

THE INTEGRATED STRESS RESPONSE PATHWAY REGULATES  
PD-L1 TRANSLATION IN HUMAN LUNG CANCER

APPROVED BY SUPERVISORY COMMITTEE

Kathryn A. O'Donnell, Ph.D.

---

Hao Zhu, M.D., Ph.D.

---

Rolf Brekken, Ph.D.

---

Steven Kliewer, Ph.D.

---

I would like to dedicate this thesis to my late friend *Priyanth Kumar Kitappa*, who dreamt  
of me getting a Ph.D. before I ever did

THE INTEGRATED STRESS RESPONSE PATHWAY REGULATES PD-L1  
TRANSLATION IN HUMAN LUNG CANCER

by

SHRUTHY SURESH

DISSERTATION / THESIS

Presented to the Faculty of the Graduate School of Biomedical Sciences

The University of Texas Southwestern Medical Center at Dallas

In Partial Fulfillment of the Requirements

For the Degree of

DOCTOR OF PHILOSOPHY

The University of Texas Southwestern Medical Center at Dallas

Dallas, Texas

May, 2019

Copyright

by

Shruthy Suresh, 2019

All Rights Reserved

THE INTEGRATED STRESS RESPONSE PATHWAY REGULATES PD-L1  
TRANSLATION IN HUMAN LUNG CANCER

SHRUTHY SURESH

The University of Texas Southwestern Medical Center at Dallas, 2019

SUPERVISOR: KATHRYN O'DONNELL, Ph.D.

Large-scale sequencing studies have comprehensively identified genomic alterations in human cancers, but they lack the ability to distinguish between cancer driver and passenger mutations. Unbiased genetic screens are a complementary approach for identifying novel cancer driving genes and establishing functional significance of clinically observed mutations. My thesis projects demonstrate how powerful this approach can be in identifying novel therapeutic targets for human cancer treatment.

Recent studies have demonstrated that human lung cancer cells express high levels of Programmed Death Ligand 1 (PD-L1), a ligand of the Programmed Death 1 (PD-1) receptor on T-cells, which allows them to directly suppress T-cell proliferation and

function. Monoclonal antibodies disrupting this pathway have yielded remarkable clinical results. However, the mechanisms of PD-L1 regulation in tumor cells remain incompletely understood. I used CRISPR-based screening to identify novel regulators of PD-L1 in human lung cancer cells, revealing potent induction of PD-L1 upon disruption of the heme biosynthesis pathway. Impairment of heme production activates the Integrated Stress Response (ISR), allowing bypass of inhibitory upstream open reading frames in the *PD-L1* 5'UTR, resulting in enhanced PD-L1 translation and immune suppression. I further demonstrated that ISR-dependent translation of PD-L1 requires the translation initiation factor EIF5B. EIF5B overexpression, which is frequent in human lung cancers and is associated with poor prognosis, is sufficient to induce PD-L1. These findings uncover a new mechanism of immune checkpoint activation and suggest novel targets for therapeutic intervention. Additionally, I have also worked on characterizing Steroid Receptor Coactivator-2, previously identified from a forward genetics screen, as a tumor suppressor in MYC-mediated liver tumorigenesis.

## Table of contents

Title Fly .....	i
Dedication .....	ii
Title Page .....	iii
Copyright .....	iv
Abstract.....	v
Table of Contents .....	vii
Prior Publications.....	xi
List of Figures .....	xiii
List of Tables .....	xviii
Chapter 1: Non-Small Cell Lung Cancer .....	1
1.1 Genomic Landscape and Molecular Origin of Non-Small Cell Lung Cancer...	1
1.2 Non-Small Cell Lung Cancer Therapy .....	2
Chapter 2: Tumor Immune Evasion .....	4
2.1 Cancer Immunity.....	4
2.2 Tumor Immune Evasion.....	4
2.3 Immune Checkpoint Pathways .....	5
2.4 PD-1/ PD-L1 Signaling Pathway .....	7
2.5 PD-1/PD-L1 Pathway in Autoimmunity and Cancer.....	8
2.6 PD-1 Checkpoint Blockade in Lung Cancer.....	9
2.7 Primary and Adaptive Resistance.....	10

Chapter 3: Unbiased Screening to Identify Cancer Drivers.....	12
3.1 Transposon Mutagenesis Screens.....	12
3.2 RNA Interference Screens .....	13
3.3 CRISPR-Cas9 Genome-Wide Screens.....	14
Chapter 4: Uroporphyrinogen Decarboxylase.....	16
4.1 Heme Synthesis in Mammalian Cells.....	16
4.2 Uroporphyrinogen Decarboxylase (UROD), a Heme Enzyme .....	18
4.3 UROD and Porphyria Cutanea Tarda .....	19
4.4 UROD in Human Cancer .....	20
Chapter 5: Integrated Stress Response .....	21
5.1 Protein Translation Initiation .....	21
5.2 The EIF2 complex and Protein Translation.....	22
5.3 EIF2 $\alpha$ Kinases: Sensors of Cellular Stress.....	22
5.4 HRI Is the Heme Sensitive EIF2 $\alpha$ Kinase .....	24
5.5 The Integrated Stress Response (ISR) Pathway .....	25
5.6 Preferential Translation Under ISR via 5'UTR Regulation .....	26
5.7 EIF2 $\alpha$ -Independent Translation .....	26
5.8 ISR in Human Disease.....	27
5.9 Pharmacological Modulation of ISR.....	29
Chapter 6: Materials and Methods .....	30
Chapter 7: Results .....	45
7.1 Experimental Strategy.....	45

7.2 A CRISPR Screen Identifies Regulators of PD-L1 in NSCLC .....	47
7.3 Loss of UROD Induces PD-L1 Protein.....	54
7.4 UROD Inhibition Promotes Tumorigenesis <i>In Vivo</i> .....	65
7.5 Mechanisms of Post-Transcriptional Regulation of PD-L1 .....	75
7.6 Loss of UROD Activates ISR to Enhance PD-L1 Translation .....	80
7.7 EIF5B Drives ISR-Dependent Translation of PD-L1 .....	98
Chapter 8: Discussion .....	104
Chapter 9: SRC-2 In Liver Cancer .....	110
9.1 Introduction .....	110
9.1.1 Human Liver Cancer .....	110
9.1.2 Mouse Models of Liver Cancer .....	111
9.1.3 SRC-2, a Master Regulator of Transcriptional Coactivation .....	112
9.1.4 SRC-2 and Human Cancer.....	113
9.2 Materials and Methods.....	114
9.3 Results.....	126
9.3.1 Deletion of <i>Src-2</i> Accelerates MYC-Mediated Liver Tumorigenesis .....	126
9.3.2 Identification of Direct SRC-2-Regulated Transcripts in MYC-Induced Liver Cancer .....	133
9.3.3 SRC-2 Targets Exhibit Tumor Suppressor Activity in Liver Cancer.....	143
9.3.4 SRC-2 Functions as a Tumor Suppressor in Human Liver Cancer .....	160
9.3.5 Analysis of Nuclear Receptor Binding Motifs Associated with SRC-2 ....	170
9.4 Discussion .....	174

Appendix A. Somatic mutations in SRC-2 target genes in human cancers.....177

Appendix B. Summary of alterations in SRC-2 targets in human liver cancer.....178

Appendix C. Other checkpoint proteins are unaltered upon UROD inhibition.....179

Acknowledgements..... 180

Bibliography ..... 184

## Prior Publications

1. **Suresh S**, Chen B, Zhu J, Golden RJ, Lu C, Evers BM, Zhan X, Schmid V, Jun S, Karacz C, Peyton M, Xiao G, Xie Y, Fu YX, Minna JD, Mendell JT, O'Donnell KA (2019). EIF5B drives integrated stress response-dependent translation of PD-L1 in lung cancer (manuscript submitted).
2. Zhou X, Padanad M, Evers BM, Smith B, Novaresi N, **Suresh S**, Richardson JA, Stein E, Zhu J, Hammer RE, O'Donnell KA (2018). Modulation of mutant KrasG12D-driven lung tumorigenesis in vivo by gain or loss of PCDH7 function, *Mol Cancer Res* PMID 30409919
3. O'Donnell KA, Guo Y, **Suresh S**, Updegraff BL, Zhou X (2019). *Ex-vivo* transposon-mediated genetic screens for cancer gene discovery, *Methods in Molecular Biology* PMID 30542998
4. **Suresh S**, Durakoglulugil D, Stashi E, York B, Xing C, Xie XJ, O'Malley BW, O'Donnell KA (2017). SRC-2-mediated coactivation of anti-tumorigenic target genes suppresses MYC-induced liver cancer. *PLoS Genetics*, PMID 29641518
5. Sreelatha, S, Kandhasamy S, Dinesh R, **Suresh S**, Shweta S, Mukesh, D, Karunagaran D, Balaji R, Mathivanan N, Perumal, PT (2014). Synthesis and SAR study of novel anticancer and antimicrobial naphthoquinone amide derivatives. *Bioorg Med Chem Lett* PMID 24913712
6. **Suresh S**, Raghu, D, Karunagaran, D (2013). Menadione (Vitamin K3) induces apoptosis of human oral cancer cells and reduces their metastatic potential by

modulating the expression of epithelial to mesenchymal transition markers and inhibiting migration. *Asian Pac J Cancer Prev*, PMID 24175842

## List of Figures

The heme biosynthetic pathway in mammalian cells .....	17
1. Cell-surface expression of PD-L1 in human NSCLC cells .....	45
2. Detection of loss and gain of cell-surface PD-L1 in H358 cells .....	46
3. Schematic outline of the CRISPR screen .....	48
4. Flow cytometry gating strategy for the CRISPR screen.....	48
5. Normalized sgRNA read counting in PD-L1 low cells .....	49
6. RIGER analysis identifies positive regulators of PD-L1 .....	50
7. Validation of positive regulators from the screen .....	51
8. RIGER analysis identifies negative regulators of PD-L1.....	52
9. Validation of negative regulators from the screen .....	53
10. Loss of UROD induces PD-L1 protein in NSCLC .....	56
11. Loss of UROD induces PD-L1 in other lung cancer cell lines.....	57
12. UROD is NOT an IFN- $\gamma$ responsive gene .....	58
13. UROD inhibition induces PD-L1 in an IFN- $\gamma$ independent manner .....	59
14. UROD is a key heme synthetic enzyme .....	60
15. Accumulated Uroporphyrinogen does not stabilize PD-L1 .....	61
16. Inhibition of ALAD induces PD-L1 .....	62
17. Inhibition of FECH induces PD-L1 .....	63
18. Hemin rescues PD-L1 in UROD knockout cells.....	64
19. Syngeneic Lewis Lung Carcinoma (LLC) Tumor Model .....	66
20. <i>Urod</i> inhibition induces PD-L1 protein but not mRNA in LLC cells. ....	66

21. <i>Urod</i> inhibition induces PD-L1 in other syngeneic tumor models .....	67
22. <i>Urod</i> inhibition promotes LLC tumor growth <i>in vivo</i> .....	68
23. <i>Urod</i> inhibition promotes tumorigenesis <i>in vivo</i> .....	69
24. <i>Urod</i> knockdown tumors grow at similar rates to controls in NSG mice .....	70
25. <i>Urod</i> knockdown tumors grow at similar rates to control tumors in CD8 <sup>+</sup> T-cell depleted mice .....	71
26. Gating strategy for TIL staining of LLC tumors .....	72
27. <i>Urod</i> inhibition leads to a reduction in CD8 <sup>+</sup> TILs .....	73
28. PD-L1 blockade controls <i>Urod</i> knockdown tumors <i>in vivo</i> .....	74
29. <i>PD-L1</i> mRNA decay is unaltered in <i>UROD</i> knockout cells .....	76
30. PD-L1 is targeted predominantly to the proteasome for degradation .....	77
31. PD-L1 protein stability is unaltered in <i>UROD</i> knockout cells .....	78
32. PD-L1 ubiquitylation is unaltered in <i>UROD</i> knockdown cells.....	79
33. <i>UROD</i> depletion activates the Integrated Stress Response (ISR) .....	81
34. A chemical activator of HRI induces PD-L1 .....	82
35. Phosphorylation of EIF2 $\alpha$ is sufficient to induce PD-L1.....	83
36. ISRIB reverses the effect of Salubrinal on PD-L1.....	84
37. ISRIB partially reverses the effect of <i>UROD</i> knockdown on PD-L1.....	85
38. EIF2 $\alpha$ phosphorylation is necessary for PD-L1 induction.....	86
39. <i>UROD</i> inhibition leads to global translation attenuation.....	87
40. <i>UROD</i> inhibition leads to reduction in polysomes.....	90
41. Salubrinal shuts down global protein translation .....	91

42. <i>UROD</i> inhibition leads to enhanced translation of PD-L1 .....	92
43. ISR activation leads to enhanced translation of PD-L1.....	93
44. Luciferase reporters harboring the wildtype or mutant human <i>PD-L1</i> 5'UTR ....	94
45. Luciferase reporter mRNA expression is similar in the various constructs .....	95
46. <i>PD-L1</i> 5'UTR harbors multiple inhibitory CUGs.....	96
47. A scanning model for <i>PD-L1</i> mRNA translation.....	97
48. EIF2Ai partially rescues PD-L1 in <i>UROD</i> knockout cells.....	99
49. EIF2Di has no effect on PD-L1 in <i>UROD</i> knockout cells .....	100
50. EIF5Bi potently rescues PD-L1 in <i>UROD</i> knockout cells.....	101
51. <i>EIF5B</i> is a clinically relevant gene in NSCLC .....	102
52. Overexpression of EIF5B induces PD-L1 .....	103
53. Working model.....	109
54. Generation of <i>Src-2<sup>-/-</sup></i> ; tet-o-MYC; LAPtTA mice .....	128
55. Western blot analysis depicting absence of SRC-2 in tet-o-MYC; LAPtTA <i>Src-2</i> wildtype (WT) or null (KO) mice .....	129
56. Hematoxylin and eosin (H&E) staining of normal liver and liver tumors from <i>Src-2<sup>-/-</sup></i> and <i>Src-2<sup>+/+</sup></i> mice .....	130
57. Periodic acid-Schiff (PAS) staining to measure glycogen storage deficiency in normal liver and tumors from <i>Src-2<sup>+/+</sup></i> and <i>Src-2<sup>-/-</sup></i> mice.....	131
58. Loss of <i>Src-2</i> accelerates MYC-mediated liver tumorigenesis <i>in vivo</i> .....	132
59. Identification of SRC-2 targets in MYC-driven liver tumors.....	135
60. Identification of targets repressed by SRC-2 in MYC-driven liver .....	136

61. Overlap of <i>in vivo</i> mouse liver SRC-2 ChIP-Seq targets and genes downregulated in <i>Src-2</i> <sup>-/-</sup> liver tumors .....	137
62. Expression analysis of direct SRC-2 targets using Geo2R in a panel of HCC tumor samples .....	139
63. Real-time PCR analysis of <i>Shp</i> , <i>Dkk4</i> , <i>Cadm4</i> and <i>Thrsp</i> in an independent set of <i>Src-2</i> <sup>-/-</sup> and <i>Src-2</i> <sup>+/+</sup> liver tumors.....	140
64. Identification of direct SRC-2 targets in MYC-induced liver cancer .....	141
65. Identification of direct targets repressed by SRC-2 in MYC-induced liver cancer .....	142
66. MYC expression is comparable in HCC cells and <i>Src-2</i> <sup>-/-</sup> ; tet-o-MYC; LAPtTA liver tumors.....	145
67. SHP depletion accelerates Huh7 cell proliferation <i>in vitro</i> .....	146
68. SHP depletion accelerates tumor formation of Huh7 cells <i>in vivo</i> .....	147
69. Overexpression of SHP reduces tumor formation of Huh7 cells <i>in vivo</i> .....	148
70. <i>Src-2</i> <sup>-/-</sup> tumors have elevated Cyp7a1 levels.....	149
71. <i>CYCLIN D1</i> mRNA levels do not change upon SHP inhibition .....	150
72. <i>CYCLIN D1</i> protein levels do not change upon SHP inhibition.....	151
73. <i>DKK4</i> depletion in HepG2 cells after inhibition with two shRNAs .....	152
74. Inhibition of <i>DKK4</i> increases HepG2 cell growth <i>in vitro</i> .....	153
75. <i>DKK4</i> depletion accelerates tumor formation of HepG2 cells <i>in vivo</i> .....	154
76. Overexpression of <i>DKK4</i> reduces tumor formation of Huh7 cells <i>in vivo</i> .....	155
77. <i>CADM4</i> depletion in HepG2 cells after inhibition with two shRNAs.....	156

78. CADM4 depletion accelerates HepG2 tumor cell growth.....	157
79. Overexpression of CADM4 reduces tumor formation of Huh7 cells.....	158
80. Overexpression of THRSP reduces tumor formation of Huh7 cells.....	159
81. Overexpression of SRC-2 upregulates candidate gene expression in HCC....	162
82. Overexpression of SRC-2 reduces HCC proliferation <i>in vitro</i> and tumor formation <i>in vivo</i> .....	163
83. Inhibition of SRC-2 accelerates Huh7 proliferation <i>in vitro</i> .....	164
84. Inhibition of SRC-2 leads to downregulation of SRC-2 target genes .....	165
85. Overexpression of each of the four targets alone or in combination in SRC-2 shRNA cells.....	166
86. SHP and CADM4 rescue enhanced cell proliferation <i>in vitro</i> .....	167
87. SHP and CADM4 rescue enhanced tumor burden upon SRC-2 inhibition .....	168
88. THRSP and DKK4 are not sufficient to rescue enhanced tumor burden upon SRC-2 inhibition.....	169
89. Putative TR binding sites in the promoter regions of SRC-2 target genes.....	171
90. <i>Shp</i> has FXR and HNF4A binding motifs in its promoter region that overlaps with SRC-2 binding site.....	172
91. Luciferase Reporters harboring either the entire <i>SHP</i> promoter or <i>SHP</i> promoter lacking the FXR element cloned upstream of Firefly Luciferase.....	173
92. SRC-2 cooperates with FXR to activate <i>SHP</i> reporter activity .....	173

## List of Tables

1. List of antibodies and chemicals .....	43
2. List of nucleotide sequences.....	44
2.1 List of sgRNA and shRNA sequences .....	44
2.2 List of primer sequences .....	44
3. Quantitative real-time PCR primer sequences .....	117
4. List of 47 downregulated genes in <i>Src-2<sup>-/-</sup></i> liver tumors and directly bound by SRC-2 in mouse liver .....	138

## Chapter 1: Non-small cell lung cancer

### 1.1 Genomic landscape and molecular origin of non-small cell lung cancer

Lung cancer is the leading cause of cancer associated deaths worldwide [1]. Non-small cell lung cancer (NSCLC) comprise 85% of all lung cancers, of which Lung Adenocarcinoma (LUAD) and Lung Squamous Carcinoma (LUSC) are the most common subtypes [2]. While smoking is the most common etiology for 80% of lung cancer cases in United States, LUAD is more common among never smokers [2, 3]. Thus, besides environmental factors, a better understanding of the biology of lung cancer as a disease is required to improve clinical outcomes in a meaningful manner.

Large-scale sequencing studies and comprehensive histological analysis of lung tumor samples have led to the identification of frequent genetic alterations in lung cancer [3, 4]. Mutations in *Kirsten Rat Sarcoma (KRAS)* and *Epidermal Growth Factor Receptor (EGFR)* each represent ~30% of all somatic mutations in LUAD and are readily detected in early stage cancers suggesting their role in tumor initiation. Several functional studies confirm a role for *KRAS* and *EGFR* as key oncogenic drivers, often mutually exclusive in LUAD [5-7]. Tumor suppressor genes such as *Tumor Suppressor Protein 53 (TP53)*, *Kelch-like ECH Associated Protein 1 (KEAP1)*, *Serine-Threonine Kinase 11 (STK11)* and *Neuro Fibromin 1 (NF1)* are also found to be inactivated in LUAD [3]. In contrast, receptor tyrosine kinases such as *EGFR* are rarely mutated in LUSC. The commonly mutated genes in LUSC include *TP53*, mutated in 90% of cases and *Cyclin Dependent Kinase*

*Inhibitor 2A (CDKN2A)*, mutated in 70% of LUSC [3]. These differences in molecular features within NSCLC subtypes are more apparent between smokers and never smokers. For instance, smokers possess a distinct genomic landscape to never smokers with the former containing high mutational burden as well as greater incidence of *KRAS* and *TP53* mutations [8]. While *KRAS* is implicated as a driver in ~32% of LUAD, it remains a non-actionable mutation that is not targeted efficiently via chemical intervention in lung cancer cells. Thus, there is a need to identify novel genetic alterations contributing to *KRAS* mediated lung cancer progression.

## **1.2 Non-small cell lung cancer therapy**

The last two decades have seen tremendous progress in therapeutic approaches to treat NSCLC. However, the five-year survival of NSCLC patients continues to be ~18% [2]. Lung cancer patients are staged I-IV based on the extent of clinical tumor progression [9, 10]. Surgical resection is the first line of treatment for early stage patients followed by adjuvant chemotherapy. Robotic and video-assisted surgeries have likely contributed to the improving clinical outcomes in early stage patients, with a 80% 5-year survival for Stage I patients. Unresectable locally advanced NSCLC on the other hand with a poorer 5-year survival rate is usually treated via thoracic radiation and cytotoxic drug regimens such as platinum-based therapy [3, 4, 9]. Identification of *EGFR* mutations as well as *Proto-oncogene tyrosine kinase (ROS1)* fusions, *Anaplastic Lymphoma Kinase (ALK)* rearrangements and *Proto-oncogene Serine Threonine Kinase (BRAF)* mutations in NSCLC patients have led to the development of effective targeted therapies to improve

clinical outcomes [3, 5, 11]. For instance, Gefitinib and Erlotinib, first generation *EGFR* Tyrosine Kinase Inhibitors (TKI) were found to be clinically superior to cytotoxic therapy. With time, clinical documentation of disease recurrence and molecular studies into resistance mechanisms paved the way for second and third generation TKI Afatinib and Osimertinib [5]. Another recent advancement in management of NSCLC has been the development of immune checkpoint blockade (ICB) to treat cancer [12, 13]. The most common ICBs approved for NSCLC include monoclonal antibodies such as Nivolumab, Pembrolizumab and Atezolizumab, which will be described in the next chapter [13, 14].

## Chapter 2: Tumor Immune Evasion

### 2.1 Cancer immunity

Cancer cells accumulate unique genetic mutations compared to normal cells that are advantageous to their proliferation and survival. However, an increase in mutational burden also increases their likelihood to be detected as foreign by the immune system [15]. Indeed, tumor specific mutations generate aberrant peptides termed neo-antigens or tumor specific antigens (TSA) that stimulate an immune response *in vivo* [16]. TSA arise from nonsynonymous mutations as well as oncogenic viral proteins and are predominantly absent in normal cells, making them an attractive target for intervention [16]. The most striking evidence supporting an important role for TSA in cancer immunity comes from clinical correlate studies of response to ICBs in patients. The frequency of somatic mutations largely correlates with sensitivity to ICBs in almost all tumor types [13, 15, 16]. Even within a tumor type, tumor mutational burden (TMB) directly correlates with response to immunotherapy, for instance, in lung cancer [17]. Similarly, mismatch repair deficiency in solid tumors was found to predict response to ICB [18]. Thus, mutational neoepitopes on tumor cells serve as key drivers of anti-cancer T lymphocyte responses.

### 2.2 Tumor Immune Evasion

The immune system is actively engaged with tumors early on from transformation and tumor initiation. Cancer cells adopt survival mechanisms to evade host immune responses over the various stages of tumorigenesis [16]. During tumor progression,

cancer cells undergo immunoediting, wherein the most immune-stimulatory antigens are lost to select for less immunogenic cancer clones [15, 19]. For example, downregulation of antigen processing and presentation on MHC class I is well documented in many tumor types [20]. Besides immunoediting, cancer cells adopt several mechanisms to mediate immune escape. For instance, factors secreted by tumors such as Vascular Endothelial Growth Factor (VEGF), adenosine, Indoleamine 2, 3-dioxygenase 1 (IDO1), Interleukin 10 (IL-10), Transforming Growth Factor- $\beta$  (TGF $\beta$ ) and galectins can mediate immune suppression [21]. Metabolic pathway activation of arginase, inducible nitric oxide and lactate dehydrogenase on tumor cells also leads to suppression of T cells [21, 22]. Tumor cells can additionally recruit immune suppressive cell populations such as myeloid suppressor dendritic cells and regulatory T cells that further promote immune escape [23, 24]. Importantly, recent studies have shown that tumor cells can co-opt immune check point proteins and anti-phagocytosis signals that allow for immune evasion [15].

### **2.3 Immune Checkpoint pathways**

Immune checkpoint proteins are cell surface molecules that either stimulate or inhibit the immune system [13]. These molecules are crucial for self-tolerance, to prevent the immune system from attacking cells indiscriminately [25]. Immune checkpoint proteins can be costimulatory or coinhibitory in nature and expressed on antigen presenting cells as well as a variety of immune cells [15]. Some important costimulatory immune checkpoint proteins include Cluster of Differentiation 28 (CD28) and Cluster of

Differentiation 40 (CD40). CD28 is a cell surface protein constitutively expressed in CD4<sup>+</sup> T cells as well as over half of CD8<sup>+</sup> T cells. Its binding to its ligands CD80 or CD86 often expressed on dendritic cells promotes T cell expansion [26]. CD40 is constitutively expressed on all antigen presenting cells, including dendritic cells, B cells and macrophages. Ligation of CD40 with its ligand on CD4<sup>+</sup> T helper cells leads to enhanced activation of both dendritic cells and macrophages, leading to both T-cell dependent and independent tumor killing [26, 27]. Clinical trials testing CD40 agonists are currently underway as potential targets of cancer immunotherapy [27, 28]. Coinhibitory immune checkpoint proteins on the other hand are expressed in various immune cells as well as overexpressed in multiple tumor types to mediate immune suppression.

**Cytotoxic T cell lymphocyte antigen-4 (CTLA-4)** was the first well characterized coinhibitory checkpoint protein. CTLA-4, a type-1 transmembrane protein, expressed on activated T cells shares the ligands CD80 and CD86 with CD28 and bind them with higher affinity [29]. Thus, by preventing CD28 co-stimulation, CTLA-4 acts as a negative regulator of T cell function [19, 30-32]. Ipilimumab, a CTLA-4 antibody has shown promising results in restoring T cell responses in advanced melanoma [19, 33].

**Lymphocyte Activation Gene-3 (LAG-3)** is a transmembrane protein expressed on activated T cells and B cells and bears structural homology to CD4 [33, 34]. MHC Class II and Galectin-3 are the most well studied ligands of LAG-3 whose engagement result in suppression of T cells [33-35].

**T cell immunoglobulin and mucin-domain containing protein-3 (TIM-3)** is a member of the TIM family whose binding partners are proposed to be

Phosphatidylserine, High mobility Protein Group B1 (HMGB-1) and Galectin-9 (LGALS9), and whose activation was found to induce T-cell dysfunction [36-38].

## **2.4 PD-1/PD-L1 signaling pathway**

**Programmed Cell Death 1 (PD-1)** is an important immune checkpoint protein expressed on T cells, B cells and activated monocytes [25]. It is a cell surface monomer with an immunoglobulin extracellular domain and a cytoplasmic domain containing two tyrosine-based signaling motifs that are activated upon ligand binding. **PD-L1** and **PD-L2** serve as ligands for PD-1, with the expression of the latter being more restricted than the former [25, 39, 40]. PD-L2 is mostly expressed on dendritic cells and macrophages. In contrast, PD-L1 is expressed in both hematopoietic cells such as T cells, B cells, dendritic cells, macrophages and non-hematopoietic cells such as vascular endothelial cells, epithelial cells of the lung and the heart, muscle cells, hepatocytes as well as sites of immune privilege, such as the placenta and eye [38, 39]. Under active T cell receptor (TCR) signaling in T cells, PD-1 ligation induces activation of the cytoplasmic tyrosine motifs that then recruits tyrosine phosphatases to dephosphorylate TCR effector molecules. PD-1 signaling also attenuates CD28-mediated activation of the Phosphoinositide 3-kinase (PI3K) pathway to disrupt T cell survival [29, 39]. Persistent PD-1 signaling results in chronic T cell dysfunction, termed as T cell exhaustion [41]. T cell exhaustion is characterized by poor effector function, sustained expression of inhibitory receptors such as PD-1 and TIM-3, and a transcriptional profile distinct from effector T cells [41]. Thus, PD-L1/PD-1 signaling results in suppression of T cell proliferation and function.

## 2.5 PD-1/PD-L1 pathway in autoimmunity and cancer

The role of PD-1/PD-L1 signaling in regulating autoimmune responses is best understood by the phenotype of *Pd1*<sup>-/-</sup> mice [39]. Loss of PD-1 results in the development of a spontaneous, late-onset lupus-like disease and a dilated cardiomyopathy characterized by autoantibodies in C57BL/6 and BALB/c mice, respectively. High expression of PD-L1 in immune privileged sites such as the placenta, eye and heart help protect these organs from self-reactive immune cells. For instance, PD-L1 in the placenta increases in the second trimester to promote fetal-maternal tolerance. Consistent with this, a PD-L1 blocking antibody increases T cell infiltration and abortion rate of allogenic fetuses [42]. Similarly, high PD-L1 in corneal cells and pancreatic islet cells help control retinal inflammation and autoimmune diabetes [25, 43]. On the other hand, active PD-1/PD-L1 signaling increases susceptibility to infectious diseases due to decreased T cell function. [15, 25, 40, 41].

PD-L1 was also found to be overexpressed in multiple human cancer types and correlated with poor patient survival [38, 44]. Mouse models of cancer demonstrate that PD-1 signaling serves as a shield for tumor cells from the immune system and monoclonal antibodies targeting PD-1 enhance tumor killing [45]. *Pd-1*<sup>-/-</sup> mice have a milder autoimmune phenotype compared to *Ctla4*<sup>-/-</sup> mice, suggesting that PD-L1 blockade in patients would be unlikely to generate severe autoimmune side effects. Consistent with this, PD-1 blockade in cancer patients has less severe side effects compared to chemotherapy and CTLA-4 blockade. However, immune-related adverse events such as

pneumonitis, nephritis and hepatitis are observed in patients treated with PD-1 blockade [46].

## **2.6 PD-1 checkpoint blockade in lung cancer**

PD-1 blockade has shown significant improvement in overall survival of NSCLC, especially in comparison to platinum-based therapy and docetaxel [47]. Patients with tumor PD-L1 expression levels of 50% or more had the most benefit from PD-1 blockade, with an objective response rate of 75% [14, 47]. Moreover, immunotherapy has less severe side effects compared to cytotoxic therapy, as well as lower fatality rates, making it an attractive treatment regimen. This has led to the establishment of PD-1 blockade as first line therapy for lung cancer patients expressing high PD-L1 [14, 47]. Patients with high PD-L1 expression as well as high TMB currently have higher response to PD-1 checkpoint blockade [17]; this comprises only about ~20% of NSCLC patients. This necessitates a better understanding of factors contributing to response to ICBs. One such factor that has just begun to be appreciated is the host microbiome which can predict and mediate sensitivity to ICBs [48, 49]. Combination of PD-1 blockade and chemotherapy or radiation have also shown promising results in clinical trials [50]. Immunotherapy however still remains challenging in patients with low T cell infiltration, low PD-L1 expression or low TMB (commonly referred to as 'cold tumors'). Moreover, several patients that initially respond to ICB eventually develop resistance [51]. Thus, it is imperative to identify better predictors for response to immunotherapy as well as understand mechanisms of immune checkpoint activation and resistance by tumor cells.

## **2.7 Primary and adaptive resistance**

PD-L1 expression on tumor cells is constitutive and can also be induced by Interferon  $\gamma$  (IFN- $\gamma$ ) in the tumor microenvironment [12, 19, 51], contributing to tumor intrinsic and extrinsic mechanisms of immune resistance.

### **Tumor extrinsic mechanisms:**

IFN- $\gamma$  secreted by effector T cells during an active anti-tumor immune response, upregulates PD-L1 and thus serves a dominant mechanism of adaptive immune resistance. In some contexts, T cell exhaustion or an absence of infiltrating T cells also contribute to resistance to anti-tumor immunity. Other tumor extrinsic mechanisms that lead to immune resistance include components of the tumor microenvironment such as regulatory T cells, myeloid-derived suppressor cells and macrophages. Several studies have shown that tumor cells for instance are more effectively cleared when PD-1 blockade was combined with inactivation of tumor associated macrophages [52, 53]. Signals that enhance anti-tumor immunity also turn on inhibitory pathways to tightly regulate immune response. For example, PD-1 blockade was found to increase TIM-3 on T cells in a mouse model of lung adenocarcinoma [54].

### **Tumor intrinsic mechanisms:**

Tumor-cell-intrinsic factors that contribute to immunotherapy resistance involve regulation of genes in tumor cells that affect immune cell infiltration and subsequent tumor clearance. Some cancers evade the immune response due to absence of antigenic cell

surface proteins [55]. Alternatively, cancer cells expressing antigens may evolve mechanisms to avoid antigen presentation by Major Histocompatibility Complex (MHC) molecules, due to dysregulation of antigen transport machinery, downregulation of Beta-2-Microglobulin or the MHC itself [56, 57]. Tumor intrinsic mechanisms of immune suppression includes genomic, transcriptional and posttranscriptional upregulation of PD-L1 itself [40, 41]. Hodgkin's lymphoma patients were found to have genomic amplifications in the PD-L1 locus in 97% of the cases [58]. Similar amplifications in PD-L1 was detected in NSCLC and SCLC [59, 60]. Truncations in the 3' Untranslated Region (3'UTR) of *PD-L1* have been documented in tumor samples and validated to contribute to immune resistance [61]. Importantly, a subset of oncogenes such as *MYC*, *KRAS*, *EGFR* have been demonstrated to induce PD-L1 transcriptionally and post transcriptionally on tumor cells to drive immune evasion [62-67]. Understanding mechanisms of PD-L1 upregulation on tumor and immune cells may help identify novel therapies in combination with PD-1 blockade and enhance anti-tumor immunity.

## Chapter 3: Unbiased screening to identify cancer drivers

### 3.1 Transposon Mutagenesis Screens

Large-scale sequencing studies have led to the comprehensive identification of genetic alterations in human cancers. However, this approach is unable to delineate the role of these mutations as driver or passenger events in tumorigenesis. Transposon-mediated mutagenesis screens have emerged as a powerful complementary approach to identify novel drivers of oncogenesis. These forward genetic screens rely on the mobilization of mutagenic DNA transposons such as *Sleeping Beauty (SB)* or *piggyBac* in transgenic mouse models [68-70]. Upon mobilization in the genome, these elements can disrupt normal gene function by activating proto-oncogenes, or by inactivating tumor suppressor genes. The transposon insertion sites can then be mapped in the genome using bioinformatic analysis to identify genes potentially regulating tumorigenesis [71]. In these studies, transposition induces tumorigenesis *in vivo* alone or in combination with an initiating event such as oncogenic activation of *Myc*, *Braf* or genetic loss of *Tp53*, or *Patch (Ptch)* tumor suppressors. Several studies have utilized transposon-based insertional mutagenesis screens in mice to identify and validate genes relevant to tumorigenesis, including T-cell leukemia, colon cancer, hepatocellular carcinoma, medulloblastoma, and nerve sheath tumors [68, 70, 72-74].

Besides *in vivo* screens which can be cost intensive, transposon mutagenesis has also been effectively adopted to identify drivers of cancer *ex vivo* [75, 76]. Unlike DNA and RNA interference-based screens, transposon-mediated mutagenesis allows the

identification of both gain-of and loss-of function mutations in the same tumor, which may be a more accurate model of tumor initiation in human patients [72].

### **3.2 RNA interference screens**

RNA interference (RNAi) screening is an alternate approach to transposon mutagenesis screens that can identify regulators of specific biological phenotypes [77]. Small interfering RNA (siRNA), 21-27 nucleotide double-stranded oligonucleotides are incorporated into a large protein complex known as the RNA-induced silencing complex (RISC), which then targets and cleaves complementary messenger RNA (mRNA) [78]. Experimentally, genome-wide RNAi can be induced in several different ways including delivery of pooled siRNAs transiently or viral transduction mediated delivery of short hairpin RNAs (shRNA) [79-82]. Pooled shRNA screens are advantageous in targeting an entire genome allowing rapid evaluation of consequences of large gene set manipulations. Cells that have altered phenotypes are analyzed for enrichment or depletion of shRNAs, which then identifies novel genes contributing to the phenotype. Such pooled shRNA screens have been an indispensable tool to identify genes regulating disease states and development in mammalian cells [83-88].

However, a major problem with RNA interference screens are off-target effects leading to false positive hit identification as well as inefficient depletion of target genes leading to false negative hits. Off-target effects can be minimized by effective RNAi library design, recapitulation of hits using multiple shRNA and importantly rescuing a phenotype using a shRNA resistant target gene product [77, 80, 82].

### 3.3 CRISPR-CAS9 genome-wide screens

RNA-guided genome editing has emerged as a new, powerful approach that circumvents the limitations of RNA interference screening and employs the RNA-guided endonuclease Cas9 from the type II microbial adaptive immune system CRISPR (Clustered Regularly Interspaced Short Palindromic Repeat) [89, 90]. Cas9 is targeted to specific genomic loci using a short guide RNA (sgRNA), which recognizes the target DNA by base pairing. Delivery of Cas9 then results in double stranded DNA breaks (DSB) at the genomic target which is often repaired by an error-prone Non-Homologous End Joining (NHEJ) resulting in insertions and deletions (indels) at the mutation site. Indels usually result in frameshift mutations or a non-functional gene product leading to effective depletion of the target gene. The commonly used Cas9 originates from *Streptococcus Pyogenes* which requires the sgRNA to contain a 20-bp guide sequence followed by a 3-bp protospacer-adjacent motif [91, 92]. Besides efficient gene knockout via Cas9, catalytically dead Cas9 (dCas9) fusion proteins have been employed to localize effector domains to specific genomic loci to either repress (CRISPRi) or activate (CRISPRa) transcription of target genes [93, 94]. Pooled CRISPR screens are powerful and less labor and resource intensive with the availability of oligonucleotide libraries. These oligonucleotides are cloned to create a plasmid library which can be used for large-scale virus production and screening. Screen readouts using Next Generation Sequencing help identify the sgRNA-encoding regions of the viral integrants, followed by mapping of sequencing reads to sgRNA libraries and enrichment of sgRNAs for a given target gene [91, 92, 95-97]. RNAi Gene Enrichment ranking enables identification of candidate hits from the screen [98]. Moreover,

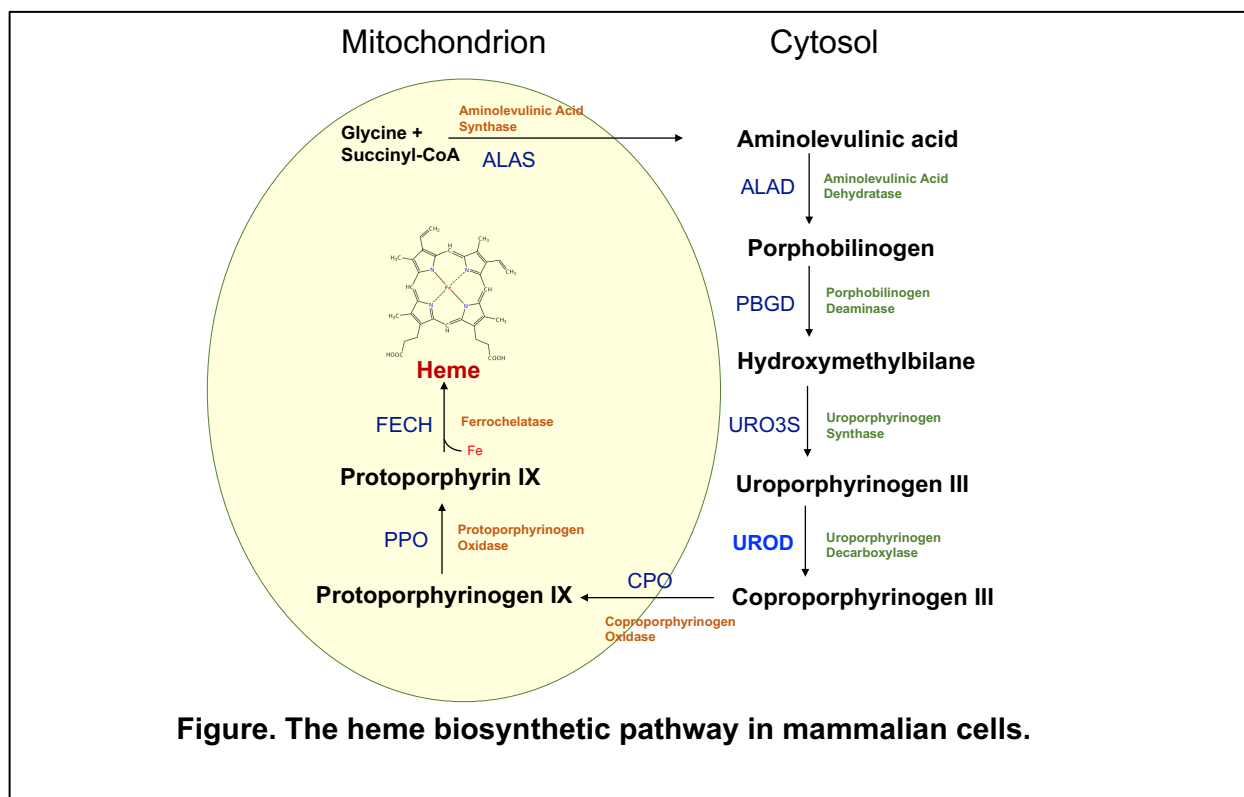
technologies such as Perturb-Sequencing [99] and Single Guide RNA (sgRNA) Lentiviral Infection with Cas9 protein Electroporation (SLICE) [100] allow for assaying complex phenotypes such as transcriptional profiles as well as performing large-scale screening in primary cells. Pooled CRISPR screens have become a vital tool in the molecular biologist arsenal to address diverse biological problems, ranging from cancer progression, susceptibility to microbial and viral infection and drug resistance [63, 91, 94, 95, 101, 102].

## Chapter 4: Uroporphyrinogen Decarboxylase

### 4.1 Heme synthesis in mammalian cells

Heme, which is 2,7,12,18-tetramethyl-3,8-divinylporphyrin-13,17-dipropionic acid iron(II) coordination complex, also known as Fe protoporphyrin IX, consists of a heterocyclic porphyrin ring surrounding one ferrous ( $\text{Fe}^{2+}$ ) iron and serves as a prosthetic group in many proteins such as hemoglobin, myoglobin, cytochromes, catalases, peroxidases, guanylate cyclase, and nitric oxide synthase [103-106]. Heme plays an important role in biological processes such as electron transport, xenobiotic detoxification, microRNA processing, signal transduction and hemoglobin homeostasis [103-109]. In metazoans, heme synthesis occurs via a conserved eight-step process [103, 104], beginning with the rate-limiting synthesis of 5-aminolevulinic acid and ending at the insertion of  $\text{Fe}^{2+}$  iron into protoporphyrin IX in the mitochondria to generate heme (**Fig. Heme Synthesis in Mammalian Cells**). Heme synthetic enzymes are encoded in the nucleus, synthesized in the cytoplasm and localized to either the cytoplasm or mitochondria. Transport of the heme synthesized in the mitochondria to other cellular compartments is not completely understood. Several heme transporter proteins such as Heme Carrier Protein 1 (HCP-1), Heme Responsive Gene 1 (HRG-1) and Feline leukemia virus subgroup C receptor-related protein 1 (FLVCR) are speculated to regulate heme import, export and intra-organelle heme translocation [110]. Degradation of free heme in cells is mediated by the Heme Oxygenase (HO) enzymes. HO-1, an ER resident enzyme encoded by the *HMOX1* gene, degrades free heme to yield equimolar amounts of three products: carbon

monoxide, iron, and biliverdin, which is converted to bilirubin by biliverdin reductase (BVR) [106, 111]. Bilirubin is converted back to biliverdin in a reactive oxygen species (ROS) dependent manner. This leads to an amplified redox cycle wherein accumulated ROS in cells is neutralized [112]. Cells replete with heme thus activate cytoprotective signaling via HO to neutralize ROS. Heme deficiency, by disrupting this HO-mediated biliverdin-bilirubin cycle leads to generation of ROS in cells. Moreover, other studies have shown that heme deficiency also impairs mitochondrial complex IV and catalases to accumulate ROS and impair cellular viability [113, 114]. Heme synthesis is thus important for survival of proliferative cells, including cancer cells [115].



## 4.2 Uroporphyrinogen Decarboxylase, a heme synthetic enzyme

Uroporphyrinogen Decarboxylase (UROD) encodes a cytosolic enzyme that catalyzes the step-wise decarboxylation of Uroporphyrinogen III to Coproporphyrinogen III (Fig. – Heme Synthesis in Mammalian Cells). The human UROD gene contains 10 exons spanning 3kb and is located on chromosome 1p34 [103, 116, 117]. *UROD* is highly expressed in erythrocytes, hepatocytes as well as several human cancers [118, 119]. Unlike other heme synthetic enzymes such as *Aminolevulinic Acid Synthase (ALAS)* and *Ferrochelatase (FECH)*, the transcriptional and post transcriptional mechanisms of regulation of *UROD* are not well understood. Additionally, in contrast to other decarboxylation enzymes, UROD's catalytic activity is independent of a metal ion or cofactor. UROD enhances the rate of substrate decarboxylation by a factor of  $1.2 \times 10^{17}$ , deeming it a benchmark for catalytic proficiency among enzymes that function without cofactors [120]. Decarboxylation of four pyrrole acetic acid side chains of Uroporphyrinogen III begins at an asymmetric D-ring and proceeds in a clockwise manner to yield the four methyl pyrrole chains of coproporphyrinogen and four molecules of carbon dioxide [120, 121]. Crystal structure studies of UROD have demonstrated that UROD is a functional homo-dimeric enzyme whose ~40 kDa protein monomer is comprised of a single domain containing an  $\alpha/\beta$ -barrel and a deep active-site cleft formed by loops at the C-terminal ends of the barrel strands [121]. While the exact sites on UROD crucial for decarboxylation is unknown, crystallization studies have identified a role for an Aspartate 86 residue in substrate binding and catalysis and of UROD. Consistent

with this, mutation of the aspartate to asparagine results in very low activity of UROD *in vitro* [120, 121].

#### **4.3 UROD and Porphyria Cutanea Tarda**

Deficiency in UROD leads to Porphyria Cutanea Tarda (PCT), the most common porphyria, occurring in 1 in 20,000 Caucasians [122-125]. PCT results from accumulation of uroporphyrin and other partially decarboxylated intermediate porphyrins in the liver, plasma and skin. PCT is characterized by hyperpigmentation, severe photosensitive dermatosis, and hypertrichosis. It can be either sporadic (type 1) or familial (type 2). For clinical symptoms to manifest in either type, the hepatic UROD activity must be <20%. Sporadic PCT patients lack *UROD* mutations and when asymptomatic, have normal UROD activity. Familial PCT patients on the other hand, are heterozygous for *UROD* mutations and asymptomatic patients have approximately 50% of enzyme activity systemically. Other environmental factors such as alcohol consumption, toxin exposure contribute to susceptibility to PCT. Mutation analysis in the UROD gene is a useful tool for diagnosis of PCT patients, with the identification of >100 *UROD* mutations in PCT patients [126]. UROD deficiency leads to a disruption of heme synthesis and accumulation of iron as well as Uroporphyrinogen. Thus, phlebotomies to decrease the hepatic iron load often is clinically beneficial to PCT patients [127, 128]. An alternative oral treatment for PCT is low dose chloroquine treatment. Since PCT can manifest sporadically without underlying *UROD* mutations, a chemical inhibitor of UROD was speculated to exist *in vivo*. Consistent with this, Uroporphomethene, an oxidized form of

Uroporphyrinogen, was shown to be the UROD inhibitor *in vivo* [124]. The oxidation of Uroporphyrinogen to Uroporphomethene was iron dependent in the liver, demonstrating how iron overload can further aggravate PCT [122, 123, 125].

#### **4.4 UROD in human cancer**

Two studies implicate UROD driven heme synthesis in providing a survival advantage for cancer progression in leukemogenesis and head and neck cancer [115, 129]. But these studies failed to capture the role of immune microenvironment in regulating tumor progression. It is thus imperative to assess the role of UROD in tumor progression in a setting relevant to the tumor microenvironment *in vivo*.

## Chapter 5: The Integrated Stress Response Pathway

### 5.1 Protein translation initiation

Translation initiation is a tightly regulated step in protein synthesis, which involves the proper assembly of competent 80S ribosomes on the mRNA. It requires at least 9 eukaryotic initiation factors (EIFs) in several stages [130-133]. These stages are:

- (1) EIF2–GTP–charged Methionyl tRNA (Met-tRNA<sub>i</sub><sup>Met</sup>) ternary complex formation
- (2) Formation of a 43S preinitiation complex comprising a 40S ribosomal subunit, EIF1, EIF1A, EIF3, EIF2–GTP–Met-tRNA<sub>i</sub><sup>Met</sup>
- (3) mRNA activation, where cap-proximal region is unwound in an ATP-dependent manner by EIF4F with EIF4B
- (4) Attachment of the 43S complex to mRNA
- (5) Scanning of the 5' UTR in a 5' to 3' direction by 43S complexes
- (6) Recognition of the initiation codon and 48S initiation complex formation, which leads to displacement of EIF1 to allow EIF5-mediated hydrolysis of EIF2-bound GTP and P<sub>i</sub> release
- (7) Joining of 60S subunits to 48S complexes and concomitant displacement of EIF2–GDP and other factors mediated by EIF5B
- (8) GTP hydrolysis by EIF5B and release of EIF1A and GDP-bound EIF5B from assembled elongation competent 80S ribosomes
- (9) Termination following elongation and leading to recycling of (1), to generate separated ribosomal units

## 5.2 The EIF2 complex and protein translation

The EIF2 complex is a heterotrimeric protein complex with a molar mass of 126 kDA that comprises of an  $\alpha$ ,  $\beta$  and  $\gamma$  subunit [132]. The EIF2 complex in eukaryotic cells is responsible for transferring charged methionyl tRNA (Met-tRNA<sub>i</sub>) to the 40S subunit in the ternary complex (TC) with the GTP. The  $\alpha$  subunit, considered the regulatory subunit of the complex contains an important phosphorylation site at Serine 51. It also contains a potential RNA binding site. The  $\beta$ -subunit also contains multiple phosphorylation sites as well as three lysine clusters in its N-terminus, important for the interaction with EIF2B. The  $\gamma$ -sub-unit comprises three guanine nucleotide-binding sites and is the crucial docking site for GTP/GDP. It also contains a tRNA-binding cavity. EIF2B is the guanine nucleotide exchange factor for EIF2 and converts the inactive EIF2-GDP to the active EIF2-GTP. Met-tRNA<sub>i</sub> has 100 times more affinity for EIF2-GTP than EIF2-GDP and thus optimal EIF2B function is essential for protein translation initiation [133, 134].

## 5.3 EIF2 $\alpha$ kinases: sensors of cellular stress

Eukaryotic cells respond to various cytoplasmic stresses by activating one of four mammalian discrete protein kinases called EIF2 $\alpha$  kinases (EIF2AKs) [135, 136]. Among these, Heme-regulated Inhibitor (HRI, EIF2AK1) is activated upon heme deprivation [137, 138], Protein Kinase R (PKR, EIF2AK2) is activated in response to double stranded RNA [136, 139], PKR like ER Kinase (PERK, EIF2AK3) is activated in response to accumulated protein load in the ER [135, 136, 140] and General Control Nondepressible 2 (GCN2, EIF2AK4) is activated in response to amino acid deprivation [139, 141, 142]. Activation

of either of the four kinases leads to phosphorylation of EIF2 $\alpha$  at Serine 51, a highly conserved adaptation to stress from yeast to mammals [134, 135, 139]. Phosphorylated EIF2-GDP then binds and inhibits the guanine nucleotide exchange factor EIF2B irreversibly, preventing the regeneration of an active EIF2-GDP to mediate translation initiation [132, 133]. This results in lower assembly of 43S preinitiation complexes and global translation attenuation.

Translational arrest can aid in cells ameliorating various cellular stresses. For instance, cells respond to Unfolded Protein Response by downregulating protein synthesis and thus reducing the total protein load in the ER [136, 140]. Erythrocytes normally produce large amounts of hemoglobin. In this setting, heme deprivation would result in the accumulation of excess globins devoid of heme and subsequent proteotoxicity. Erythrocytes thus activate HRI in response to heme deficiency to phosphorylate EIF2 $\alpha$  and attenuate globin synthesis as a cytoprotective mechanism [143]. Another strong line of evidence supporting a stress adaptive role for EIF2 $\alpha$  phosphorylation comes from *in vivo* studies [144]. Homozygous mutation at Serine 51 prevents EIF2 $\alpha$  phosphorylation permitting normal mRNA translation even under stress. Mice with homozygous mutation of the EIF2 $\alpha$  phosphorylation site die shortly after birth due to prolonged hypoglycemia, demonstrating that EIF2 $\alpha$  phosphorylation is crucial to sustain the physiological function of the liver and pancreas after birth, especially in the induction of gluconeogenic enzymes and insulin.

#### 5.4 HRI is the heme sensitive EIF2 $\alpha$ kinase

HRI is the predominant EIF2 $\alpha$  kinase in erythroid lineage, although it is expressed in other somatic tissues such as liver, lung and placenta [118, 137, 143, 145]. In the absence of HRI, excessive globins synthesized during heme deficiency can aggregate in cells to cause proteotoxicity. Thus, HRI is crucial to coordinate translation of globin mRNAs in response to heme levels in cells [137]. HRI is also activated by non-heme cytoplasmic stresses such as oxidative stress induced by sodium arsenite and heat shock [143, 146]. Due to its role in regulating translation under heme and non-heme stress, HRI plays an essential protective role in anemias of iron deficiency, erythroid protoporphyria,  $\beta$ -thalassemia and arsenite induced stress *in vivo* [137, 145, 147]. HRI exists as a dimer in cells and has three unique regions in its amino acid sequences relative to other EIF2 $\alpha$  kinases, the N terminus (amino acids 1–160), the kinase insertion region (amino acids 236–380), and the C-terminus (amino acids 507–626). Biochemical studies have identified two distinct heme-binding sites in each HRI monomer. Heme bound to the N-terminal domain is stable and co-purifies with HRI to homogeneity. When heme levels are abundant, heme binds to the second heme-binding site in the kinase insertion domain reversibly and inhibits HRI kinase activity upon binding. Thus, under high levels of heme, HRI is bound by four molecules of heme and lacks kinase activity. Under heme deficiency, HRI gets activated by autophosphorylation of Threonine-485 in the activation loop of HRI, which allows it to attain EIF2 $\alpha$  kinase activity to phosphorylate EIF2 $\alpha$  [138, 148, 149].

## 5.5 The Integrated Stress Response (ISR) pathway

Activation of one of the four EIF2 $\alpha$  kinases in response to various physiological and pathological stresses all converge at the phosphorylation of EIF2 $\alpha$  at Serine 51. While this results in a reduction in global protein translation, it allows for preferential translation of select mRNAs that often aid in ameliorating cellular stress and restoring homeostasis. This together is called the Integrated Stress Response (ISR) [140, 150]. Examples of preferentially translated mRNAs include *Activating Transcription Factor 4 (ATF4)*, *Activating Transcription Factor 5 (ATF5)*, *C-EBP Homologous Protein (CHOP)*, *Inhibitor of Bruton Tyrosine Kinase (IBTK $\alpha$ )*, and *Growth Arrest and DNA Damage-Inducible (GADD34)*. It is not clear whether all four EIF2 $\alpha$  kinases mediate the same translational program in response to cellular stress. For example, HRI activation, and not any other EIF2 $\alpha$  kinase, was found to selectively induce fetal hemoglobin translation in erythroid cells. ATF4 is the most well-characterized mRNA induced by all four EIF2 $\alpha$  kinases [151, 152].

ISR signal termination requires the dephosphorylation of EIF2 $\alpha$  to restore normal protein synthesis and homeostasis. Protein phosphatase 1 (PP1) complex recruits a PP1 catalytic subunit (PP1c) to mediate EIF2 $\alpha$  dephosphorylation. In eukaryotic cells, GADD34, induced under ISR, or the constitutively expressed paralogue Constitutive Repressor of EIF2 $\alpha$  Phosphorylation (CReP) are responsible for targeting the PP1 enzyme to EIF2 $\alpha$  [135, 153, 154]. Recently, in addition to PP1c and GADD34, G-actin was identified as a crucial and conserved component of the EIF2 $\alpha$  phosphatase complex, providing an insight into the importance of cytoskeletal dynamics in regulating the ER

stress-induced ISR [155]. It is possible that the EIF2 $\alpha$  phosphatase complex contains other important regulatory factors that may differ among cell types or species.

### **5.6 Preferential translation under ISR via 5'UTR regulation**

During protein translation initiation, the 43S PIC scans the mRNA from 5'-3' until it encounters the first AUG triplet, preferably flanked by a favorable sequence called the Kozak sequence (5' (A/G)CCAUGG 3') [130, 156]. mRNAs that contain upstream AUG can regulate downstream translation from the main Open Reading Frame (ORF) [156-159]. Near cognate triplets such as CUG can also be selected by the PIC at lower frequencies. Genome-wide sequencing and ribosomal footprint studies of 5'UTRs reveal that upstream ORFs (uORFs) are pervasive in ~50% of mammalian mRNAs with translation activity [156]. Despite their widespread occurrence, evidence that uORFs can inhibit downstream translation exist only for a small number of genes. Previous studies suggest that inhibitory uORFs may serve as barriers to downstream translation, and ISR activation through an unknown mechanism allows for leaky scanning of these inhibitory uORF to enhance translation at the main ORF [156, 159]. The presence of multiple uORFs such as in *ATF4* allow for dynamic regulation of its translation via multiple mechanisms [152, 154, 160].

### **5.7 EIF2 $\alpha$ -independent translation**

EIF2 $\alpha$ -independent translation was first described in viruses that utilize Internal Ribosomal Entry Site (IRES) mechanism of translation initiation, which is insensitive to

reduced availability of ternary complex [161]. For example, Hepatitis C virus (HCV) and Classical Swine Fever Virus (CSFV) both employ EIF5B as an alternate initiator to deliver the initiator tRNA [161-164]. While the canonical role of EIF5B is in ribosome subunit joining, it is known to compensate for EIF2 complex during ISR activation [164]. EIF5B-dependent translation has additionally been shown to regulate *X-linked Inhibitor of Apoptosis (XIAP)* mRNA translation upon serum deprivation [165]. Recently, hypoxia was found to induce an EIF5B-dependent translation program [162, 166]. Besides EIF5B, EIF2D was reported to be able to deliver tRNA into the P site of the ribosome during HCV IRES-mediated translation. Experiments revealed that EIF2D promotes re-initiation of translation on these mRNAs, a mechanism distinct from the classical uORF-dependent mode that is used by ATF4 [162, 167, 168]. Another alternate initiator protein is EIF2A, a protein distinct from the EIF2 complex. EIF2A, unlike EIF2 complex mediates translation from upstream CUGs with a leucine-tRNA recruitment instead of the classical methionyl-tRNA [162, 169, 170]. Recent studies show that EIF2A dependent oncogenic translation is a key event in tumor initiation of squamous cell cancer [158, 169, 171].

## **5.8 ISR in human disease**

The ISR pathway activated under various stress stimuli is reported to have both cytoprotective as well as pro-apoptotic functions. The ISR pathway activation allows cells to slow down protein synthesis, thereby providing time to ramp up transcription and translation of genes involved in cell survival and proper protein folding. Thus, absence of ISR signaling in response to stress can lead to severe metabolic consequences. For

example, mice with a non-phosphorylatable EIF2 $\alpha$  become obese, suffer oxidative damage and develop diabetes on a high-fat diet due to pancreatic cell failure [144, 172, 173]. On the other hand, other studies have demonstrated that persistent ISR signaling can be detrimental and cause apoptosis in various tissues. For example, CHOP, a classical downstream target of ISR, promotes apoptosis in various tissues in response to cellular stress. ISR activation induced pancreatic islet cell apoptosis and poor diabetes tolerance [174, 175]. The ISR pathway is also implicated in promoting neurological diseases, such as Vanishing White Matter [176]. Indeed, inhibiting the ISR pathway has been found to be clinically beneficial *in vivo* to improve cognitive memory [176-180]. Thus, the pathological consequences of ISR pathway activation involves a fine interplay of its pro-survival and apoptotic functions, often in a tissue and context specific manner.

The role of ISR pathway activation in tumor progression has only recently begun to be appreciated. Several lines of evidence support a pro-tumorigenic role for ISR pathway activation. Pancreatic cancer cells were found to activate ISR to mediate resistance to gemcitabine [181]. In this model, inhibiting PERK activation was found to have anti-tumorigenic and anti-angiogenic activity [182]. The ISR pathway was also found to promote tolerance to a hypoxic microenvironment and enhance tumor growth *in vivo* [160, 182-184]. Additionally, in a mouse model of squamous carcinoma, ISR pathway allowed cells to activate an alternate oncogenic translational program to promote tumor initiation [158]. ISR activation was also found to promote metastasis of prostate cancer [185]. Thus, ISR pathway activation represents a strategy for tumor cells to promote growth in an often metabolically challenging tumor microenvironment.

## 5.9 Pharmacological Modulation of ISR pathway

The ISR pathway can be activated pharmacologically either by activation of EIF2 $\alpha$  kinases or by inhibiting EIF2 $\alpha$  dephosphorylation using phosphatase inhibitors. For example, activators of HRI include BTdCPU and related N,N'-diarylureas [186]. Histidinol, Halofuginone, Asparaginase, and Arginine Deiminase are found to activate GCN2 [142]. BEPP monohydrochloride is a specific PKR activator while DHBDC is a dual activator of PKR and PERK [187]. Inhibitors of EIF2 $\alpha$  dephosphorylation include drugs such as Salubrinal which inhibits GADD34-mediated dephosphorylation of EIF2 $\alpha$  [175, 188]. Other phosphatase inhibitors include Guanabenz and its derivative Sephin1. Guanabenz also has nanomolar affinity for the  $\alpha$ 2-adrenergic receptor, and thus Sephin1, a more specific inhibitor of GADD34 is preferred *in vivo* [173].

Inhibitors of the ISR pathway on the other hand, represent a strategy to overcome resistant cancers, and in the treatment of neurodegenerative diseases. GSK2606414 and GSK2656157 that trap PERK in an inactive state and prevent its autophosphorylation were found to have antitumor activity *in vivo* [182]. Similarly, small-molecule inhibitors have been discovered to inhibit PKR and HRI [189, 190]. Recently, two new small-molecule inhibitors of the ISR, Integrated Stress Response Inhibitor (ISRIB) and EIF2B Activator (2BAct) were discovered, which stabilize EIF2B and thus function downstream of EIF2 $\alpha$  phosphorylation to render cells insensitive to EIF2 $\alpha$  phosphorylation [178-180].

## Chapter 6: Materials and methods

### Lentiviral Library Generation

The human Genome-wide CRISPR Knockout (GeCKO) v2 library was obtained from Addgene (#1000000048) and amplified according to instructions provided. Plasmids were electroporated and subsequently purified from bacterial pellets using the Qiagen plasmid maxi kit. To generate GeCKO v2 lentivirus,  $3 \times 10^6$  293T cells were first seeded per 10 cm dish. Libraries A and B were prepared independently using 20 dishes per library. The next day, each dish was transfected using 10  $\mu$ g of total plasmid (5:3:2 ratio of GeCKO library:psPAX2:pMD2.G), 30  $\mu$ L of FuGENE HD in 900  $\mu$ L of Opti-MEM. Fresh medium was added the following day. The media containing virus was harvested at 48 and 72 hours post transfection and filtered through a 0.45  $\mu$ m Surfactant-free Cellulose Acetate (SFCA) sterile filter. Aliquots of the library were snap frozen on dry ice and ethanol and then stored at  $-80^{\circ}\text{C}$ . Library viral titer was determined as described [91].

### Lentiviral Infection

The Genome-wide CRISPR Cas9 screen was performed in human lung carcinoma H358 cells using both GeCKO v2 libraries A and B, in biological replicates. To achieve 300X or greater coverage, at least 50 million cells were transduced with each library. For each transduction, ten 12-well plates were seeded with  $3.5 \times 10^5$  H358 cells per well. An overnight transduction was performed at a viral MOI of 0.2-0.4 along with 8  $\mu$ g/mL polybrene. Cells were then trypsinized and pooled before being plated into fresh medium

in eight 15 cm dishes. 48 hours later, cells were trypsinized, pooled and plated into fresh medium containing 1ug/mL puromycin. In parallel, a small aliquot of cells was used to confirm that a MOI of 0.2-0.4 was achieved. Cells were passaged in puromycin for 14 days before cell sorting. At every passage,  $12 \times 10^6$  cells were seeded per dish into 15 cm dishes with medium containing puromycin.

### **Fluorescence Activated Cell Sorting**

Confluent H358 cells were trypsinized and centrifuged at 300g for 5 minutes. The cells were then counted using the Countess Automated Cell Counter and washed with cell staining buffer (BioLegend). Cells were then incubated in the dark for 20 minutes on ice in cell staining buffer containing APC-PD-L1 antibody (BioLegend) at a concentration of 0.4 ug antibody per million cells. Stained cells were centrifuged at 300g for 5 minutes to discard unbound antibody and washed with cell staining buffer two times. The final cell pellets were resuspended at a cell density of  $15 \times 10^6$  cells per mL of complete RPMI media. The cells were sorted at the UT Southwestern Flow Cytometry Core Facility (MoFlo cell sorter, Beckman Coulter). The highest and lowest 0.5% cells were gated based on APC fluorescence and collected. 100-200 million cells were sorted to collect  $2-4 \times 10^5$  PD-L1 high and low cells. The cells were washed once with PBS and frozen at -80C. Unsorted cells were frozen similarly at -80C.

## Genomic DNA Extraction

Genomic DNA was extracted from the unsorted cells using the Qiagen DNeasy Blood & Tissue Kit according to the manufacturer's instructions. Extractions were performed on  $40\text{-}80 \times 10^6$  unsorted cells to ensure 300X coverage or higher of the library. DNA was eluted twice in 125  $\mu\text{L}$  of nuclease free water and its concentration was assessed using the Qubit dsDNA BR assay kit (Thermo Fisher). To facilitate maximum recovery of gDNA from the sorted cells, a previously described method [101] was used with the following modifications: Sorted cell pellets were resuspended in 500  $\mu\text{L}$  of tissue lysis buffer, consisting of 460  $\mu\text{L}$  of STE buffer [1 mM EDTA (pH 8.0), 10 mM Tris-HCl (pH 8.0), 100 mM NaCl] supplemented with 10  $\mu\text{L}$  of 0.5 M EDTA, 10  $\mu\text{L}$  of proteinase K [10 mg/mL in TE buffer containing 10 mM Tris-HCl (pH 8.0) and 1 mM EDTA], and 20  $\mu\text{L}$  of 10% SDS. Pellets were digested overnight at 55°C while shaking at 600 rpm on a Thermomixer (Eppendorf). The following day, 5  $\mu\text{L}$  of 2 mg/mL RNase A was added to each tube and incubated at 37°C for 1 hr while shaking at 600 rpm. Extractions were first performed with equal volumes of pH 7.9-buffer saturated phenol, followed by phenol:chloroform:isoamyl alcohol (25:24:1) and then chloroform. Following this, DNA was precipitated in 100% ethanol and glycogen (Roche) at -80°C for 1 hr followed by centrifugation at 18,000 g for 10 min at 4°C. Pellets were washed with 75% ethanol, dried, and resuspended in 21  $\mu\text{L}$  of water by incubating at 37°C overnight. DNA concentration was determined with the Qubit dsDNA BR assay kit.

### **Preparation of sequencing Libraries**

PCR amplicon libraries for deep sequencing were prepared based on a protocol adapted from [91, 101]. All primer sequences are provided in Table 2. The first round of PCR (PCR I) was performed on DNA from unsorted cells using 6.6 µg of gDNA per 100 µL PCR reaction. To maintain 300X coverage, 20 reactions were assembled for each sample. For sorted cells, all extracted gDNA for a given sample was distributed into two 100 µL reactions. In both cases, 18-20 cycles of amplification were performed using Herculase II Fusion polymerase (Agilent). The reactions for a given sample from PCR I were pooled together and used as a template for the second round of PCR (PCR II), to add the necessary adapters for Illumina sequencing. To adjust for varying PCR efficiency between the samples, the cycle number for PCR II was adjusted such that each library was amplified in a 50 µL reaction to generate approximately 50 ng of DNA library. The final DNA for sequencing was purified using AMPure XP beads (Agencourt) according to the manufacturer's instructions with the following modifications: Each 50 µL PCR II reaction was mixed with 25 µL of beads and incubated for 5 minutes. Magnetic separation was used to collect the supernatant. The supernatant was then mixed with 90 µL of beads and incubated for 5 minutes. The supernatant was discarded and the beads were washed twice with 200 µL of 70% ethanol. The beads were then dried for 10-15 minutes. Bound DNA was eluted from the beads using 40 µL of water.

## **Next Generation Sequencing**

Prior to sequencing, all DNA libraries were analyzed using the Bioanalyzer High Sensitivity DNA Analysis Kit (Agilent). Library concentration was then determined by qPCR using the KAPA Library Quantification Kit for Illumina platforms. All samples were sequenced on an Illumina HiSeq 2500 or a NextSeq 500 with 75 bp single reads. ~15-20 million reads were sequenced per library.

## **Sequencing Data Analysis**

A reference file for all sgRNAs in the library was acquired from Addgene, and identical sgRNAs targeting more than one protein-coding gene were removed. Demultiplexed FASTQ files were mapped to the reference file using Bowtie 2 requiring unique alignments with no mismatches. Normalized read counts were calculated as described previously [91]. Screen hits were identified using RIGER16 with the following parameters: log fold-change ranking,  $1 \times 10^6$  permutations, second best rank (SBR) scoring algorithm.

## **Ethics statement on animal study**

Mice were monitored closely throughout all experimental protocols to minimize discomfort, distress or pain. Signs of pain and distress include disheveled fur, decreased feeding, significant weight loss (>20% body mass), limited movement, or abnormal gait. If any of these signs were detected, the animal was removed from the study immediately and euthanized. All sacrificed animals were euthanized with CO<sub>2</sub>. The animals were placed in a clear chamber and 100% CO<sub>2</sub> was introduced. Animals were left in the

container until clinical death ensued. To ensure death prior to disposal, cervical dislocation was performed while the animal was still under CO<sub>2</sub> narcosis. All methods were performed in accordance with the recommendations of the Panel on Euthanasia of the American Veterinary Medical Association and protocols approved by the UT Southwestern Institutional Animal Care and Use Committee (protocol # 2017-102112). The Institutional Animal Care and Use Committee (IACUC) of UT Southwestern Medical Center approved all procedures involving mice. C57BL/6J and NSG mice were obtained from The Jackson Laboratory and the UT Southwestern Breeding core, respectively.

### **Cell culture**

All human lung cancer cell lines (obtained from Dr. John Minna) were cultured in RPMI 1640 media supplemented with 5% FBS (Sigma) and 1% antibiotic-antimycotic (anti-anti, Invitrogen). WT and EIF2 $\alpha$  mutant Mouse Embryonic Fibroblasts (MEFs), obtained from Dr. Randal Kaufman, were cultured in DMEM supplemented with 10% FBS, 1 % anti-anti, 2mM Glutamine, 2% MEM amino acid solutions (Gibco) and 1mM Sodium pyruvate (Invitrogen). Lewis Lung Carcinoma (LLC) (obtained from Dr. Don Gibbons) were cultured in DMEM media supplemented with 10% FBS and 1% penicillin and anti-mycotic. For the hemin rescue experiment, Control or UROD knockout H1944 cells were treated with 1uM and 10uM Hemin Chloride (Sigma) for 48h. For the ISR pathway activation experiments, H1944 cells were treated with 100uM or 200uM Salubrinal (Tocris) and 200nM ISRIB (Sigma) for 24h.

## **Plasmids**

LentiCRISPR V2, PAX2 and MD2 plasmids were obtained from Addgene ( #52961, #12260, #12259). sgRNAs targeting candidates from the screen were selected from the human GeCKO libraries (Addgene Library #1000000048, #1000000049) and described in Table 2. pTRIPZ plasmid was obtained from Dharmacon (#RHS5087). pGL3 and Renilla firefly plasmids were a gift from Dr. Joshua Mendell.

## **Generation of knockout cell lines using CRISPR-Cas9**

Human Embryonic Kidney 293T (HEK 293T, 1x10<sup>8</sup>) cells were co-transfected with lentiCRISPR V2 (10ug) and PAX2 (4ug), MD2 (2.66ug) helper plasmids using Lipofectamine 3000 (Life technologies). Lentiviral supernatant was collected 48 and 72 hours post transfection and filtered. Recipient cells were infected overnight with the viral supernatant containing 8ug/mL polybrene (Sigma) and then replenished with fresh media. 48 hours later, transduced cells were cultured in fresh media containing 1ug/mL puromycin for 10-12 days.

## **RNA extraction and qRT-PCR analysis**

Total RNA was isolated from cells using the RNeasy Mini Kit (Qiagen). For qRT-PCR of mRNA, cDNA synthesis was performed with 1-5 µg RNA for reverse transcription using Superscript IV Vilo Master Mix (5X) (Invitrogen). mRNA expression was assessed using quantitative real-time PCR with a 2X SYBR Green Master Mix (R&D Systems). mRNA levels were normalized to β-actin or 18S mRNA expression, with gene expression levels

measured using a standard curve for each set of primers crossing exon-exon junctions for each gene. All PCR assays were performed in triplicate. PCR primers are shown in Table 2. To monitor *PD-L1* mRNA decay, cells expressing Control or UROD sgRNA were treated with ActinomycinD (10ug/ml) to halt transcription and RNA was isolated at various time points.

### **Western blotting**

Cells and tissues were lysed in RIPA buffer containing Halt Protease Inhibitor cocktail (Invitrogen) and then homogenized using a Bioruptor (Diagenode). Proteins were quantified using the Bicinchoninic Acid (BCA) assay (Thermo Scientific) and subject to separation by using NuPage Bis-Tris gels (Invitrogen) for electrophoresis. The proteins were subsequently transferred to a nitrocellulose membrane. The membranes were blocked for 1 hour at room temperature in 5% milk and subsequently probed with primary antibodies in 5% milk overnight at 4°C. After incubating the membrane with the appropriate secondary antibody conjugated to horseradish peroxidase, protein levels were detected with SuperSignal Extended Dura substrate (Thermo Scientific). All antibodies are listed in Table 1. For cycloheximide chase experiments, control or UROD knockout H1944 cells were treated with 100ug/ml Cycloheximide (Sigma) and protein was isolated at various timepoints and subsequently used to perform western blotting for PD-L1 to monitor PD-L1 protein stability over time.

### **Inducible knockdown of *Urod* in LLC cells**

HEK 293T cells were co-transfected with pTRIPZ (Dharmacon, RHS5087, Table 2) along with helper plasmids as described above. LLC cells were infected overnight with a scrambled shRNA or *Urod* shRNA (2 independent shRNAs) lentiviral supernatant along with 8ug/mL polybrene. Transduced cells were selected in 2ug/mL puromycin for a week and then cultured in 2-3ug/mL doxycycline for 4 days. The cells were then harvested for RNA and protein analysis to assess extent of knockdown.

### **Immunoprecipitation assay**

Control or *UROD* knockdown H1944 cells at 90% confluency were treated with Velcade (10uM, Sigma) for 24 hours to inhibit the proteasome. The following day, cells were scraped in cold PBS and lysed in IP lysis buffer (Invitrogen). Lysates were centrifuged at 15,000 rpm for 5 minutes and supernatants containing protein were quantified using BCA assay. 300mg of protein lysate was immunoprecipitated with 5ug PD-L1 antibody (Cell Signaling Technology, E1L3N XP) using the Protein G Dynabeads kit (Invitrogen). The IP samples were then subject to western blotting and probed with a Ubiquitin antibody (Cell Signaling Technology, P4D1) to assess PD-L1 ubiquitylation.

### **Transient knockdown using siRNA**

H1944 ( $2 \times 10^6$ ) cells were seeded in 10 cm<sup>2</sup> dishes. The following day, cells were transfected with siRNA pools (5uM, siGENOME Dharmacon pools) and Dharmafect solution 4 in Opti-MEM media according to manufacturer's instructions. The cells were

replenished with fresh complete media the next day and harvested 48 hours later for RNA and western blot analysis.

### **Measurement of heme synthesis levels**

Heme synthesis in cells was measured using a previously published protocol [191]. H1944 cells ( $4 \times 10^5$ ) cells were seeded in triplicates in 6-well plates and transfected with control or *UROD* siRNAs. 72 hr post transfection, cells were incubated with 0.3  $\mu\text{Ci}$  [ $^{14}\text{C}$ ] 5- $\alpha$  aminolevulinic acid (ALA) overnight. The next day, cells were scraped in cold PBS in a radioactive safe area and subject to diethyl ether- HCl phase extractions to extract [ $^{14}\text{C}$ ] labelled heme as previously described [191]. Radioactivity was measured in triplicate using a scintillation counter and normalized to total protein to obtain heme synthesis levels in cells.

### **Metabolic labeling ( $\text{S}^{35}$ ) to monitor translation**

H1944 cells ( $4 \times 10^5$ ) cells were seeded in triplicates in 6-well plates and transfected with control or *UROD* siRNAs. 72 hours post transfection, cells (at 90% confluency) were cultured in methionine/cysteine free RPMI media for one hour and then incubated with 75 $\mu\text{Ci}$  EasyTag Express Protein Labeling Mix [ $\text{S}^{35}$ ] (Perkin Elmer) for 15 minutes. Cells were lysed in 1X SDS lysis buffer and proteins were subject to separation by electrophoresis. The proteins were subsequently transferred to a nitrocellulose membrane and analyzed for  $\text{S}^{35}$  incorporation using autoradiography.

### **Tumor implantation assays**

LLC cells ( $4 \times 10^5$ ) expressing a scrambled shRNA lentivirus or *Urod* shRNA lentiviruses were injected subcutaneously into the right flanks of 6-8-week-old C57BL/6J female mice (Jackson laboratory). On Day 10, 10-15 mice each bearing scrambled shRNA and *Urod* shRNA tumors were randomized into groups receiving Control or PD-1 antibody (BioXCell, *InvivoMab* Clone 29F.1A12). Mice were injected with 200ug antibody intraperitoneally every three days. All mice were kept on doxycycline water (2g/L doxycycline, 2% sucrose) for the entire duration of the experiment. Tumor volume was measured using calipers every 3 days until the average tumor mass reached  $2\text{cm}^3$ . Tumor volume was calculated using the formula  $(\text{length} \times \text{width}^2)/2$ .

### **Flow cytometry multi-color staining of tumor infiltrating lymphocytes (TIL)**

Tumors were excised from euthanized mice and homogenized using a Tissue Chopper. The tumor cells were then digested at  $37^\circ\text{C}$  at 70 rpm for 1 hour in digest buffer (RPMI 1640 containing 5% FBS, 0.5mg/mL Hyaluronidase, 0.5mg/mL Collagenase IV (Sigma) and 20ug/mL DNase I (Sigma). All subsequent steps were performed on ice. The digested cells were centrifuged at 1500 rpm for 5 minutes and the cell pellet was resuspended in 5mL Cell Staining Buffer (CSB, BioLegend) and filtered using a 70uM cell strainer. The cells were then centrifuged again and resuspended in 50-100uL blocking-dead mix (CSB containing 5% FBS, 10% mouse serum, 1uL CD16/CD32 Fc blocking antibody (BioLegend, #101302) and 3uL ef506 viability dye (eBioscience, #65-0866-18) for 30 minutes on ice. The samples were then incubated with 50-100uL of primary

antibodies (Table 1) diluted in CSB for 30 minutes on ice. Cells were washed twice with CSB and filtered through a nylon membrane into flow cytometry tubes for analysis. Samples were run on LSRII (BD Biosciences) and single-color stained C57/BL6 splenocytes were used as compensation controls. FlowJo software was used to calculate the % CD8<sup>+</sup> T-cells of the CD45<sup>+</sup> live cells. Gating strategy for TIL staining is described in Fig. 26.

### **Polysome Profiling**

Sucrose gradients were prepared in advance in Beckman ultracentrifuge tubes as described in and stored at -80°C. One day before the experiment, gradients were allowed to diffuse for 16 hours at 4°C. The next day, 20-40 million H1944 cells per sample were trypsinized and washed twice with ice -cold PBS (second wash containing 100ug/mL cycloheximide). After the second wash, the PBS was discarded and cell pellets were resuspended in 750uL of Polysome Extraction Buffer (20mM Tris-HCl (pH 7.5), 100mM NaCl, 5mM MgCl<sub>2</sub>, 0.1% NP-40 in distilled water) containing cycloheximide, protease inhibitor cocktail and RNase inhibitors. The cells were lysed in Eppendorf tubes for 10 minutes on ice and then sheared through a 27.5-gauge needle 3-4 times. The lysates were then centrifuged at 15000 rpm for 5 minutes on ice and the supernatant lysate RNA concentration was quantified on a Nanodrop. Equal amount of lysate (at least 500-600ug RNA) was loaded across all gradients. The gradients were then centrifuged at 35,000 rpm for 2 hours at 4°C and run on a fractionator machine (Biorad) to visualize and collect polysome fractions. Each collected polysome fraction was mixed 3 times with 100%

ethanol and 10ug glycogen carrier and incubated overnight in  $-20^{\circ}\text{C}$ . The next day, fractions were centrifuged at 20,000g for 30 minutes at  $4^{\circ}\text{C}$  to precipitate RNA pellets. Pellets were dried for 20 minutes at RT, resuspended in 100uL Nanopure water and 350uL RNeasy RLT lysis buffer and loaded onto RNeasy columns. The RNeasy kit was used to isolate RNA as previously described.

### **Dual luciferase assays**

$50 \times 10^3$  MEF cells were seeded per well in 12-well plates in triplicate and transfected with a Renilla plasmid (20ng), Firefly luciferase pGL3 plasmid expressing *PD-L1* wildtype 5'UTR or various mutant constructs as described (200ng) and a carrier pUC19 plasmid (400ng) per well using Fugene HD (Promega) at a 3:1 Fugene:DNA ratio. Luciferase activity was measured 48 hours post transfection using a Luminescence plate reader (Promega). Firefly luciferase activity was normalized to its corresponding Renilla luciferase activity to obtain Relative luciferase levels for each sample.

### **Statistical analysis**

A Student t-test was used for comparisons between two groups with normal data distribution (for real time qPCR, MTS, and xenograft assays). A Two-Sample Fisher-Pitman Permutation Test was performed for comparing % CD8+ T-cells.

**Table 1. List of antibodies and chemicals**

<b>Antibody</b>	<b>Source</b>	<b>Catalog No.</b>	<b>Clone</b>
Human PD-L1 (WB, IP)	CST	13684S	E13LN
Mouse PD-L1 (WB)	Abcam	Ab213480	EPR20529
Mouse PD-L1 (WB)	R&D Systems	MAB90781	2096C
UROD (WB)	Abcam	Ab196562	
pEIF2 $\alpha$ (WB)	CST	9721S	
Total EIF2 $\alpha$ (WB)	CST	9722S	
Ubiquitin (WB)	CST	3936S	P4D1
Tubulin (WB)	Calbiochem	CP06	DM1A
APC PD-L1 ab (FC)	BioLegend	329708	29E.2A3
FITC PD-L1 ab (FC)	BioLegend	393605	MIH2
APC CD3E (FC)	BioLegend	100312	145-2C11
PE CD4 (FC)	BioLegend	100408	GK1.5
FITC CD8A (FC)	BioLegend	100705	53-6.7
PURE CD16/32 (FC)	BioLegend	101302	93
APC-Cy7 CD45 (FC)	BioLegend	103116	30-F11
<i>InvivoMab</i> PD-1	BioXCell	BE0273	29F.1A12
<i>InvivoMab</i> CD8 $\alpha$	BioXCell	BE0004	53-6.7
<i>InvivoMab</i> IgG2a control	BioXCell	BE0089	2A3
<b>Chemical</b>	<b>Source</b>	<b>Catalog No.</b>	
eFLUOR viability dye	Invitrogen	65-0865-14	
Salubrinal	Tocris	2347	
ISRIB	Sigma	SML0843	
Cycloheximide	Sigma	01810	
Succinyl Acetone	Sigma	D1415	
BtDCpu	Sigma	324892	
Puromycin	Gibco	A1113803	
Doxycycline	Sigma	D9891	
Hemin chloride	Alfa Aesar	A1116503	
EasyTag Express Mix	Perkin Elmer	NEG77200	
Velcade/ Bortezomib	Sigma	5043140001	
RNAseOUT	Invitrogen	10777019	
Collagenase	Sigma	C0130	
DNase I	Roche	11284932001	
Glycogen	Invitrogen	R0561	

**Table 2.1 List of sgRNA and shRNA sequences**

<b>sgRNA Sequences for generating LentiCRISPR knockout cells</b>		
	sgRNA 1	sgRNA 2
<b><i>PDL1</i></b>	TCTTTATATTCATGACCTAC	ACCGTTCAGCAAATGCCAGT
<b><i>CMTM6</i></b>	TGCAATACACAATCAGTATA	AGCTGAAGTCCTGTCATGTG
<b><i>SMAD4</i></b>	AACTCTGTACAAAGACCGCG	TTCTTCCTAAGGTTGCACAT
<b><i>DPAGT1</i></b>	AAGCCCTTCGCCCCGATACT	ACCTACCTTCCAACCTCTACC
<b><i>UROD</i></b>	AAACAGACTACACTCCCGTT	CGACATCCTTGTTGTACCCC
<b><i>MUL1</i></b>	GGAATCGAACCACCCACCTT	
<b><i>MRPS12</i></b>	CACTCGACAGCACTTGCGAT	
<b><i>UQCR10</i></b>	GAACATGACGCCACGATGA	
<b><i>DNAJC13</i></b>	ATTTGCAGCATCAGCCCTGT	

<b>Mouse <i>Urod</i> shRNA antisense sequence</b>	
Scrambled	ATCTCGCTTGGGCGAGAGTAAG
<i>mUrod</i> shRNA-1	TGCTGGATCCCGTAGACGC
<i>mUrod</i> shRNA-2	CAATTAGTGGCACACGTCC

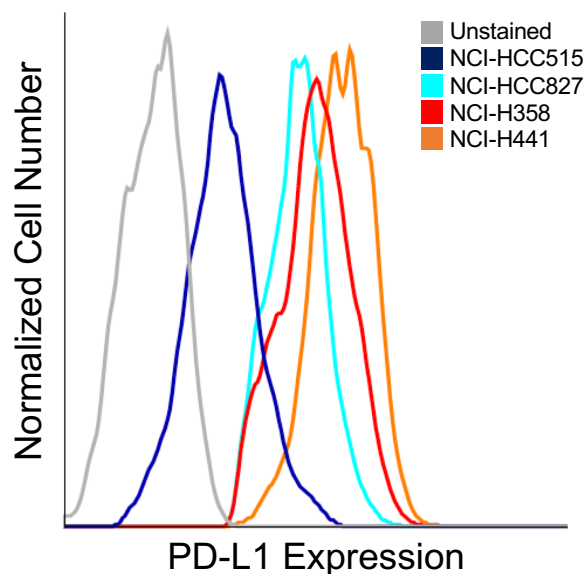
**Table 2.2 List of primer sequences**

	Forward	Reverse
<b><i>hPDL1</i></b>	GCTGCATGATCAGCTATGGT	GTGACTGGATCCACAACCAA
	TGGTAATTCTGGGAGCCATC	TCTTTGAGTTTGTATCTTGGATGC
<b><i>hActin</i></b>	ATTGCCGACAGGATGCAGAA	ACATCTGCTGGAAGGTGGACAG
<b><i>hUROD</i></b>	GCCCAGGACTTTTTTCAGCAC	GGGGTACAACAAGGATGTCCG
<b><i>hUROS</i></b>	GAAAAATGGAATGCCAAGTCA	GCAAGCTTTTCTGCATTCC
<b><i>hATF4</i></b>	CTTACGTTGCCATGATCCCT	CTTCTGGCGGTACCTAGTGG
<b><i>Luciferase</i></b>	GAGGCGAACTGTGTGTGAGA	GAGCCACCTGATAGCCTTTG
<b><i>mPd-11</i></b>	GCTCCAAAGGACTTGTACGTG	TGATCTGAAGGGCAGCATTTC
<b><i>mActin</i></b>	CGGTTCCGATGCCCTGAGGCTCTT	CGTCACACTTCATGATGGAATTGA
<b><i>18S</i></b>	GTAACCCGTTGAACCCATT	CCATCCAATCGGTAGTAGCG

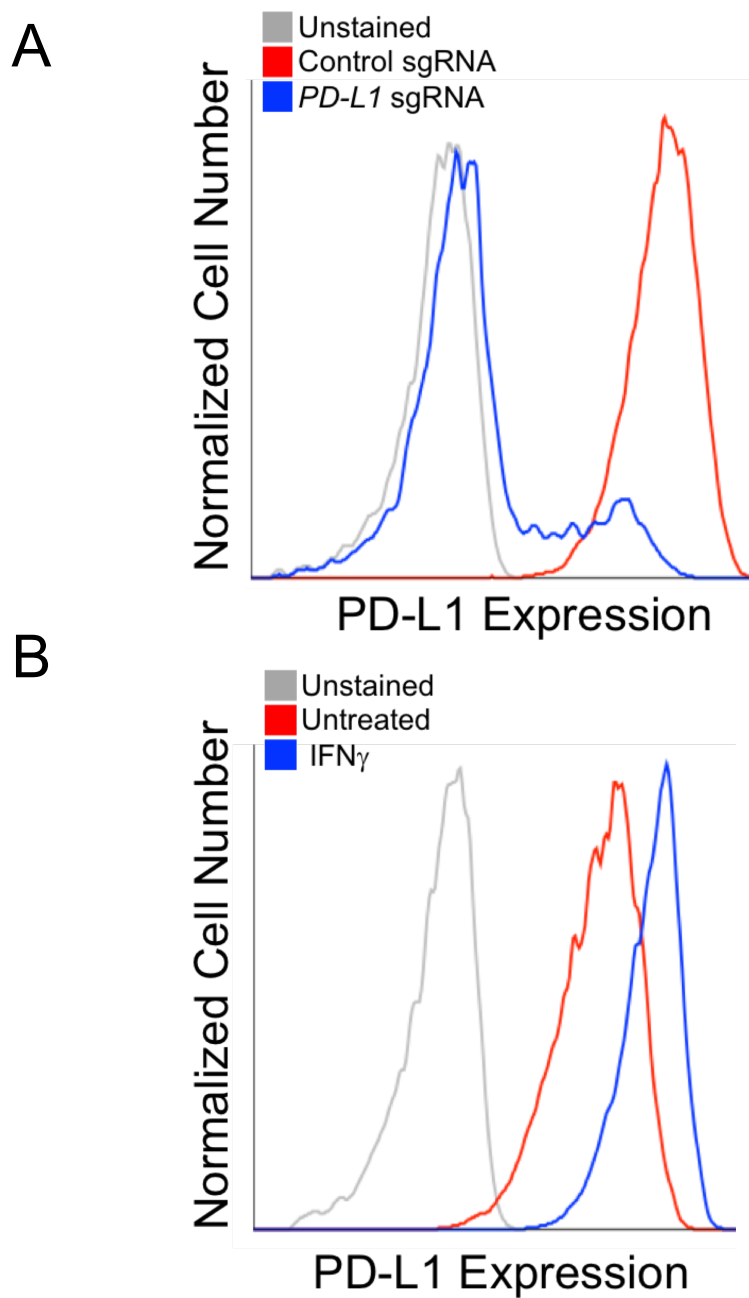
## Chapter 7: Results

### 7.1 Experimental Strategy

To identify regulators of PD-L1 in non-small cell lung cancer (NSCLC) in an unbiased and rigorous manner, we undertook a genome-wide loss of function screening approach in human lung cancer cells. First, we assessed endogenous PD-L1 expression in a panel of NSCLC cell lines by flow cytometry using an Allophycocyanin (APC)-conjugated PD-L1 antibody (Fig. 1). NCI-H358, a *KRAS* (*G12C*) mutant lung cancer cell line expressed moderately high PD-L1 (Fig. 1). Endogenous PD-L1 in these cells can be suppressed by a sgRNA targeting *PD-L1* (Fig. 2A), or induced by IFN- $\gamma$  treatment (Fig. 2B). Since the loss or gain of PD-L1 in these cells can be readily detected by flow cytometry, we performed the screen in H358 cells.



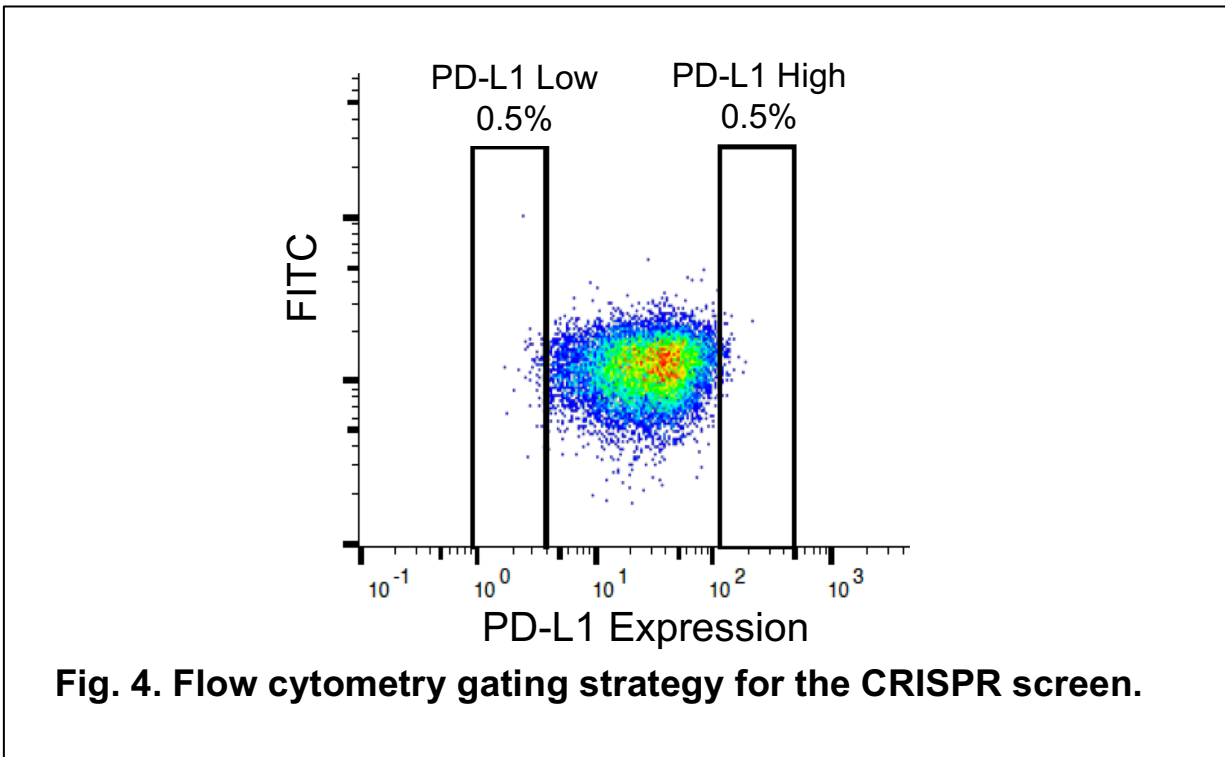
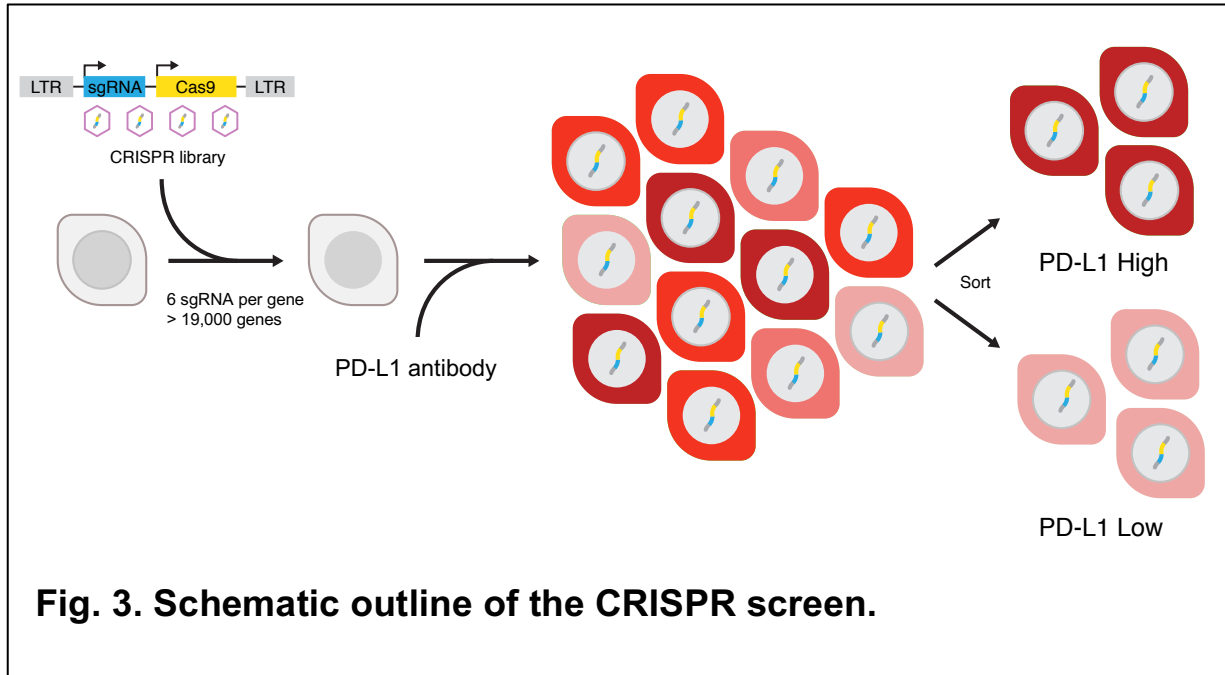
**Fig. 1. Cell-surface expression of PD-L1 in human NSCLC cells.**

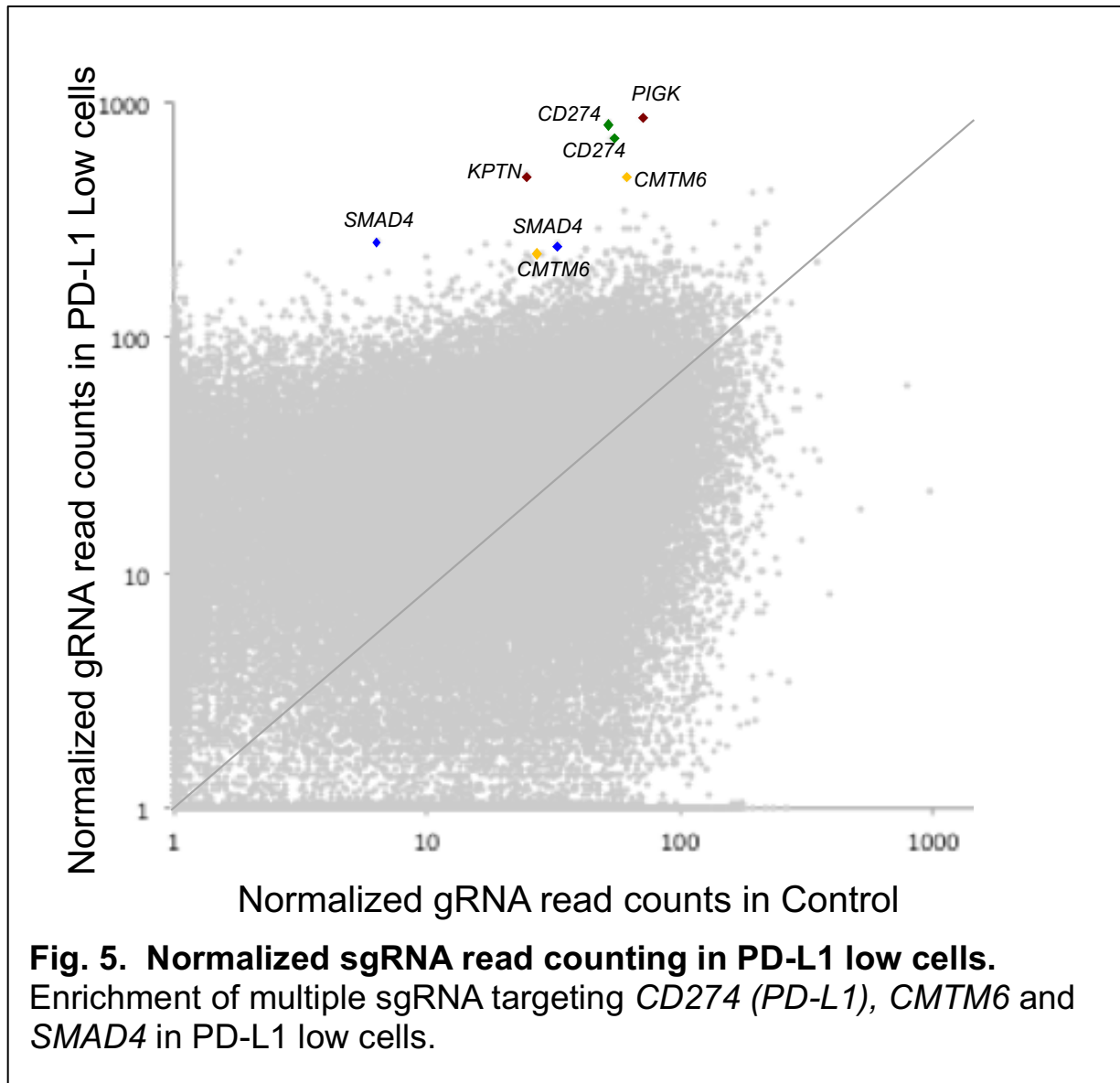


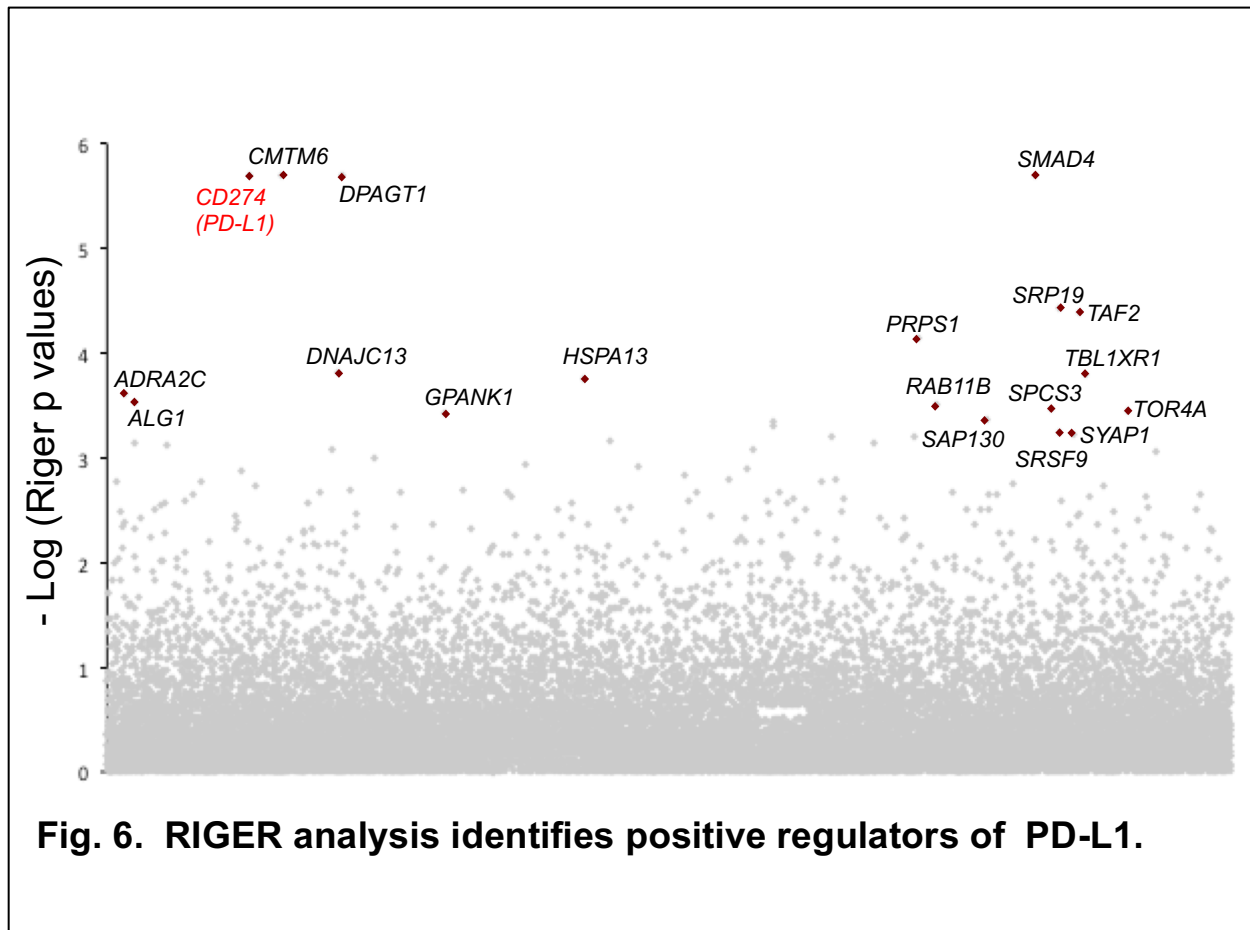
**Fig. 2. Detection of loss and gain of cell-surface PD-L1 in H358 cells.** (A) CRISPR-Cas9 targeting of PD-L1 in H358 cells. (B) Induction of PD-L1 in cells treated with 10ng/mL IFN- $\gamma$  for 24h.

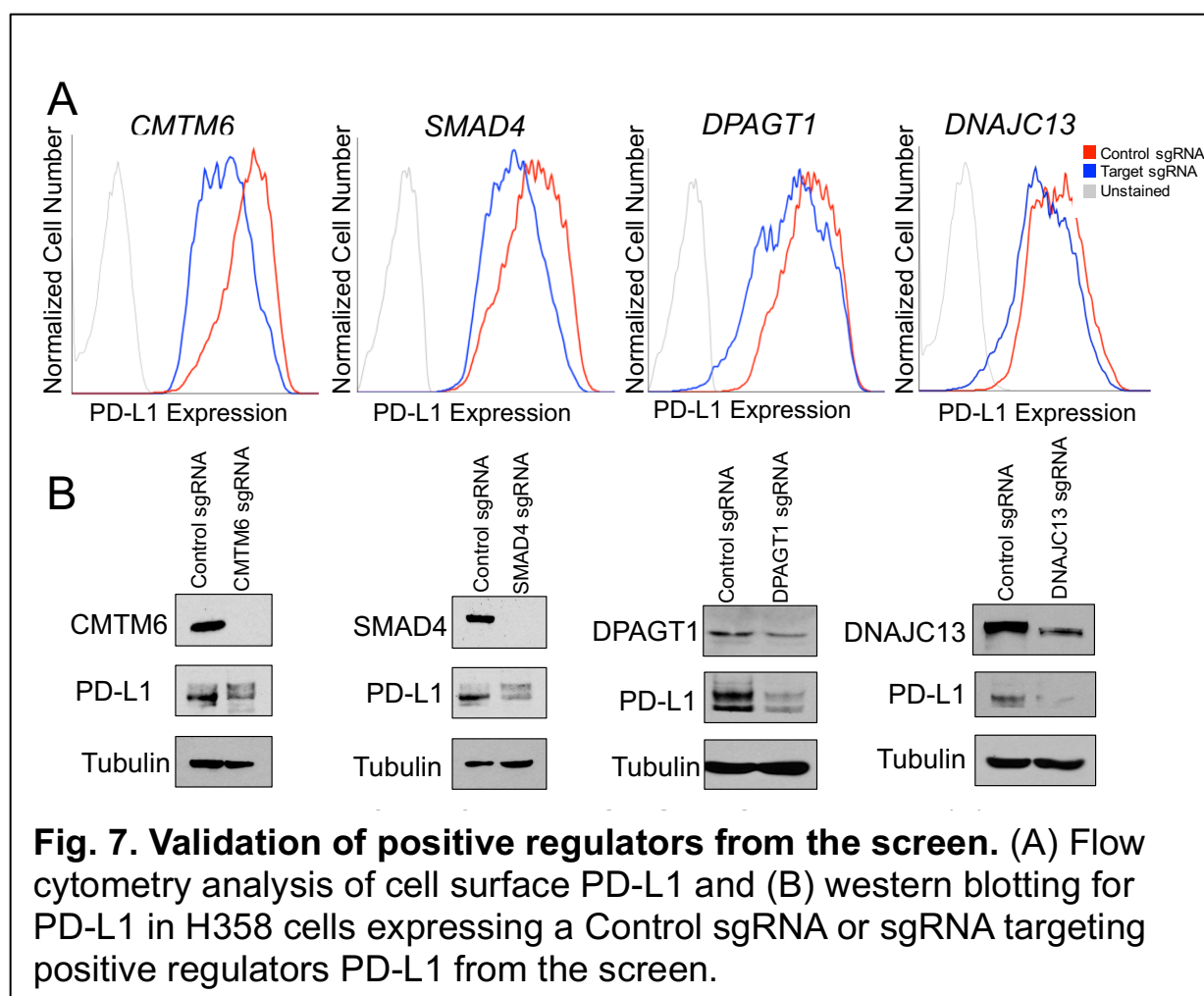
## 7.2 A CRISPR screen identifies regulators of PD-L1 in NSCLC

The genome-wide CRISPR-Cas9 loss of function screen was performed in H358 cells using the LentiCRISPR GeCKO library (Fig.3, [91]). After selection in puromycin for 2 weeks, transduced cells were stained with PD-L1 antibody and sorted based on PD-L1 expression. The 0.5% PD-L1 high and PD-L1 low cells were sorted (Fig. 4), genomic DNA was isolated and deep sequencing was performed to identify sgRNAs enriched in sorted cells compared to unsorted control cells (Fig. 3). Preliminary analysis of enriched sgRNAs identified multiple sgRNAs targeting *PD-L1* enriched in PD-L1 low cells (Fig. 5). RIGER analysis identified several high-confidence positive regulators of PD-L1 (Fig. 6), including *CKLF-like MARVEL transmembrane domain containing protein 6 (CMTM6)*, encoding a cell surface protein that was recently shown to bind and prevent PD-L1 degradation [63, 64]. CRISPR-Cas9 mediated knockout of *CMTM6* as well as several top hits from the screen downregulated PD-L1 expression (Fig. 7). *SMAD family member 4 (SMAD4)* was found to induce PD-L1 levels (Fig. 7), which identifies a new arm of TGF- $\beta$  signaling mediating tumor immune suppression [192]. Among the negative regulators, we identified *Uroporphyrinogen Decarboxylase (UROD)*, a key enzyme in the heme biosynthetic pathway, as the top negative regulator of PD-L1 from the screen (Fig. 9). We also identified and validated several other genes involved in mitochondrial homeostasis including Mitochondrial E3 Ubiquitin Protein Ligase 1 (*MUL1*), Mitochondrial Ribosomal Protein S12 (*MRPS12*), and *Ubiquinol-Cytochrome C Reductase, Complex III Subunit X (UQCR10)* (Fig. 9, Fig. 10).









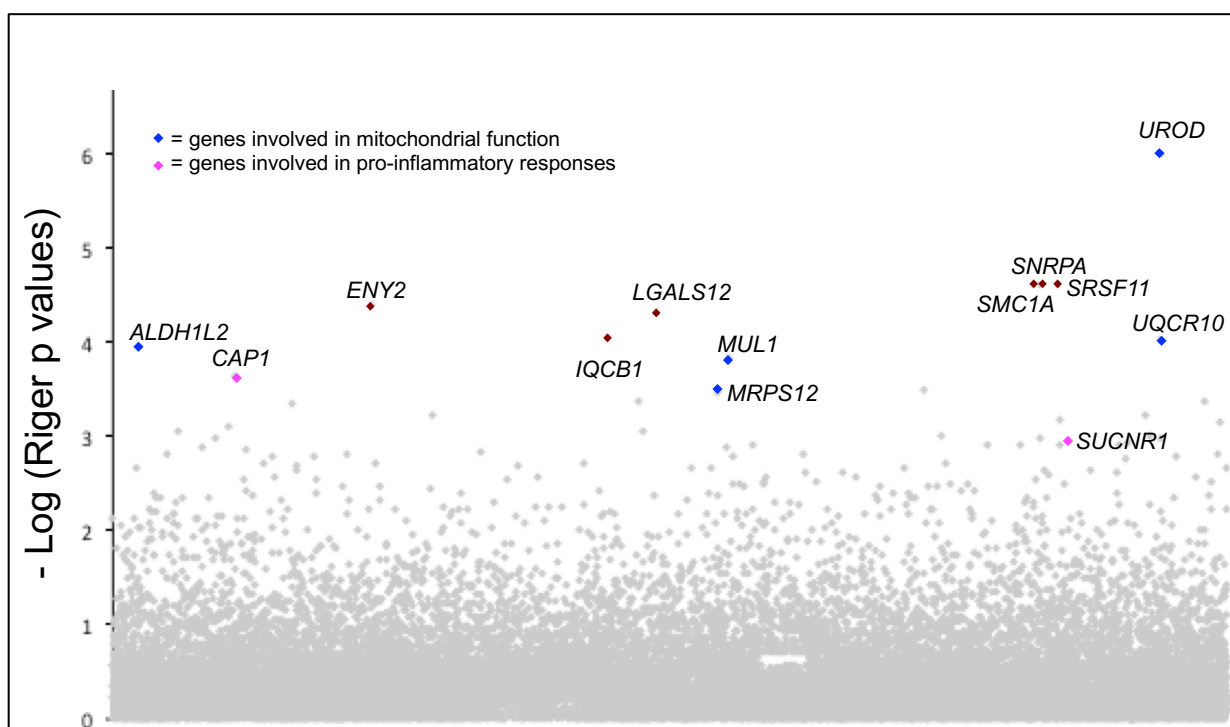
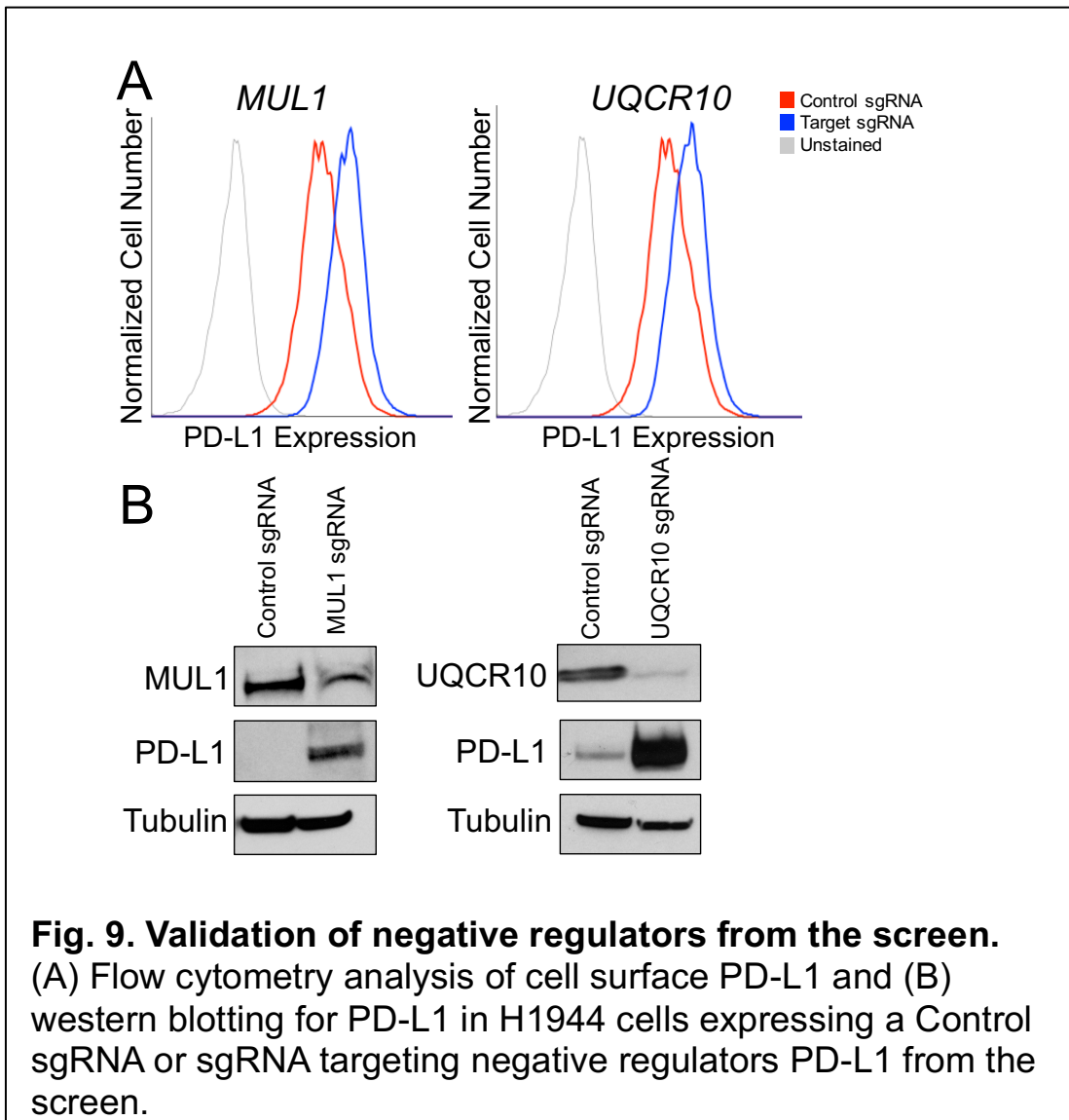


**Fig. 8. RIGER analysis identifies negative regulators of PD-L1.** Blue dots are genes involved in mitochondrial function, pink dots are genes involved in inflammatory signaling.

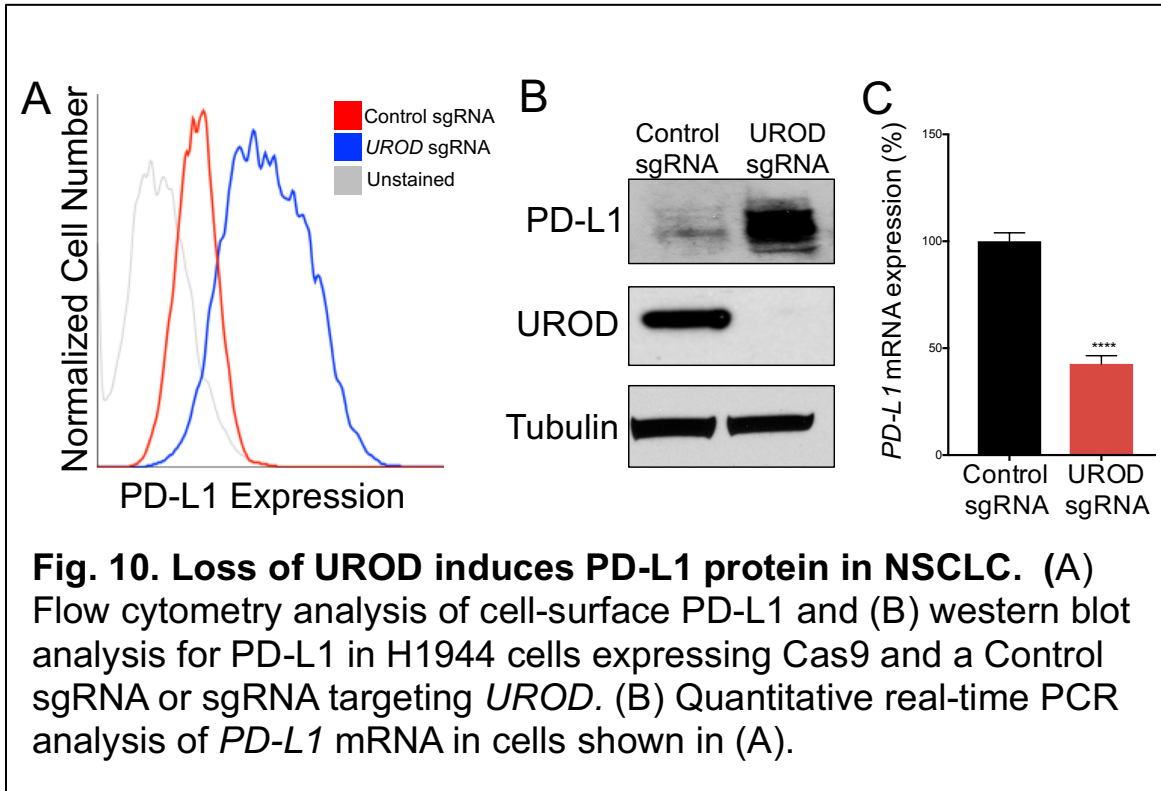


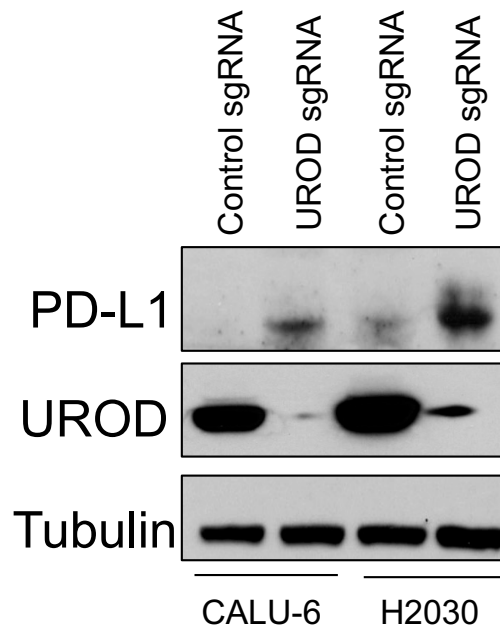
### 7.3 Loss of UROD induces PD-L1 protein

To functionally validate *UROD* as a negative regulator of PD-L1, we knocked out UROD using a sgRNA targeting *UROD* in multiple independent NSCLC cell lines. Loss of UROD potently induced total cellular levels and cell-surface PD-L1 (Fig. 10A, Fig. 10B, Fig. 11). Notably, *PD-L1* mRNA levels decreased in UROD knockout cells (Fig. 10C), suggesting that loss of UROD post-transcriptionally induces PD-L1 in NSCLC. Since PD-L1 is predominantly regulated by IFN- $\gamma$  from the tumor microenvironment, we investigated if PD-L1 upregulation upon loss of UROD is mediated via IFN- $\gamma$  signaling. First, we assessed if *UROD* was an IFN- $\gamma$  responsive gene. UROD levels were not influenced by IFN- $\gamma$  stimulation in NSCLC cells (Fig. 12). Next, to test if PD-L1 upregulation was mediated via IFN- $\gamma$  signaling, *UROD* knockdown cells were treated with Ruxolitinib, a downstream inhibitor of IFN- $\gamma$  signaling. Treatment with Ruxolitinib inhibited IFN- $\gamma$  mediated transcriptional upregulation of *PD-L1* (Fig. 13A), but failed to suppress PD-L1 protein induction in UROD knockout cells (Fig. 13B). Thus, taken together, loss of PD-L1 post-transcriptionally induces PD-L1 in an IFN- $\gamma$  independent manner.

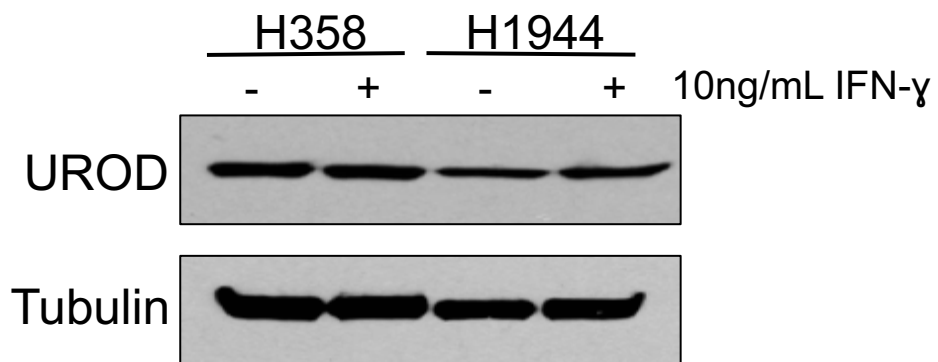
*UROD* catalyzes the step-wise decarboxylation of Uroporphyrinogen to Coproporphyrinogen (Fig. 14A) in the heme biosynthetic pathway [103]. Deficiency of UROD in human patients results in heme deficiency and PCT due to the disruption of heme synthesis and the accumulation of Uroporphyrinogen [124, 127]. Consistent with this, UROD inhibition resulted in a 50% reduction in heme synthesis (Fig. 14B). To test if Uroporphyrinogen accumulation in UROD knockout cells stabilizes PD-L1, we knocked down *URO3S* (*Uroporphyrinogen Synthase*), which encodes the enzyme that functions

directly upstream of UROD. Simultaneous inhibition of *URO3S* and *UROD* still leads to potent PD-L1 induction (Fig. 15), ruling out a role for Uroporphyrinogen in PD-L1 stabilization. Moreover, knockdown of *URO3S* alone potently induced PD-L1 (Fig. 15), demonstrating that disruption of the heme synthesis pathway likely induces PD-L1 in NSCLC cells. In support of this, chemical inhibition of Aminolevulinic Acid Dehydratase (ALAD) enzyme by Succinylacetone treatment or Ferrochelatase (FECH) enzyme by N-Methyl Porphyrin IX also induced PD-L1 protein in H1944 cells (Fig. 16A, Fig. 17A) without increasing *PD-L1* transcript levels (Fig. 16B, Fig. 17B). Importantly, exogenous hemin restored PD-L1 levels to baseline in UROD knockout cells (Fig. 18), demonstrating that heme deficiency leads to upregulation of PD-L1 protein in NSCLC cells.

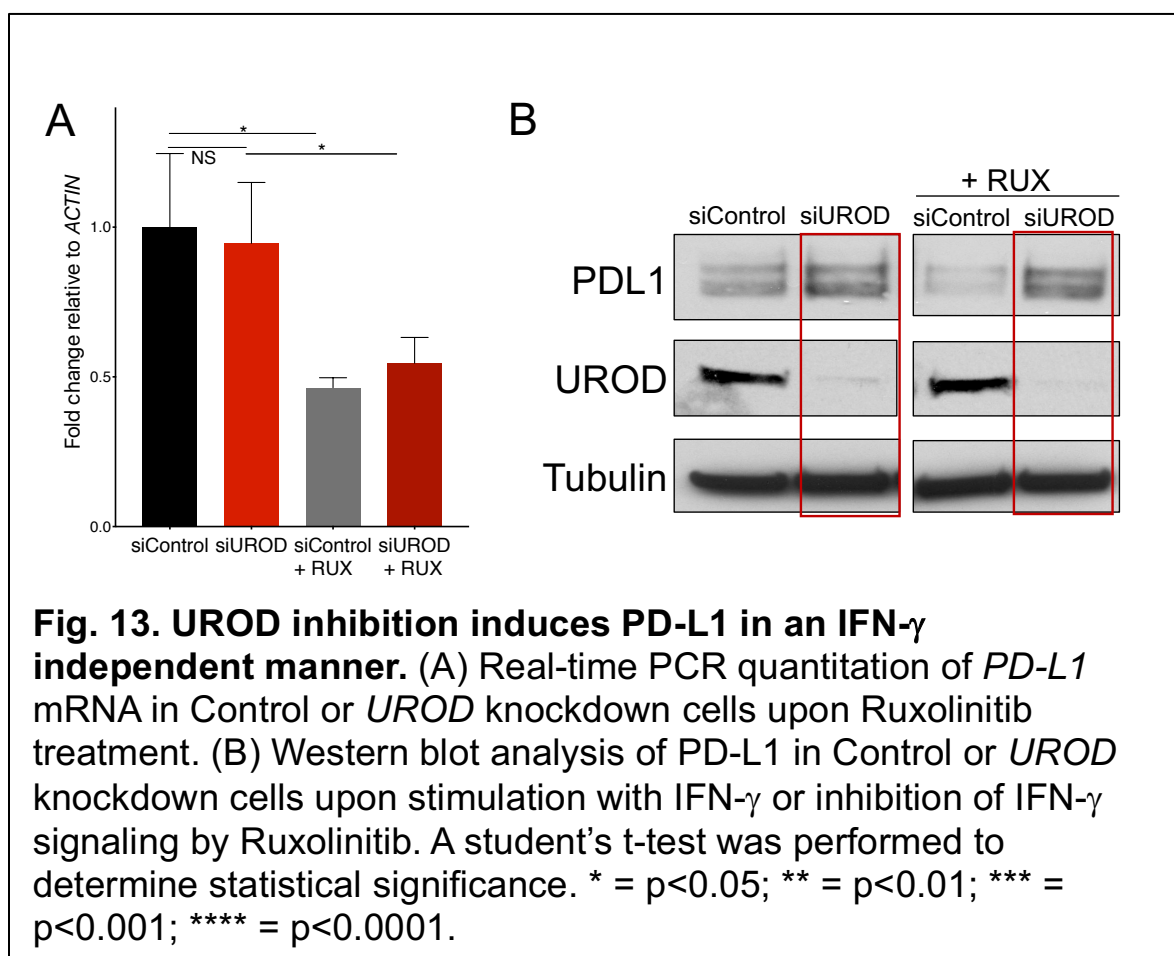


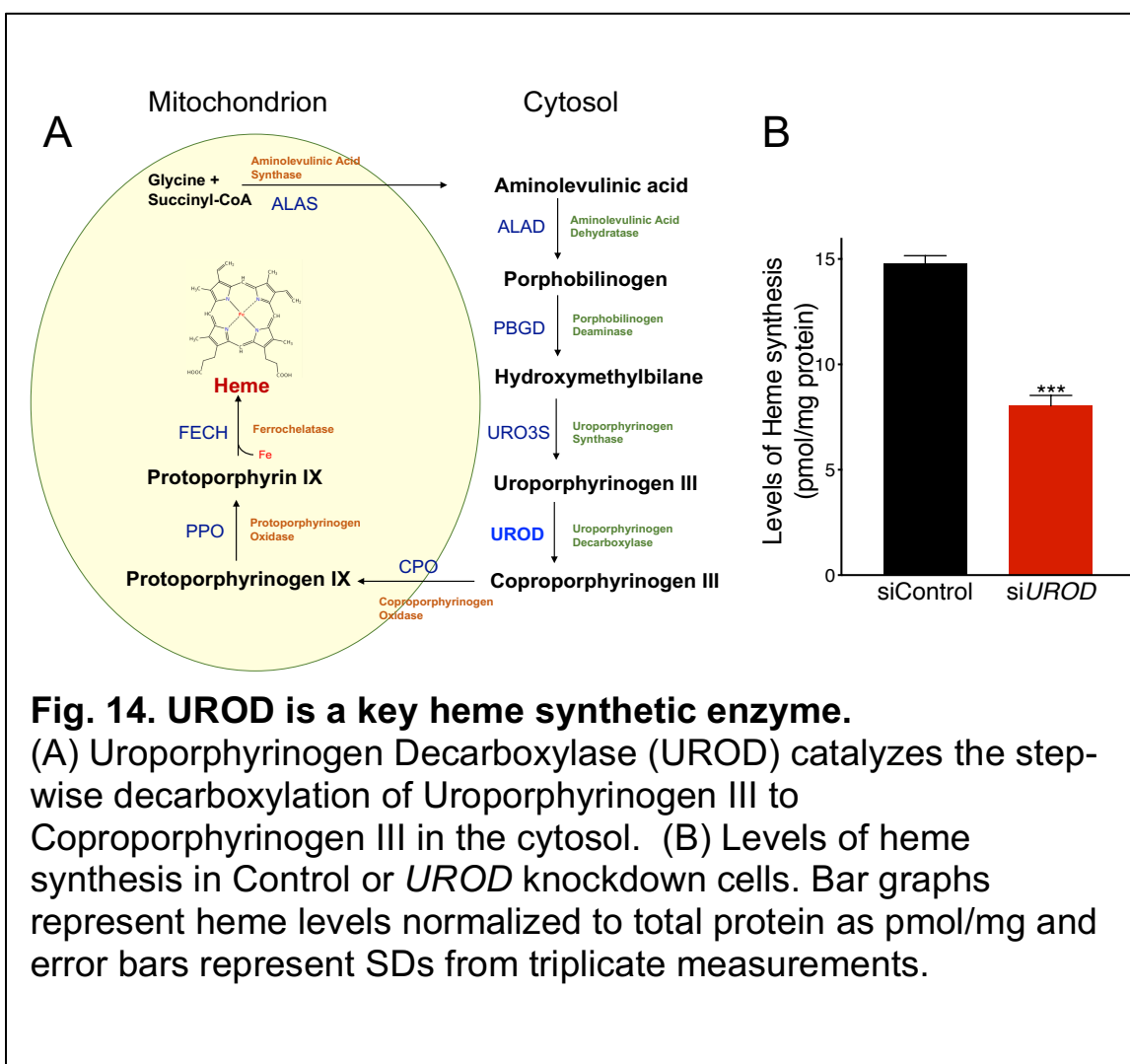


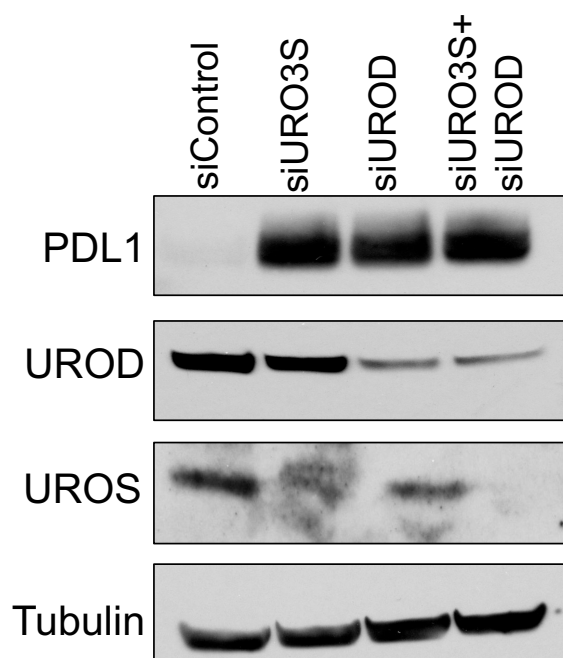
**Fig. 11. Loss of UROD induces PD-L1 in other lung cancer cell lines.** Western blot analysis of PD-L1 in Calu-6 and H2030 cells expressing a Control or UROD sgRNA.



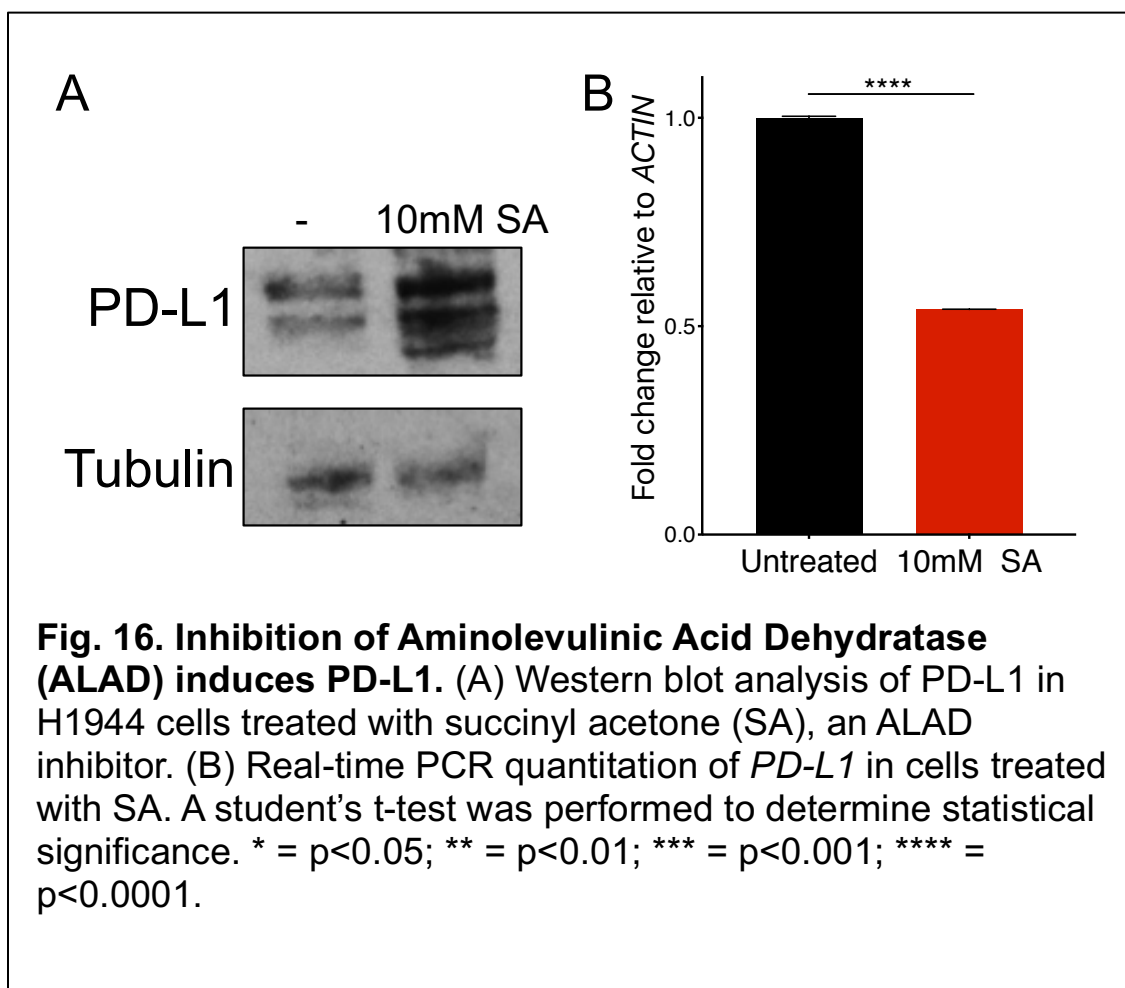
**Fig. 12. UROD is NOT an IFN- $\gamma$  responsive gene.** Western blot analysis of UROD in lung cancer cells stimulated with IFN- $\gamma$  for 24h.

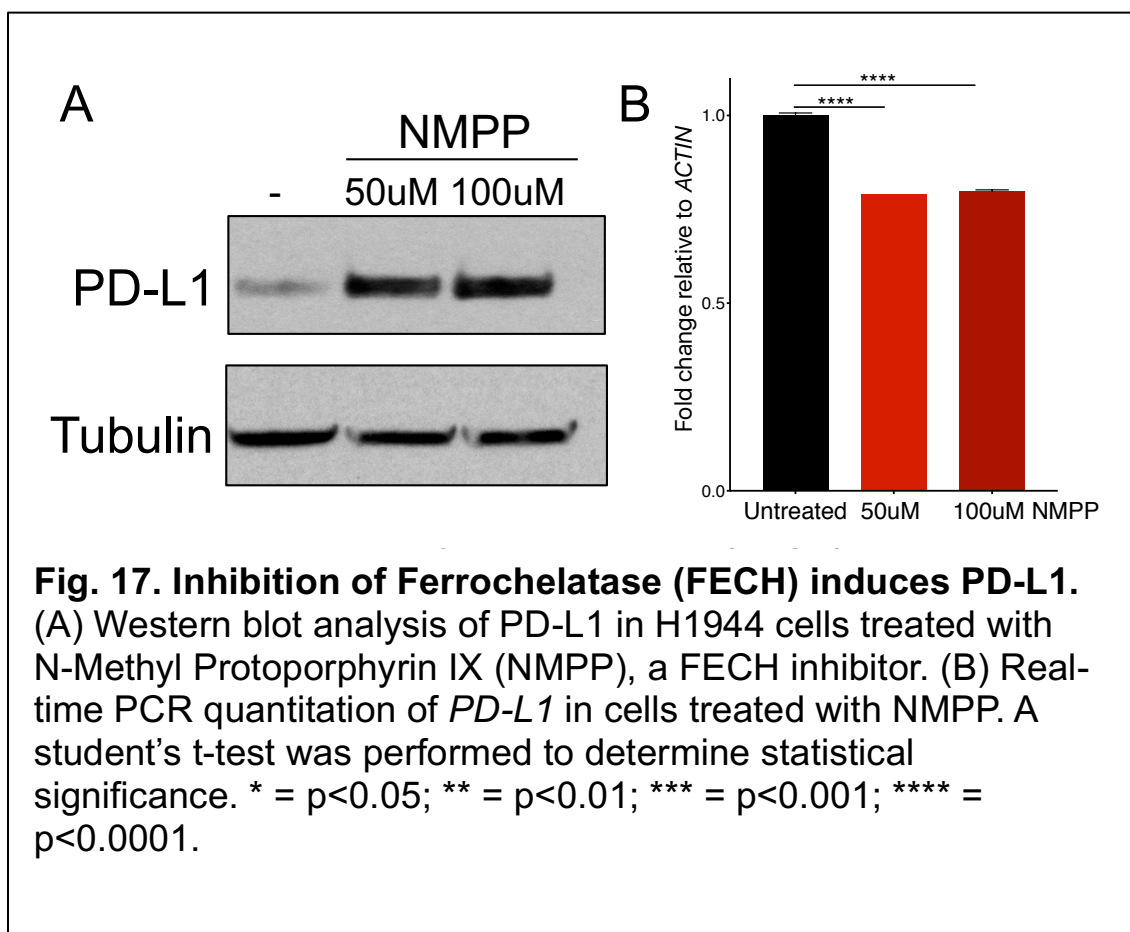






**Fig. 15. Accumulated Uroporphyrinogen does not stabilize PD-L1.** Western blot analysis of PD-L1 measured in H1944 cells upon transient knockdown of heme synthesis pathway enzymes *UROD*, *URO3S*, or both in combination.





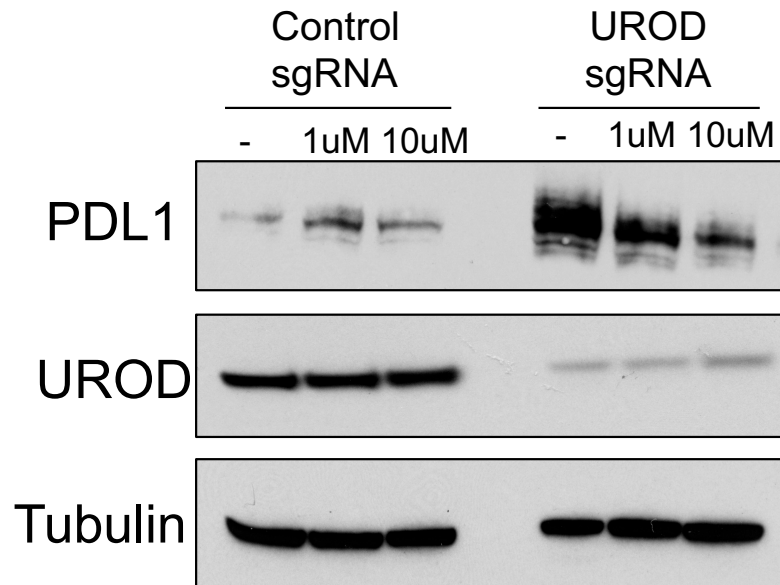
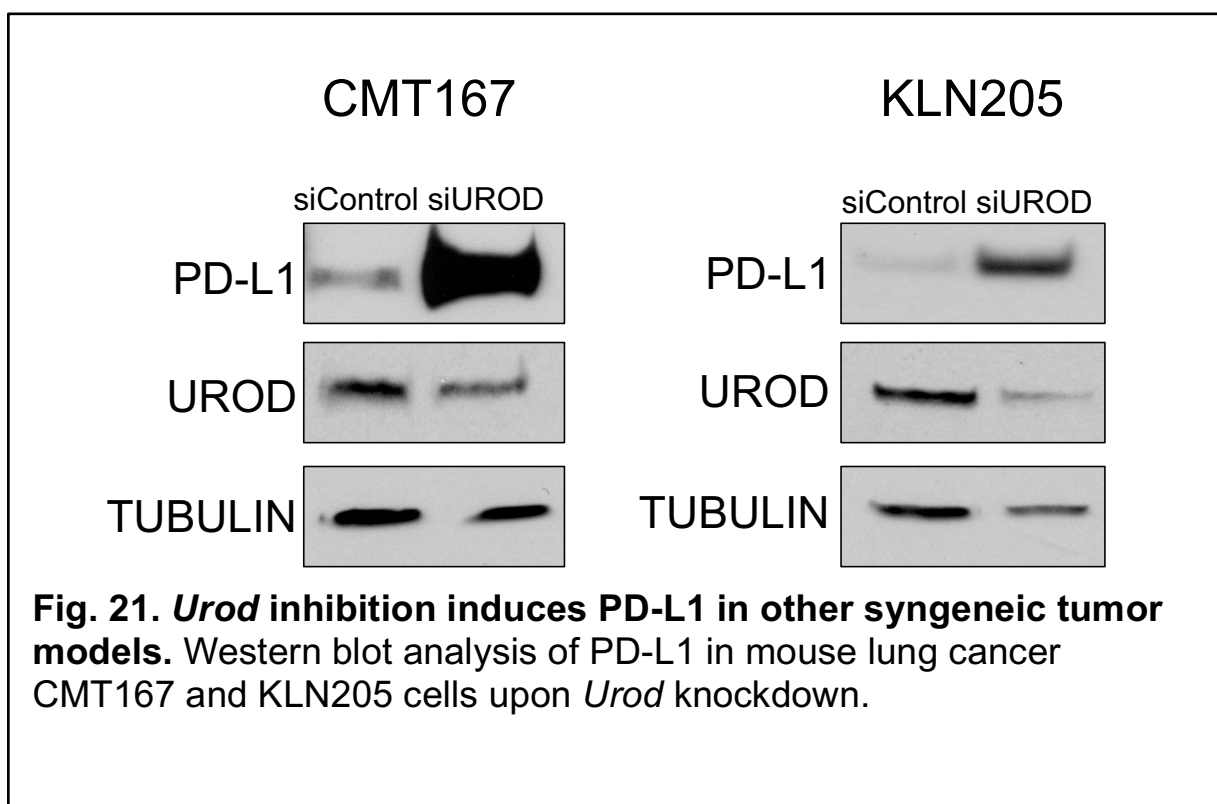


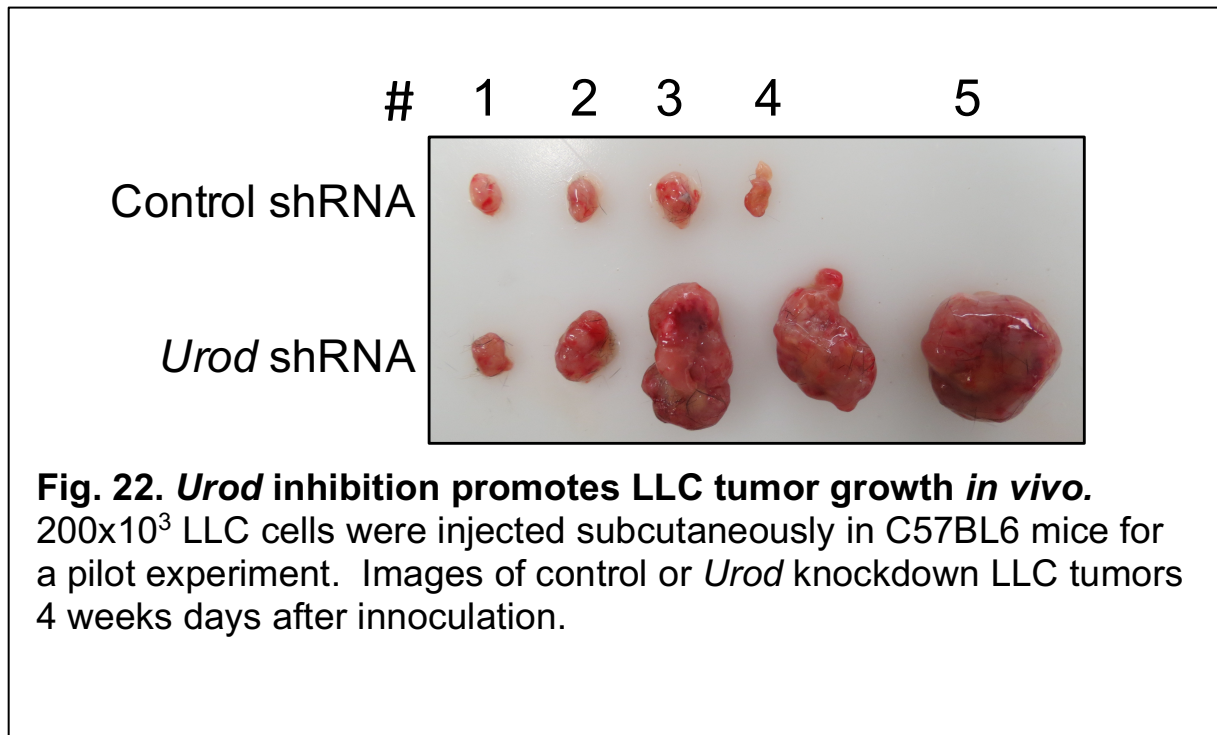
**Fig. 18. Hemin rescues PD-L1 in UROD knockout cells.** Western blot analysis of PD-L1 expression in H1944 cells expressing Cas9 and a control sgRNA or sgRNA targeting UROD upon supplementation with exogenous heme.

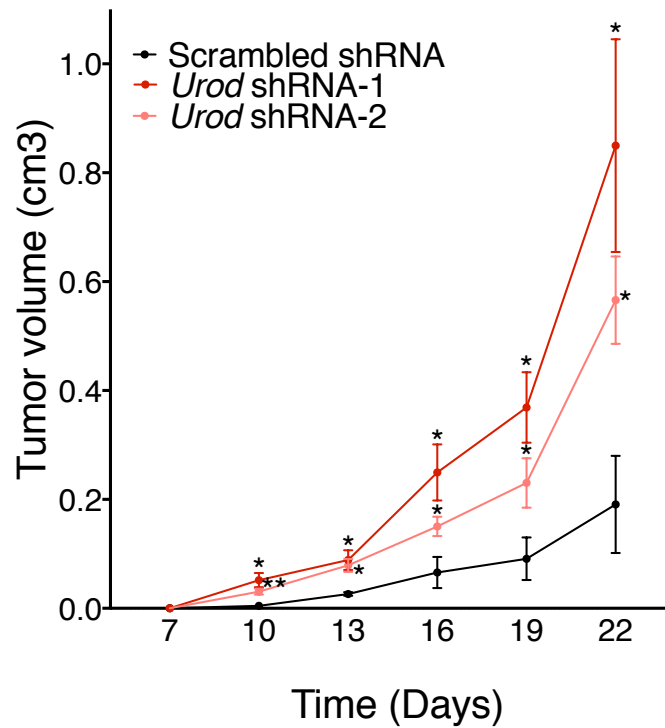
#### **7.4 *Urod* inhibition suppresses CD8<sup>+</sup> T cells to promotes tumorigenesis *in vivo***

To examine the effects of UROD inhibition on tumor growth *in vivo*, we used Tet-ON doxycycline inducible (pTRIPZ) shRNA to deplete *Urod* in a syngeneic murine lung cancer model, Lewis Lung Carcinoma (LLC) cells [193] (Fig. 19). Inhibition of UROD in LLC cells led to potent upregulation of PD-L1 protein without altering *Pd-11* transcript levels, demonstrating that this pathway is conserved between human and mouse (Fig. 20A, Fig. 20B). Additionally, *Urod* inhibition induced PD-L1 in two other murine syngeneic lung cancer models, CMT167 and KLN205 cells (Fig. 21). *Urod* shRNA LLC cells grew significantly faster than control cells in immunocompetent C57BL/6 mice (Fig. 22, Fig. 23). However, *Urod* shRNA cells grew at similar rates to control cells in immunodeficient NOD-*scid* IL2R $\gamma$ <sup>null</sup> mice (Fig. 24), suggesting that *Urod* suppression may modulate the tumor immune microenvironment to sustain growth *in vivo*. Indeed, we observed that the growth advantage was diminished upon depletion of CD8<sup>+</sup> T cells in C57BL/6 mice (Fig. 25), implying that *Urod* inhibition suppresses CD8<sup>+</sup> tumor infiltrating lymphocyte (TIL) function *in vivo* via PD-L1 upregulation. To test this hypothesis, we performed TIL staining in LLC tumors expressing a Control or *Urod* shRNA +/- PD-1 blockade (Fig. 26). We found that *Urod* shRNA tumors exhibited significantly lower numbers of CD8<sup>+</sup> TILs compared to control tumors (Fig. 27). Furthermore, we observed that disruption of the PD-1/ PD-L1 signaling axis with administration of  $\alpha$ -PD1 blocking antibody markedly controlled growth of *Urod* knockdown tumors *in vivo* (Fig. 28), along with a significant increase in CD8<sup>+</sup> TILs (Fig. 27). Taken together, these data demonstrate that *Urod*



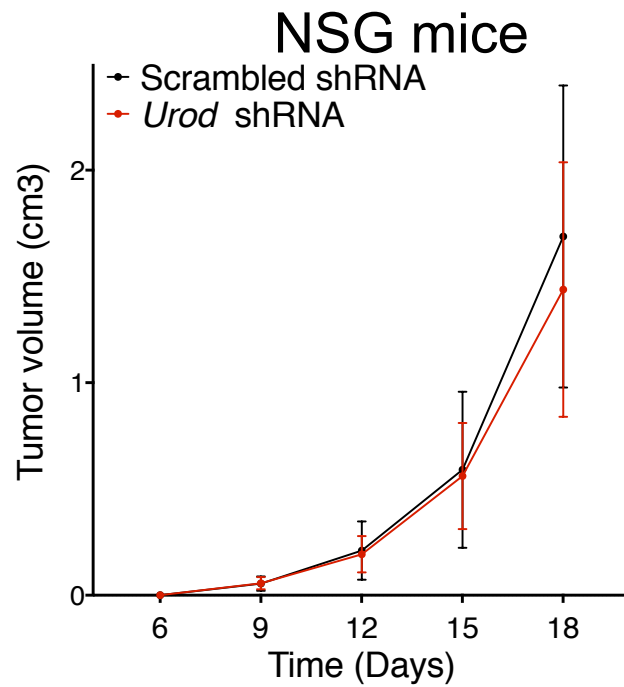




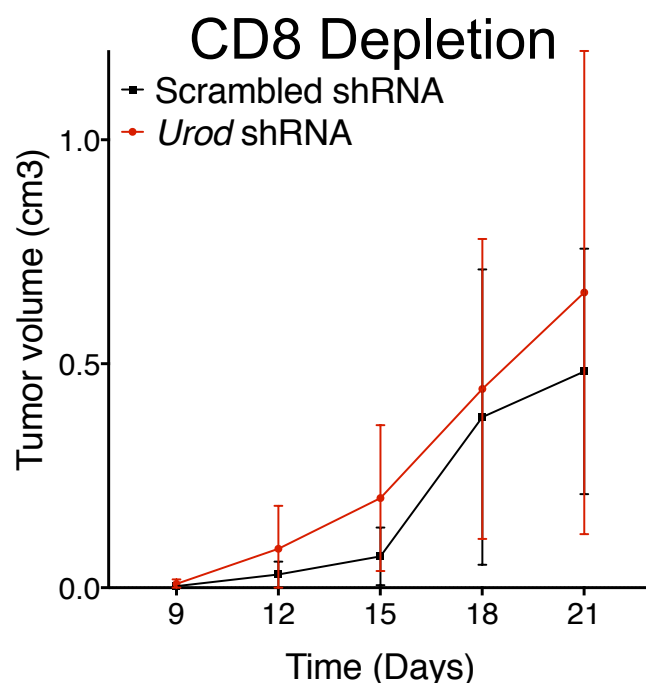


**Fig. 23. *Urod* inhibition promotes tumorigenesis *in vivo*.**

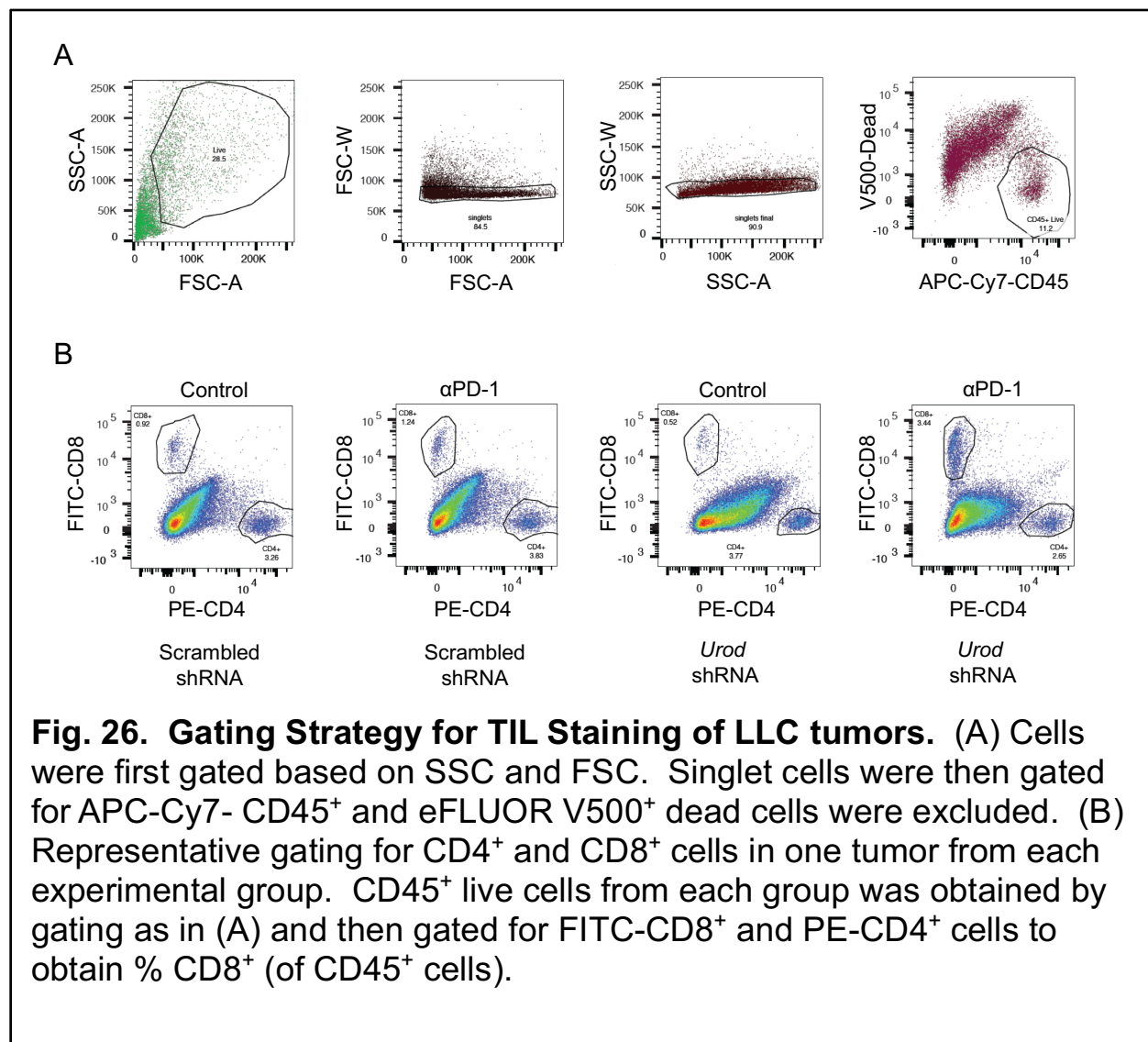
$400 \times 10^3$  LLC cells expressing either a scrambled shRNA or two independent *Urod* shRNAs were injected subcutaneously in C57BL6 mice (n=12-15 mice per group). Bar graph represents mean tumor volumes per experimental group.



**Fig. 24. *Urod* knockdown tumors grow at similar rates to controls in NSG mice.**  $400 \times 10^3$  LLC cells expressing a scrambled or *Urod* shRNA were injected subcutaneously into NSG mice (n=12-15 per group). Bar graphs represents mean tumor volumes per group.



**Fig. 25. *Urod* knockdown tumors grow at similar rates to control tumors in CD8<sup>+</sup> T cell depleted mice.** 400x 10<sup>3</sup> LLC cells expressing either a scrambled shRNA or *Urod* shRNA were injected subcutaneously in C57BL6 mice treated intraperitoneally with 200ug CD8<sup>+</sup> T cell depleting antibody every three days (n=12-15 mice per group). Bar graph represents mean tumor volumes per experimental group.



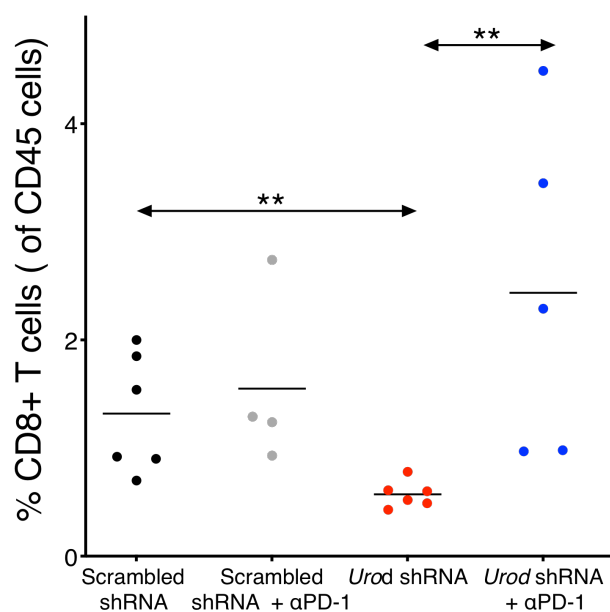


**Fig. 27. *Urod* inhibition leads to a reduction in CD8<sup>+</sup> TILs.**

400x 10<sup>3</sup> LLC cells expressing either a scrambled shRNA or *Urod* shRNA were injected subcutaneously in C57BL6 mice treated intraperitoneally every three days with 200ug control or PD-1 antibody (n=12-15 mice per group). TILs from tumors were stained and gated as described in Fig. 26. Graph represents % CD8<sup>+</sup> T cells (of CD45<sup>+</sup> TILs) measured in 4-6 tumors per group.

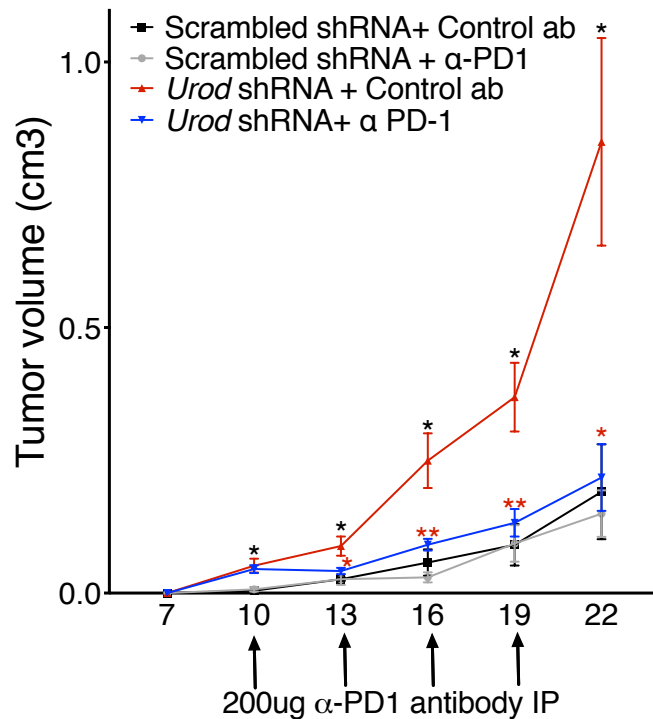


**Fig. 28. PD-1 blockade controls *Urod* knockdown tumors *in vivo*.**  $400 \times 10^3$  LLC cells expressing either a scrambled shRNA or *Urod* shRNA were injected subcutaneously in C57BL6 mice and treated intraperitoneally every three days with 200ug control or PD-1 antibody every three days (n=12-15 mice per group). Graph represents mean tumor volumes per group.

### **7.5 Mechanisms of post-transcriptional regulation of PD-L1**

To probe the mechanisms underlying PD-L1 upregulation in UROD knockout cells, we first monitored *PD-L1* mRNA abundance over time and observed no significant difference in mRNA decay rate between control and UROD knockout cells (Fig. 29). To test if loss of UROD affected PD-L1 protein degradation, we first treated H1944 cells with a proteasomal inhibitor (Velcade) or lysosomal inhibitors (Chloroquine, Baflomycin) and observed that PD-L1 protein was degraded via the proteasomal pathway, and to a lesser extent by the lysosome (Fig. 30). Cycloheximide treatment however revealed that PD-L1 protein degraded at similar rates in Control and UROD knockout cells (Fig. 31). Furthermore, PD-L1 ubiquitylation was unaltered in UROD knockout cells (Fig. 32), ruling out a role for UROD in regulating ubiquitin-mediated proteasomal degradation of PD-L1.

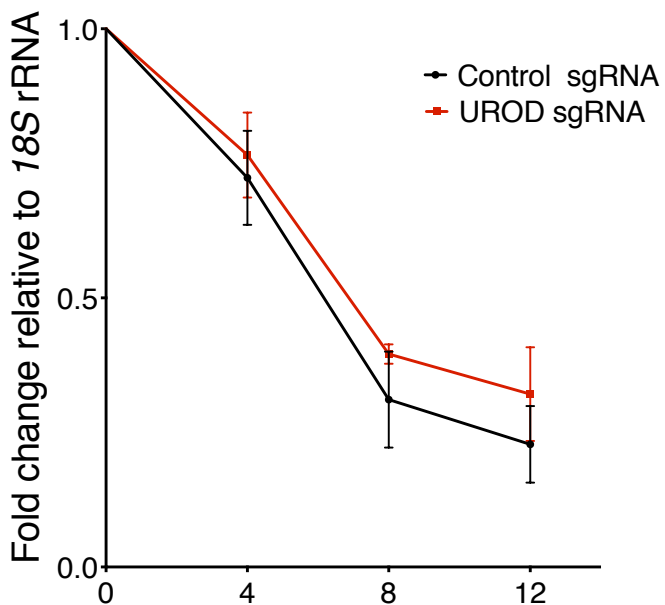


**Fig. 29. *PD-L1* mRNA decay is unaltered in UROD knockout cells.** Real-time PCR to monitor *PD-L1* mRNA decay rate with time in cells expressing a Control or UROD sgRNA upon treatment with 10uM Actinomycin D.

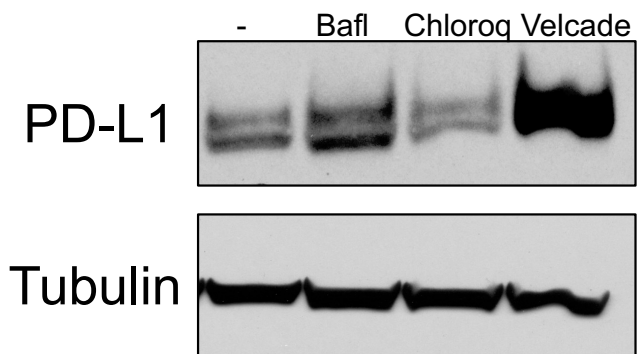


**Fig. 30. PD-L1 protein is targeted predominantly to the proteasome for degradation.** Western blot analysis of PD-L1 in cells treated with lysosomal inhibitors (Baflomycin BafI, Chloroquine, Chloroq) or a proteosomal inhibitor (Velcade).

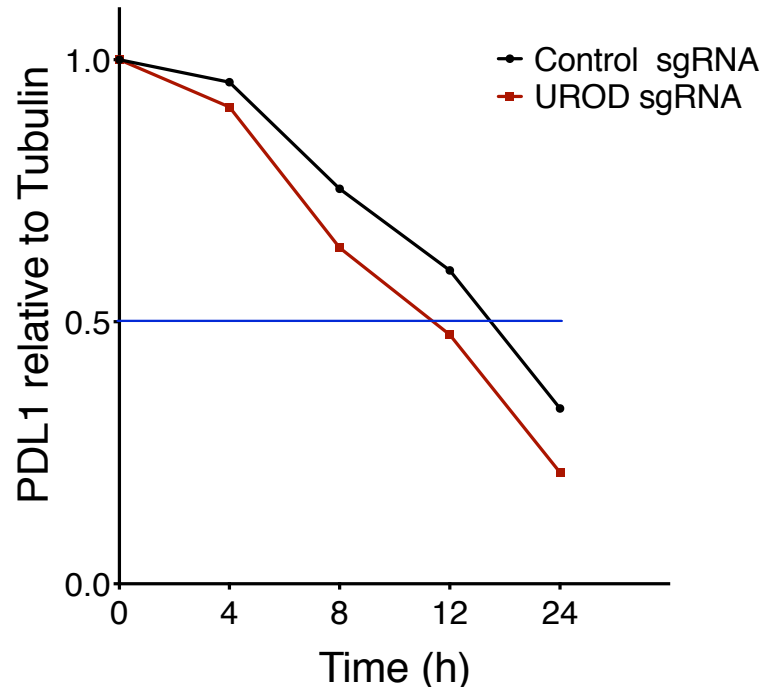
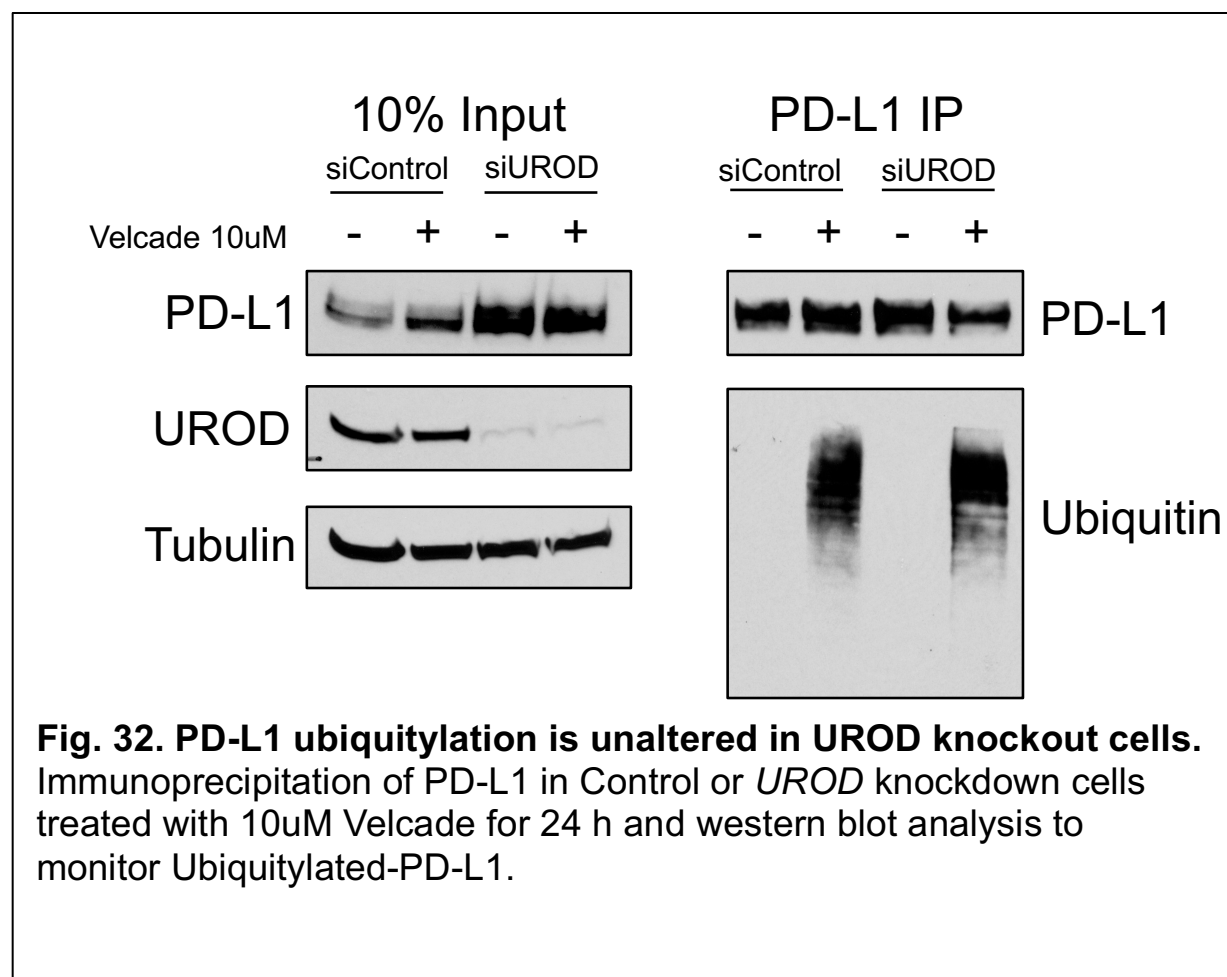


**Fig. 31. PD-L1 protein stability is unaltered in UROD knockout cells.** PD-L1 protein abundance monitored with time in cells expressing a Control or UROD sgRNA upon treatment with 50uM cycloheximide.

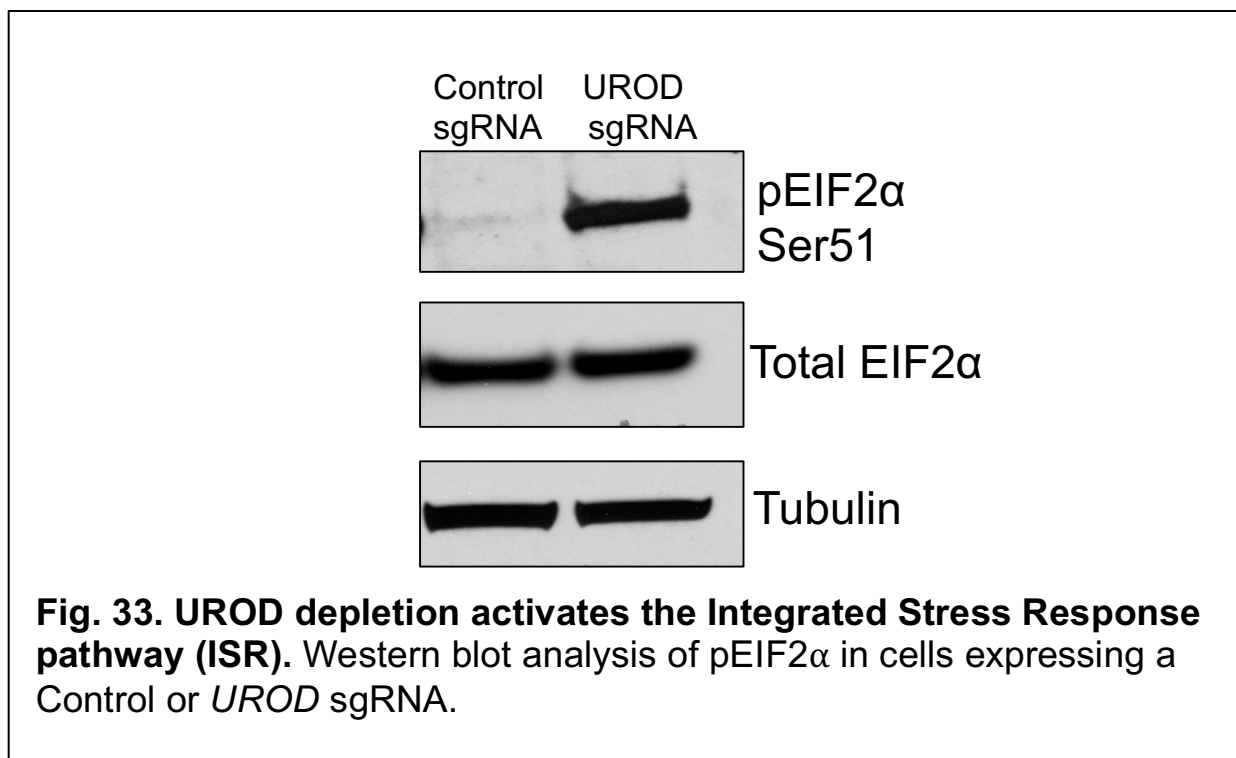


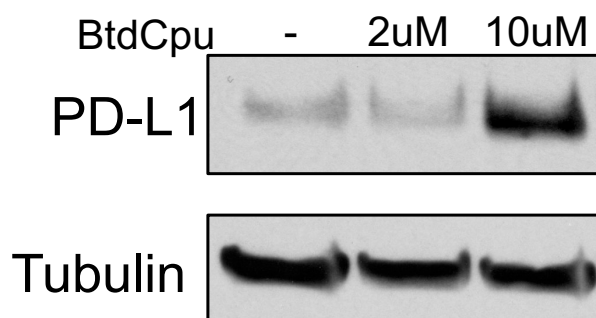
## 7.6 Loss of UROD activates ISR to enhance *PD-L1* translation in NSCLC

We hypothesized that loss of UROD promotes *PD-L1* mRNA translation in NSCLC. Heme deficiency activates the Heme-Regulated Inhibitor HRI to phosphorylate its substrate EIF2 $\alpha$  at Serine 51 (Ser-51) [137, 138, 143]. Phosphorylation of EIF2 $\alpha$  leads to inhibition of global translation initiation and simultaneous translation of select mRNAs. This is commonly known as the Integrated Response (ISR) pathway [135, 140, 194, 195]. Since *UROD* loss results in heme deficiency, we hypothesized that inhibition of UROD may activate the ISR and enhance translation of *PD-L1* mRNA. UROD depletion led to potent phosphorylation of EIF2 $\alpha$  at Ser-51 (Fig. 33). Moreover, treatment with the HRI agonist BtDCpu leads to PD-L1 induction (Fig. 34). Additionally, Salubrinal, a selective inhibitor of EIF2 $\alpha$  de-phosphorylation [188], induced PD-L1 in NSCLC cells (Fig. 35). The small molecule ISRIB (Integrated Stress Response Inhibitor) was recently found to reverse the effects of EIF2 $\alpha$  phosphorylation on translation [178, 179]. Accordingly, treatment with ISRIB could completely reverse PD-L1 upregulation induced by Salubrinal treatment (Fig. 36). Additionally, ISRIB partially restored PD-L1 levels in UROD knockout cells (Fig. 37) further implicating a role for ISR in enhancing PD-L1 protein levels.

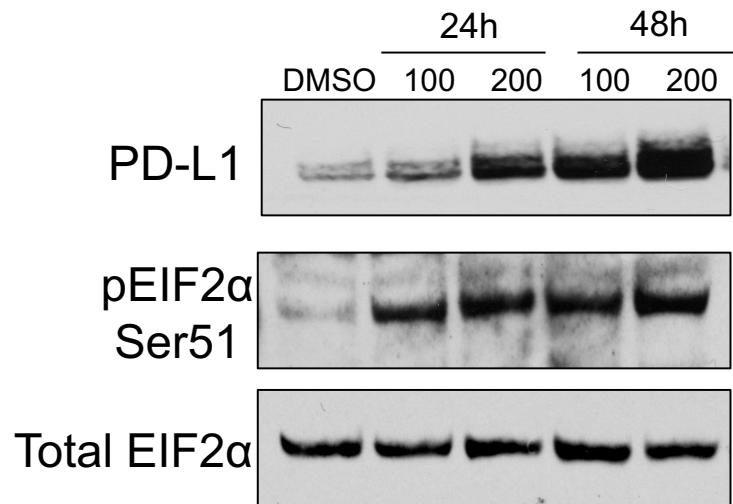
To determine whether phosphorylation of EIF2 $\alpha$  is necessary for PD-L1 induction, we inhibited *Urod* in MEFs expressing either wildtype EIF2 $\alpha$  (S/S cells) or a mutant EIF2 $\alpha$  with Serine-51 mutated to Alanine (A/A cells). Loss of *Urod* led to phosphorylation of EIF2 $\alpha$  at Ser-51 and a potent induction in PD-L1 protein without increasing *Pd-11* mRNA levels in the S/S cells, but not in the A/A cells (Fig. 38A, Fig. 38B). Moreover, consistent with activation of ISR, we observed a 50% reduction in global translation in UROD

depleted cells (Fig. 39A, 39B). Taken together, these data demonstrate that UROD inhibition activates the ISR pathway and that phosphorylation of EIF2 $\alpha$  at Ser-51 is required for PD-L1 protein induction.

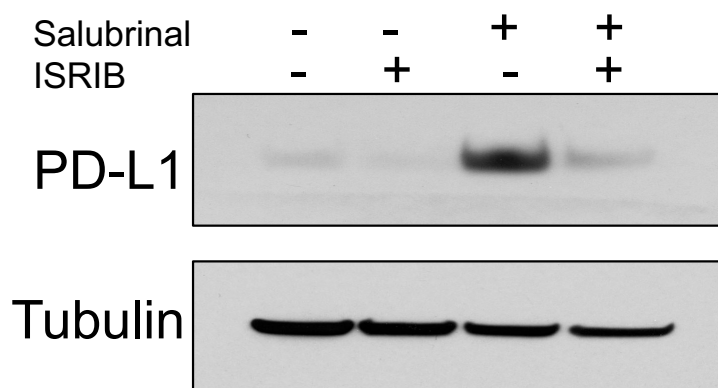




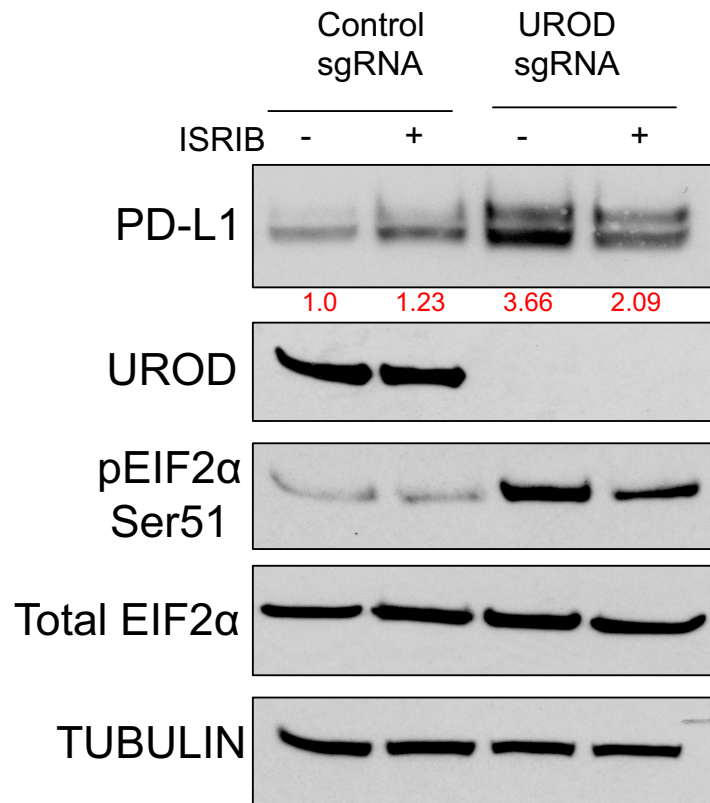
**Fig. 34. A chemical activator of HRI (BtDCpu) induces PD-L1.** Western blot analysis of PD-L1 in H1944 cells treated with BtDCpu for 24h.



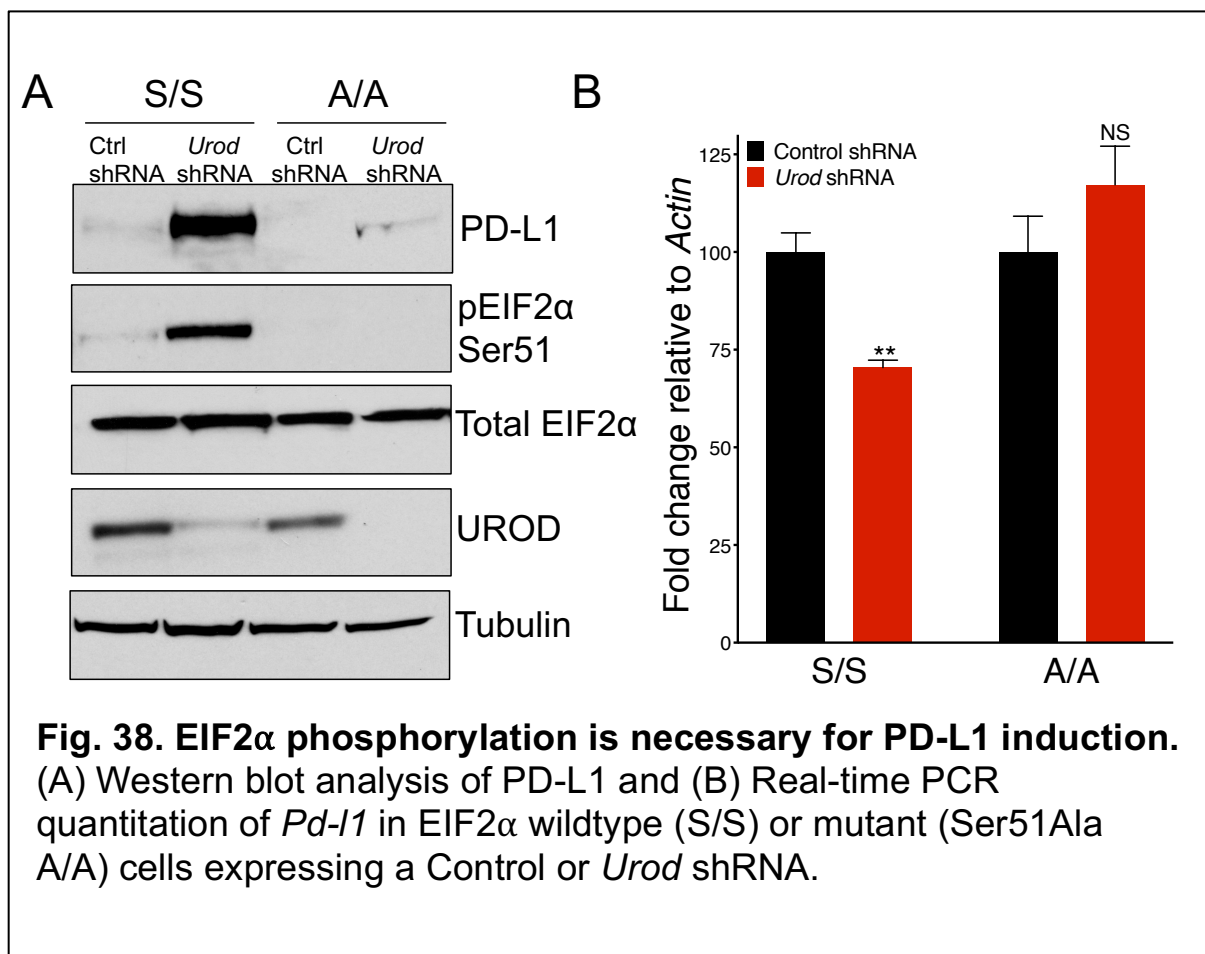
**Fig. 35. Phosphorylation of EIF2 $\alpha$  is sufficient to induce PD-L1.** Western blot analysis of PD-L1 and pEIF2 $\alpha$  in cells treated with Salubrinal (in uM), a specific inhibitor of EIF2 $\alpha$  dephosphorylation.

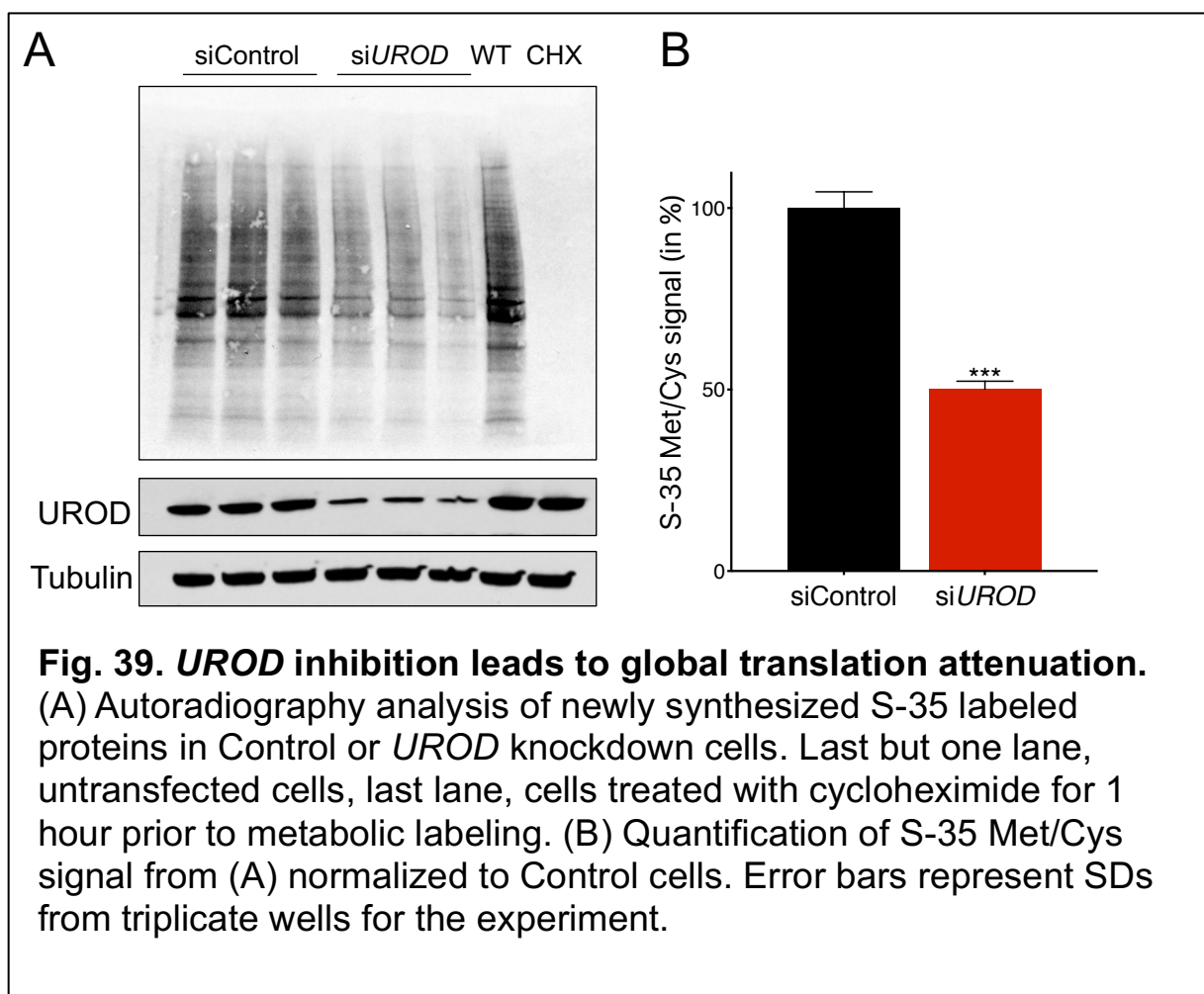


**Fig. 36. Integrated Stress Response Inhibitor (ISRIB) reverses the effect of Salubrinal on PD-L1.** Western blot analysis of PD-L1 in H1944 cells treated with 100uM Salubrinal and/or 200nM ISRIB, a chemical inhibitor of the ISR pathway for 24h.



**Fig. 37. ISRIB partially reverses the effect of *UROD* knockdown on PD-L1.** Western blot analysis of PD-L1 in H1444 cells treated with ISRIB (200 nM) in UROD knockout cells for 48h.

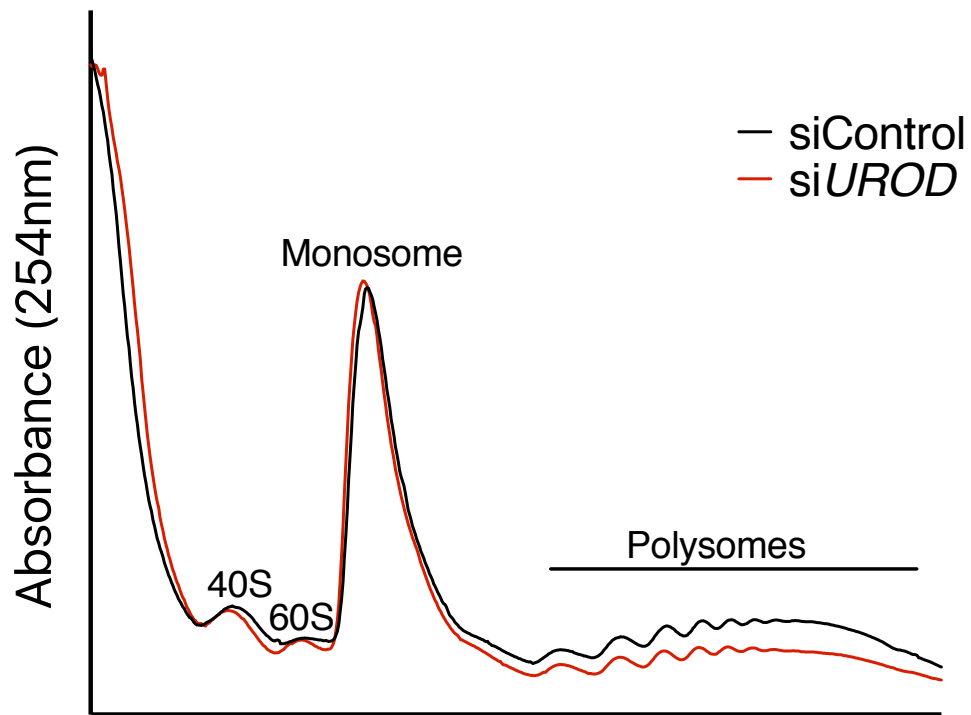




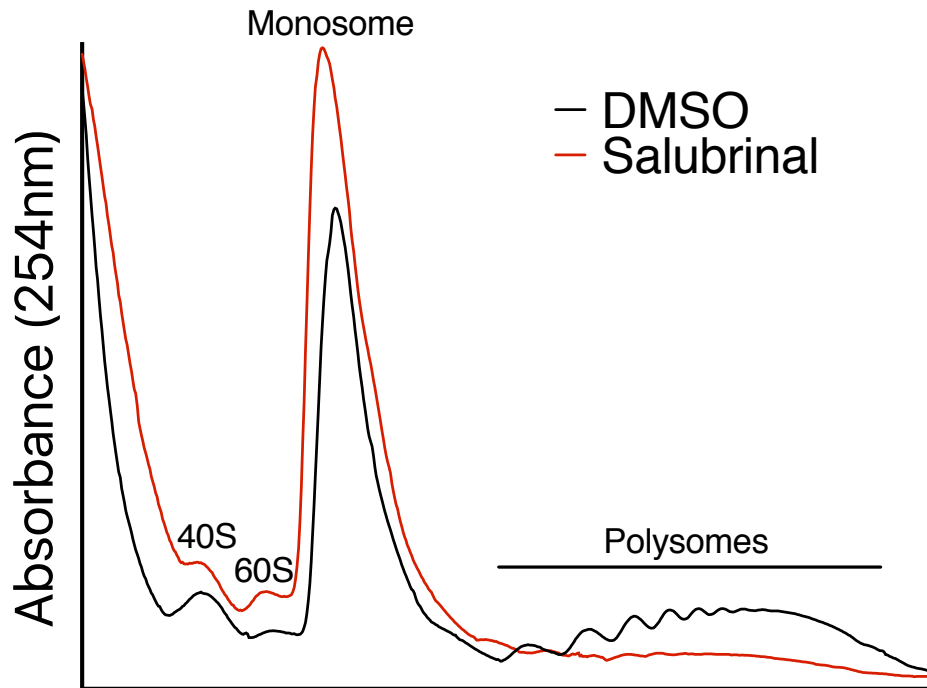
Next, to test if *PD-L1* mRNA translation is selectively enhanced under these conditions, we performed polysome profiling of control and UROD siRNA-treated cells. UROD inhibition resulted in an overall decrease in polysomes (Fig. 40), consistent with the reduction in global translation (Fig. 39). Salubrinal treatment also led to an overall decrease in polysomes consistent with its role in translation attenuation (Fig. 41). mRNA isolation from polysome fractions was performed to assess *PD-L1* mRNA association with actively translating ribosomes (Fig. 42). Notably, *PD-L1* mRNA redistributed to heavier polysomes in *UROD* depleted cells, indicating increased association with actively translated ribosomes (Fig. 42A). *PD-L1* mRNA was also more abundant in actively translated ribosome fractions upon Salubrinal treatment (Fig. 43A). As expected, *ATF4* was enriched in polysome fractions in *UROD* siRNA-treated cells and with Salubrinal treatment (Fig. 42B, Fig. 43B).

Recent studies have demonstrated that activation of the ISR pathway promotes translation through upstream ORFs (uORF) present in the 5'UTR of select genes [135, 140, 157, 159, 160, 195]. Under conditions of cellular stress, phosphorylation of EIF2 $\alpha$  is hypothesized to weaken activity of the EIF2 complex. This is speculated to result in leaky scanning of the 5'UTR, thereby allowing bypass of inhibitory uORFs and enhancing translation at the canonical AUG start site [156]. To test whether the *PD-L1* 5'UTR harbors putative elements that are critical for translation, we cloned the human *PD-L1* 5'UTR upstream of a Firefly Luciferase reporter (Fig. 44). While the human *PD-L1* 5'UTR lacks an upstream AUG that may serve as a uORF, it harbors one in-frame CUG and four out-of-frame CUGs. To determine the role of these upstream CUGs in *PD-L1* translation,

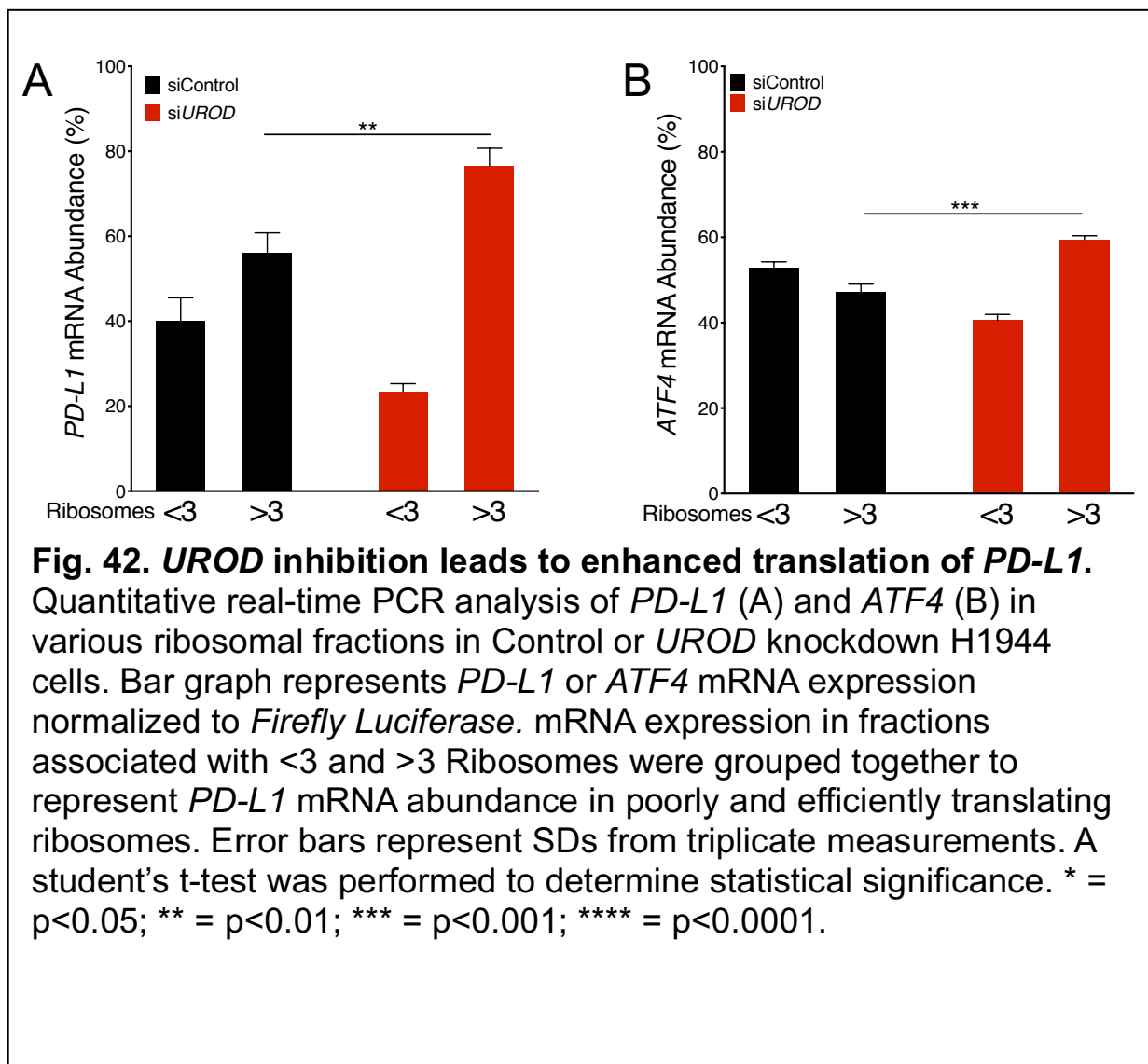
we generated a series of mutant reporter constructs by mutating each CUG to CUC, alone and in combination (Fig. 44). While no significant alterations in *Luciferase* mRNA levels were observed, mutation of the third, fourth and fifth CUG led to a ~8-15- fold increase in luciferase activity (Fig. 45, Fig. 46), relative to the wild-type (WT) construct. This suggests that these CUGs are inhibitory to downstream translation. Taken together, these data demonstrate that *UROD* inhibition activates the ISR pathway, which may result in leaky scanning of the *PD-L1* 5'UTR (Fig. 47) by the EIF2 complex, thereby enhancing *PD-L1* translation.

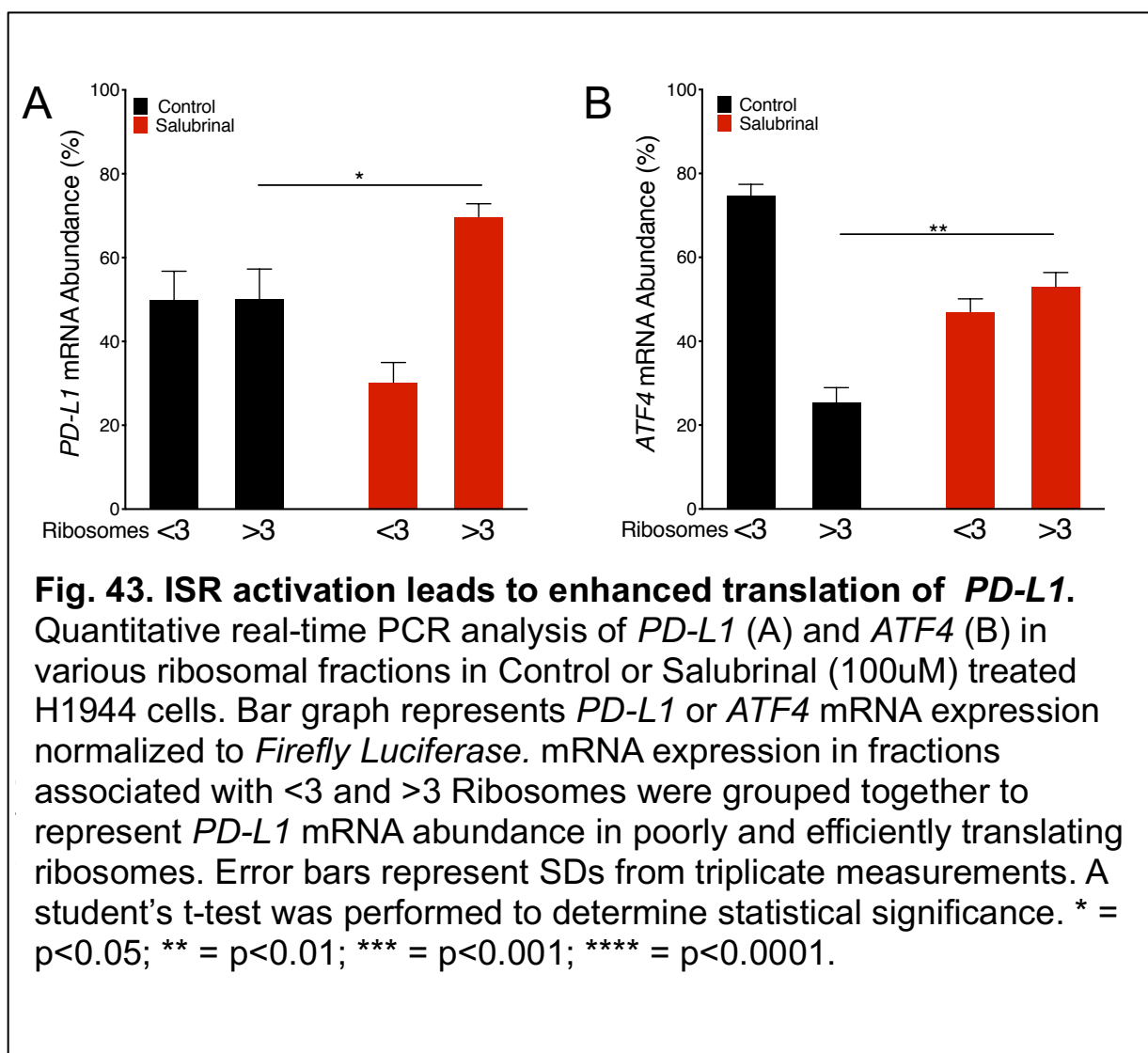


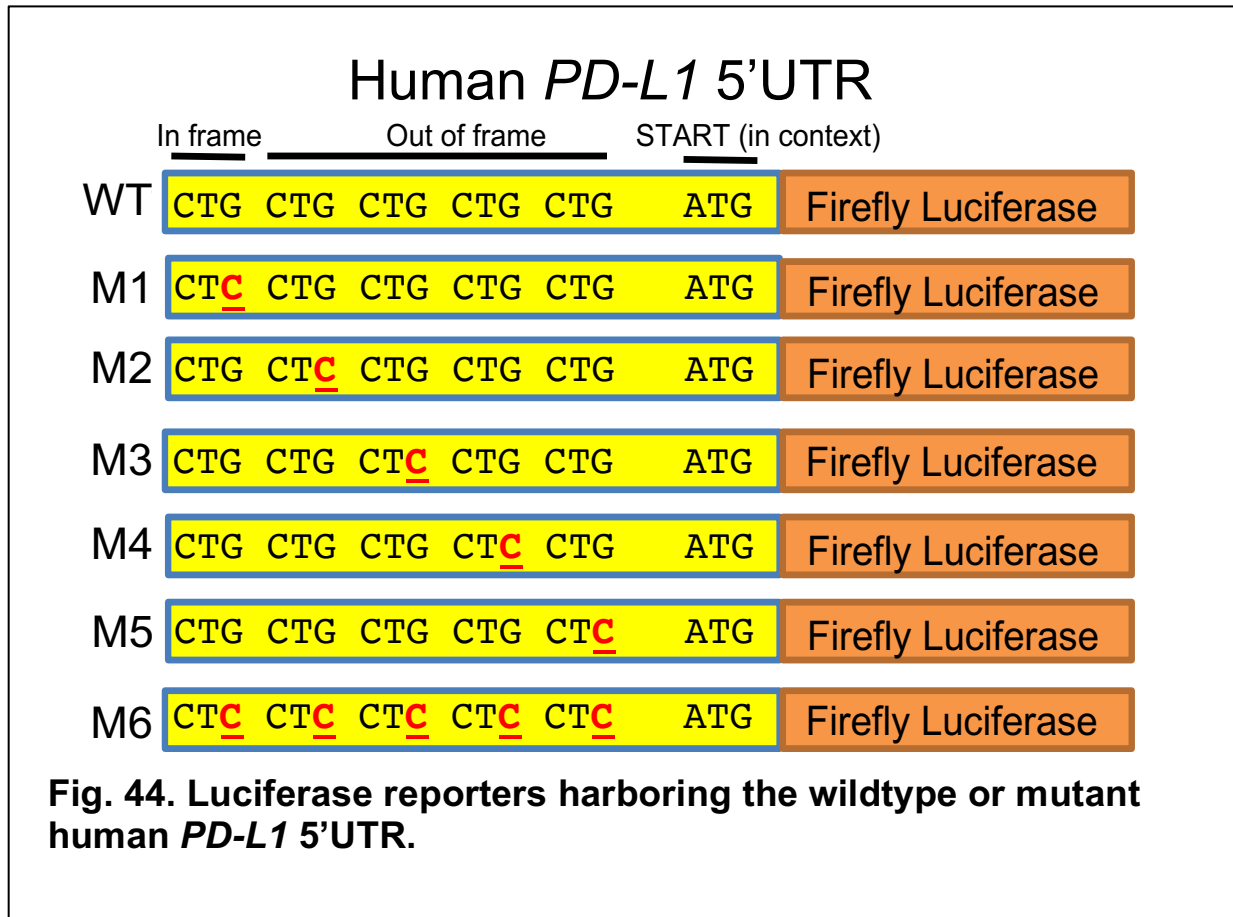
**Fig. 40. *UROD* inhibition leads to reduction in polysomes.** Polysome Profiling of Control or *Urod* knockdown H1944 cells.



**Fig. 41. Salubrinal treatment shuts down global protein translation.** Polysome Profiling of H1944 cells treated with 100uM Salubrinal for 48h.







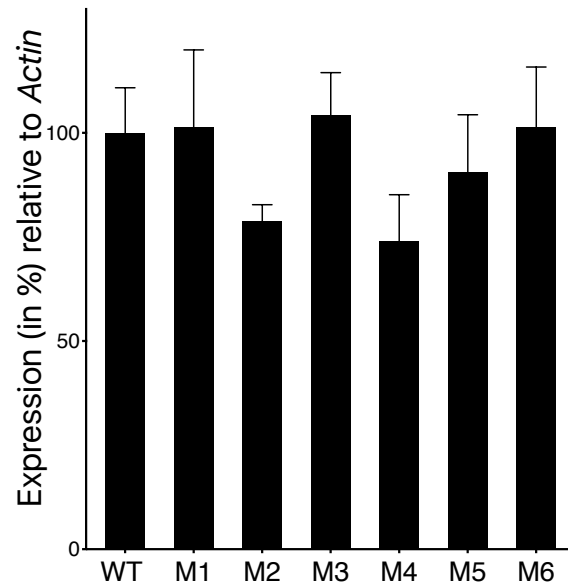


**Fig. 45. Luciferase reporter mRNA expression is similar in the various constructs.** MEF cells were transfected with various luciferase constructs and *Luciferase* mRNA expression was measured by real-time quantitative PCR and normalized to *Actin*.

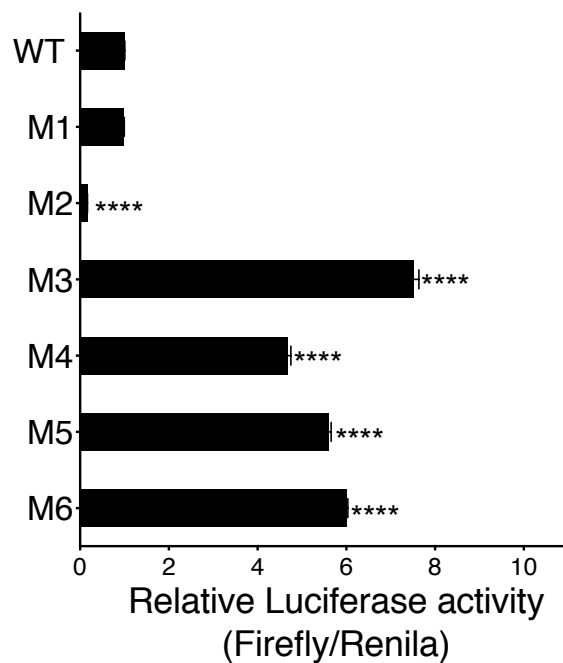
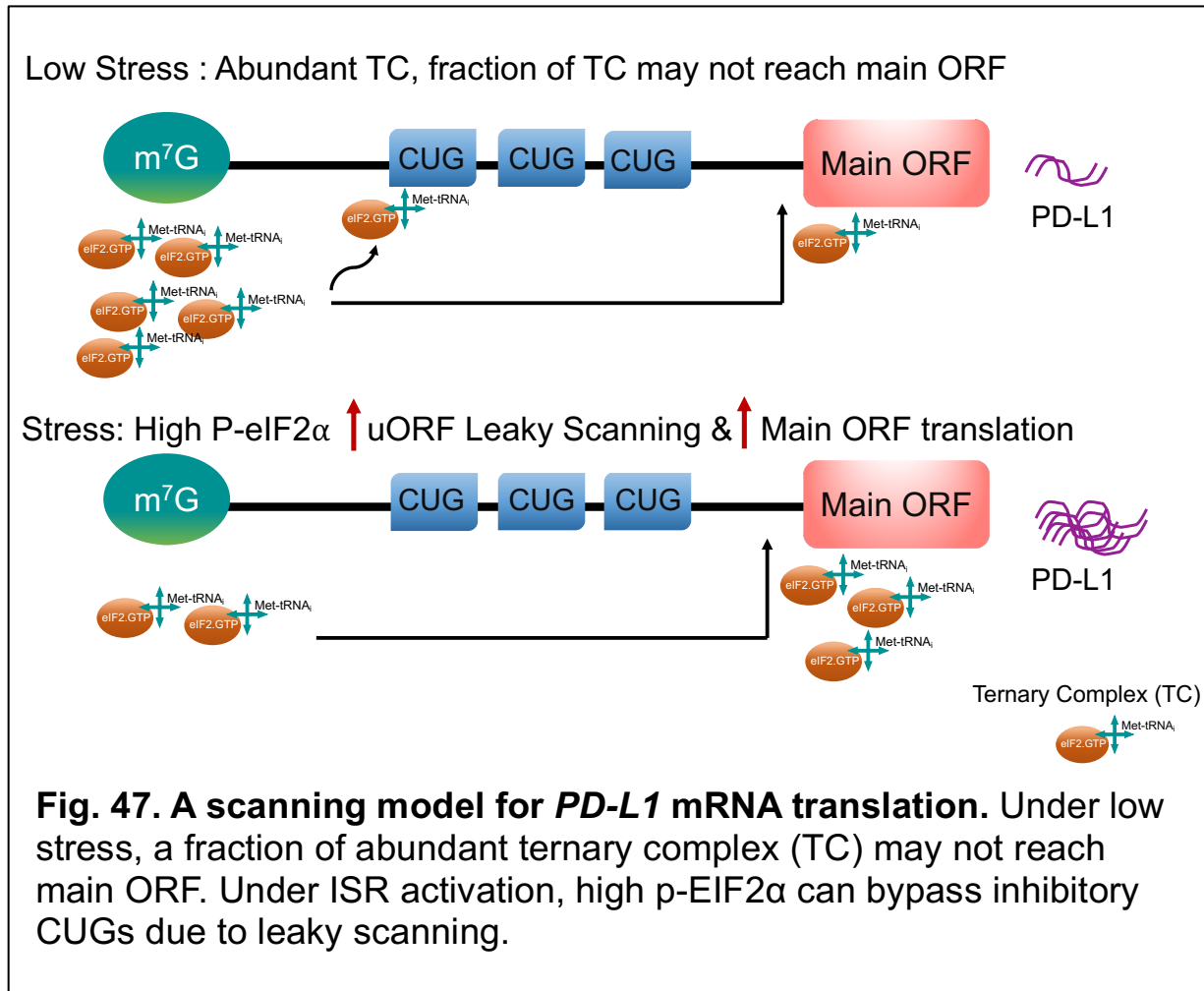
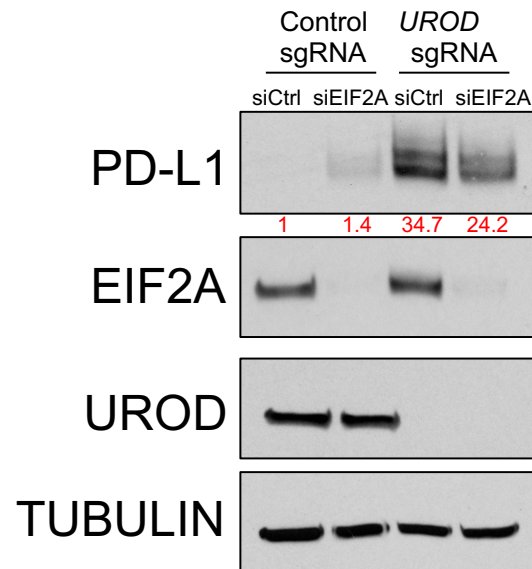


**Fig. 46. *PD-L1* 5'UTR harbors multiple inhibitory CUGs.** MEFs were transfected with various Luciferase reporter constructs and luciferase activity was measured after 48h. Firefly luciferase activity was normalized to Renilla luciferase activity.

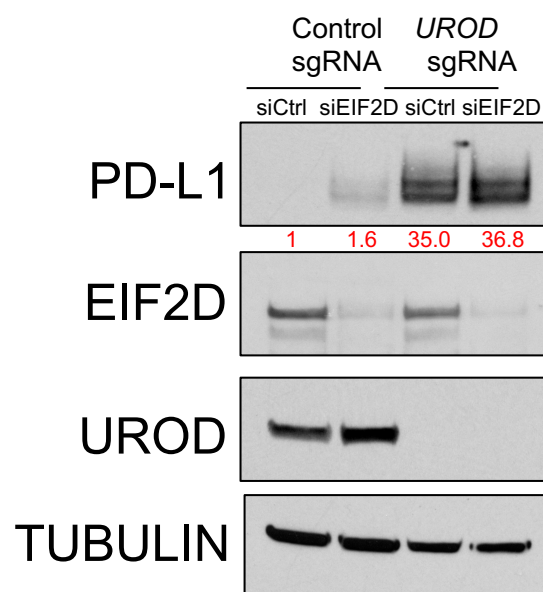


## 7.7 EIF5B drives ISR-dependent translation of PD-L1

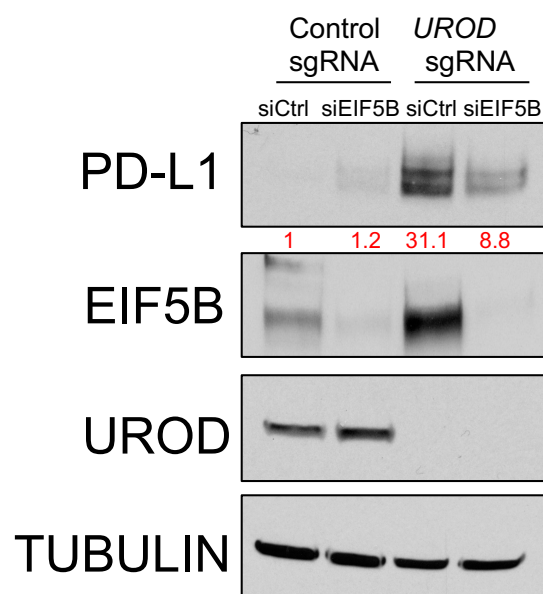
Alternative translation initiation factors, including EIF2A, EIF2D, and EIF5B, substitute for EIF2 $\alpha$  under stress conditions [164, 167]. To determine if any these factors play a role in ISR-dependent PD-L1 translation, each were depleted individually with siRNAs in *UROD* knockout cells. While EIF2A knockdown modestly reduced PD-L1 induction (Fig. 48), EIF2D knockdown had no effect on PD-L1 (Fig. 49). In contrast, EIF5B depletion strongly downregulated PD-L1 expression in *UROD* knockout cells (Fig. 50), demonstrating that EIF5B is necessary for ISR-dependent *PD-L1* translation. Examination of TCGA data revealed that high expression of *EIF5B* correlates with poor overall survival of human lung adenocarcinoma patients (Fig. 51A) and *EIF5B* amplification or mRNA upregulation occurs in nearly 20% of lung adenocarcinomas (Fig. 51B). Remarkably, overexpression of EIF5B in human lung cancer cells was sufficient to induce PD-L1 protein (Fig. 52A) without altering *PD-L1* mRNA expression (Fig. 52B), even in the absence of ISR activation (Fig. 52A). Thus, EIF5B gain-of-function represents a previously unrecognized mechanism that is employed by human lung cancer cells to activate the PD-L1 immune checkpoint.



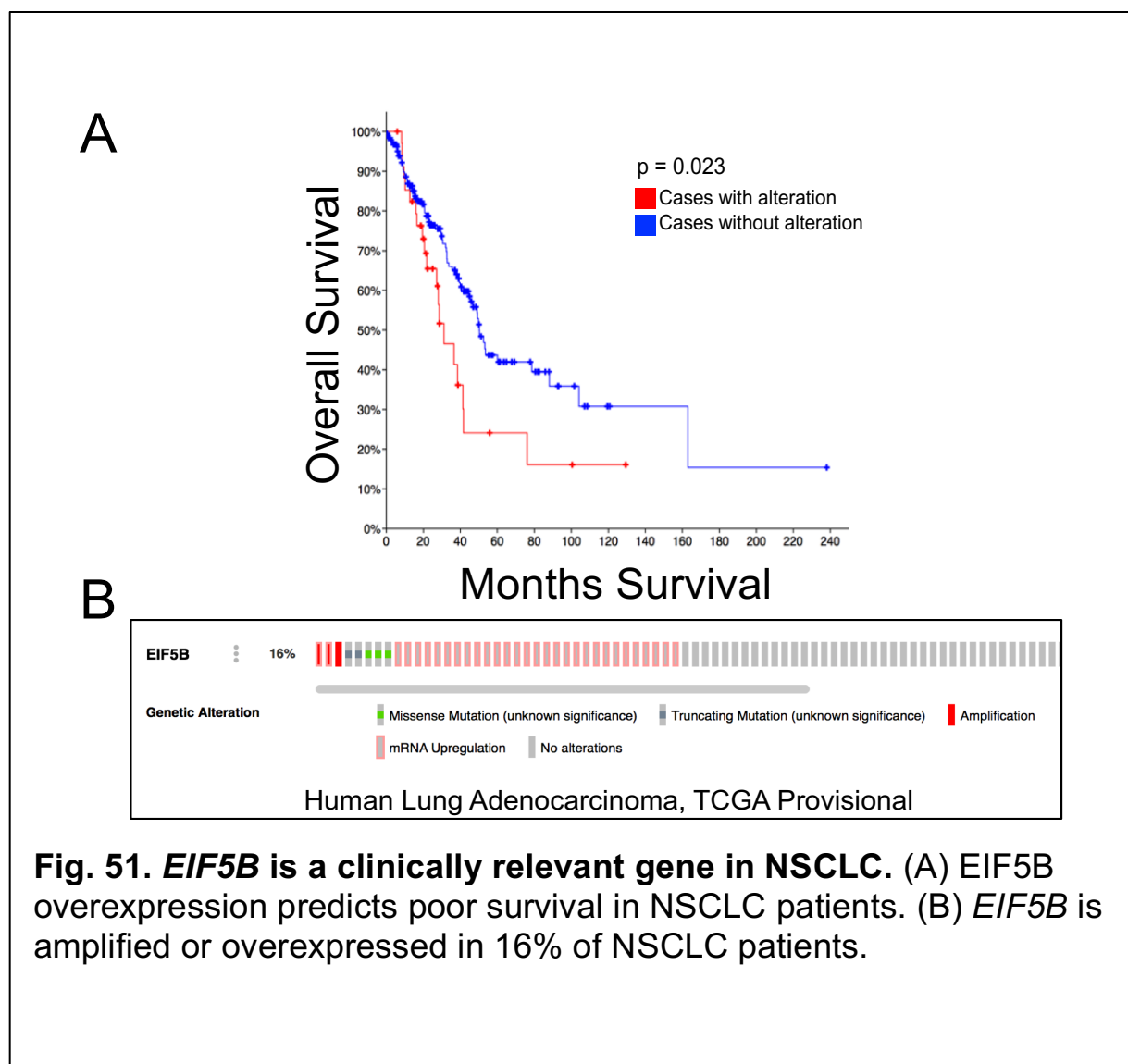
**Fig. 48. EIF2Ai partially rescues PD-L1 in UROD knockout cells.** Western blot analysis of PD-L1 in Control or UROD knockout cells upon EIF2A knockdown.

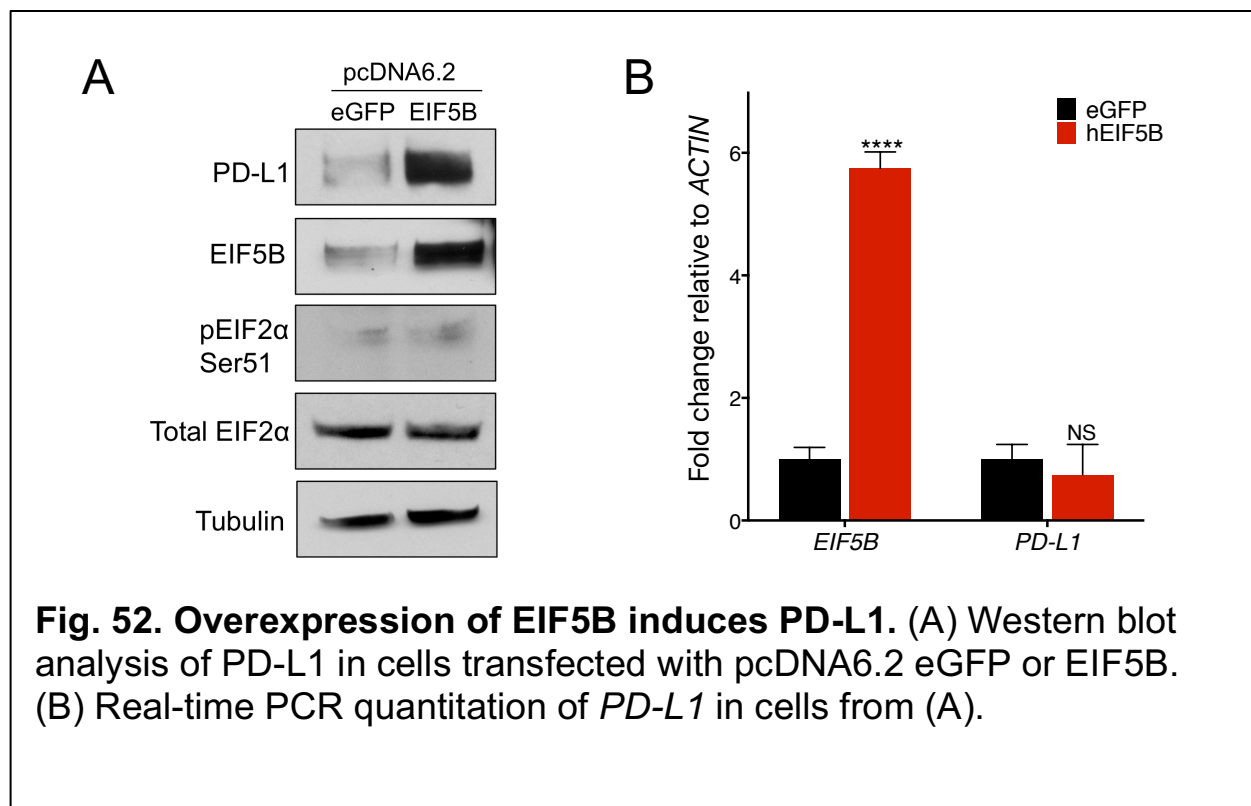


**Fig. 49. EIF2Di has no effect on PD-L1 in UROD knockout cells.** Western blot analysis of PD-L1 in Control or UROD knockout cells upon EIF2D knockdown.



**Fig. 50. EIF5Bi potently rescues PD-L1 in UROD knockout cells.** Western blot analysis of PD-L1 in Control or UROD knockout cells upon EIF5B knockdown.





## Chapter 8: Discussion

Immune checkpoint blockade has emerged as an indispensable modality in cancer therapy. While monoclonal antibodies against the PD-L1/PD-1 axis have been approved as first-line therapy for NSCLC, only ~20% of patients currently respond to the therapy [4, 14, 47]. An open question in the field is thus understanding what factors contribute to resistance to checkpoint blockade in non-responders. Among other factors, PD-L1 expression on tumor cells and in the myeloid compartment, tumor mutational burden as well as presence of infiltrating immune cells are clinically predictive of response to therapy [17]. Moreover, analysis of tumor and immune compartments of non-responders have helped identify important gene expression signatures that enhance immune infiltration and response to checkpoint blockade [196-198]. Additionally, understanding tumor intrinsic mechanisms of PD-L1 checkpoint regulation will be critical for improving patient outcomes [12, 19, 51, 199].

Using an unbiased screening approach, we discovered that impairment of the heme biosynthesis pathway induces PD-L1 expression in lung cancer cells. Heme synthesis is a highly conserved biological pathway, with heme incorporated in several proteins important for cell survival such as mitochondrial complexes, catalases, as well as hemoglobin, a protein critical for erythrocyte function [103]. Thus, heme disruption impedes mitochondrial respiration and proliferation of cells *in vitro* [113, 114]. Heme has been implicated as an important metabolite for survival of cancer cells as well. Inhibition of UROD, a key enzyme in the heme pathway was found to induce oxidative damage and synergize with radiotherapy to promote apoptosis of head and neck cancer cells [200].

Gene amplifications in *UROD* have been observed in head and neck cancers as well as other tumor types [119]. This suggests a pro-tumorigenic role for *UROD* and the heme pathway. However, several observations highlight the contrary and necessitate further studies to understand the role of heme metabolism on tumorigenesis. Firstly, *UROD* amplifications in patient tumor samples do not correlate with patient survival [119]. Secondly, deep deletions of other heme synthetic genes such as *UROS*, *FECH* and *PBGD* are observed in human lung adenocarcinoma (Lung Cancer TCGA Provisional dataset). Thus, it is unclear if dysregulation of heme pathway is clinically advantageous or deleterious to human cancers. Thirdly, most studies examining the consequences of heme deprivation on tumor progression have been performed *in vitro* or in immunodeficient mice. Since tumor cells adapt and evolve *in vivo* in response to their microenvironment, these studies fail to capture the role of heme metabolism in an actual tumor setting. For instance, dysregulation of the heme pathway in the liver leads to elevated levels of hepatic porphyrins, liver damage and an increased incidence of hepatocellular carcinoma [201].

Our study unexpectedly discovered that heme deprivation potently induces the PD-L1 immune checkpoint protein in NSCLC. We showed that heme deficiency in lung cancer cells signals the heme responsive kinase HRI to phosphorylate EIF2 $\alpha$  and activate the ISR pathway. Our data furthermore demonstrates that activation of the ISR pathway promotes PD-L1 translation, thereby suppressing CD8<sup>+</sup> T cells to sustain tumorigenesis *in vivo* (Fig. 53). Recently, another group showed that inhibition of heme synthesis induced metabolic stress and hindered the proliferative capacities of lung cancer cells *in*

*vitro* [129]. In contrast to that, our study demonstrates that activation of ISR upon heme impairment provides lung cancer cells an opportunity to respond to the metabolic stress by slowing down uncontrolled global protein synthesis, but at the same time preferentially enhancing PD-L1 translation to suppress cytotoxic T cells and promote tumorigenesis *in vivo*. Thus, ISR activation upon heme impairment provides a crucial survival mechanism for lung cancer cells in the tumor microenvironment.

In agreement with these results, there is a growing appreciation that the ISR pathway contributes to cancer progression. Prostate cancer cells experiencing proteotoxic stress activate the ISR pathway to sustain growth and promote metastasis [185]. EIF2 $\alpha$  phosphorylation triggers an alternative translation program that promotes oncogene expression in a mouse model of skin squamous carcinoma [158]. While these studies have established a role for ISR in tumor initiation and metastasis, the findings of our work highlight a new role for ISR in immune checkpoint control by regulation the translation of *PD-L1*. Consistent with the findings reported here, uORFs in the mouse PD-L1 5' UTR were shown to suppress translation in *Kras*<sup>G12D</sup>-induced liver tumors [202]. Transgenic expression of MYC in this model results in EIF2 $\alpha$  phosphorylation, resulting in induction of PD-L1 translation and tumor progression [202]. Future studies will involve evaluating if the ISR pathway can induce PD-L1 in myeloid cells of the tumor immune microenvironment. Interestingly, other immune checkpoint proteins such as PD-L2, LGALS9 and LGALS3 were unaffected upon UROD inhibition in human lung cancer cells (Appendix C). The factors that dictate which transcripts are translationally upregulated upon discrete physiological stress cues remains yet to be explored. Additionally, while

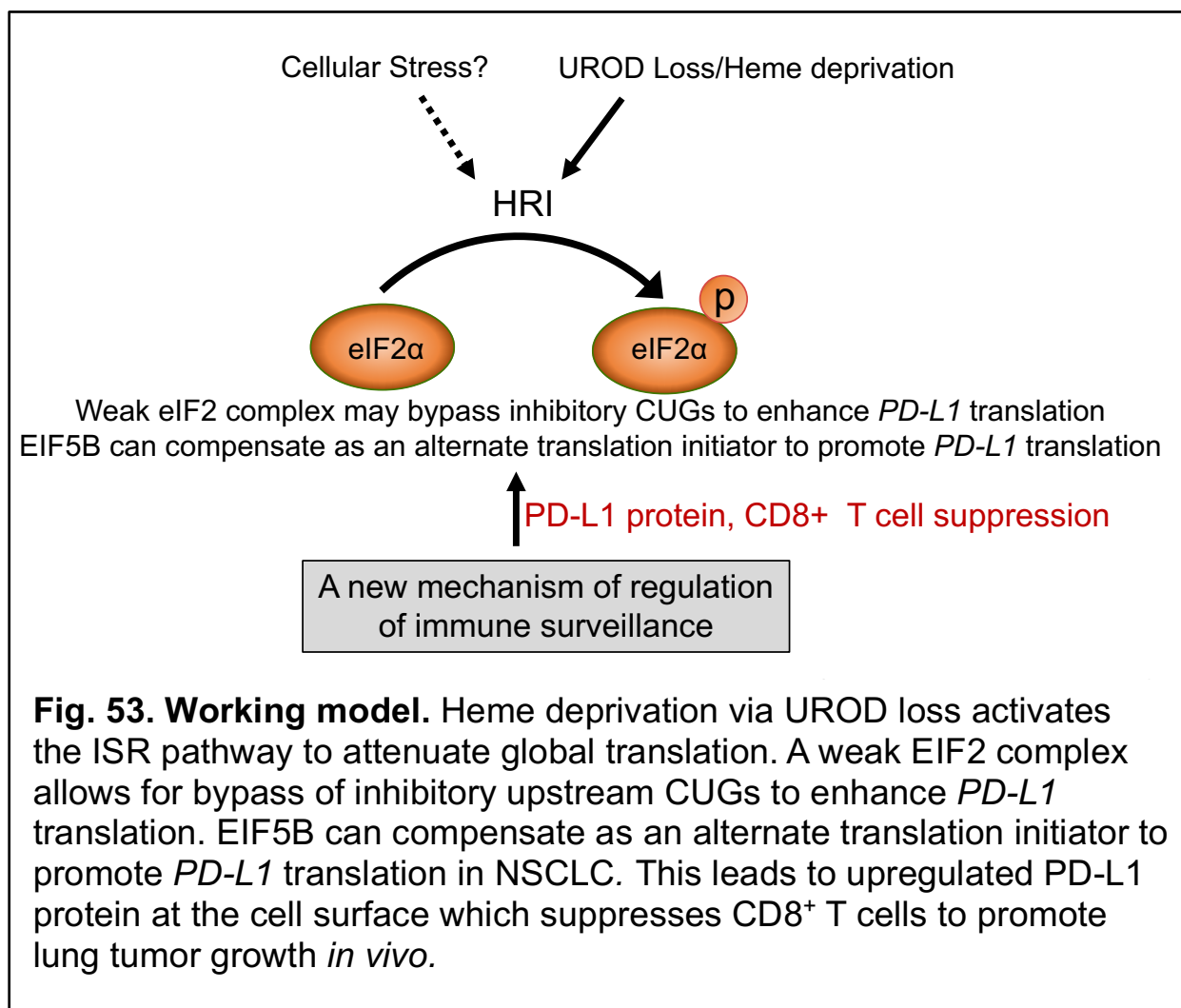
our data show that HRI activates the ISR in response to UROD inhibition, it is important to determine the extent to which other EIF2 $\alpha$  kinases play a role in ISR-mediated PD-L1 translation in NSCLC. Overall, based on these prior findings and the results described here, further investigation of the prevalence, consequences and targeting the ISR in cancer will be an important priority for future work.

The ISR pathway-targeting drug ISRIB induces cytotoxicity in patient derived xenografts in immunocompromised mice [179, 185]. Our data show that ISRIB also suppresses PD-L1 protein levels in the setting of ISR pathway activation in lung cancer cells, suggesting that ISR pathway inhibition may induce anti-tumor immunity alone or in combination with existing immunotherapies. Recently, another novel ISR inhibitor called 2BAct, with better pharmacokinetics than ISRIB, was shown to inhibit ISR mediated neurodegeneration in mice [180]. Future directions include assessing the ability of 2BAct in inducing anti-tumor immunity in mouse models of lung cancer.

Perhaps even more importantly, our data pinpoint the alternative initiation factor EIF5B as a key mediator of ISR-dependent *PD-L1* translation (Fig. 53). Strikingly, EIF5B overexpression, a frequent event in lung adenocarcinoma patients that portends poor survival, was sufficient to potently increase PD-L1 levels in lung cancer cells, even in the absence of ISR. A recent study suggests that EIF5B and EIF2A interact and mediate EIF2 $\alpha$ -independent translation [170]. This may explain why EIF2A knockdown partially rescues PD-L1 in UROD knockdown cells (Fig. 48); wherein EIF2A and EIF5B may be cooperating to mediate translation of PD-L1 in UROD knockdown cells. Surprisingly, we observed that UROD knockout cells had elevated EIF5B protein levels (Fig. 50). We

speculate that inhibition of UROD induces EIF5B through an unknown mechanism to compensate for the impaired EIF2 $\alpha$  dependent translation in NSCLC. How EIF5B is induced or recruited to promote translation initiation under ISR is a future question to be investigated. While the canonical function of EIF5B is in joining of the large and small ribosomal subunits, EIF5B was recently found to be directly bound to Met-tRNA<sup>Met</sup> under hypoxia and shown to be a key driver of translation of anaerobic mRNAs [166]. Thus, additional contexts such as hypoxic stress may engage this mechanism to activate PD-L1 in cancer cells.

Our findings highlight the importance of future studies to examine the complete translational program orchestrated by EIF5B as a translation initiator in cancer. Our data, taken together with the clinical correlates of EIF5B expression and lung cancer patient survival leads us to hypothesize that EIF5B may promote translation of oncogenic mRNAs in lung cancer. Functional studies of EIF5B dysregulation on lung tumorigenesis via gain and loss of function experiments will further shed light on the role of EIF5B as an oncogene in NSCLC. Additionally, since EIF5B is an enzyme, chemical library screens to identify inhibitors of this enzyme is another exciting avenue to be pursued, to explore its potential as a therapeutic target in NSCLC.



## Chapter 9: SRC-2 in liver cancer

### 9.1 Introduction

#### 9.1.1 Human Liver Cancer

Hepatocellular carcinoma (HCC) is the fifth most common solid tumor and the second leading cause of cancer-related deaths [203, 204]. Liver tumorigenesis usually occurs in settings of chronic liver disease, such as ongoing inflammation, cirrhosis, or glycogen storage disease [203]. Previous studies have described genomic alterations in human HCC, with recurrent loss of the *TP53* and *Retinoblastoma RB* tumor suppressor genes, and amplification or overexpression of the *MYC* oncogene in 40-60% of HCCs [205]. Despite this wealth of data, the critical genes and pathways that contribute to HCC development are incompletely understood. Early stage HCC is surgically resected (partial hepatectomy) and/or subject to chemoembolization. Currently, the only targeted therapies for late-stage HCC are the multi-kinase inhibitors Sorafenib and Regorafenib [203, 204, 206, 207]. However, they only modestly significantly improve the survival of HCC patients [206]. Nivolumab, the PD-1 blockade therapy was approved in 2017 for HCC patients who progressed on targeted therapy but the median survival still remains a clinical outcome worth improving [208]. Thus, a better understanding of the mechanisms underlying HCC initiation and progression may accelerate the development of novel therapeutic strategies.

### 9.1.2 Mouse models of liver cancer

Mouse models of liver cancer involve genetically engineered mice (GEM), carcinogen induced models and implantation models [209-211]. Since HCC is often thought to be a step-wise progression involving various genetic and epigenetic changes, GEM models have been developed where activation of common oncogenes or inactivation of tumor suppressors in HCC can induce tumor formation. Additionally, mice expressing fragments of Hepatitis B/Hepatitis C virus have also been developed to study virus induced liver cancer [210, 212]. Liver specific deletion of *p53* was found to induce tumors in 14 months [213]. An additional deletion of *Phosphatase and Tensin Homolog (PTEN)* led to tumors as early as 4 months in mice [209]. Recently, liver specific somatic deletions of *P53* and *PTEN* was performed utilizing CRISPR-Cas9 delivery to hepatocytes via rapid hydrodynamic tail vein injection [214]. This technique has proved to be a quick and powerful method to ensure high expression of transgene in the liver. In contrast to inactivation of tumor suppressors, overexpression or amplification of *MYC* oncogene is a common event in human HCCs [215]. Mouse models using tetracycline-controlled transcriptional activation of *MYC* have been developed [216]. The transcription factor *E2F1* is also commonly found overexpressed in HCC, and transgenic mice overexpressing *E2f1* and *Myc* develop HCC more rapidly and with a higher frequency than mice over-expressing *Myc* alone [217].

Alternatively, stem cell transduction can be used to induce HCC in a healthy liver. This may be more accurate model of HCC progression because the tumor microenvironment is genetically wildtype and only the tumor cells have the mutation

driving cancer. Hepatoblasts isolated from fetal livers are retrovirally transduced to introduce specific mutations and transplanted intra-splenically into recipient mice, allowing for HCC from the induced stem cells [218, 219]. Besides GEMs, carcinogen-induced liver cancer offers a complementary system to study HCC progression as induced by environmental challenges. Diethylnitrosamine (DEN), a DNA alkylating agent, is commonly used to induce HCC, which shows the disease progression from hyperplastic nodules, adenoma and finally resulting in HCC [73, 209, 220].

Implantation models on the other hand offer a rapid and reproducible method to study growth of liver cancer cells *in vivo*. This may involve subcutaneous or orthotopic injection of human or mouse liver cancer cells. To study tumor-immune interactions, syngeneic models are preferred. In contrast, human xenograft models use human cancer cell lines such as HepG2, Hep3B and Huh7 or primary tumors freshly isolated from patients in immunocompromised mice such as athymic nude mice or non-obese-diabetic-severe combined immunodeficient mice [221].

### **9.1.3 SRC-2, a master regulator of transcriptional coactivation**

The *Sleeping Beauty* (*SB*) DNA transposon system was previously used to identify mutations that cooperate with MYC to accelerate liver tumorigenesis in mice [73]. This led to the identification of Steroid Receptor Coactivator 2 (SRC-2, also known as NCOA2, TIF2, GRIP1) as a novel gene that functions to restrain MYC-induced liver cancer. SRC-2 belongs to the Steroid Receptor Coactivator family (SRC-1,2 and 3) and encodes a transcriptional coactivator that cooperates with nuclear receptors (NRs) to control multiple

physiological processes including glucose homeostasis, energy metabolism, and reproduction [222-231]. The SRC family share five fundamental motifs [232]. Of these, the N-terminal basic helix loop helix domain is highly conserved and essential for protein-protein interactions. The middle region of SRC proteins contain a highly conserved LXXLL (X=any amino acid) motif which is essential for nuclear receptor interaction and activation. The C-terminus contains activation domains that bind CBP/p300 to regulate histone acetylation [233]. Mice with whole-body or liver-specific deletion of *Src-2* develop glycogen storage disease Type 1 (Von Gierke's disease), and exhibit decreased expression of the SRC-2 target *Glucose 6 phosphatase (G6pc)* [223]. Interestingly, a significant fraction of patients with Von Gierke's disease develop hepatic adenomas and are susceptible to developing HCC [234].

#### **9.1.4 SRC-2 and human cancer**

A transposon mutagenesis screen previously identified SRC-2/NCOA2 as a novel tumor suppressor gene in MYC mediated liver tumorigenesis [73]. Several observations from previous studies suggested a tumor suppressive role for SRC-2 in liver cancer. Inhibition of *Src-2* using shRNAs promoted tumor formation by mouse hepatoblasts in immunocompromised mice [73]. Furthermore, deletion of *Src-2* predisposed mice to diethylnitrosamine (DEN)-induced liver tumorigenesis. Nevertheless, multiple observations suggest that further functional studies are required to establish whether SRC-2 is a bona fide tumor suppressor in liver cancer. For instance, copy number gains of SRC-2 are frequent in liver cancer although this is likely due to the proximity of this

gene to the *MYC* gene on chromosome 8q [235-237]. A recent study demonstrated that SRC-2 promotes lipogenesis and enhanced cell survival and metastasis in prostate cancer [238]. Another study implicates SRC-2 in maintaining EMT in breast cancer [239]. Additionally, SRC-2 was required for proliferation of endometrial cancer cells [240]. This suggests a tissue-specific and context-dependent role for SRC-2 in tumorigenesis. Thus, to definitively test the tumor suppressive role of SRC-2 in liver cancer, we assessed the consequences of genetic ablation of *Src-2* in a MYC-induced liver cancer mouse model.

## 9.2 Materials and methods

### Cell culture

HepG2 and Huh7 cells were cultured in Dulbecco's Modified Eagle Medium (GIBCO) supplemented with 10% FBS (Invitrogen) and 1% Penicillin/Streptomycin (Invitrogen). Huh7 and HepG2 cells were a gift from Hao Zhu (UT Southwestern Medical Center).

### Animals

The Institutional Animal Care and Use Committee (IACUC) of UT Southwestern Medical Center approved all procedures involving mice. *Src-2<sup>-/-</sup>* mice were obtained from Pierre Chambon and maintained on a mixed C57BL/6J and 129sV background. LAPtTA and tet-O-MYC mice were obtained from Dean Felsher and maintained on a FVB/NJ background. Simultaneously, *Src-2<sup>+/-</sup>* mice were bred with tet-o-MYC and LAPtTA mice to generate *Src-2<sup>+/-</sup>*; tet-o-MYC and *Src-2<sup>+/-</sup>*; LAPtTA mice, respectively. In the final cross, *Src-2<sup>+/-</sup>*; LAPtTA females were bred with *Src-2<sup>+/-</sup>*; tet-o-MYC males to obtain tet-o-MYC;

LAPtTA mice with all 3 alleles of *Src-2* (WT, heterozygous, or homozygous null). The MYC transgene is on chromosome Y, precluding analysis of females.

### Plasmids

The following plasmids were used: TRC shRNA for *SHP* (UT Southwestern core facility, Jerry Shay laboratory V2LHS\_239330, V2LHS\_72556); TRC shRNA constructs for *DKK4* (GE Dharmacon RHS4430-200191360 V2LHS\_197942 RHS4430-200173366 V2LHS\_204025); GIPZ shRNA for *CADM4* (GE Dharmacon V3LHS\_375253, V3LHS\_375254); GIPZ shRNA for *SRC-2* (GE Dharmacon V2LHS\_199063, V2LHS\_357381). pLJM1-EGFP was a gift from David Sabatini (Addgene plasmid # 19319), and pLX304, which also harbors a V5 tag, was a gift from David Root (Addgene plasmid # 25890). A human *SHP* plasmid was a gift from Steven Kliewer (UT Southwestern Medical Center); pCMX-FXR and h*SHP*-LUC plasmids were a gift from David Mangelsdorf (UT Southwestern Medical Center). A *SHP* $\Delta$ 215-569-LUC deletion mutant construct lacking the FXR response element was generated by PCR amplification as previously described. The pHRL-SV40 Renilla reporter plasmid was a gift from Joshua Mendell (UT Southwestern Medical Center).

### Liver tumor analysis

Whole liver was dissected from euthanized mice, washed, and placed in ice-cold PBS. At the time of dissection, images were captured of both the dorsal and ventral sides of the intact liver, and estimated the mean percent tumor burden for each mouse using NIH

Image J software. The surface area of the liver tumors was measured as well as the total surface area (including normal liver and all tumors). For percent tumor burden calculation, the surface area of the liver tumors was divided by the total surface area (including normal liver and tumors) and then multiplied by 100. For histological analysis, tissues were fixed in 10% formalin, embedded in paraffin, and sectioned. Hematoxylin and eosin (H &E) and Periodic acid-Schiff (PAS) staining were performed on normal liver and liver tumor tissues at the Pathology Core, UT Southwestern Medical Center.

### **RNA extraction and qRT-PCR analysis**

Total RNA was isolated from liver tumors and normal tissues using Trizol (Invitrogen) followed by additional cleanup and DNase digestion using the RNeasy Mini Kit (Qiagen). Total RNA was isolated from cells using only the RNeasy Mini Kit (Qiagen). For qRT-PCR of mRNA, cDNA synthesis was performed with 1 µg RNA for reverse transcription using Superscript III First Strand synthesis kit (Invitrogen). mRNA expression was assessed using quantitative real-time PCR with a 2X SYBR Green Master Mix (R&D Systems). mRNA levels were normalized to  $\beta$ -actin mRNA expression, with gene expression levels measured using a standard curve for each set of primers crossing exon-exon junctions for each gene. All PCR assays were performed in triplicate. PCR primers are shown below in Table 3.

**Table 3. Quantitative real-time PCR primer sequences**

<b>Gene</b>	<b>Sequence</b>	<b>Exon-exon junction</b>
<i>Thbs1</i>	5'-GCATCTTCACCAGGGATCTG-3'	3-4 Forward
<i>Thbs1</i>	5'- CTGGGGTGGTTCCAAGAC -3'	3-4 Reverse
<i>Thbs4</i>	5'- TCCTCAAGTGACAACAGCAA -3'	2-3 Forward
<i>Thbs4</i>	5'- GTTGAACACCACCAGATGGA -3'	2-3 Reverse
<i>Cadm4</i>	5'- ACGATGGGTCCATAGTCGTC -3'	2-3 Forward
<i>Cadm4</i>	5'- GATCTGATGGTGGGTGTCCT -3'	2-3 Reverse
<i>Cldn7</i>	5'- CTGTGGGGGAGATGACAAAG -3'	2-3 Forward
<i>Cldn7</i>	5'- TGACAATCTGATGACCAATCC -3'	2-3 Reverse
<i>Cldn4</i>	5'- ATGGTCATCAGCATCATCGT -3'	2 Forward
<i>Cldn4</i>	5'- CATGATCTTGGCCTTGACG -3'	2 Reverse
<i>Gadd45b</i>	5'- CCTCACCGTGGGGGTGTA -3'	2-3 Forward
<i>Gadd45b</i>	5'- TCTGCAGAGCGATATCATCC-3'	2-3 Reverse
<i>Gramd4</i>	5'- GAGACGAGATCCCCCTGAA -3'	2-3 Forward
<i>Gramd4</i>	5'- GTCCTGTTGAAGTCCTGCAC -3'	2-3 Reverse
<i>Unc5b</i>	5'- GGAGCTCTTCGGGAACTACC -3'	3-4 Forward
<i>Unc5b</i>	5'- GCAGAAGGACCTCATGATCC -3'	3-4 Reverse
<i>Eda2r</i>	5'- CCAAGAATGCATCCCATGTA -3'	5-6 Forward
<i>Eda2r</i>	5'- AGTGCAACAAGTGTGGCTTC -3'	5-6 Reverse
<i>G6pc</i>	5'- GCGCAGCAGGTGTATACTATG -3'	3-4 Forward
<i>G6pc</i>	5'- GCTGCACAGCCCAGAATC -3'	3-4 Reverse
<i>Pck1</i>	5'- GACTTTGAGAAAGCATTCAACG -3'	3-4 Forward
<i>Pck1</i>	5'- GCGAGTCTGTCAGTTCAATACC -3'	3-4 Reverse

<i>Scd1</i>	5'- AAAGAGAAGGGCGGAAAAC -3'	4-5 Forward
<i>Scd1</i>	5'- GTGGGCAGGATGAAGCAC -3'	4-5 Reverse
<i>Acacb</i>	5'- CCGTAATGAACGTGCCATC -3'	4-5 Forward
<i>Acacb</i>	5'- TATTGGGTCCTCCTGGGACA -3'	4-5 Reverse
<i>Masp1</i>	5'- GATTTCTCCAATGAGGAACGA -3'	3-4 Forward
<i>Masp1</i>	5'- GGTCACAGGACAGCTCTTCA -3'	3-4 Reverse
<i>Cd24a</i>	5'- CTAGGGCTGGGGTTGCTG -3'	1-2 Forward
<i>Cd24a</i>	5'- GGATTTGGGGAAGCAGAAAT -3'	1-2 Reverse
<i>Ccl24</i>	5'- AATTCCAGAAAACCGAGTGG -3'	2-3 Forward
<i>Ccl24</i>	5'- AGCAGCTTGGGGTCAGTACA -3'	2-3 Reverse
<i>C1rb</i>	5'- CTTCTGTTCTGCCATCCTG -3'	4-5 Forward
<i>C1rb</i>	5'- GGCTGGAGACATAGCCTGAG -3'	4-5 Reverse
<i>Bmp2</i>	5'- AAGTCAGTGGGAGAGCTTCG -3'	3- Forward
<i>Bmp2</i>	5'- GAGACACCTGGGTTCTCCTCT -3'	3- Reverse
<i>Vegfc</i>	5'- CTACAGATGTGGGGTTGCT -3'	3-4 Forward
<i>Vegfc</i>	5'- GACTGGTTTGGGGCCTTG -3'	3-4 Reverse
<i>Fgf1</i>	5'- GGGGCCACTTCTTGAGGAT -3'	2-3 Forward
<i>Fgf1</i>	5'- CCGGTCTCCGTACCCTTTAT -3'	2-3 Reverse
<i>Gdf10</i>	5'- CTCTCCCAAATCCTTTGACG -3'	2-3 Forward
<i>Gdf10</i>	5'- CACAGCTCTGACGATGCTCT -3'	2-3 Reverse
<i>Shp</i>	5'- AGCTGGGTCCCAAGGAGTAT -3'	1-2 Forward
<i>Shp</i>	5'- AGCCTCCTGTTGCAGGTGT -3'	1-2 Reverse
<i>Dkk4</i>	5'- GCCAGCAGAGGAAAACAGAC -3'	3-4 Forward
<i>Dkk4</i>	5'- AGGGCCACAGTCAGAGGTT -3'	3-4 Reverse

<i>Thrsp</i>	5'- ACGGAGCCCCTGATCTCTAT-3'	1-2 Forward
<i>Thrsp</i>	5'- TTTCGTTGCCAGCCACCT-3'	1-2 Reverse
<i>NR0B2</i>	5'- GCTTAGCCCCAAGGAATATG-3'	1-2 Forward
<i>NR0B2</i>	5'- CCAGTGAGCCTCCTGCTG-3'	1-2 Reverse
<i>DKK4</i>	5'- AGGAGGTGCCAGCGAGAT-3'	1-2 Forward
<i>DKK4</i>	5'- TTGCTCATCAAGCTGCCTTT-3'	1-2 Reverse
<i>THRSP</i>	5'- AAGGCCATCTGTGTGGATGT-3'	1- Forward
<i>THRSP</i>	5'- GCACTCTCGTCCTCGACTTC-3'	1- Reverse
<i>CADM4</i>	5'- CGAGGCGTCCAATAAGCAC-3'	2-3 Forward
<i>CADM4</i>	5'- CACAATGGCATAGGGAACC-3'	2-3 Reverse
<i>SRC2</i>	5'- CGCAGCATGAAGGAGAATC -3'	9-10 Forward
<i>SRC2</i>	5'- GCAACAAGAGTGCCATCAGA -3'	9-10 Reverse
<i>CCND1</i>	5'- CCTGTCCTACTACCGCCTCA-3'	4-5 Forward
<i>CCND1</i>	5'- TGA CTCCAGCAGGGCTTC-3'	4-5 Reverse
<i>mActin</i>	5'-CGGTTCCGATGCCCTGAGGCTCTT-3'	4-5 Forward
<i>mActin</i>	5'-CGTCACACTTCATGATGGAATTGA-3'	4-5 Reverse
<i>hACTIN</i>	5'-ATTGCCGACAGGATGCAGAA-3'	5-6 Forward
<i>hACTIN</i>	5'-ACATCTGCTGGAAGGTGGACAG -3'	5-6 Reverse

## RNA sequencing and gene ontology analysis

RNA sequencing was performed in the McDermott Center Sequencing Core at UTSW Medical Center. RNA was extracted from tet-o-MYC; LAPtTA; *Src-2*<sup>+/+</sup> and tet-o-MYC; LAPtTA; *Src-2*<sup>-/-</sup> liver tumors. Four µg of total DNase treated RNA was prepared with the TruSeq Stranded Total RNA LT Sample Prep Kit from Illumina. Poly-A RNA was purified and fragmented before strand specific cDNA synthesis. cDNA was A-tailed and indexed adapters were ligated. Samples were PCR amplified and purified with AmpureXP beads and validated on the Agilent 2100 Bioanalyzer. Samples were quantified by Qubit (Invitrogen) prior to normalization and pooling. Sequencing was performed on an Illumina HiSeq 2500 to generate 51-bp single end reads. Reads were trimmed to remove low-quality regions in the ends.

Trimmed reads were mapped to the mouse genome (mm10) using TopHat v2.0.1227. Alignments with mapping quality less than 10 were discarded. Expression abundance estimation and differential expression analysis were carried out using Cufflinks/Cuffdiff (v2.1.1) software. Genes with the nominal p-value cutoff of 0.05 were considered significantly differentially expressed between the tet-o-MYC; LAPtTA; *Src-2*<sup>+/+</sup> and tet-o-MYC; LAPtTA; *Src-2*<sup>-/-</sup> liver tumors. Gene Ontology analysis was performed using the DAVID Functional Annotation tool on differentially expressed genes between the tet-o-MYC; LAPtTA; *Src-2*<sup>+/+</sup> and tet-o-MYC; LAPtTA; *Src-2*<sup>-/-</sup> liver tumors to identify biological processes specifically enriched in the *Src-2*<sup>-/-</sup> group. Biological processes were assessed for statistical significance ( $p < 0.05$ ). (<http://david.abcc.ncifcrf.gov/>)

**ChIP-Seq**

ChIP-Seq for SRC-2 (at CT4) was performed by Active Motif, Inc. (Carlsbad, CA) as previously described with no additional filtering. Briefly, mouse liver samples were submerged in PBS containing 1% formaldehyde, cut into small (~1 mm<sup>3</sup>) pieces with a razor blade and incubated at room temperature for 15 minutes. Fixation was stopped by the addition of 0.125M glycine (final concentration). The tissue pieces were then treated with a TissueTearer and finally spun down and washed twice in PBS. Chromatin was isolated by the addition of lysis buffer, followed by disruption with a Dounce homogenizer. Lysates were sonicated and the DNA was sheared to an average length of 300±500 bp. Genomic DNA (Input) was prepared by treating aliquots of chromatin with RNase, Proteinase K and heated for reverse-crosslinking, followed by ethanol precipitation. Pellets were resuspended and the resulting DNA was quantified on a NanoDrop spectrophotometer. An aliquot of chromatin (30 µg) was precleared with protein A agarose beads (Invitrogen). Genomic DNA regions of interest were isolated using 4 µg of antibody. Complexes were washed, eluted from the beads with SDS buffer, and subjected to RNase and proteinase K treatment. Crosslinking was reversed by incubation overnight at 65°C, and ChIP DNA purified by phenol-chloroform extraction and ethanol precipitation. Illumina sequencing libraries were prepared from the ChIP and input DNAs by the standard consecutive enzymatic steps of end-polishing, dA-addition, and adaptor ligation. After a final PCR amplification step, the resulting DNA libraries were quantified and sequenced on Illumina NextSeq 500 (75 nt reads, single-end).

### **ChIP-Seq peak calling and data normalization**

The sequences identified were mapped to the mouse genome (NCBI37/UCSC mm9) using BOWTIE function in Galaxy. Only the sequences uniquely mapped with no more than 2 mismatches were kept and used as valid reads. PCR duplicates were also removed. Peak calling was carried out by MACS (version 1.4.2 20120305) in Galaxy/Cistrome (options  $\text{fold } 10, 30$   $\text{pvalue } 1 \times 10^{-5}$ ), on each ChIP-Seq file against the matching input file. To account for the different sequencing depths between samples, the signal files generated from MACS were normalized to sequencing depth. The peak summits were used as the binding site centers, and the normalized signal files were used as the binding strength for further analysis. Assigning peaks to a given gene was performed with the Genomic Regions Enrichment of Association Tool (version 3.0.0) using the basal plus extension setting.

### **Western blotting**

Cells and tissues were lysed in RIPA buffer and then homogenized using a Bioruptor sonicator (Diagenode). Proteins were quantified using the Bicinchoninic Acid (BCA) assay (ThermoScientific) and subject to separation by using NuPage Bis-Tris gels (Invitrogen) for electrophoresis. The proteins were subsequently transferred to a nitrocellulose membrane. The membranes were blocked for 1 hour at room temperature and subsequently probed with primary antibodies overnight at 4°C. After incubating the membrane with the appropriate secondary antibody conjugated to horseradish peroxidase, protein levels were detected with SuperSignal Dura substrate (Thermo

Scientific). Primary antibodies were prepared in 5% Milk or BSA in TBST. Antibodies were purchased from the following sources: SRC-2 (BD Biosciences, 1:250); DKK4 (Abgent, 1:1000); CADM4 (Neuromabs, 1:500); THRSP (Santa-cruz, 1:500); FXR (Santa Cruz, 1:50). SHP overexpression was detected with a V5 antibody (Invitrogen, 1:5000).

### **shRNA mediated depletion**

Human Embryonic Kidney 293T (HEK 293T,  $1 \times 10^8$ ) cells were co-transfected with pLKO shRNA constructs (TRC, GE Dharmacon), and PAX2, MD2 helper plasmids using Lipofectamine 2000 (Life technologies). Following transfection, the lentiviral supernatant was collected, filtered and supplemented with 8ug/ml hexadimethrene bromide (Sigma). Human HCC cell lines Huh7 and HepG2 ( $3 \times 10^5$ ) were infected overnight twice with the viral supernatant and 24h after the second infection transferred into fresh media containing Puromycin (2  $\mu$ g/ml). Cells were selected in puromycin media for at least 7 days and then harvested for RNA or western blot analysis to assess extent of knockdown.

### **Lentiviral overexpression**

To overexpress candidate genes in human HCC cells, human ORFs corresponding to each gene were cloned into the PLX304 or PLJM1 lentiviral plasmids. PLJM-eGFP or PLX303-empty constructs were used as negative controls. HEK 293T cells ( $1 \times 10^8$  cells) were then co-transfected with lentiviral overexpression or control constructs and helper plasmids PAX2 and MD2 using Lipofectamine 2000 (Life Technologies). Following transfection, the lentiviral supernatant was collected, filtered and supplemented with 8

$\mu\text{g/ml}$  hexadimethrine bromide (Sigma). Human Huh7 cells ( $3 \times 10^5$ ) were infected overnight twice with the viral supernatant and 24h after the second infection transferred into fresh media containing blasticidin ( $4 \mu\text{g/ml}$ ) or puromycin ( $2 \mu\text{g/ml}$ ). Control cells and cells overexpressing SRC-2 or SRC-2 target genes were selected in antibiotic-containing media for at least 7 days and then harvested for RNA and western blot analysis to assess overexpression.

### **Xenograft assays**

Human HCC cells ( $3 \pm 5 \times 10^6$ ) expressing shRNA lentiviruses or lentiviruses overexpressing candidate genes in PBS were injected subcutaneously into both the left and right flanks of 6-week-old immunocompromised athymic nude mice (Charles River, strain 490). Tumor volume was measured using calipers every  $3 \pm 4$  days until the average tumor mass reached  $2 \text{cm}^3$ . Tumor volume was calculated using the formula  $(\text{length} \times \text{width}^2)/2$ . A total of five mice were injected per experimental group, corresponding to ten experimental samples per group.

### **Cell proliferation assays**

To measure in vitro proliferation of cells, the CellTiter 96 Aqueous Non-Radioactive Cell Proliferation assay kit (Promega) was used. 1000 cells per well were plated in 96-well plates in triplicate overnight. The MTS/PMS agent was added to the media according to the manufacturer's protocol and incubated at  $37^\circ\text{C}$  for 1.5 hours. Absorbance was then

measured at 490 nm every 24 hours for 6±7 days. All experiments were performed in triplicate and performed at least two times.

### **Nuclear hormone receptor (NR) binding site analysis**

To predict NRs that interact with SRC-2, promoter regions (spanning 10kb on either side) of candidate SRC-2 target genes were screened for NR binding motifs using the NHR scan tool ([http://www.cisreg.ca/cgi-bin/NHR-scan/nhr\\_scan.cgi](http://www.cisreg.ca/cgi-bin/NHR-scan/nhr_scan.cgi)). SRC-2 binding regions in candidate genes were overlapped with predicted NR binding motifs to predict potential SRC-2/NR interactions.

### **Dual luciferase assays**

5 x10<sup>4</sup> Huh7 cells expressing an eGFP control or SRC-2 lentivirus were seeded per well in 12-well plates in triplicate. Cells were transfected 24 hours later using Fugene HD (Promega) with 20 ng FXR plasmid, 80 ng SHP-LUC or SHP $\Delta$ 215-569-LUC reporter plasmids, 1 ng Renilla control reporter plasmid and 199ng pUC19 plasmid to give a total of 300 ng DNA per well. Empty pCMX vector was used as a no receptor control. The same transfection plan was followed for a replicate set of plates for downstream protein analysis by immunoblotting. Cells were lysed 48 h later and luciferase activity was measured in Glo-Max Microplate reader (Promega) using the Dual Luciferase assay reporter system (Promega). Luciferase data was obtained by normalizing Firefly activity to Renilla control activity and fold change induction was calculated relative to activity in eGFP control cells.

## Statistical analysis

A Student t-test was used for comparisons between two groups with normal data distribution (for real time qPCR, MTS, and xenograft assays). A nonparametric method (Wilcoxon Rank Sum test) was used when data were not normally distributed (for the liver tumor burden analysis). In the Wilcoxon Rank Sum test, the *Src-2<sup>+/+</sup>* group served as the reference, and was compared to either the *Src-2<sup>-/-</sup>* or *Src-2<sup>+/-</sup>* groups (multiple comparisons were not adjusted). SAS 9.4 TS Level 1M2 (Cary, NC) was used for data analysis. For survival analysis, survival functions were constructed using Kaplan-Meier method and were compared using the log-rank test.

## 9.3 Results

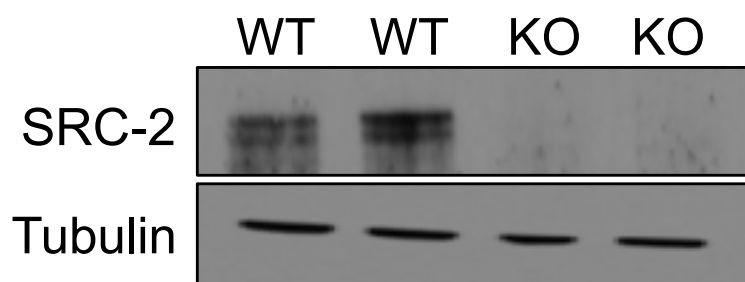
### 9.3.1 Deletion of *Src-2* accelerates MYC-mediated liver tumorigenesis

To first determine whether SRC-2 suppresses MYC-mediated liver cancer *in vivo*, we employed a mouse model of MYC-induced liver cancer. In this model, mice harboring a MYC transgene under the control of a doxycycline-regulatable promoter (tet-o-MYC) are crossed with mice expressing tet-transactivator protein (tTA) driven by the liver-activator protein (LAP) promoter. Removal of doxycycline leads to MYC induction specifically in the liver and development of tumors that resemble human hepatocellular cancer [212, 216]. We bred this mouse model to *Src-2<sup>+/-</sup>* mice and generated tet-o-MYC; LAPtTA animals harboring wild type, heterozygous, or homozygous null alleles of *Src-2* (Fig. 54A). To induce MYC in our experiment, doxycycline was withdrawn at 6 weeks, and

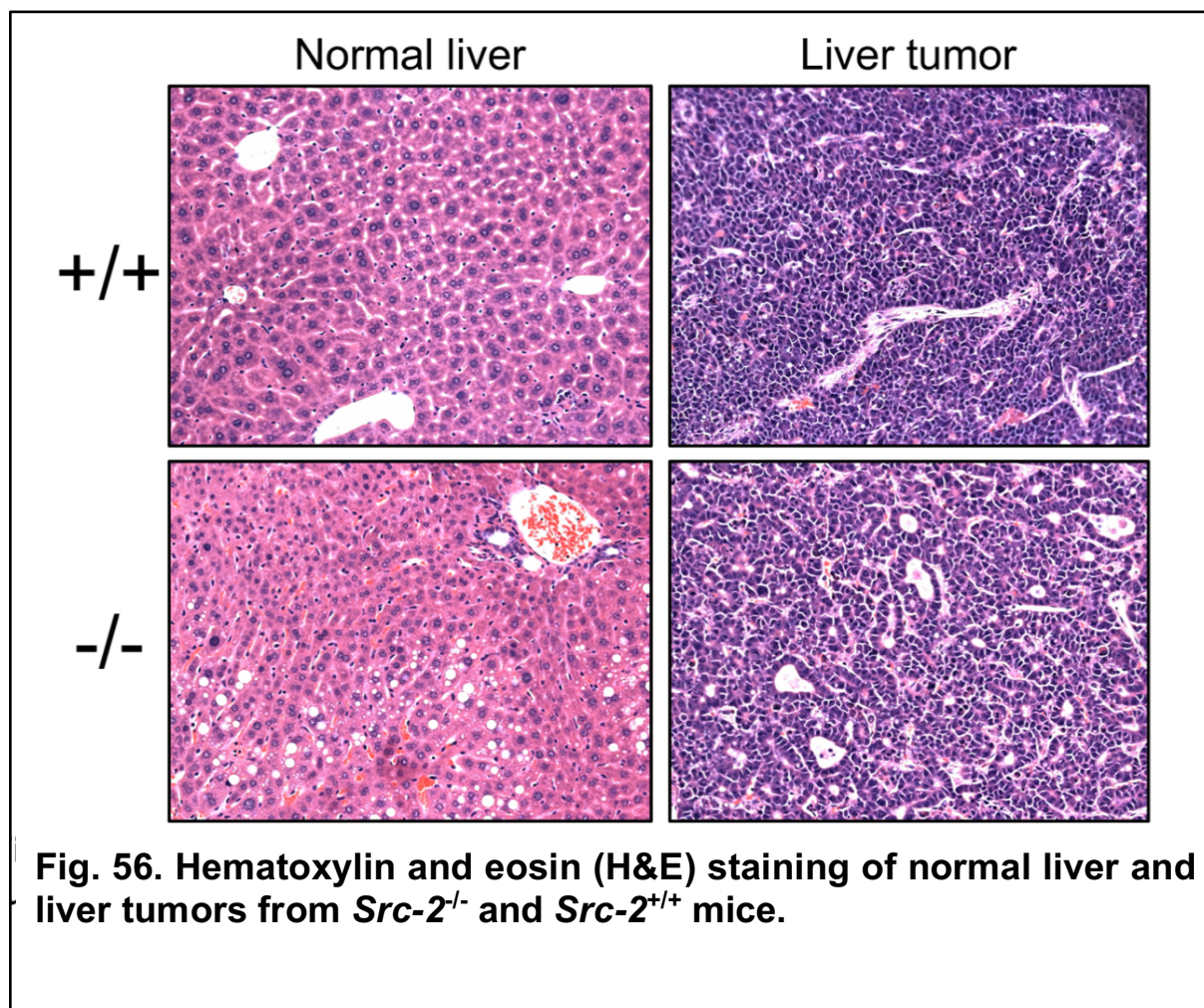
mice were monitored for early-developing tumors (Fig. 54B). All animals were euthanized and dissected at 15 weeks of age (9 weeks after MYC induction).

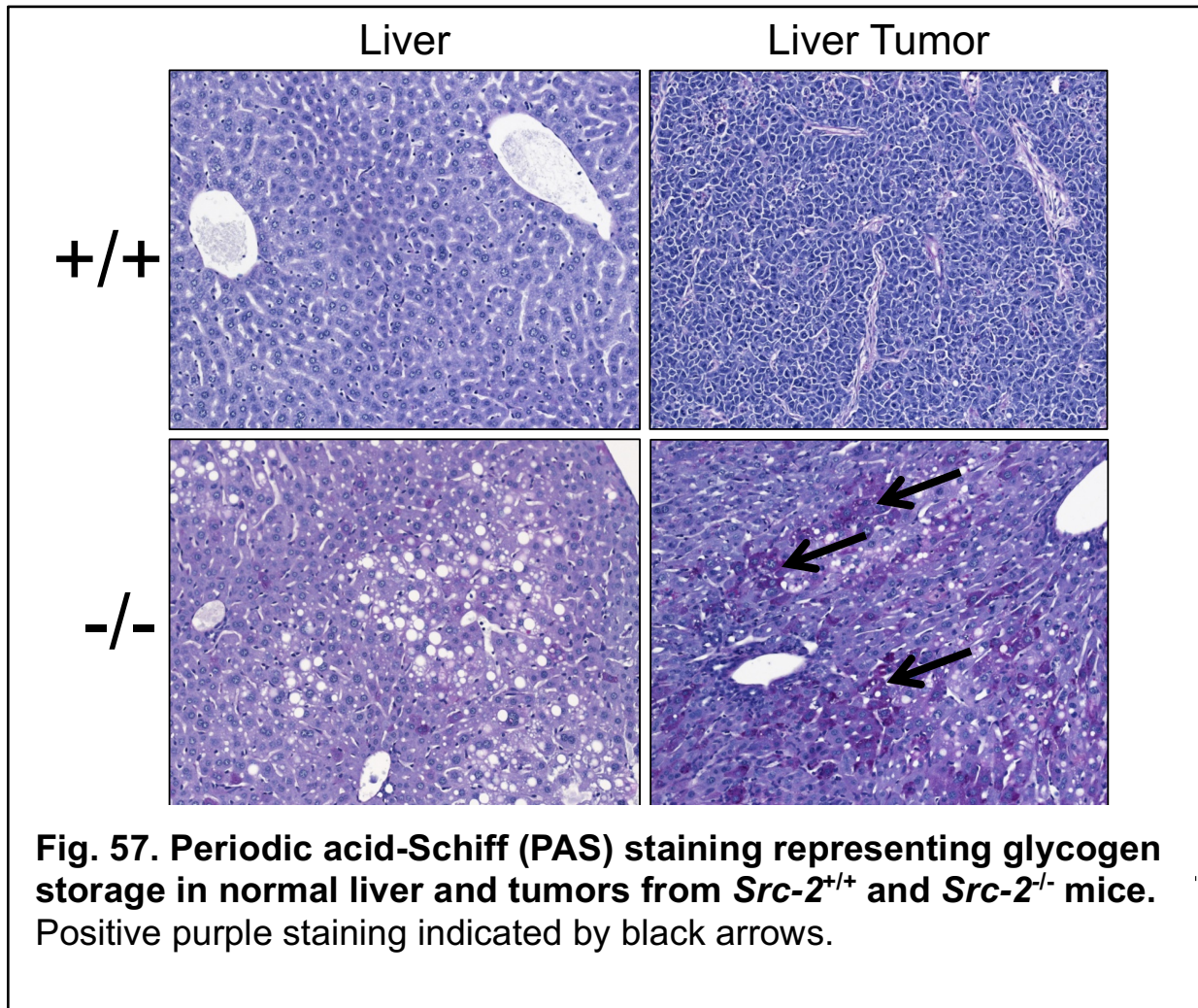
Loss of SRC-2 in the *Src-2<sup>-/-</sup>* mice was confirmed by western blotting with tumor lysates from *Src-2<sup>+/+</sup>* and *Src-2<sup>-/-</sup>* animals (Fig. 55). Histologic analysis confirmed that tumors arising in these animals resembled human hepatocellular cancer (Fig. 56). Consistent with prior findings, *Src-2<sup>-/-</sup>* mice displayed an accumulation of glycogen and lipid droplets in both non-neoplastic hepatocytes as well as liver tumors (Fig. 57). Importantly, *Src-2<sup>-/-</sup>* mice exhibited a significant enhancement of liver tumor burden compared to *Src-2<sup>+/+</sup>* animals (Fig. 58). Thus, genetic inactivation of *Src-2* is sufficient to accelerate MYC-mediated liver tumorigenesis, supporting a tumor suppressive role for SRC-2 in liver cancer.





**Fig. 55. Western blot analysis depicting absence of SRC-2 protein in tet-o-MYC; LAPtTA *Src-2* wildtype (WT) or null (KO) mice.**







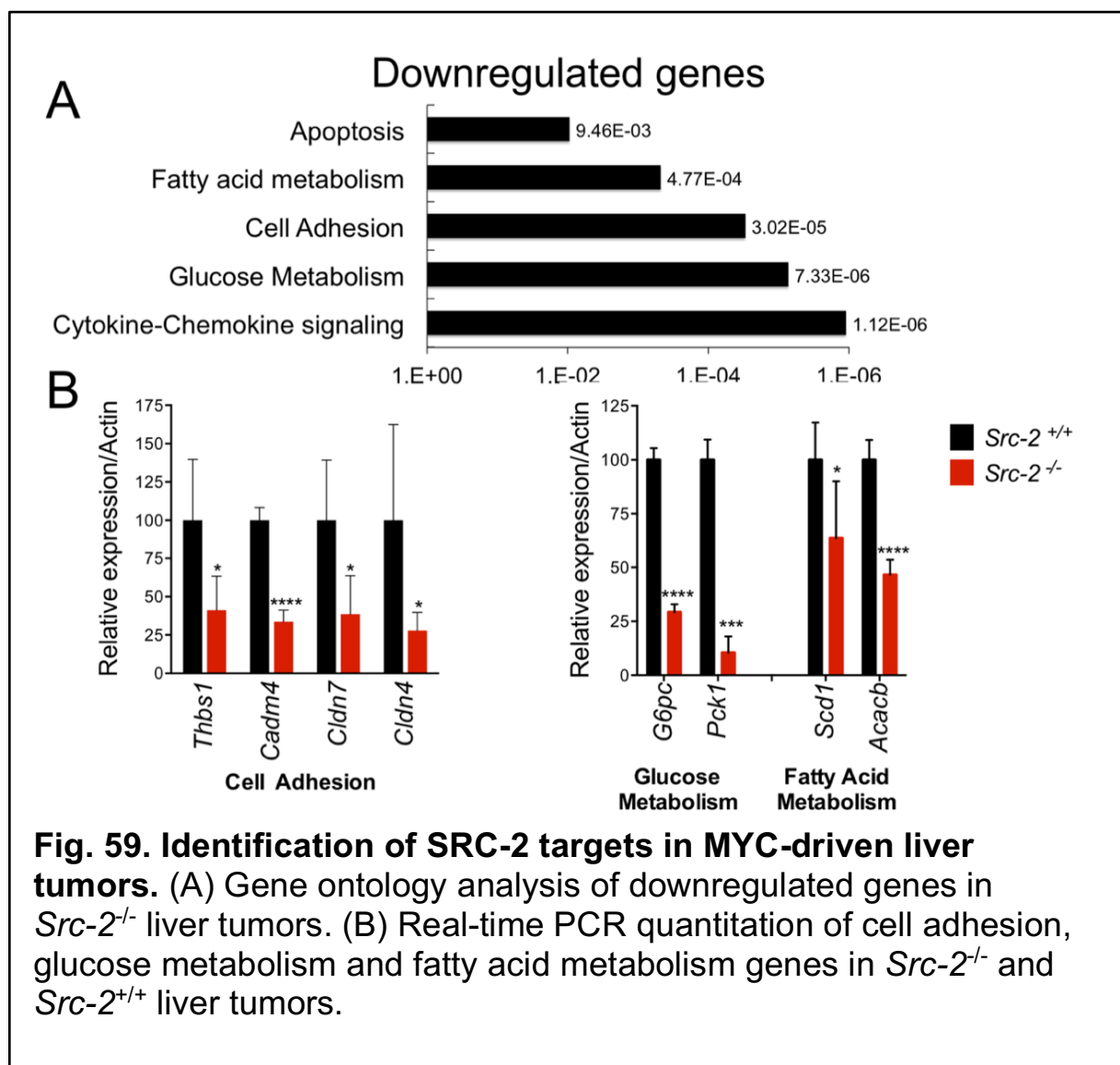
### 9.3.2 Identification of direct SRC-2-regulated transcripts in MYC-induced liver

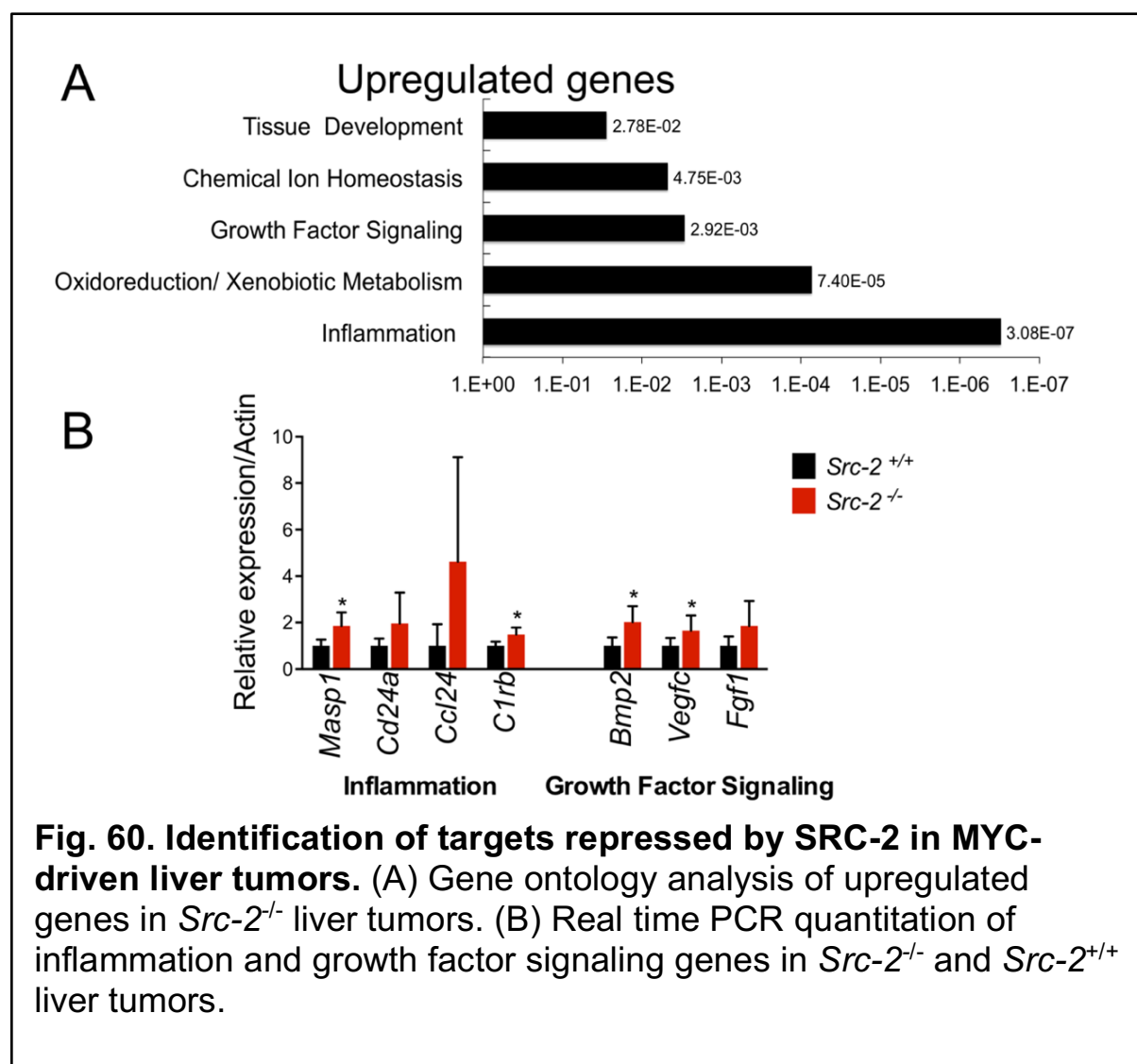
To investigate the mechanisms through which SRC-2 suppresses liver tumorigenesis, we used RNA-Seq to assess global gene expression in liver tumor nodules from *Src-2<sup>+/+</sup>* and *Src-2<sup>-/-</sup>* animals. We identified 865 differentially expressed genes between wild type and knockout tumors. DAVID Gene Ontology analysis identified biological processes enriched in *Src-2<sup>-/-</sup>* liver tumors (Fig. 59A, Fig. 60A). Downregulated genes included regulators of fatty acid and glucose metabolism, and cell adhesion. Upregulated genes included mediators of growth factor signaling and inflammation. Key genes from each of these categories were validated using quantitative real-time PCR (qRT-PCR) (Fig. 59B, Fig. 60B).

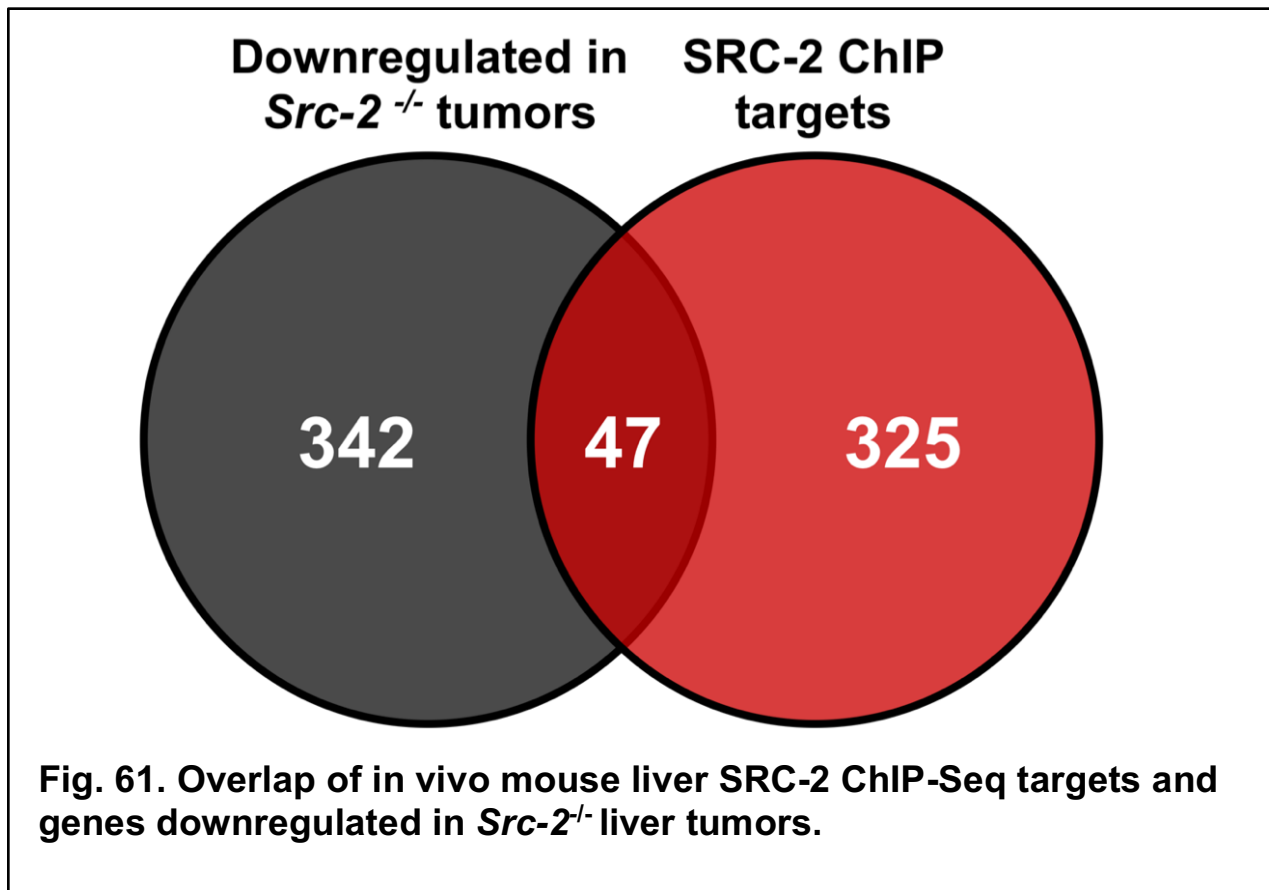
Since SRC-2 is a transcriptional coactivator, we hypothesized that *Src-2* may function to restrain HCC by coactivating transcription of target genes relevant to tumorigenesis. To identify direct SRC-2 target genes, we overlapped the list of genes that were downregulated in *Src-2<sup>-/-</sup>* liver tumors with genes that were bound by SRC-2 in genome-wide chromatin immunoprecipitation (ChIP) Seq analysis of murine liver [228] (Fig. 61). We identified 47 genes that were bound by SRC-2 and downregulated in *Src-2<sup>-/-</sup>* liver tumors (Table 4). To identify clinically relevant candidate genes, we used data from a previously described gene expression analysis of human liver tumors and paired adjacent normal tissue to assess expression of 23 of these genes that were downregulated by at least 2-fold in *Src-2<sup>-/-</sup>* liver tumors and were expressed in the human dataset. Of these, 19/23 genes were downregulated in human HCC samples (Fig. 62).

We selected four putative downstream targets of SRC-2 for further study: *Small Heterodimer Partner (Shp)* , *Dickkopf 4 (Dkk4)* , *Cell Adhesion Molecule 4 (Cadm4)*, and *Thyroid hormone responsive (Thrsp)*. These genes were selected because they were downregulated in *Src-2<sup>-/-</sup>* tumors and in human HCCs, they harbored mutations in human cancers (Appendix A,B), and they were directly bound by SRC-2. Indeed, we confirmed using qRT-PCR that expression of three out of four of these genes (*Shp*, *Dkk4*, and *Cadm4*) was significantly downregulated in an independent set of *Src-2<sup>-/-</sup>* liver tumors (Fig. 63), and identified SRC-2 ChIP-seq peaks in the proximal promoter and/or enhancer regions of each gene (Fig. 64).

Interestingly, in our ChIP-Seq analysis, we also found that SRC-2 bound to the proximal promoter of *Vascular Endothelial Growth Factor C (Vegfc)*, *Fibroblast Growth Factor 1 (Fgf1)*, and *Mannan binding Lectin Serine Peptidase 1(Masp1)*, and their mRNA expression was upregulated in *Src-2<sup>-/-</sup>* liver tumors (Fig. 65). *Vegfc* and *Fgf1* encode growth factors that promote cell growth and survival [241, 242]. *Masp1* is a key component of the complement cascade, which has also been implicated in promoting tumorigenesis [243, 244]. Although activation of gene targets is thought to serve as the primary function of this nuclear receptor coactivator, SRC-2 was previously reported to cooperate with NRs such as Estrogen Receptor to mediate transcriptional repression [224, 245]. Therefore, we speculate that SRC-2 might repress downstream pro-tumorigenic genes and mediate tumor suppression.

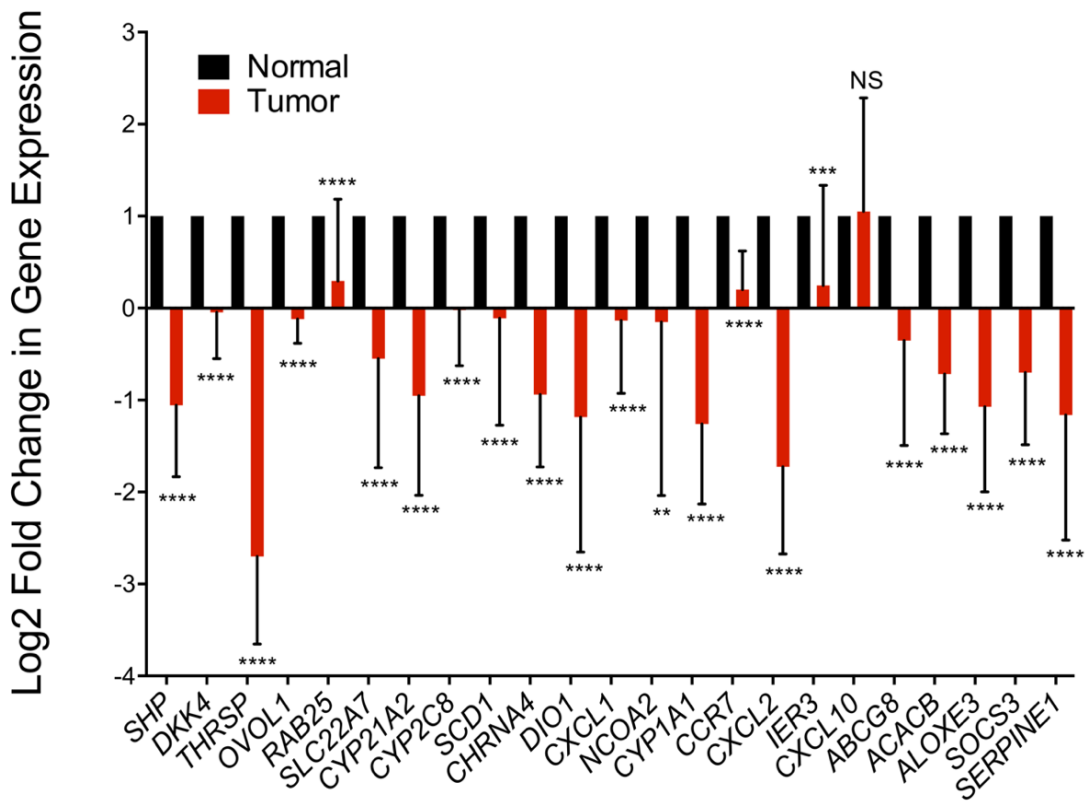




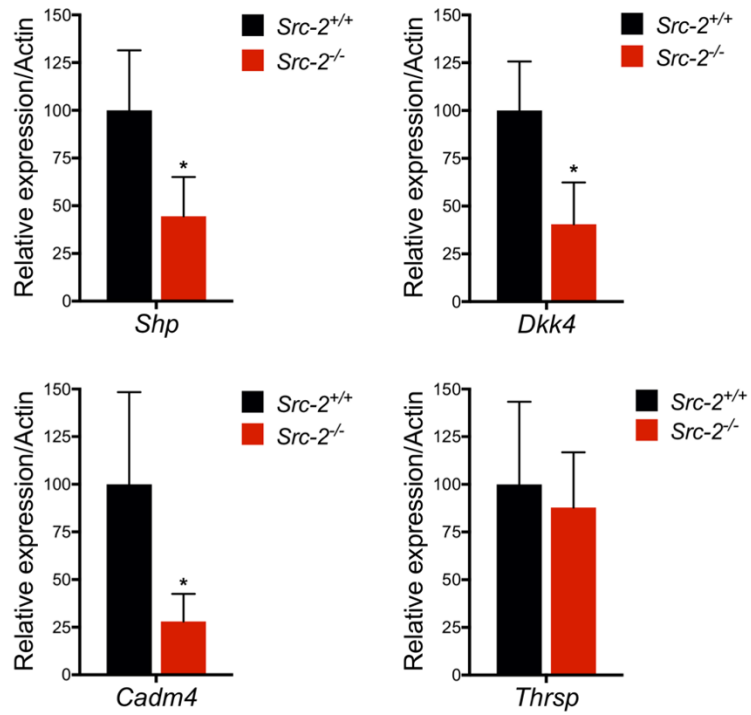


<u>MOUSE GENE ID</u>	<u>HUMAN GENE ID</u>	<u>Fold Decrease</u>	<u>p-value</u>	<u>q-value</u>
<i>Mug2</i>		7.03	5.00E-05	0.0076
<i>Slc22a7</i>	<i>SLC22A7</i>	5.7316	2.00E-04	0.02396
<i>Cyp21a1</i>	<i>CYP21AIP</i>	4.2942	5.00E-05	0.0076
<i>Cyp2c29</i>	<i>CYP2C8</i>	4.004	5.00E-05	0.0076
<i>Scd1</i>	<i>SCD1</i>	3.9866	5.00E-05	0.0076
<i>Chrna4</i>	<i>CHRNA4</i>	3.636	0.00035	0.03585
<i>Nr0b2</i>	<i>SHP</i>	3.497	0.01515	0.43285
<i>Dio1</i>	<i>DIO1</i>	3.35	0.00085	0.06788
<i>Cxcl1</i>	<i>CXCL1</i>	3.281	5.00E-05	0.0076
<i>Ncoa2</i>	<i>NCOA2</i>	3.1	5.00E-05	0.0076
<i>Cadm4</i>	<i>CADM4</i>	2.9311	0.00025	0.02718
<i>Cyp1a1</i>	<i>CYP1A1</i>	2.8489	0.00165	0.1032
<i>Thrsp</i>	<i>THRSP</i>	2.805	5.00E-05	0.0076
<i>Ccr7</i>	<i>CCR7</i>	2.798	0.0034	0.15966
<i>Rab25</i>	<i>RAB25</i>	2.785	0.0173	0.46139
<i>Cxcl2</i>	<i>CXCL2</i>	2.7403	0.01075	0.34931
<i>Ovol1</i>	<i>OVOL1</i>	2.7229	0.00255	0.13399
<i>Ier3</i>	<i>IER3</i>	2.4307	0.00355	0.16561
<i>Scml4</i>	<i>SCML4</i>	2.4166	0.0052	0.21367
<i>Cxcl10</i>	<i>CXCL10</i>	2.3654	5.00E-05	0.0076
<i>Abcg8</i>	<i>SBCG8</i>	2.302	0.0019	0.11237
<i>Igsf11</i>	<i>IGSF11</i>	2.1678	5.00E-05	0.0076
<i>Acacb</i>	<i>ACACB</i>	2.16081	5.00E-05	0.0076
<i>Gltd1d1</i>	<i>GLT1D1</i>	2.1524	0.00025	0.02718
<i>Aloxe3</i>	<i>ALOXE3</i>	2.0871	0.02665	0.59888
<i>Dkk4</i>	<i>DKK4</i>	2.0432	0.0357	0.69126
<i>Socs3</i>	<i>SOCS3</i>	2.0223	0.00065	0.05671
<i>Serpine1</i>	<i>SERPINE1</i>	2.019	5.00E-05	0.0076
<i>Il33</i>	<i>IL33</i>	1.9771	0.0388	0.71879
<i>Mapkapk3</i>	<i>MAPKAPK3</i>	1.9757	5.00E-05	0.0076
<i>Gata6</i>	<i>GATA6</i>	1.897	0.03425	0.67742
<i>Tmem79</i>	<i>TMEM79</i>	1.879	0.0178	0.47029
<i>Cnksr1</i>	<i>CNKSR1</i>	1.85233	0.00275	0.14084
<i>Tm6sf2</i>	<i>TM6SF2</i>	1.7702	0.0172	0.46139
<i>Igfbp1</i>	<i>IGFBP1</i>	1.7481	5.00E-05	0.0076
<i>Egr1</i>	<i>EGR1</i>	1.74384	0.0013	0.09052
<i>Mospd3</i>	<i>MOSPD3</i>	1.6902	0.0049	0.20675
<i>Cldn6</i>	<i>CLDN6</i>	1.6712	5.00E-05	0.0076
<i>Mug1</i>		1.5769	8.00E-04	0.06536
<i>Mal2</i>	<i>MAL2</i>	1.5614	0.00085	0.06788
<i>Cblc</i>	<i>CBLC</i>	1.5545	0.02895	0.61668
<i>Ccbl2</i>	<i>CCBL2</i>	1.549	0.00135	0.09174
<i>Pmm1</i>	<i>PMM1</i>	1.517	0.00135	0.09174
<i>Hgfac</i>	<i>HGFAC</i>	1.4755	0.0061	0.2343
<i>Tat</i>	<i>TAT</i>	1.458	0.02205	0.53923
<i>Permt</i>	<i>PEMT</i>	1.4371	0.0208	0.51853
<i>Acss2</i>	<i>ACSS2</i>	1.4343	0.0222	0.54132

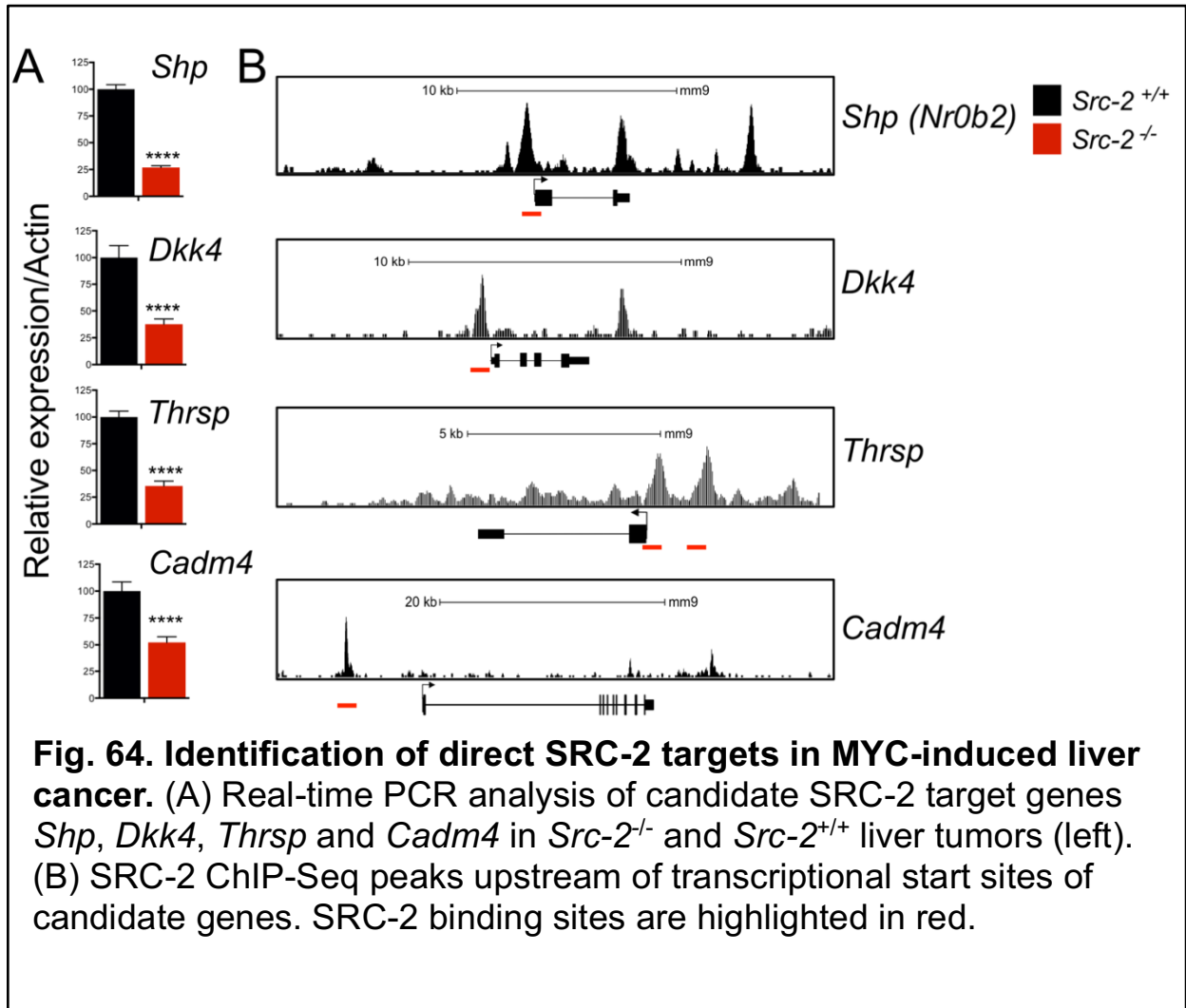
**Table 4. List of 47 downregulated genes in SRC-2 KO liver tumors and directly bound by SRC-2 in mouse liver. Genes above black line have at least 2-fold decrease in mRNA expression.**

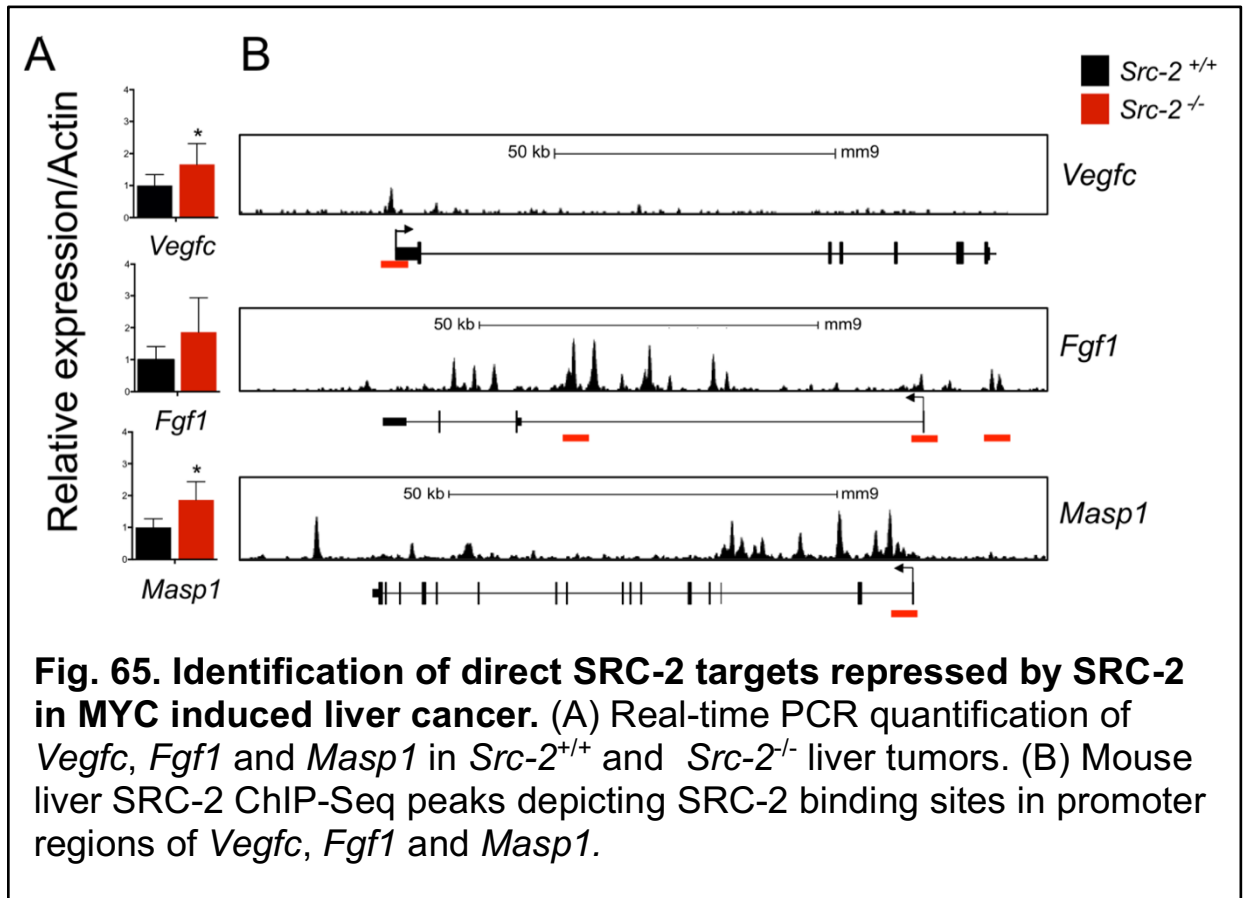


**Fig. 62. Expression analysis of direct SRC-2 targets (GSE1898) using Geo2R in a panel of 91 HCC tumor samples.**



**Fig. 63. Real-time PCR analysis of *Shp*, *Dkk4*, *Cadm4* and *Thrsp* in an independent set of *Src-2<sup>-/-</sup>* and *Src-2<sup>+/+</sup>* liver tumors.**





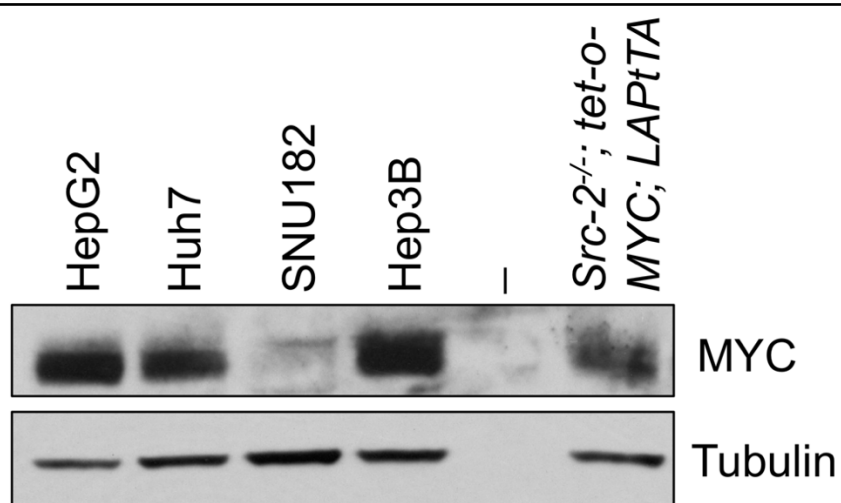
### 9.3.3 SRC-2 targets exhibit tumor suppressor activity in liver cancer cells

To functionally validate SRC-2 target genes as putative tumor suppressors, we performed loss-of-function experiments in human HCC cells. HepG2 and Huh7 were chosen for these studies since these cell lines are widely used for functional analysis of genes in HCC and they express MYC at levels comparable to liver tumors in *Src-2<sup>-/-</sup>*; tet-o-MYC; LAPtTA mice (Fig. 66). *DKK4* and *CADM4* were expressed at high levels in HepG2 cells, and *SHP* was highly expressed in Huh7 cells, allowing examination of the consequences of their inhibition in either of these cell lines. To determine whether SHP inhibition promotes proliferation and tumorigenesis in human cells, we utilized shRNAs to suppress *SHP* in Huh7 cells. qRT-PCR confirmed inhibition of SHP mRNA using two independent shRNAs (Fig. 67A). Cells with stable inhibition of SHP grew significantly faster than control cells (Fig. 67B). Moreover, *SHP* depletion accelerated tumor formation of Huh7 cells in immunocompromised mice (Fig. 68). Complementary to this approach, we overexpressed a V5-tagged SHP (Fig. 69A) in Huh7 cells and assessed its consequences on tumor growth in immunocompromised mice. Overexpression of SHP potently reduced tumor growth *in vivo* (Fig. 69B). Taken together, our data provide evidence that SHP is a downstream target of SRC-2 that inhibits liver tumorigenesis.

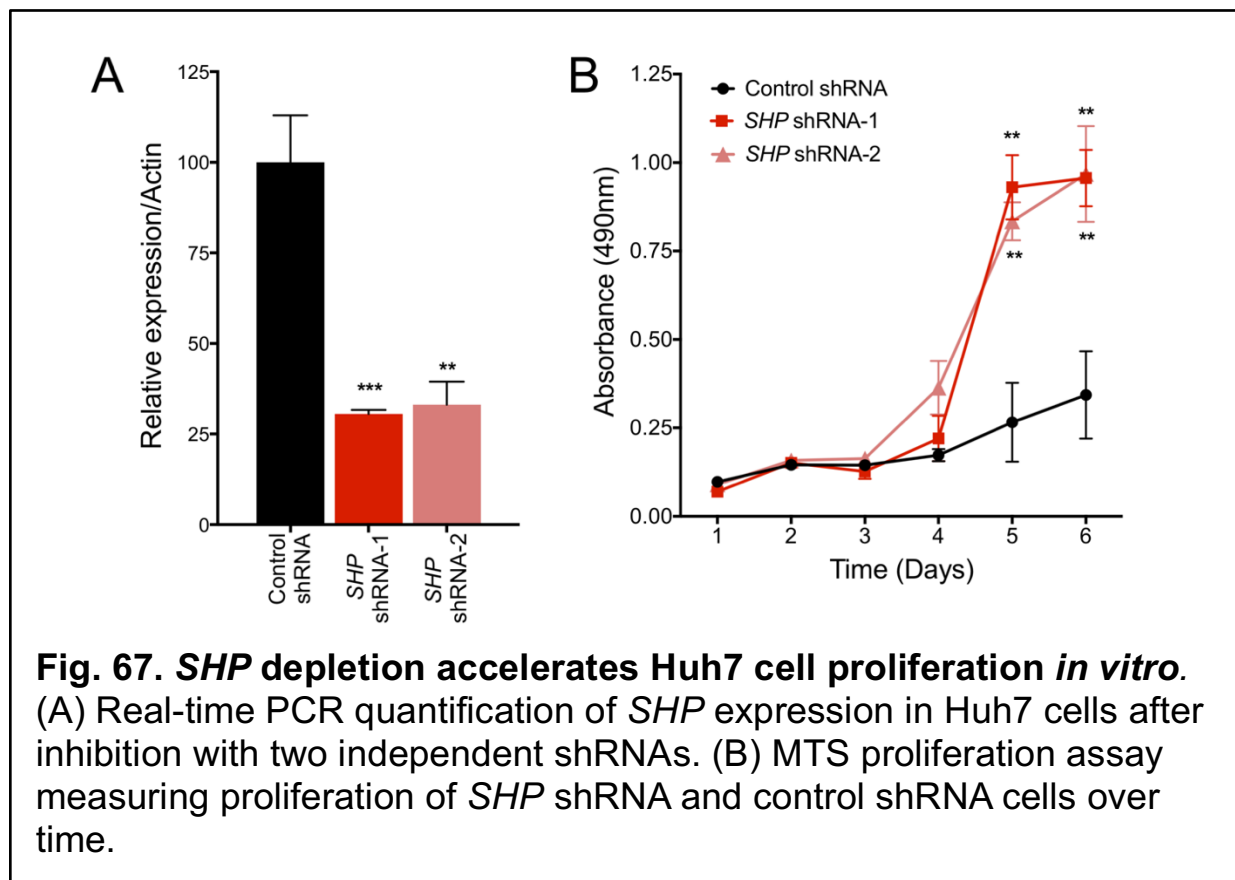
Since SHP is a repressor of bile synthesis in the liver, we measured *CYP7A1*, the bile synthetic enzyme repressed by SHP in the liver. *CYP7A1* was not expressed in human HCC cells but we detected an increase in *Cyp7a1* in *Src-2<sup>-/-</sup>* tumors (Fig. 70). A previous study suggested that SHP suppressed proliferation by transcriptionally repressing *CYCLIN D1* (*Ccnd1*) and that *Shp<sup>-/-</sup>* liver tumors exhibited increased *Ccnd1*

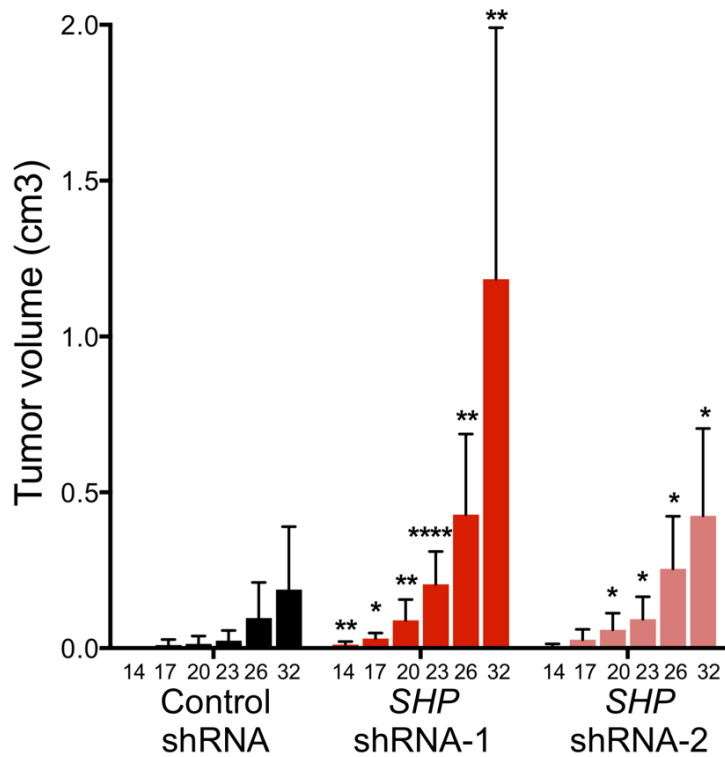
expression [246]. However, it was also reported that *CCND1* levels were unaffected in livers of mice overexpressing SHP [247]. Notably, we failed to observe a significant change in *CCND1* mRNA in Huh7 cells after SHP knockdown (Fig. 71A). Similarly, we failed to detect a difference in *CCND1* mRNA and protein in Huh7 xenograft tumors lacking SHP (Fig. 71B, Fig. 72). These findings suggest that in addition to its known effects on bile acid homeostasis, SHP suppresses liver tumorigenesis by regulating tumor cell proliferation through a mechanism that is independent of *CCND1*.

We next tested the tumor suppressive role of *DKK4* and *CADM4* through loss of function experiments in HepG2 cells. qRT-PCR and western blotting confirmed a reduction in *DKK4* mRNA and protein, respectively (Fig. 73A-B). *DKK4* shRNA cells grew faster than control cells (Fig. 74). Moreover, depletion of *DKK4* enhanced tumorigenesis *in vivo* (Fig. 75). Consistent with this, overexpression of *DKK4* (Fig. 76A) in Huh7 cells reduced tumor growth *in vivo* (Fig. 76B). Similarly, inhibition of *CADM4* via shRNAs (Fig. 77) significantly increased cell proliferation and tumorigenesis *in vivo* (Fig. 78), while overexpression of *CADM4* (Fig. 79A) reduced tumor growth of Huh7 cells *in vivo* (Fig. 79B). *THRSP* was not expressed in Huh7 or HepG2 cells, precluding loss of function studies in these cells. However, overexpression of *THRSP* (Fig. 80A) significantly reduced tumor burden *in vivo* (Fig. 80B). Thus, multiple SRC-2 target genes, including SHP, *CADM4*, and *DKK4*, exhibit tumor suppressor activity in human HCC cells.

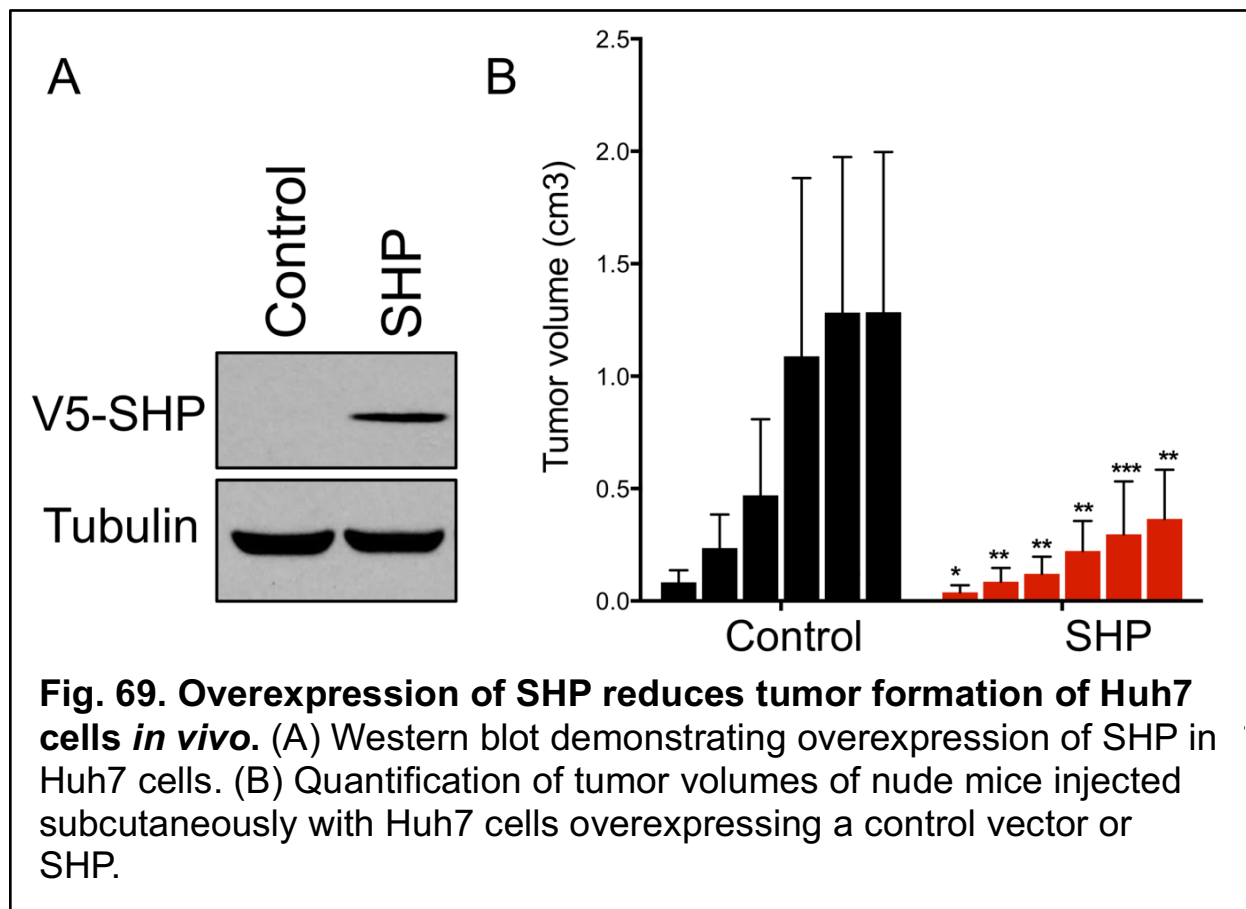


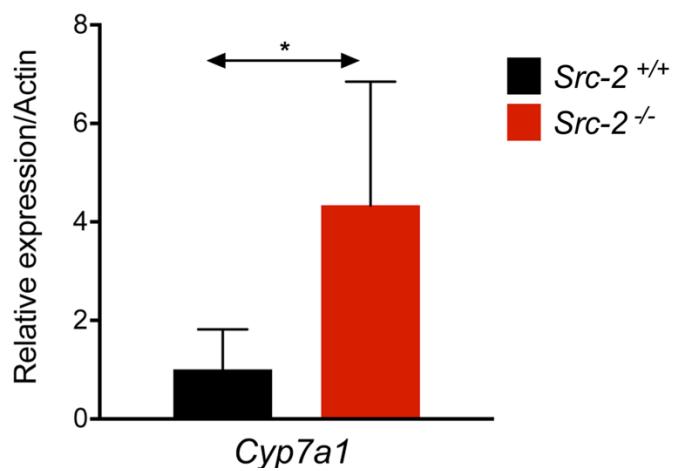
**Fig. 66. MYC expression is comparable in human liver cancer cells and *Src-2<sup>-/-</sup>; tet-o-MYC; LAPtTA* liver tumors.** Western blot analysis depicting MYC protein levels in a panel of human liver cancer cells and a liver tumor from an *Src-2<sup>-/-</sup>; tet-o-MYC; LAPtTA* animal (after dox removal, with MYC overexpression).



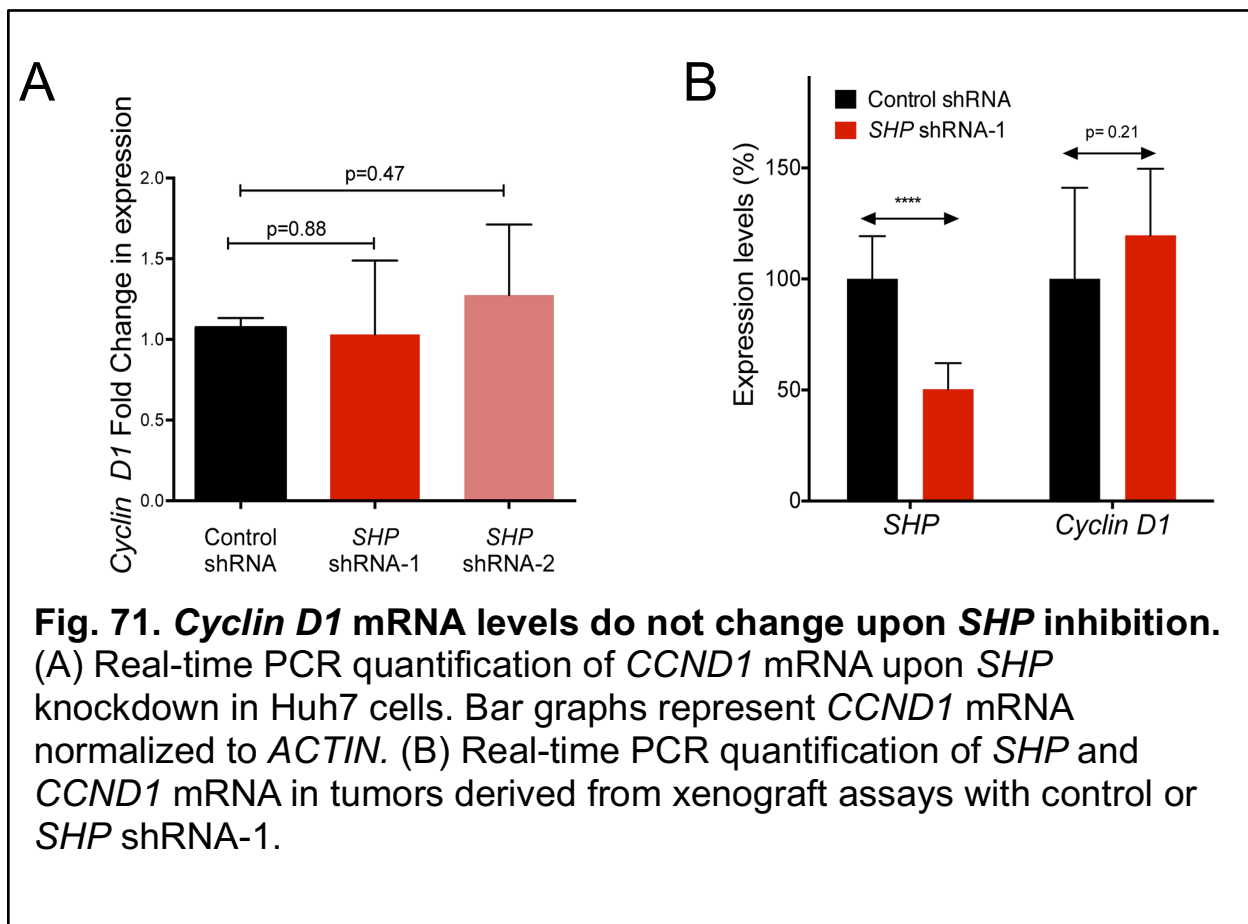


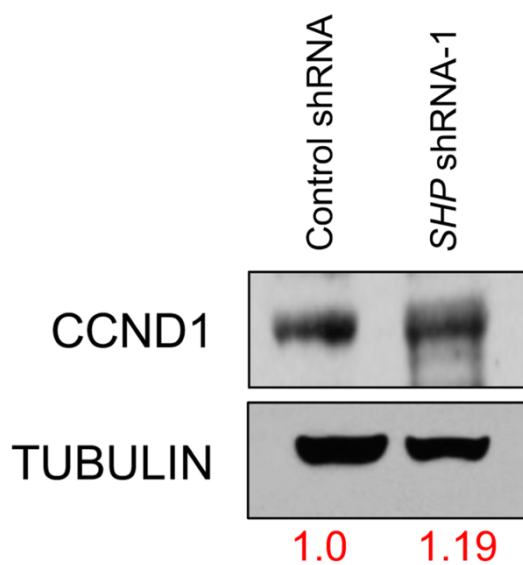
**Fig. 68. *SHP* depletion accelerates tumor formation of Huh7 cells *in vivo*.** Quantification of tumor volumes in nude mice injected with Huh7 cells with *SHP* shRNAs or control shRNA.



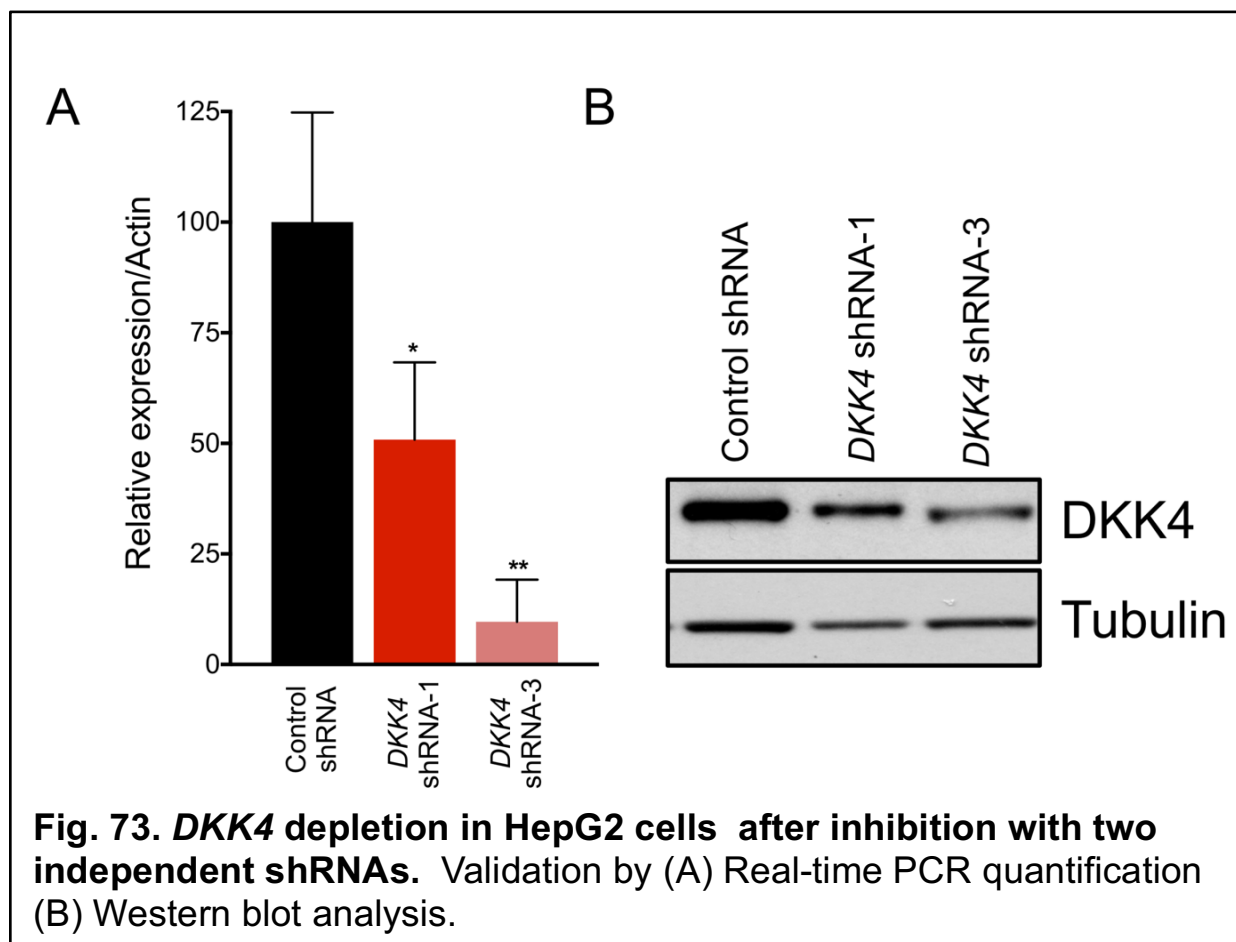


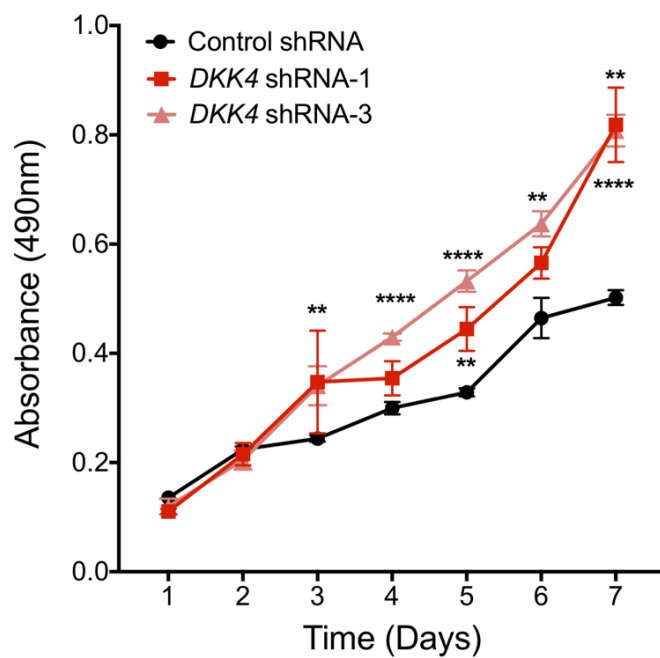
**Fig. 70. *Src-2*<sup>-/-</sup> tumors have elevated *Cyp7a1* levels.** Real-time PCR quantification of *Cyp7a1*, which encodes a bile synthetic gene that is repressed by SHP in the liver.



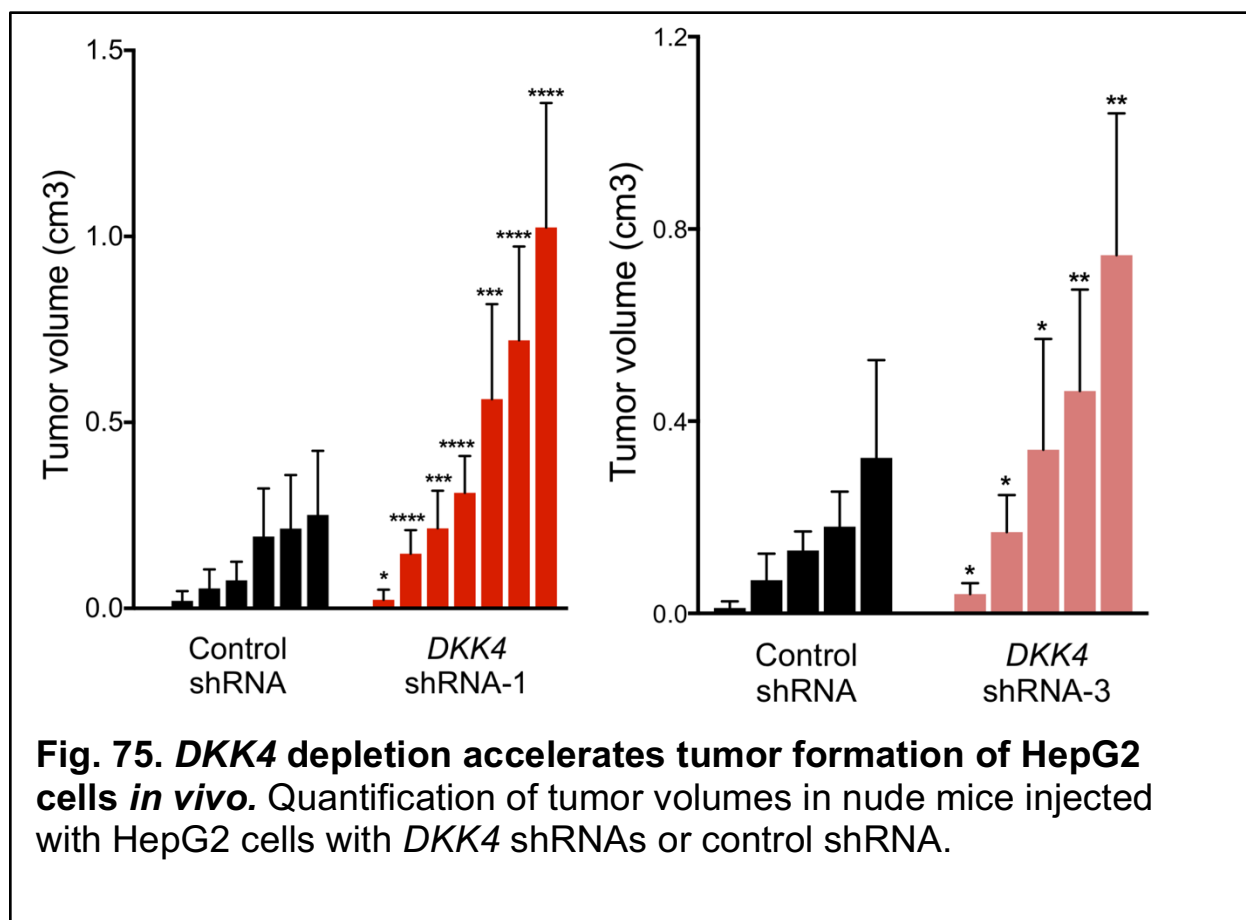


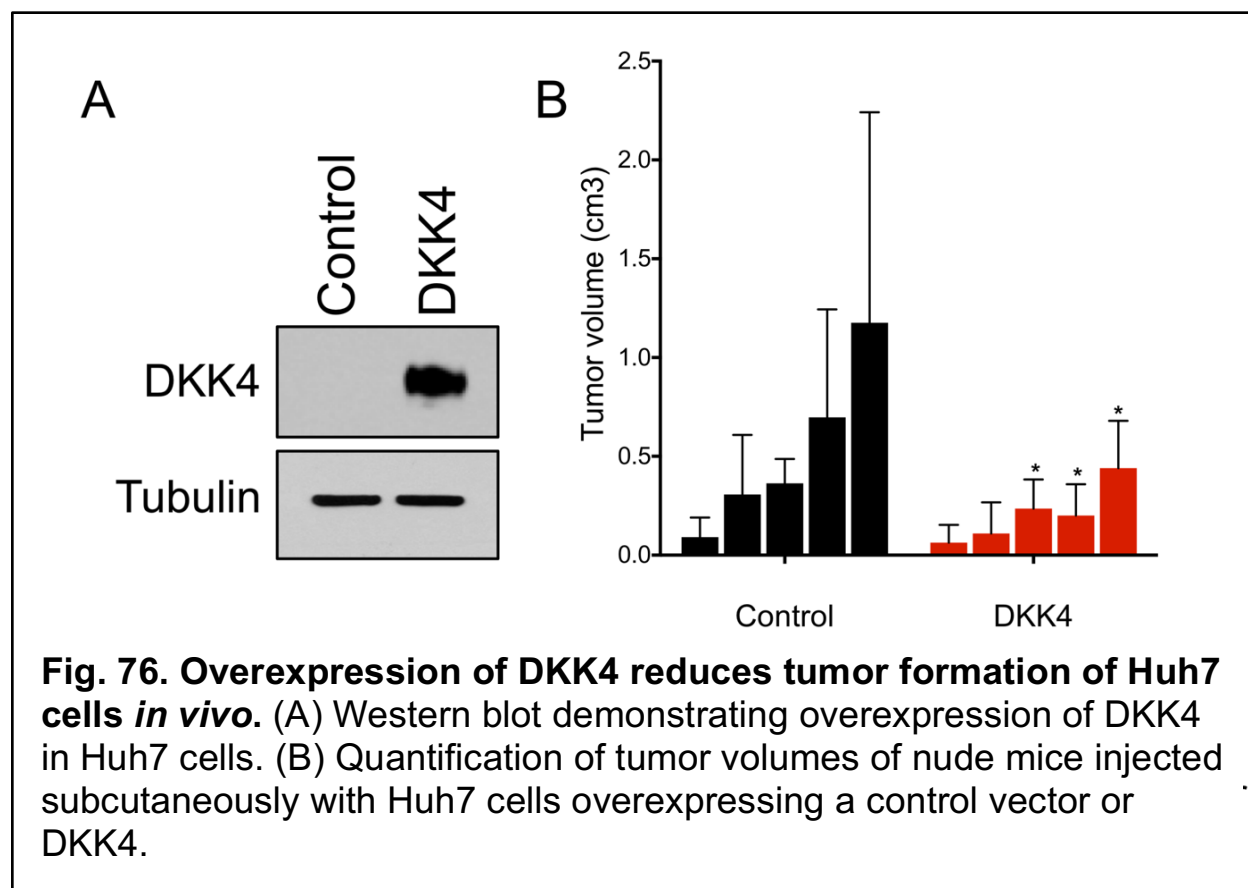
**Fig. 72. CYCLIN D1 protein levels do not change upon *SHP* inhibition.** Western blotting of CCND1 protein in tumors derived from xenograft assays with control or *SHP* shRNA-1.

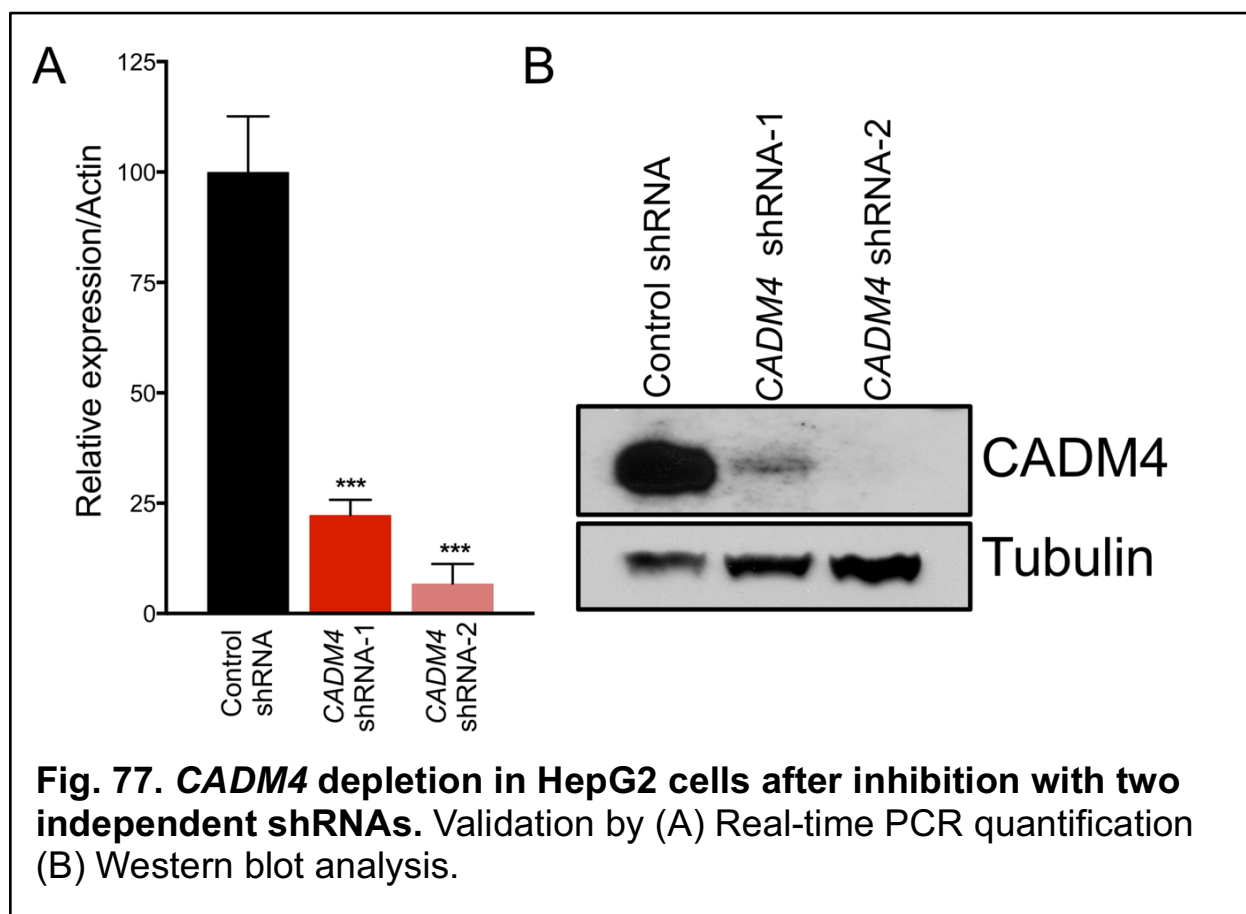


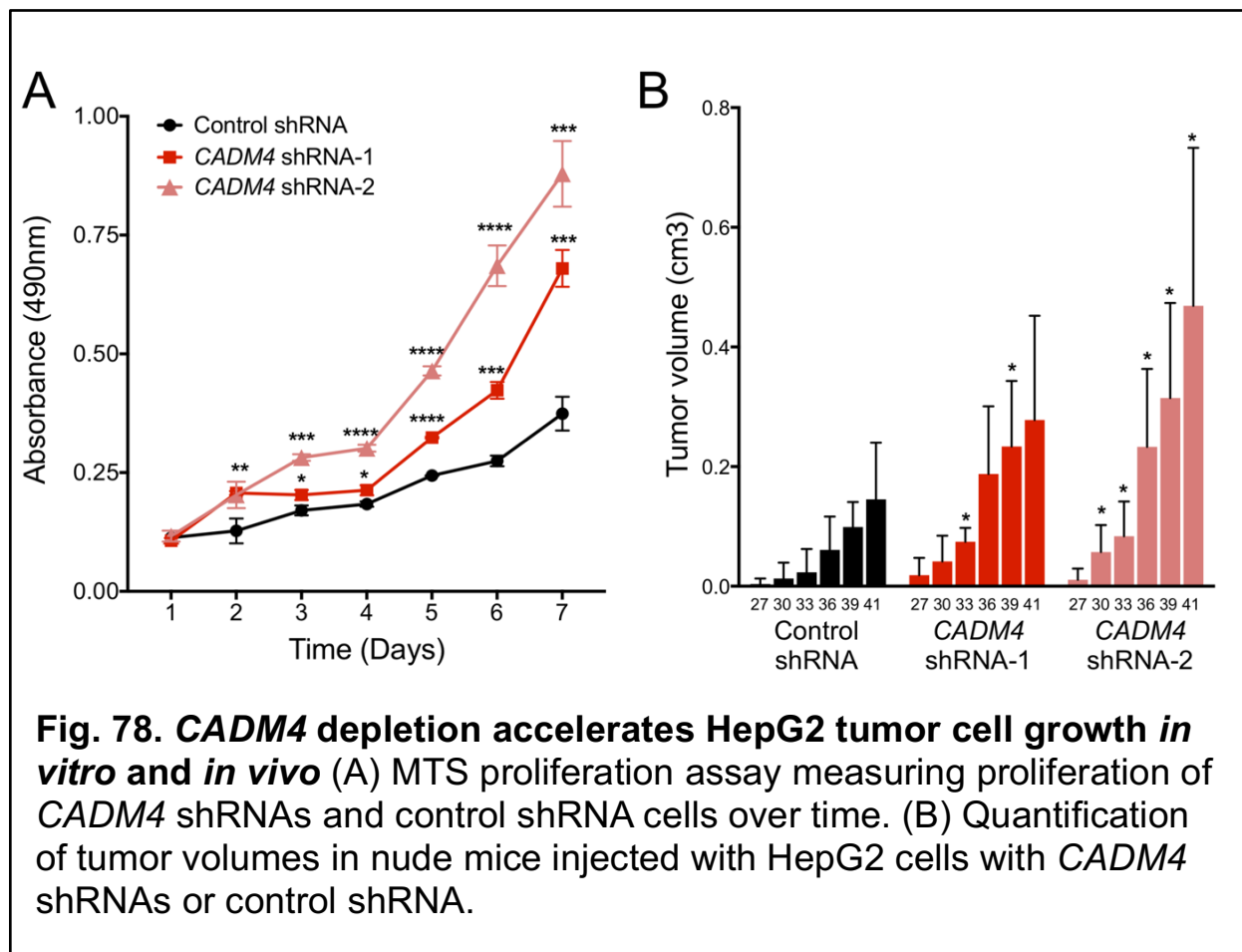


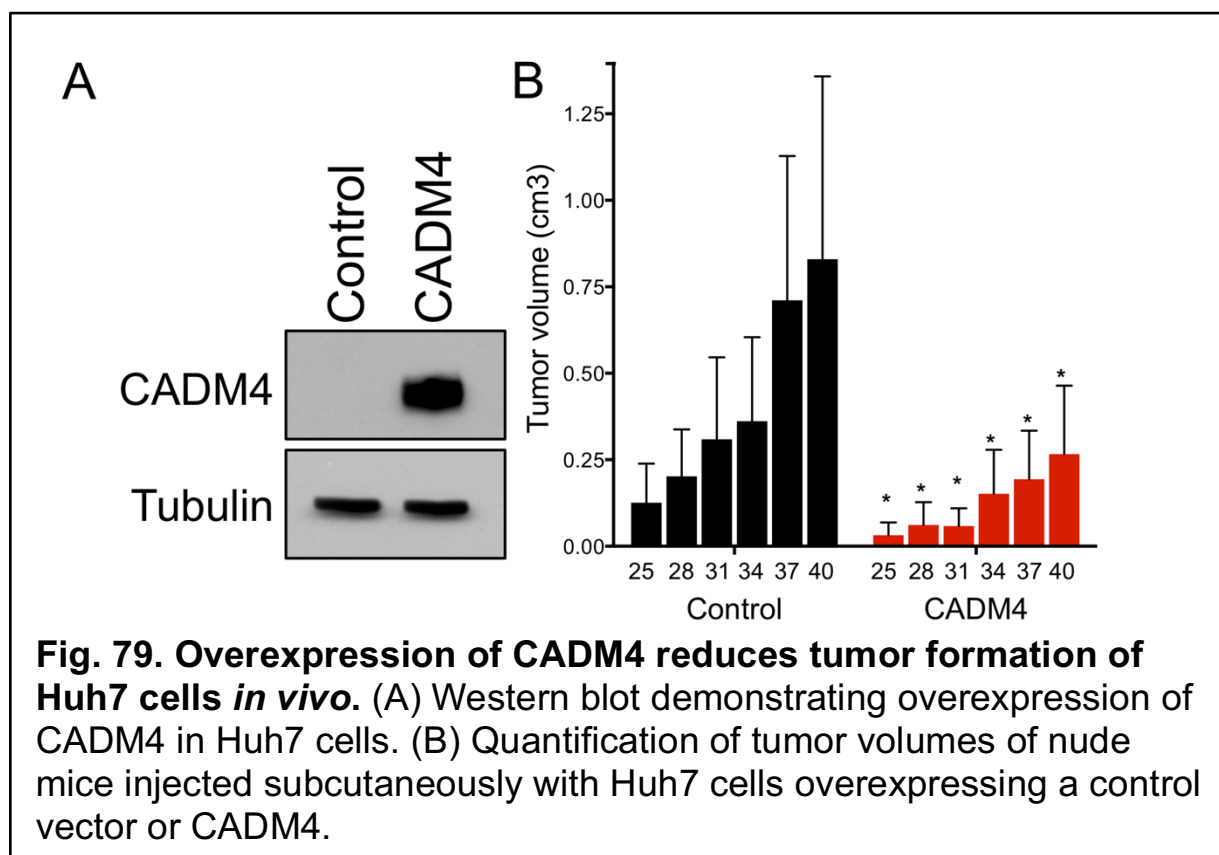
**Fig. 74. Inhibition of *DKK4* increases HepG2 cell growth *in vitro*.** MTS proliferation assay measuring the proliferation of *DKK4* shRNA and control shRNA cells over time.

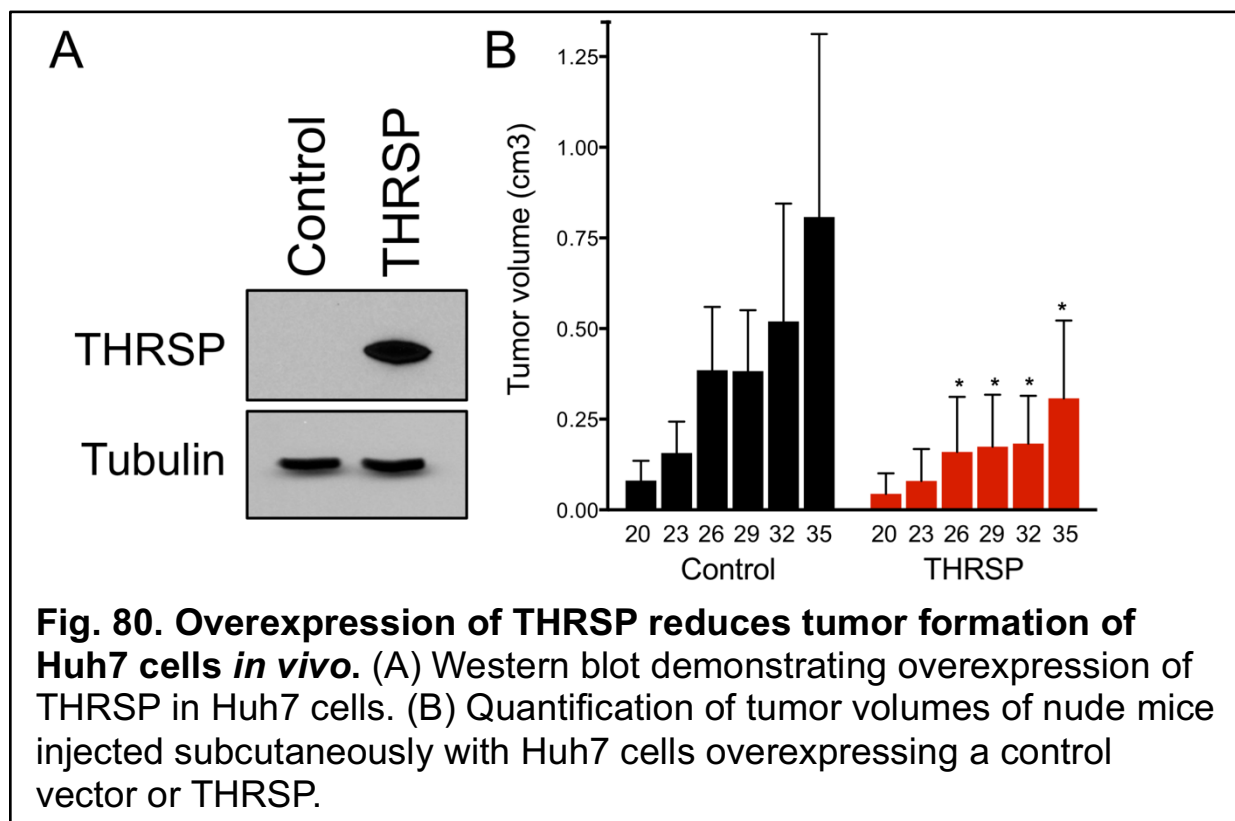












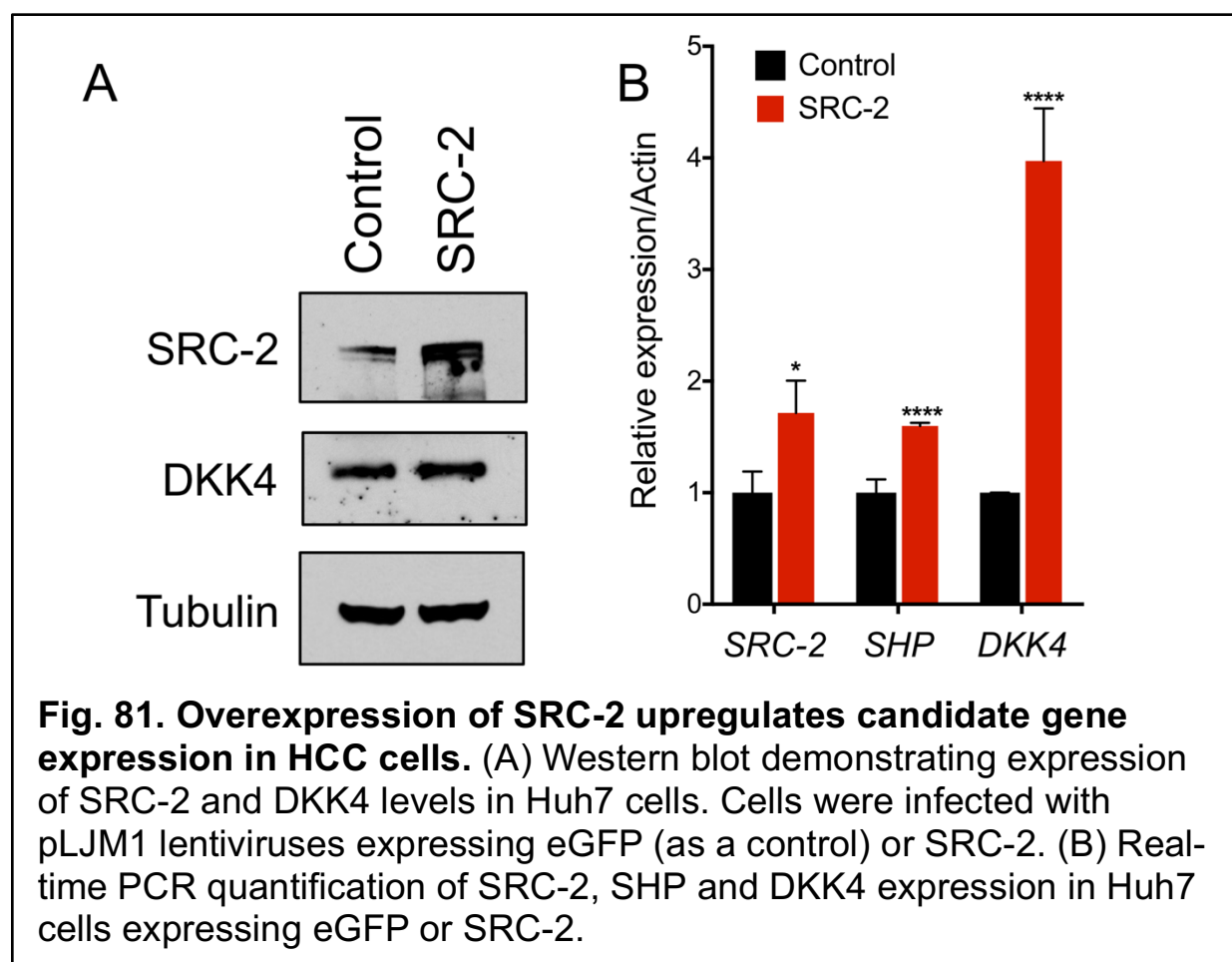
### 9.3.4 SRC-2 functions as tumor suppressor in human liver cancer

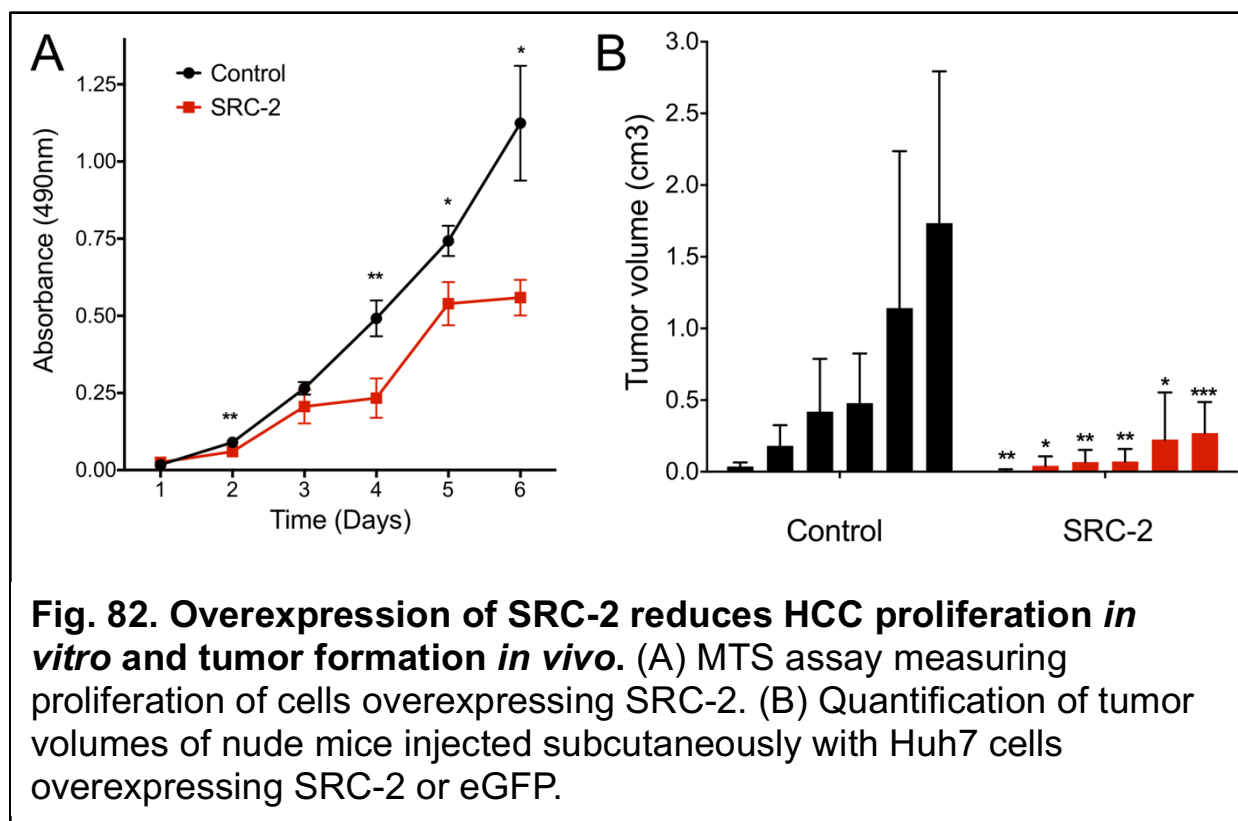
Through the use of mice lacking *Src-2* we demonstrated that inactivation of *Src-2* accelerated MYC mediated liver tumorigenesis *in vivo*. To test if SRC-2 similarly functions as a tumor suppressor in human liver cancer, we first assessed if overexpression of SRC-2 was sufficient to suppress tumorigenesis in HCC cells. Huh7 cells were infected with an SRC-2-expressing or an eGFP control lentivirus, and overexpression of SRC-2 was confirmed by western blotting (Fig. 81A) and quantitative RT-PCR (Fig. 81B). Upregulation of SRC-2 and its target *SHP* (Fig. 81B) were associated with a decrease in cell proliferation as well as tumorigenesis in immunocompromised mice (Fig. 82A, Fig. 82B). Notably, although *DKK4* transcript levels increased by 4-fold upon SRC-2 overexpression, *DKK4* protein levels were only modestly affected, suggesting the existence of post-transcriptional mechanisms that control *DKK4* expression independently of SRC-2 in these cells.

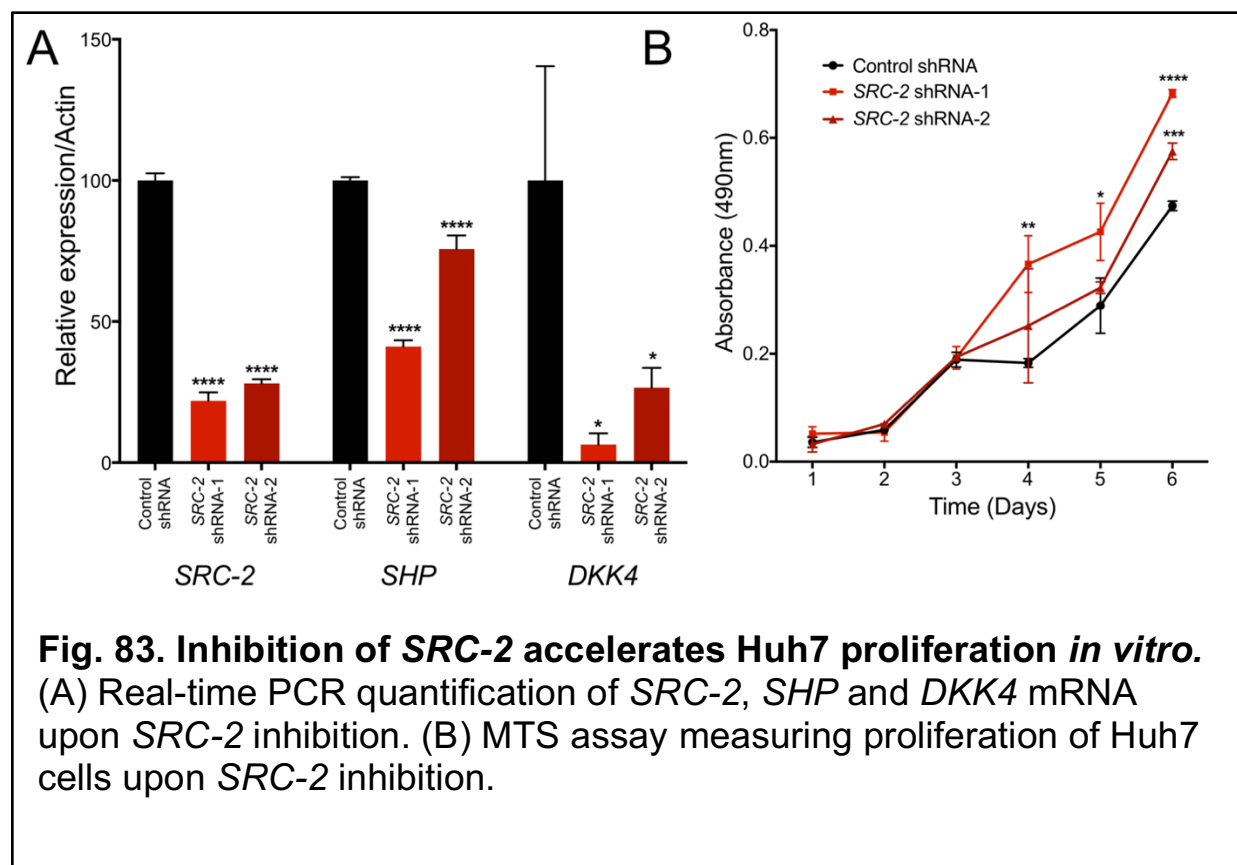
In addition to the gain-of-function approach, we depleted *SRC-2* in HepG2 and Huh7 cells to assess its consequences on cell proliferation and tumor growth *in vivo*. As expected, *SRC-2* inhibition in Huh7 cells through two independent shRNAs resulted in decreased *SHP* and *DKK4* expression (Fig. 83A) and significantly increased cell proliferation (Fig. 83B). Similarly, inhibition of SRC-2 in HepG2 cells led to a decrease in *SHP* and *CADM4* expression (Fig. 84).

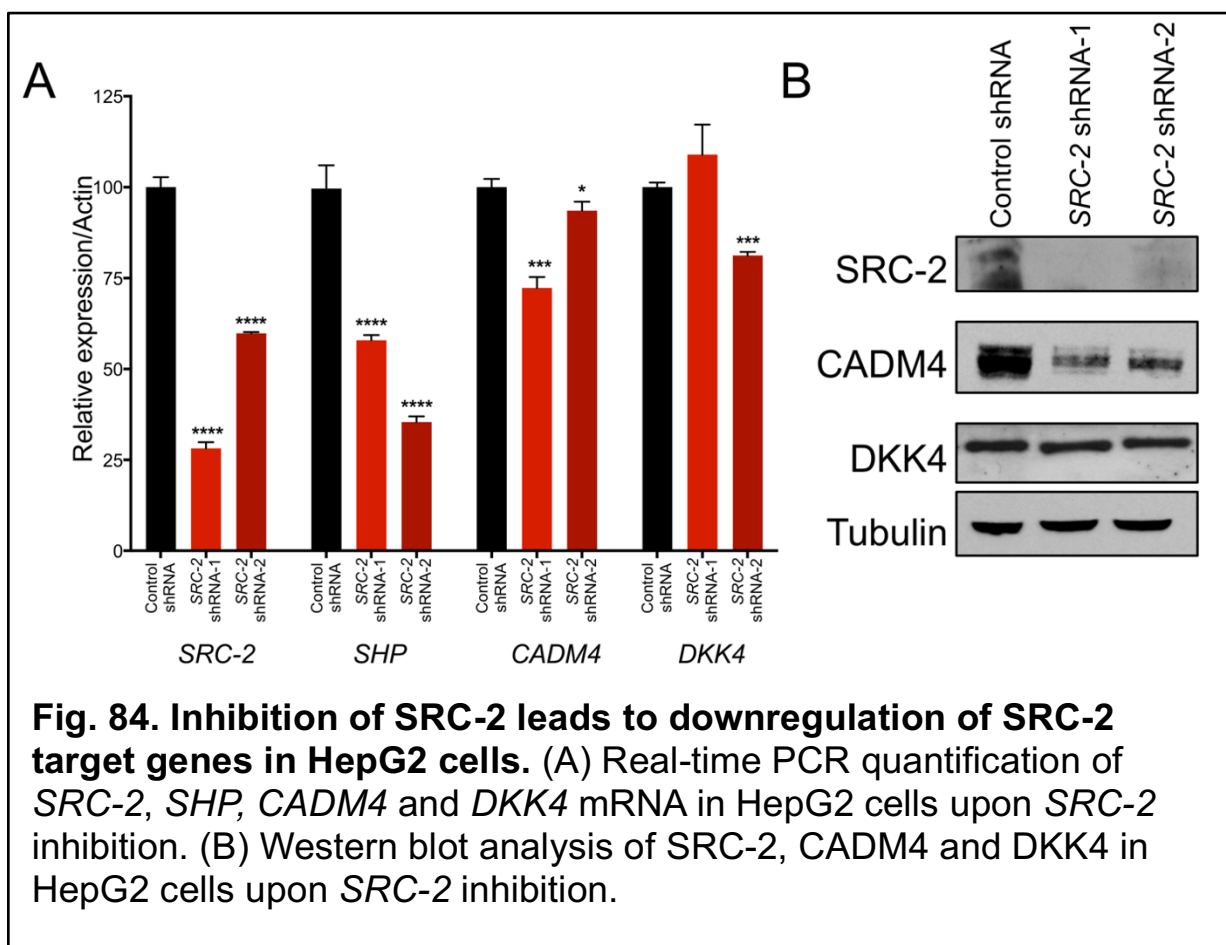
We next sought to determine whether any of the SRC-2 targets alone or in combination were sufficient to rescue the enhanced cell proliferation and tumor burden resulting from SRC-2 knockdown. Rescue experiments were performed in HepG2 cells

because three of the four putative SRC-2 target genes (SHP, CADM4, and DKK4) were expressed in these cells. Enforced expression of SHP, CADM4, DKK4, and THSRP (Fig. 85) in combination significantly reduced proliferation and tumor burden (Fig. 86, Fig. 87). Moreover, individual overexpression of CADM4 and SHP were sufficient to suppress the increase in cell proliferation and tumorigenesis of SRC- 2 knockdown cells (Fig. 86, Fig. 87). In contrast, overexpression of either DKK4 or THRSP alone significantly impacted rates of cell proliferation but not tumor burden (Fig. 88). These data taken together, provide convincing evidence that SHP and CADM4 function as important antitumorigenic SRC-2 target genes in human liver cancer cells.









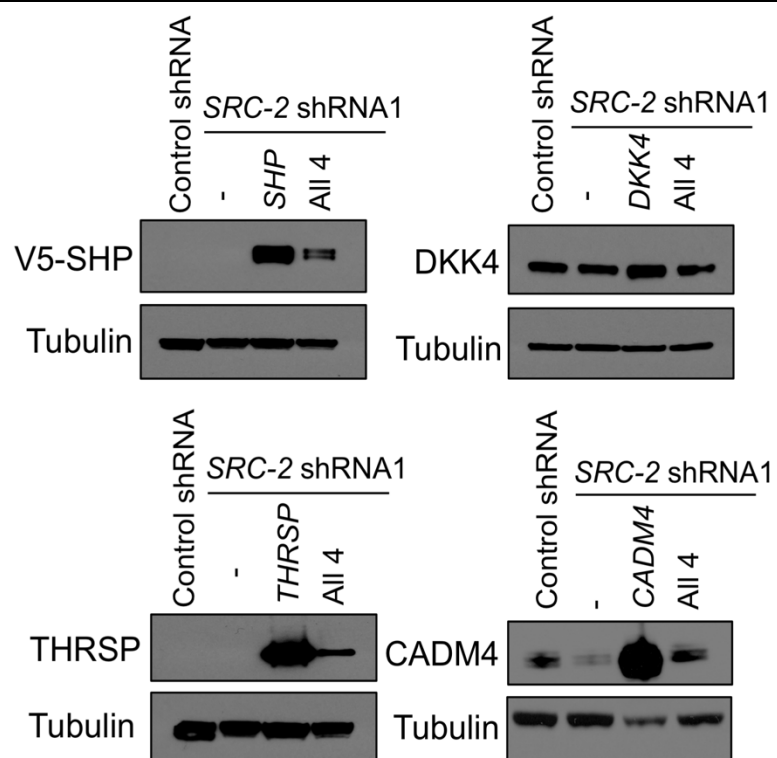


**Fig. 85. Western blot analysis demonstrating overexpression of each of the four targets alone or in combination in SRC-2 shRNA cells.** The V5 antibody detects V5-tagged SHP in the rescue experiment, but does not recognize endogenous SHP.

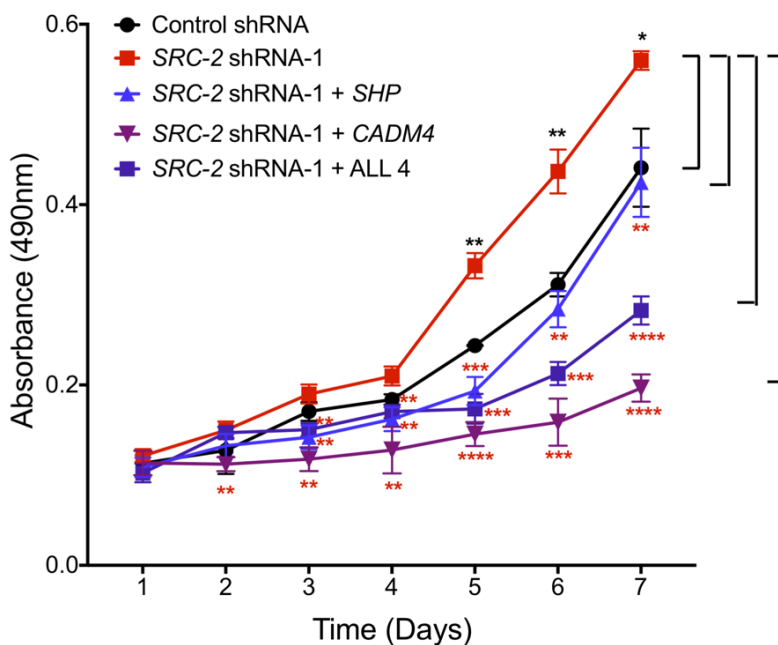


**Fig. 86. SHP and CADM4 rescue enhanced cell proliferation *in vitro* upon SRC-2 inhibition.** MTS assay measuring proliferation of HepG2 cells with control shRNA, SRC-2 shRNA-1, or SRC-2 shRNA-1 with overexpression of SHP or CADM4 alone, or in combination with THRSP and DKK4 (labeled as ALL 4).

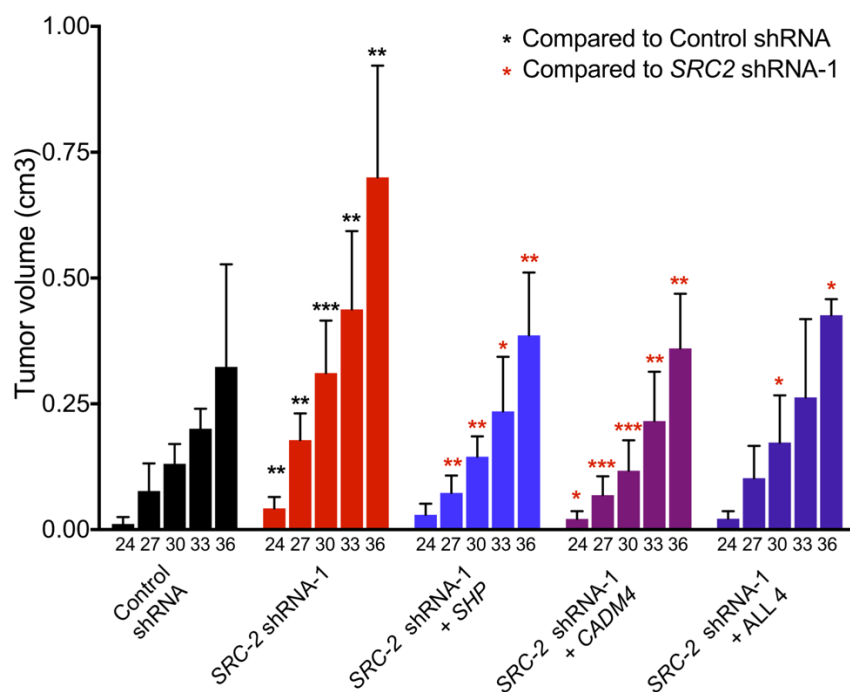
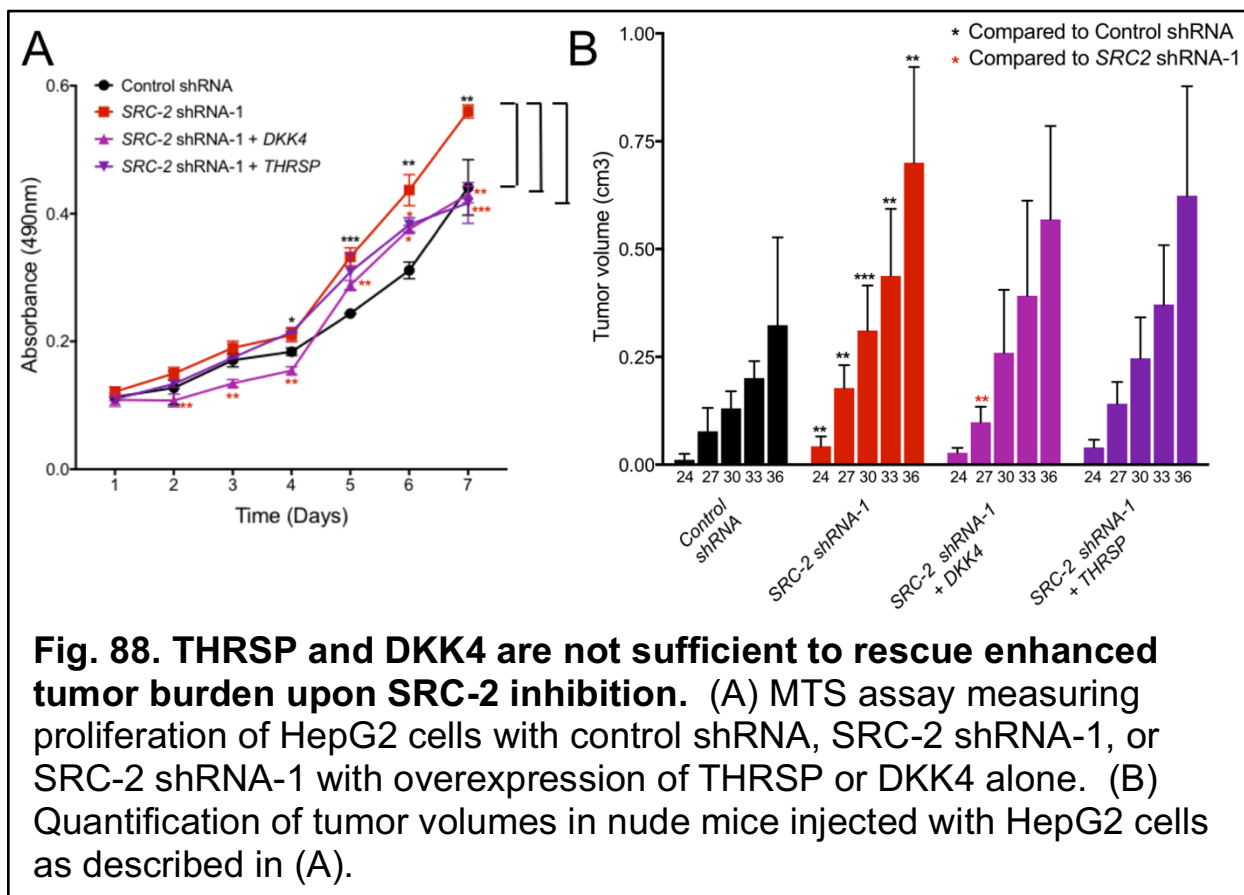


**Fig. 87. SHP and CADM4 rescue enhanced tumor burden upon SRC-2 inhibition.** Quantification of tumor volumes in nude mice injected with HepG2 cells with control shRNA, SRC-2 shRNA-1, or SRC-2 shRNA-1 with overexpression of SHP or CADM4 alone, or in combination with THRSP and DKK4 (labeled as ALL 4).

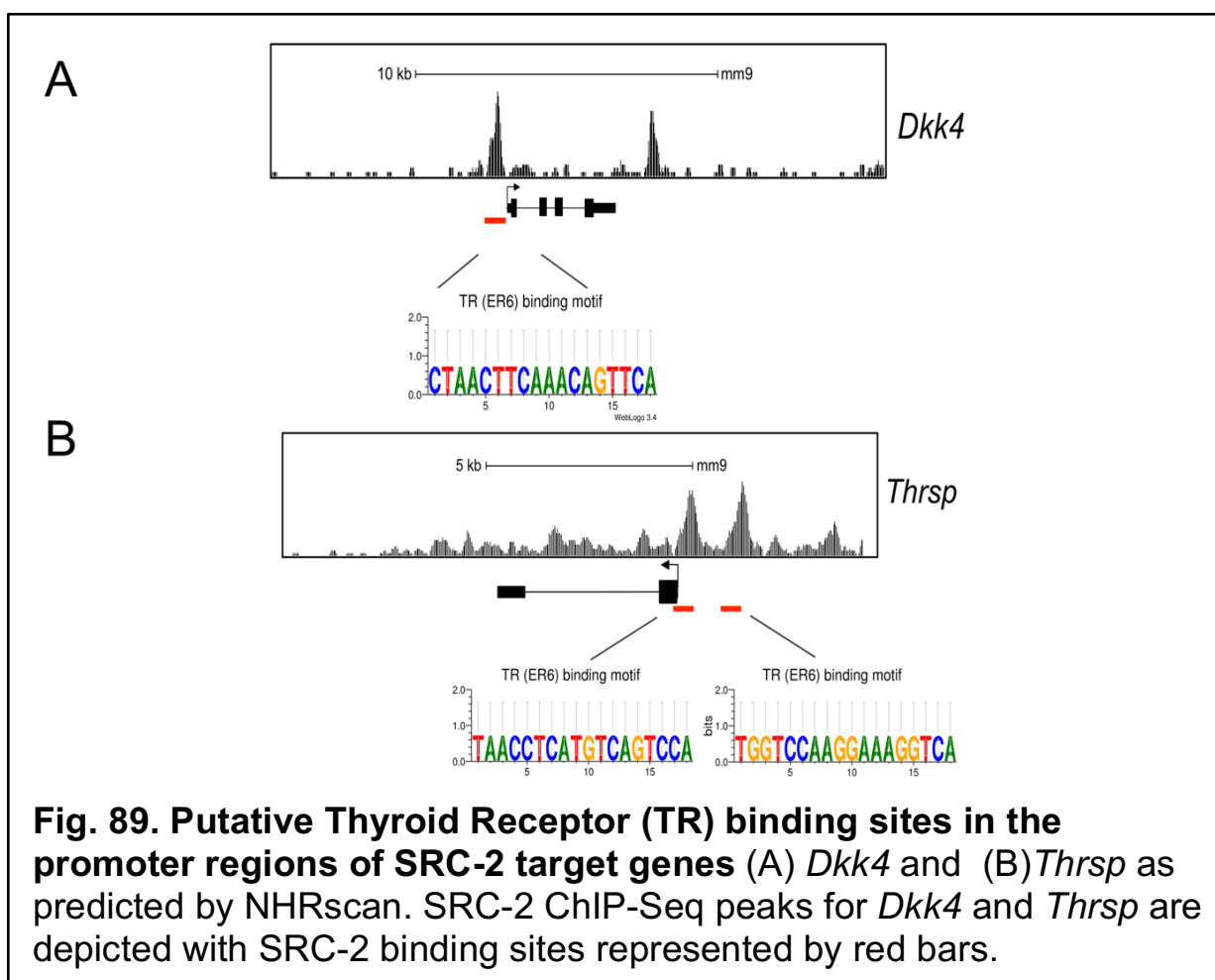


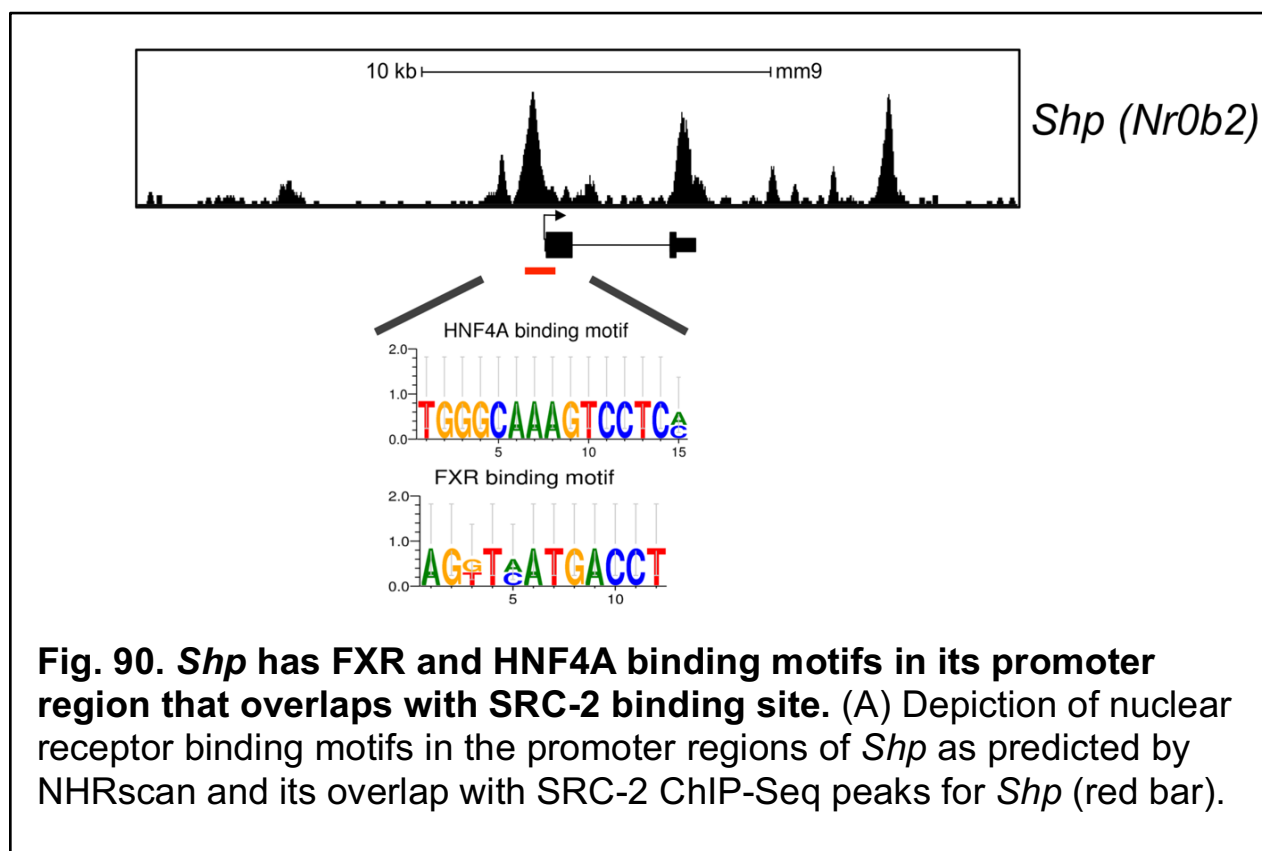
### 9.3.5 Analysis of nuclear receptor binding motifs associated with SRC-2

To identify the putative NRs that cooperate with SRC-2 to activate transcription of target gene expression and suppress proliferation and tumorigenesis, the promoter regions of *DKK4*, *THRSP*, *CADM4*, and *SHP* was screened for NR binding motifs using NHRscan, a computational predictor of nuclear hormone receptor binding sites [248]. The overlap of NR binding motifs with SRC-2 ChIP-Seq peaks identified in this study was then performed. This analysis revealed that the promoter regions of *Dkk4* and *Thrsp* both contained Thyroid Receptor (TR) binding motifs, denoted as Everted Repeat 6 (ER6), which is consistent with previous reports (Fig. 89). NR binding motif analysis also revealed that the *Shp* promoter harbors Hepatocyte Nuclear Factor 4 Alpha (HNF4A) and Farnesoid X Receptor (FXR) binding motifs (also reported in ChIP-Seq studies) overlapping with SRC-2 ChIP-Seq peaks (Fig. 90).

To determine whether SRC-2 cooperates with FXR in activating SHP expression in human liver cancer cells, transactivation assays were performed with a luciferase reporter construct harboring the proximal promoter of SHP, and a truncated reporter construct harboring a deletion that encompasses the FXR binding site (Fig. 91). FXR was expressed in Huh7 cells infected with an eGFP control or SRC-2 lentivirus. Overexpression of SRC-2 and FXR increased SHP reporter activity by approximately 9-fold in Huh7 cells compared to cells expressing FXR alone (Fig. 92). Interestingly, while the truncated reporter construct was significantly less active in control cells, it was also measurably stimulated by SRC-2 expression. This suggests that SRC-2 can interact with other nuclear receptors to transactivate the SHP promoter. Taken together, these data

provide additional evidence that SRC-2 directly induces SHP expression. Future studies are warranted to dissect additional SRC-nuclear receptor interactions in liver cancer and in different tumorigenic contexts.





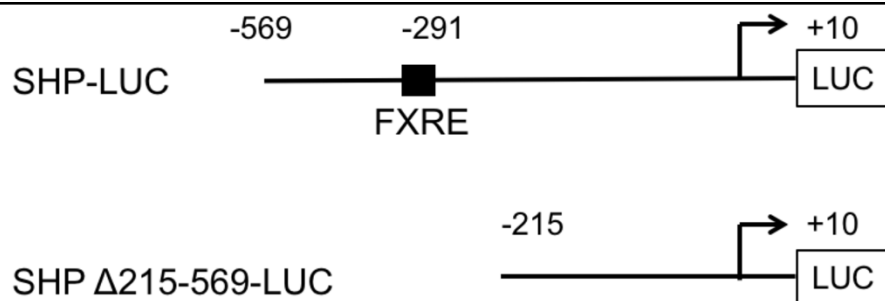


**Fig. 91. Luciferase Reporters harboring either the entire *SHP* promoter or *SHP* promoter lacking the FXR element cloned upstream of Firefly Luciferase.**

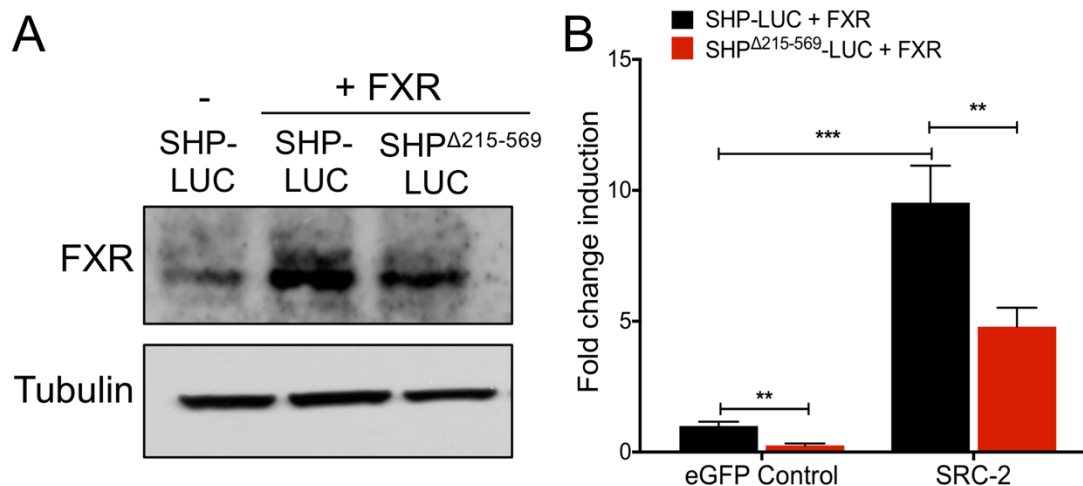


**Fig. 92. SRC-2 cooperates with FXR to activate SHP reporter activity.** (A) Western blot demonstrating expression of FXR in Huh7 cells transfected with SHP-LUC plasmids with and without FXR. (B) Quantification of SHP-luciferase fold-induction relative to Renilla luciferase in eGFP control and SRC-2 expressing cells.

## 9.4 Discussion

Recently, large-scale studies have identified multiple types of recurrent genomic alterations of SRC-2 in human HCC, including missense mutations and amplifications [249, 250]. Notably, *SRC-2* and *MYC* are both located on the short arm of chromosome 8. *MYC* is amplified or overexpressed in 40±60% of human HCCs and a number of studies have previously documented 8q gains in a significant fraction of liver cancers [235]. Thus, it is possible that *SRC-2* copy number gains may occur simply due to a passenger effect associated with *MYC* amplification and may not functionally contribute to tumorigenesis. In support of this concept, Kaplan-Meier analysis revealed that survival of HCC patients with *SRC-2* amplification or mRNA upregulation was not significantly different than survival of patients lacking these alterations [251]. In contrast, low expression of *SRC-2* in tumors is strongly associated with poor survival in HCC patients and HCC patients harboring *SRC-2* missense mutations similarly exhibit poorer overall survival [73]. Taken together, these studies point to a tumor suppressor role for SRC-2 in HCC.

Nevertheless, in light of recent evidence indicating that SRC-2 has oncogenic activity in prostate cancer [238], a direct demonstration of the tumor suppressor activity of SRC-2 in liver cancer, and a better understanding of the underlying mechanisms, would provide important insight into the role of SRC-2 in HCC. Through the use of *Src-2<sup>-/-</sup>* mice, my work has provided unequivocal evidence that this protein restrains MYC-mediated liver tumorigenesis *in vivo* and led to the identification of key downstream SRC-2 target genes that mediate this effect [251].

The orphan nuclear receptor SHP represents one such direct SRC-2 target gene with strong anti-tumorigenic activity. SHP has been extensively studied for its role in liver bile acid homeostasis and as a transcriptional repressor of other NRs. Mice lacking *Shp* accumulate bile acids due to de-repression of the SHP target *Cyp7a1* and develop HCC [252-255]. SHP is also downregulated in liver cancer and low expression of SHP is associated with poor survival of HCC patients [247, 256, 257]. Accordingly, our data demonstrate that SHP inhibition accelerates tumor formation by human HCC cells in mice. Although we detected an increase in *Cyp7a1* in *Src-2*<sup>-/-</sup> tumors, we did not detect expression of CYP7A1 in human HCC cells, nor did we detect a difference in expression of another putative SHP target, *CCND1*. These data suggest that SHP represses hepatic tumorigenesis through mechanisms that are independent of these genes. Importantly, overexpression of SHP alone was sufficient to reverse the tumor enhancing effect of SRC-2 knockdown in HepG2 cells. In light of these findings, future studies are warranted further characterize SHP targets that control proliferation and metabolism in liver cancer and other tumor types. These studies may impact our understanding and treatment of additional types of cancers as SHP was recently found to be downregulated in lung tumors and low expression was associated with poor survival of stage I non-small cell lung cancer patients [258].

DKK4, an inhibitor of Wnt signaling [259] was also identified as a novel anti-tumorigenic SRC-2 target gene in this study. We also demonstrated that two additional genes without a prior known role in liver cancer, *CADM4* and *THRSP*, have strong anti-tumorigenic activity in this tumor type. Consistent with these results, expression of

CADM4, which encodes a member of the immunoglobulin superfamily of proteins, is reduced in multiple tumor types and suppresses tumor formation of prostate, renal and colon cancer cells in immunocompromised mice [260-264]. Moreover, overexpression of CADM4 was sufficient to reverse tumor acceleration by SRC-2 knockdown in HepG2 cells. These findings set the stage for further study of the role of CADM4 in HCC pathogenesis.

In summary, this project has firmly established the potent anti-tumorigenic activity of SRC-2 in human and mouse liver cancer and helped dissect SRC-2 target genes that mediate these effects. In the prostate, SRC-2 amplification coactivates androgen receptor-mediated gene transcription to promote prostate lipogenesis, tumor progression, and metastasis [238]. In liver, SRC-2 cooperates with multiple nuclear receptors, several of which are documented tumor suppressors, including TR, ER, HNF4A, and FXR [224-226, 230, 265] to coactivate a distinct program of target genes resulting in tumor suppression. Recently, a small molecule that stimulated SRC transcriptional activity was developed and shown to promote cell death in breast cancer cells [266]. Determining whether small molecule-mediated activation of SRC-2 can attenuate liver tumorigenesis represents an exciting area for future investigation.

## Appendix A

Gene	Chromosome	Mutations	Nonsense mutations	Missense mutations
<i>NR0B2</i>	1	31 (4 in Breast, 5 in Stomach, 4 in Uterine, 1 in Colon, 2 in GBM, 2 Head and Neck Cancers, 2 in Liver, 4 in Lung and 7 in Melanoma)	1	30
<i>DKK4</i>	8	47 (15 in Colon, 7 in Melanoma, 6 in Uterine, 4 in Breast, 4 in Stomach, 3 in Lung, 3 in Bladder, 2 in Esophagus, 2 in Thyroid, 1 in Pancreas)	2	45
<i>THRSP</i>	11	21 (2 in Bladder, 2 in Breast, 2 in GBM, 5 in Melanoma, 2 in liver and 2 in Stomach)	0	21
<i>CADM4</i>	19	43 (10 in Melanoma, 6 in Stomach, 6 in Lung, 4 in Uterine, 3 in Colon and 3 in Prostate)	7	36

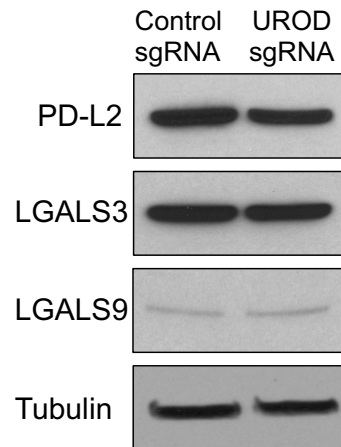
**Appendix A. Analysis of somatic mutations in SRC-2 target genes in human cancers.** Table containing somatic mutations was analyzed from Cosmic database v77.

## Appendix B

Gene	Missense mutations (Y/N)	Deletions	mRNA Downregulation	
			GSE1898** Log2 (T/N)	Other dataset(s) with downregulation
	HCC TCGA Provisional*			
<i>NR0B2</i>	Y, 0.9%	1.1%	-1.056	Chen <i>et al</i> , <i>MBoC</i> 2002
<i>DKK4</i>	N	3.4%	-0.046	Fatima <i>et al</i> , <i>Oncogene</i> , 2012
<i>THRSP</i>	Y, 0.7%	-	-2.700	
<i>CADM4</i>	Y, 0.2%	-	0.219	

**Appendix B. Summary of alterations in SRC-2 targets in human liver cancer.** Table containing alterations in SRC-2 targets were obtained from \*Cbioportal, \*\*NCBI GSE1898 and other datasets. T: Tumor, N: Normal Liver, %: Percentage of cases with alteration.

## Appendix C



**Appendix C. Other checkpoint proteins are unaltered upon UROD inhibition.** Western blot analysis of PD-L2, LGALS3, LGALS9 in H1944 cells expressing a Control or *UROD* sgRNA.

## Acknowledgements

I would like to express my gratitude to several people who have made my research training possible, including my mentor, colleagues, friends and family. First and foremost, I am deeply thankful to my mentor Dr. Kathryn O'Donnell. I have grown immensely both scientifically and as a person under her guidance and mentorship during this important phase of my research career. Dr. O'Donnell has been a great source of inspiration and support since 2014, when I first joined her lab as a meek, underconfident student with minimal research experience but enormous excitement to do science. I greatly admire and have benefited from her enthusiasm and energy to work on great science, her expansive knowledge in the fields of genetics and cancer biology and her expertise in directing and pushing projects aggressively to completion under high pressure deadlines. She has trained me to do great science, communicate my science effectively, prepare scientifically sound and good quality manuscripts and posters, set up important collaborations for our work and enabled me to attend exciting conferences to share my work. She will continue to be a mentor and a role model I look up to for the rest of my scientific career and life. It is a privilege to work in Dr. O'Donnell's lab and receive resources and funding to fulfill my scientific curiosities. Finally, I cannot forget to acknowledge Dr. O'Donnell's personality and its role in shaping me as of today. Thanks to her, I have learnt how to better handle tricky situations with colleagues, collaborators and other researchers in a collegiate fashion. Her kind, considerate nature and immense

patience with trainees allowed me time and space to build my confidence and independence as a scientist over the years while at the same time maintain a positive attitude towards science, the lab and graduate school in general. I feel the key to a successful and happy graduate school experience lies in picking a good mentor, and in this regard, I am deeply grateful to Dr. O'Donnell and feel very fortunate to have joined her lab.

Along with having a great thesis advisor, I had the privilege of having other excellent mentors. Dr. Joshua Mendell has been a very inspiring scientist and an excellent person to discuss scientific ideas with. My dissertation committee members who are experts in their specialized fields of research — Drs. Hao Zhu, Rolf Brekken and Steven Kliewer. Their varied research expertise and critical feedback contributed to a wholesome experience in my thesis committee meetings and played an important role in giving my dissertation work a proper direction. I thank my committee members for their constant understanding and support, as well as looking out for my future beyond graduate school.

In addition to having such role models to look up to, I have had great peers to learn from, discuss exciting new science and share a happy and healthy experience in graduate school. For this reason and many more, I am thankful to my lab mates. Deniz Durakoglugil was a great friend and collaborator in the first half of my thesis and Jingfei Zhu is very helpful with animal handling work in my current project. Dr. Barrett Updegraff, a senior student in the lab and the student I worked with as a rotation student has always challenged my ideas, data and enabled me to do better science. Senior postdocs from

my lab Dr. Yabin Gao, Dr. Mahesh Padanabandula and Dr. Xiaorong Zhou have also been a great source of inspiration and guidance during my research life at UT Southwestern. Members of the Mendell lab have been great friends over the years as well as great folks to discuss my scientific ideas and technical issues. The newcomers in O'Donnell lab, Bethany Smith and Nicole Novaresi as well as various summer students and rotation students have made the lab atmosphere vibrant and happy, their excitement to discuss new papers and constant cheer for me have helped make the past few stressful months much more enjoyable. I am especially grateful to Sojeong Jun, Ester Alvarez Benedicto and Chelsea Karacz for their contribution to my projects during their rotation.

Outside of the O'Donnell lab, several people at UT Southwestern have supported my journey in graduate school. I thank the Cancer Biology graduate program - Drs. Jerry Shay and Rolf Brekken and our coordinators Priya Sen and Laura Henry. I am also grateful to Dr. Helen Yin for selecting me in the MoDTS track, and giving me an opportunity to have such an incredible clinical immersion experience. On this note, I would like to thank my clinical mentors, Dr. Shalaan Beg and Dr. David Gerber, who are inspiring oncologists and terrific human beings. I am grateful to Dr. Melanie Cobb and Dr. John Minna, two great senior investigators who have been inspiring role models and have always had their doors open for me to seek their guidance and advice. I am also grateful to Dr. Eric Olson and the Department of Molecular Biology for being an enthusiastic, fun and over-achieving department to do cutting edge science. I am also grateful to Dr. Stuart Ravnitzky and the International Office for supporting me as an international student. I would like to thank the various Core facilities at UT Southwestern

for their enthusiastic collaboration and timely help in our projects. I would also like to thank various collaborators inside and outside of UT Southwestern who helped make our projects a success.

During this half a decade of stay at UT Southwestern Graduate School, the friends that I made have been more like family and helped me stay happy and positive during the various ups and downs of research. When I moved to Texas, I was a naïve 21-year old who had never lived away from home in her life. The friends I made from various parts of the world helped me feel less lonely and are now my friends for life.

Last but not the least, I express my heartfelt gratitude to my family for believing in me and encouraging me the past 5 years. My parents have always motivated me and have been pillars of support throughout the very tumultuous five years. I am also incredibly fortunate to have met my husband Ayoosh during my PhD. His unbridled enthusiasm to overcome challenges and rise stronger, and his love and complete belief in me helped me rise up during one of my biggest lows in graduate school. Having him by my side as a companion has made me much more productive and happier as a graduate student. I am also thankful to my parents-in-law, who knew nothing about academic research but have invested the time and energy to understand my work and support me emotionally. I would also like to thank my brother, my friends and various well-wishers who always blessed me with positivity and love to do better and cheered me up during stagnant times in my research. Finally, as cheesy as it may be, I would like to thank the United States of America, for truly being the land of opportunity and freedom and giving me this avenue to be the best I could be.

## Bibliography

1. Parkin, D.M., P. Pisani, and J. Ferlay, *Global cancer statistics*. CA Cancer J Clin, 1999. **49**(1): p. 33-64, 1.
2. Gridelli, C., et al., *Non-small-cell lung cancer*. Nat Rev Dis Primers, 2015. **1**: p. 15009.
3. Reck, M., et al., *Management of non-small-cell lung cancer: recent developments*. Lancet, 2013. **382**(9893): p. 709-19.
4. Herbst, R.S., D. Morgensztern, and C. Boshoff, *The biology and management of non-small cell lung cancer*. Nature, 2018. **553**(7689): p. 446-454.
5. Kosaka, T., et al., *Mutations of the epidermal growth factor receptor gene in lung cancer: biological and clinical implications*. Cancer Res, 2004. **64**(24): p. 8919-23.
6. Rotow, J. and T.G. Bivona, *Understanding and targeting resistance mechanisms in NSCLC*. Nat Rev Cancer, 2017. **17**(11): p. 637-658.
7. Suda, K., K. Tomizawa, and T. Mitsudomi, *Biological and clinical significance of KRAS mutations in lung cancer: an oncogenic driver that contrasts with EGFR mutation*. Cancer Metastasis Rev, 2010. **29**(1): p. 49-60.
8. Alexandrov, L.B., et al., *Mutational signatures associated with tobacco smoking in human cancer*. Science, 2016. **354**(6312): p. 618-622.
9. Detterbeck, F.C., et al., *The Eighth Edition Lung Cancer Stage Classification*. Chest, 2017. **151**(1): p. 193-203.

10. Woodard, G.A., K.D. Jones, and D.M. Jablons, *Lung Cancer Staging and Prognosis*. *Cancer Treat Res*, 2016. **170**: p. 47-75.
11. Pakkala, S. and S.S. Ramalingam, *Personalized therapy for lung cancer: Striking a moving target*. *JCI Insight*, 2018. **3**(15).
12. Pardoll, D.M., *The blockade of immune checkpoints in cancer immunotherapy*. *Nat Rev Cancer*, 2012. **12**(4): p. 252-64.
13. Topalian, S.L., C.G. Drake, and D.M. Pardoll, *Immune checkpoint blockade: a common denominator approach to cancer therapy*. *Cancer Cell*, 2015. **27**(4): p. 450-61.
14. Herbst, R.S., et al., *Predictive correlates of response to the anti-PD-L1 antibody MPDL3280A in cancer patients*. *Nature*, 2014. **515**(7528): p. 563-7.
15. Chen, D.S. and I. Mellman, *Elements of cancer immunity and the cancer-immune set point*. *Nature*, 2017. **541**(7637): p. 321-330.
16. Yarchoan, M., et al., *Targeting neoantigens to augment antitumour immunity*. *Nat Rev Cancer*, 2017. **17**(9): p. 569.
17. Rizvi, N.A., et al., *Cancer immunology. Mutational landscape determines sensitivity to PD-1 blockade in non-small cell lung cancer*. *Science*, 2015. **348**(6230): p. 124-8.
18. Le, D.T., et al., *Mismatch repair deficiency predicts response of solid tumors to PD-1 blockade*. *Science*, 2017. **357**(6349): p. 409-413.
19. Pardoll, D.M., *Immunology beats cancer: a blueprint for successful translation*. *Nat Immunol*, 2012. **13**(12): p. 1129-32.

20. Matsushita, H., et al., *Cancer exome analysis reveals a T-cell-dependent mechanism of cancer immunoediting*. *Nature*, 2012. **482**(7385): p. 400-4.
21. Singer, K., et al., *Suppression of T-cell responses by tumor metabolites*. *Cancer Immunol Immunother*, 2011. **60**(3): p. 425-31.
22. Chang, C.H., et al., *Metabolic Competition in the Tumor Microenvironment Is a Driver of Cancer Progression*. *Cell*, 2015. **162**(6): p. 1229-41.
23. Serafini, P., I. Borrello, and V. Bronte, *Myeloid suppressor cells in cancer: recruitment, phenotype, properties, and mechanisms of immune suppression*. *Semin Cancer Biol*, 2006. **16**(1): p. 53-65.
24. Jang, J.E., et al., *Crosstalk between Regulatory T Cells and Tumor-Associated Dendritic Cells Negates Anti-tumor Immunity in Pancreatic Cancer*. *Cell Rep*, 2017. **20**(3): p. 558-571.
25. Sharpe, A.H., et al., *The function of programmed cell death 1 and its ligands in regulating autoimmunity and infection*. *Nat Immunol*, 2007. **8**(3): p. 239-45.
26. Van Gool, S.W., et al., *CD80, CD86 and CD40 provide accessory signals in a multiple-step T-cell activation model*. *Immunol Rev*, 1996. **153**: p. 47-83.
27. Vonderheide, R.H., *The Immune Revolution: A Case for Priming, Not Checkpoint*. *Cancer Cell*, 2018. **33**(4): p. 563-569.
28. Hoves, S., et al., *Rapid activation of tumor-associated macrophages boosts preexisting tumor immunity*. *J Exp Med*, 2018. **215**(3): p. 859-876.
29. Alegre, M.L., K.A. Frauwirth, and C.B. Thompson, *T-cell regulation by CD28 and CTLA-4*. *Nat Rev Immunol*, 2001. **1**(3): p. 220-8.

30. Lee, K.M., et al., *Molecular basis of T cell inactivation by CTLA-4*. Science, 1998. **282**(5397): p. 2263-6.
31. Schneider, H., et al., *Reversal of the TCR stop signal by CTLA-4*. Science, 2006. **313**(5795): p. 1972-5.
32. Walker, L.S. and D.M. Sansom, *The emerging role of CTLA4 as a cell-extrinsic regulator of T cell responses*. Nat Rev Immunol, 2011. **11**(12): p. 852-63.
33. De Sousa Linares, A., et al., *Not All Immune Checkpoints Are Created Equal*. Front Immunol, 2018. **9**: p. 1909.
34. Triebel, F., et al., *LAG-3, a novel lymphocyte activation gene closely related to CD4*. J Exp Med, 1990. **171**(5): p. 1393-405.
35. Lui, Y. and S.J. Davis, *LAG-3: a very singular immune checkpoint*. Nat Immunol, 2018. **19**(12): p. 1278-1279.
36. Freeman, G.J., et al., *TIM genes: a family of cell surface phosphatidylserine receptors that regulate innate and adaptive immunity*. Immunol Rev, 2010. **235**(1): p. 172-89.
37. Zhu, C., et al., *The Tim-3 ligand galectin-9 negatively regulates T helper type 1 immunity*. Nat Immunol, 2005. **6**(12): p. 1245-52.
38. Zou, W. and L. Chen, *Inhibitory B7-family molecules in the tumour microenvironment*. Nat Rev Immunol, 2008. **8**(6): p. 467-77.
39. Freeman, G.J., et al., *Engagement of the PD-1 immunoinhibitory receptor by a novel B7 family member leads to negative regulation of lymphocyte activation*. J Exp Med, 2000. **192**(7): p. 1027-34.

40. Sun, C., R. Mezzadra, and T.N. Schumacher, *Regulation and Function of the PD-L1 Checkpoint*. *Immunity*, 2018. **48**(3): p. 434-452.
41. Thommen, D.S. and T.N. Schumacher, *T Cell Dysfunction in Cancer*. *Cancer Cell*, 2018. **33**(4): p. 547-562.
42. Petroff, M.G., et al., *B7 family molecules: novel immunomodulators at the maternal-fetal interface*. *Placenta*, 2002. **23 Suppl A**: p. S95-101.
43. Hori, J., et al., *B7-H1-induced apoptosis as a mechanism of immune privilege of corneal allografts*. *J Immunol*, 2006. **177**(9): p. 5928-35.
44. Dong, H., et al., *Tumor-associated B7-H1 promotes T-cell apoptosis: a potential mechanism of immune evasion*. *Nat Med*, 2002. **8**(8): p. 793-800.
45. Hirano, F., et al., *Blockade of B7-H1 and PD-1 by monoclonal antibodies potentiates cancer therapeutic immunity*. *Cancer Res*, 2005. **65**(3): p. 1089-96.
46. Wang, D.Y., et al., *Fatal Toxic Effects Associated With Immune Checkpoint Inhibitors: A Systematic Review and Meta-analysis*. *JAMA Oncol*, 2018. **4**(12): p. 1721-1728.
47. Herbst, R.S., et al., *Pembrolizumab versus docetaxel for previously treated, PD-L1-positive, advanced non-small-cell lung cancer (KEYNOTE-010): a randomised controlled trial*. *Lancet*, 2016. **387**(10027): p. 1540-50.
48. Iida, N., et al., *Commensal bacteria control cancer response to therapy by modulating the tumor microenvironment*. *Science*, 2013. **342**(6161): p. 967-70.
49. Sivan, A., et al., *Commensal Bifidobacterium promotes antitumor immunity and facilitates anti-PD-L1 efficacy*. *Science*, 2015. **350**(6264): p. 1084-9.

50. Pfirschke, C., et al., *Immunogenic Chemotherapy Sensitizes Tumors to Checkpoint Blockade Therapy*. *Immunity*, 2016. **44**(2): p. 343-54.
51. Sharma, P., et al., *Primary, Adaptive, and Acquired Resistance to Cancer Immunotherapy*. *Cell*, 2017. **168**(4): p. 707-723.
52. Mok, S., et al., *Inhibition of CSF-1 receptor improves the antitumor efficacy of adoptive cell transfer immunotherapy*. *Cancer Res*, 2014. **74**(1): p. 153-161.
53. Lim, S.O., et al., *Deubiquitination and Stabilization of PD-L1 by CSN5*. *Cancer Cell*, 2016. **30**(6): p. 925-939.
54. Koyama, S., et al., *Adaptive resistance to therapeutic PD-1 blockade is associated with upregulation of alternative immune checkpoints*. *Nat Commun*, 2016. **7**: p. 10501.
55. Gubin, M.M., et al., *Checkpoint blockade cancer immunotherapy targets tumour-specific mutant antigens*. *Nature*, 2014. **515**(7528): p. 577-81.
56. Marincola, F.M., et al., *Escape of human solid tumors from T-cell recognition: molecular mechanisms and functional significance*. *Adv Immunol*, 2000. **74**: p. 181-273.
57. Sucker, A., et al., *Genetic evolution of T-cell resistance in the course of melanoma progression*. *Clin Cancer Res*, 2014. **20**(24): p. 6593-604.
58. Ansell, S.M., et al., *PD-1 blockade with nivolumab in relapsed or refractory Hodgkin's lymphoma*. *N Engl J Med*, 2015. **372**(4): p. 311-9.

59. Ikeda, S., et al., *PD-L1 Is Upregulated by Simultaneous Amplification of the PD-L1 and JAK2 Genes in Non-Small Cell Lung Cancer*. *J Thorac Oncol*, 2016. **11**(1): p. 62-71.
60. George, J., et al., *Genomic Amplification of CD274 (PD-L1) in Small-Cell Lung Cancer*. *Clin Cancer Res*, 2017. **23**(5): p. 1220-1226.
61. Kataoka, K., et al., *Aberrant PD-L1 expression through 3'-UTR disruption in multiple cancers*. *Nature*, 2016. **534**(7607): p. 402-6.
62. Casey, S.C., et al., *MYC regulates the antitumor immune response through CD47 and PD-L1*. *Science*, 2016. **352**(6282): p. 227-31.
63. Burr, M.L., et al., *CMTM6 maintains the expression of PD-L1 and regulates anti-tumour immunity*. *Nature*, 2017. **549**(7670): p. 101-105.
64. Mezzadra, R., et al., *Identification of CMTM6 and CMTM4 as PD-L1 protein regulators*. *Nature*, 2017. **549**(7670): p. 106-110.
65. Zhang, J., et al., *Cyclin D-CDK4 kinase destabilizes PD-L1 via cullin 3-SPOP to control cancer immune surveillance*. *Nature*, 2018. **553**(7686): p. 91-95.
66. Akbay, E.A., et al., *Activation of the PD-1 pathway contributes to immune escape in EGFR-driven lung tumors*. *Cancer Discov*, 2013. **3**(12): p. 1355-63.
67. Coelho, M.A., et al., *Oncogenic RAS Signaling Promotes Tumor Immunoresistance by Stabilizing PD-L1 mRNA*. *Immunity*, 2017. **47**(6): p. 1083-1099.e6.
68. Collier, L.S., et al., *Cancer gene discovery in solid tumours using transposon-based somatic mutagenesis in the mouse*. *Nature*, 2005. **436**(7048): p. 272-6.

69. DeNicola, G.M., et al., *The utility of transposon mutagenesis for cancer studies in the era of genome editing*. *Genome Biol*, 2015. **16**: p. 229.
70. Dupuy, A.J., et al., *Mammalian mutagenesis using a highly mobile somatic Sleeping Beauty transposon system*. *Nature*, 2005. **436**(7048): p. 221-6.
71. Brett, B.T., et al., *Novel molecular and computational methods improve the accuracy of insertion site analysis in Sleeping Beauty-induced tumors*. *PLoS One*, 2011. **6**(9): p. e24668.
72. O'Donnell, K.A., *Advances in functional genetic screening with transposons and CRISPR/Cas9 to illuminate cancer biology*. *Curr Opin Genet Dev*, 2018. **49**: p. 85-94.
73. O'Donnell, K.A., et al., *A Sleeping Beauty mutagenesis screen reveals a tumor suppressor role for Ncoa2/Src-2 in liver cancer*. *Proc Natl Acad Sci U S A*, 2012. **109**(21): p. E1377-86.
74. Starr, T.K., et al., *A Sleeping Beauty transposon-mediated screen identifies murine susceptibility genes for adenomatous polyposis coli (Apc)-dependent intestinal tumorigenesis*. *Proc Natl Acad Sci U S A*, 2011. **108**(14): p. 5765-70.
75. Guo, Y., et al., *Comprehensive Ex Vivo Transposon Mutagenesis Identifies Genes That Promote Growth Factor Independence and Leukemogenesis*. *Cancer Res*, 2016. **76**(4): p. 773-86.
76. O'Donnell, K.A., et al., *Ex Vivo Transposon-Mediated Genetic Screens for Cancer Gene Discovery*. *Methods Mol Biol*, 2019. **1907**: p. 145-157.

77. Boutros, M. and J. Ahringer, *The art and design of genetic screens: RNA interference*. Nat Rev Genet, 2008. **9**(7): p. 554-66.
78. Hannon, G.J., *RNA interference*. Nature, 2002. **418**(6894): p. 244-51.
79. Demir, K. and M. Boutros, *Cell perturbation screens for target identification by RNAi*. Methods Mol Biol, 2012. **910**: p. 1-13.
80. Echeverri, C.J. and N. Perrimon, *High-throughput RNAi screening in cultured cells: a user's guide*. Nat Rev Genet, 2006. **7**(5): p. 373-84.
81. Mohr, S.E. and N. Perrimon, *RNAi screening: new approaches, understandings, and organisms*. Wiley Interdiscip Rev RNA, 2012. **3**(2): p. 145-58.
82. Sharma, S. and A. Rao, *RNAi screening: tips and techniques*. Nat Immunol, 2009. **10**(8): p. 799-804.
83. Bric, A., et al., *Functional identification of tumor-suppressor genes through an in vivo RNA interference screen in a mouse lymphoma model*. Cancer Cell, 2009. **16**(4): p. 324-35.
84. Cronin, S.J., et al., *Genome-wide RNAi screen identifies genes involved in intestinal pathogenic bacterial infection*. Science, 2009. **325**(5938): p. 340-3.
85. Gonsalves, F.C., et al., *An RNAi-based chemical genetic screen identifies three small-molecule inhibitors of the Wnt/wingless signaling pathway*. Proc Natl Acad Sci U S A, 2011. **108**(15): p. 5954-63.
86. Meacham, C.E., et al., *In vivo RNAi screening identifies regulators of actin dynamics as key determinants of lymphoma progression*. Nat Genet, 2009. **41**(10): p. 1133-7.

87. Paul, P., et al., *A Genome-wide multidimensional RNAi screen reveals pathways controlling MHC class II antigen presentation*. Cell, 2011. **145**(2): p. 268-83.
88. Premsrirut, P.K., et al., *A rapid and scalable system for studying gene function in mice using conditional RNA interference*. Cell, 2011. **145**(1): p. 145-58.
89. Jinek, M., et al., *A programmable dual-RNA-guided DNA endonuclease in adaptive bacterial immunity*. Science, 2012. **337**(6096): p. 816-21.
90. Wiedenheft, B., et al., *RNA-guided complex from a bacterial immune system enhances target recognition through seed sequence interactions*. Proc Natl Acad Sci U S A, 2011. **108**(25): p. 10092-7.
91. Shalem, O., et al., *Genome-scale CRISPR-Cas9 knockout screening in human cells*. Science, 2014. **343**(6166): p. 84-87.
92. Shalem, O., N.E. Sanjana, and F. Zhang, *High-throughput functional genomics using CRISPR-Cas9*. Nat Rev Genet, 2015. **16**(5): p. 299-311.
93. Deans, R.M., et al., *Parallel shRNA and CRISPR-Cas9 screens enable antiviral drug target identification*. Nat Chem Biol, 2016. **12**(5): p. 361-6.
94. Gilbert, L.A., et al., *Genome-Scale CRISPR-Mediated Control of Gene Repression and Activation*. Cell, 2014. **159**(3): p. 647-61.
95. Koike-Yusa, H., et al., *Genome-wide recessive genetic screening in mammalian cells with a lentiviral CRISPR-guide RNA library*. Nat Biotechnol, 2014. **32**(3): p. 267-73.
96. Morgens, D.W., et al., *Systematic comparison of CRISPR/Cas9 and RNAi screens for essential genes*. Nat Biotechnol, 2016. **34**(6): p. 634-6.

97. Wang, T., et al., *Genetic screens in human cells using the CRISPR-Cas9 system*. Science, 2014. **343**(6166): p. 80-4.
98. Luo, B., et al., *Highly parallel identification of essential genes in cancer cells*. Proc Natl Acad Sci U S A, 2008. **105**(51): p. 20380-5.
99. Dixit, A., et al., *Perturb-Seq: Dissecting Molecular Circuits with Scalable Single-Cell RNA Profiling of Pooled Genetic Screens*. Cell, 2016. **167**(7): p. 1853-1866.e17.
100. Shifrut, E., et al., *Genome-wide CRISPR Screens in Primary Human T Cells Reveal Key Regulators of Immune Function*. Cell, 2018. **175**(7): p. 1958-1971.e15.
101. Golden, R.J., et al., *An Argonaute phosphorylation cycle promotes microRNA-mediated silencing*. Nature, 2017. **542**(7640): p. 197-202.
102. Parnas, O., et al., *A Genome-wide CRISPR Screen in Primary Immune Cells to Dissect Regulatory Networks*. Cell, 2015. **162**(3): p. 675-86.
103. Ajioka, R.S., J.D. Phillips, and J.P. Kushner, *Biosynthesis of heme in mammals*. Biochim Biophys Acta, 2006. **1763**(7): p. 723-36.
104. May, B.K. and M.J. Bawden, *Control of heme biosynthesis in animals*. Semin Hematol, 1989. **26**(2): p. 150-6.
105. Ponka, P., *Cell biology of heme*. Am J Med Sci, 1999. **318**(4): p. 241-56.
106. Tsiftoglou, A.S., A.I. Tsamadou, and L.C. Papadopoulou, *Heme as key regulator of major mammalian cellular functions: molecular, cellular, and pharmacological aspects*. Pharmacol Ther, 2006. **111**(2): p. 327-45.

107. Faller, M., et al., *Heme is involved in microRNA processing*. Nat Struct Mol Biol, 2007. **14**(1): p. 23-9.
108. Hamza, I., *Intracellular trafficking of porphyrins*. ACS Chem Biol, 2006. **1**(10): p. 627-9.
109. Mense, S.M. and L. Zhang, *Heme: a versatile signaling molecule controlling the activities of diverse regulators ranging from transcription factors to MAP kinases*. Cell Res, 2006. **16**(8): p. 681-92.
110. Rouault, T.A., *The intestinal heme transporter revealed*. Cell, 2005. **122**(5): p. 649-51.
111. Khan, A.A. and J.G. Quigley, *Control of intracellular heme levels: heme transporters and heme oxygenases*. Biochim Biophys Acta, 2011. **1813**(5): p. 668-82.
112. Baranano, D.E., et al., *Biliverdin reductase: a major physiologic cytoprotectant*. Proc Natl Acad Sci U S A, 2002. **99**(25): p. 16093-8.
113. Atamna, H., et al., *Heme deficiency may be a factor in the mitochondrial and neuronal decay of aging*. Proc Natl Acad Sci U S A, 2002. **99**(23): p. 14807-12.
114. Atamna, H., J. Liu, and B.N. Ames, *Heme deficiency selectively interrupts assembly of mitochondrial complex IV in human fibroblasts: relevance to aging*. J Biol Chem, 2001. **276**(51): p. 48410-6.
115. Fukuda, Y., et al., *Upregulated heme biosynthesis, an exploitable vulnerability in MYCN-driven leukemogenesis*. JCI Insight, 2017. **2**(15).

116. Romana, M., et al., *Structure of the gene for human uroporphyrinogen decarboxylase*. Nucleic Acids Res, 1987. **15**(18): p. 7343-56.
117. Romeo, P.H., et al., *Molecular cloning and nucleotide sequence of a complete human uroporphyrinogen decarboxylase cDNA*. J Biol Chem, 1986. **261**(21): p. 9825-31.
118. Uhlen, M., et al., *Proteomics. Tissue-based map of the human proteome*. Science, 2015. **347**(6220): p. 1260419.
119. Cerami, E., et al., *The cBio cancer genomics portal: an open platform for exploring multidimensional cancer genomics data*. Cancer Discov, 2012. **2**(5): p. 401-4.
120. Lewis, C.A., Jr. and R. Wolfenden, *Uroporphyrinogen decarboxylation as a benchmark for the catalytic proficiency of enzymes*. Proc Natl Acad Sci U S A, 2008. **105**(45): p. 17328-33.
121. Phillips, J.D., et al., *Structural basis for tetrapyrrole coordination by uroporphyrinogen decarboxylase*. Embo j, 2003. **22**(23): p. 6225-33.
122. Franklin, M.R., J.D. Phillips, and J.P. Kushner, *Uroporphyrin in the uroporphyrinogen decarboxylase-deficient mouse: Interplay with siderosis and polychlorinated biphenyl exposure*. Hepatology, 2002. **36**(4 Pt 1): p. 805-11.
123. Franklin, M.R., J.D. Phillips, and J.P. Kushner, *Accelerated development of uroporphyrin in mice heterozygous for a deletion at the uroporphyrinogen decarboxylase locus*. J Biochem Mol Toxicol, 2001. **15**(5): p. 287-93.

124. Phillips, J.D., et al., *A porphomethene inhibitor of uroporphyrinogen decarboxylase causes porphyria cutanea tarda*. Proc Natl Acad Sci U S A, 2007. **104**(12): p. 5079-84.
125. Phillips, J.D., et al., *A mouse model of familial porphyria cutanea tarda*. Proc Natl Acad Sci U S A, 2001. **98**(1): p. 259-64.
126. Weiss, Y., et al., *Porphyria cutanea tarda and hepatoerythropoietic porphyria: Identification of 19 novel uroporphyrinogen III decarboxylase mutations*. Mol Genet Metab, 2018.
127. Balwani, M. and R.J. Desnick, *The porphyrias: advances in diagnosis and treatment*. Blood, 2012. **120**(23): p. 4496-504.
128. Puy, H., L. Gouya, and J.C. Deybach, *Porphyrias*. Lancet, 2010. **375**(9718): p. 924-37.
129. Hooda, J., et al., *Enhanced heme function and mitochondrial respiration promote the progression of lung cancer cells*. PLoS One, 2013. **8**(5): p. e63402.
130. Hinnebusch, A.G. and J.R. Lorsch, *The mechanism of eukaryotic translation initiation: new insights and challenges*. Cold Spring Harb Perspect Biol, 2012. **4**(10).
131. Jackson, R.J., C.U. Hellen, and T.V. Pestova, *The mechanism of eukaryotic translation initiation and principles of its regulation*. Nat Rev Mol Cell Biol, 2010. **11**(2): p. 113-27.
132. Krishnamoorthy, T., et al., *Tight binding of the phosphorylated alpha subunit of initiation factor 2 (eIF2alpha) to the regulatory subunits of guanine nucleotide*

- exchange factor eIF2B is required for inhibition of translation initiation. Mol Cell Biol*, 2001. **21**(15): p. 5018-30.
133. Pavitt, G.D., *eIF2B, a mediator of general and gene-specific translational control. Biochem Soc Trans*, 2005. **33**(Pt 6): p. 1487-92.
134. Yatime, L., et al., *Structure of an archaeal heterotrimeric initiation factor 2 reveals a nucleotide state between the GTP and the GDP states. Proc Natl Acad Sci U S A*, 2007. **104**(47): p. 18445-50.
135. Harding, H.P., et al., *Regulated translation initiation controls stress-induced gene expression in mammalian cells. Mol Cell*, 2000. **6**(5): p. 1099-108.
136. Harding, H.P., Y. Zhang, and D. Ron, *Protein translation and folding are coupled by an endoplasmic-reticulum-resident kinase. Nature*, 1999. **397**(6716): p. 271-4.
137. Han, A.P., et al., *Heme-regulated eIF2alpha kinase (HRI) is required for translational regulation and survival of erythroid precursors in iron deficiency. Embo j*, 2001. **20**(23): p. 6909-18.
138. Rafie-Kolpin, M., et al., *Two heme-binding domains of heme-regulated eukaryotic initiation factor-2alpha kinase. N terminus and kinase insertion. J Biol Chem*, 2000. **275**(7): p. 5171-8.
139. Dey, M., et al., *PKR and GCN2 kinases and guanine nucleotide exchange factor eukaryotic translation initiation factor 2B (eIF2B) recognize overlapping surfaces on eIF2alpha. Mol Cell Biol*, 2005. **25**(8): p. 3063-75.
140. Harding, H.P., et al., *An integrated stress response regulates amino acid metabolism and resistance to oxidative stress. Mol Cell*, 2003. **11**(3): p. 619-33.

141. Guo, F. and D.R. Cavener, *The GCN2 eIF2alpha kinase regulates fatty-acid homeostasis in the liver during deprivation of an essential amino acid*. *Cell Metab*, 2007. **5**(2): p. 103-14.
142. Zhang, P., et al., *The GCN2 eIF2alpha kinase is required for adaptation to amino acid deprivation in mice*. *Mol Cell Biol*, 2002. **22**(19): p. 6681-8.
143. Lu, L., A.P. Han, and J.J. Chen, *Translation initiation control by heme-regulated eukaryotic initiation factor 2alpha kinase in erythroid cells under cytoplasmic stresses*. *Mol Cell Biol*, 2001. **21**(23): p. 7971-80.
144. Scheuner, D., et al., *Translational control is required for the unfolded protein response and in vivo glucose homeostasis*. *Mol Cell*, 2001. **7**(6): p. 1165-76.
145. Liu, S., et al., *The function of heme-regulated eIF2alpha kinase in murine iron homeostasis and macrophage maturation*. *J Clin Invest*, 2007. **117**(11): p. 3296-305.
146. McEwen, E., et al., *Heme-regulated inhibitor kinase-mediated phosphorylation of eukaryotic translation initiation factor 2 inhibits translation, induces stress granule formation, and mediates survival upon arsenite exposure*. *J Biol Chem*, 2005. **280**(17): p. 16925-33.
147. Bahnan, W., et al., *The eIF2alpha Kinase Heme-Regulated Inhibitor Protects the Host from Infection by Regulating Intracellular Pathogen Trafficking*. *Infect Immun*, 2018. **86**(3).

148. Bauer, B.N., et al., *Multiple autophosphorylation is essential for the formation of the active and stable homodimer of heme-regulated eIF2alpha kinase*. *Biochemistry*, 2001. **40**(38): p. 11543-51.
149. Rafie-Kolpin, M., A.P. Han, and J.J. Chen, *Autophosphorylation of threonine 485 in the activation loop is essential for attaining eIF2alpha kinase activity of HRI*. *Biochemistry*, 2003. **42**(21): p. 6536-44.
150. Pakos-Zebrucka, K., et al., *The integrated stress response*. *EMBO Rep*, 2016. **17**(10): p. 1374-1395.
151. Grevet, J.D., et al., *Domain-focused CRISPR screen identifies HRI as a fetal hemoglobin regulator in human erythroid cells*. *Science*, 2018. **361**(6399): p. 285-290.
152. Hahn, C.K. and C.H. Lowrey, *Eukaryotic initiation factor 2alpha phosphorylation mediates fetal hemoglobin induction through a post-transcriptional mechanism*. *Blood*, 2013. **122**(4): p. 477-85.
153. Jousse, C., et al., *Inhibition of a constitutive translation initiation factor 2alpha phosphatase, CReP, promotes survival of stressed cells*. *J Cell Biol*, 2003. **163**(4): p. 767-75.
154. Kojima, E., et al., *The function of GADD34 is a recovery from a shutoff of protein synthesis induced by ER stress: elucidation by GADD34-deficient mice*. *Faseb j*, 2003. **17**(11): p. 1573-5.
155. Chen, R., et al., *G-actin provides substrate-specificity to eukaryotic initiation factor 2alpha holophosphatases*. *Elife*, 2015. **4**.

156. Hinnebusch, A.G., I.P. Ivanov, and N. Sonenberg, *Translational control by 5'-untranslated regions of eukaryotic mRNAs*. Science, 2016. **352**(6292): p. 1413-6.
157. Andreev, D.E., et al., *Translation of 5' leaders is pervasive in genes resistant to eIF2 repression*. Elife, 2015. **4**: p. e03971.
158. Sendoel, A., et al., *Translation from unconventional 5' start sites drives tumour initiation*. Nature, 2017. **541**(7638): p. 494-499.
159. Vattem, K.M. and R.C. Wek, *Reinitiation involving upstream ORFs regulates ATF4 mRNA translation in mammalian cells*. Proc Natl Acad Sci U S A, 2004. **101**(31): p. 11269-74.
160. Blais, J.D., et al., *Activating transcription factor 4 is translationally regulated by hypoxic stress*. Mol Cell Biol, 2004. **24**(17): p. 7469-82.
161. Dmitriev, S.E., et al., *GTP-independent tRNA delivery to the ribosomal P-site by a novel eukaryotic translation factor*. J Biol Chem, 2010. **285**(35): p. 26779-87.
162. Holcik, M., *Could the eIF2alpha-Independent Translation Be the Achilles Heel of Cancer?* Front Oncol, 2015. **5**: p. 264.
163. Lancaster, A.M., E. Jan, and P. Sarnow, *Initiation factor-independent translation mediated by the hepatitis C virus internal ribosome entry site*. Rna, 2006. **12**(5): p. 894-902.
164. White, J.P., L.C. Reineke, and R.E. Lloyd, *Poliovirus switches to an eIF2-independent mode of translation during infection*. J Virol, 2011. **85**(17): p. 8884-93.

165. Ross, J.A., et al., *Eukaryotic initiation factor 5B (eIF5B) provides a critical cell survival switch to glioblastoma cells via regulation of apoptosis*. *Cell Death Dis*, 2019. **10**(2): p. 57.
166. Ho, J.J.D., et al., *Oxygen-Sensitive Remodeling of Central Carbon Metabolism by Archaic eIF5B*. *Cell Rep*, 2018. **22**(1): p. 17-26.
167. Skabkin, M.A., et al., *Activities of Ligatin and MCT-1/DENR in eukaryotic translation initiation and ribosomal recycling*. *Genes Dev*, 2010. **24**(16): p. 1787-801.
168. Weisser, M., et al., *Structural and Functional Insights into Human Re-initiation Complexes*. *Mol Cell*, 2017. **67**(3): p. 447-456.e7.
169. Kearse, M.G. and J.E. Wilusz, *Non-AUG translation: a new start for protein synthesis in eukaryotes*. *Genes Dev*, 2017. **31**(17): p. 1717-1731.
170. Kim, E., et al., *eIF2A, an initiator tRNA carrier refractory to eIF2alpha kinases, functions synergistically with eIF5B*. *Cell Mol Life Sci*, 2018. **75**(23): p. 4287-4300.
171. Starck, S.R., et al., *Translation from the 5' untranslated region shapes the integrated stress response*. *Science*, 2016. **351**(6272): p. aad3867.
172. Scheuner, D., et al., *Control of mRNA translation preserves endoplasmic reticulum function in beta cells and maintains glucose homeostasis*. *Nat Med*, 2005. **11**(7): p. 757-64.
173. Das, I., et al., *Preventing proteostasis diseases by selective inhibition of a phosphatase regulatory subunit*. *Science*, 2015. **348**(6231): p. 239-42.

174. Abdulkarim, B., et al., *A Missense Mutation in PPP1R15B Causes a Syndrome Including Diabetes, Short Stature, and Microcephaly*. *Diabetes*, 2015. **64**(11): p. 3951-62.
175. Cnop, M., et al., *Selective inhibition of eukaryotic translation initiation factor 2 alpha dephosphorylation potentiates fatty acid-induced endoplasmic reticulum stress and causes pancreatic beta-cell dysfunction and apoptosis*. *J Biol Chem*, 2007. **282**(6): p. 3989-97.
176. Wong, Y.L., et al., *The small molecule ISRIB rescues the stability and activity of Vanishing White Matter Disease eIF2B mutant complexes*. *Elife*, 2018. **7**.
177. Sidrauski, C., et al., *Pharmacological brake-release of mRNA translation enhances cognitive memory*. *Elife*, 2013. **2**: p. e00498.
178. Sidrauski, C., et al., *The small molecule ISRIB reverses the effects of eIF2alpha phosphorylation on translation and stress granule assembly*. *Elife*, 2015. **4**.
179. Sidrauski, C., et al., *Pharmacological dimerization and activation of the exchange factor eIF2B antagonizes the integrated stress response*. *Elife*, 2015. **4**: p. e07314.
180. Wong, Y.L., et al., *eIF2B activator prevents neurological defects caused by a chronic integrated stress response*. *Elife*, 2019. **8**.
181. Palam, L.R., et al., *Integrated stress response is critical for gemcitabine resistance in pancreatic ductal adenocarcinoma*. *Cell Death Dis*, 2015. **6**: p. e1913.

182. Atkins, C., et al., *Characterization of a novel PERK kinase inhibitor with antitumor and antiangiogenic activity*. *Cancer Res*, 2013. **73**(6): p. 1993-2002.
183. Bi, M., et al., *ER stress-regulated translation increases tolerance to extreme hypoxia and promotes tumor growth*. *Embo j*, 2005. **24**(19): p. 3470-81.
184. Dey, S., et al., *ATF4-dependent induction of heme oxygenase 1 prevents anoikis and promotes metastasis*. *J Clin Invest*, 2015. **125**(7): p. 2592-608.
185. Nguyen, H.G., et al., *Development of a stress response therapy targeting aggressive prostate cancer*. *Sci Transl Med*, 2018. **10**(439).
186. Chen, T., et al., *Chemical genetics identify eIF2alpha kinase heme-regulated inhibitor as an anticancer target*. *Nat Chem Biol*, 2011. **7**(9): p. 610-6.
187. Bai, H., et al., *Dual activators of protein kinase R (PKR) and protein kinase R-like kinase PERK identify common and divergent catalytic targets*. *Chembiochem*, 2013. **14**(10): p. 1255-62.
188. Boyce, M., et al., *A selective inhibitor of eIF2alpha dephosphorylation protects cells from ER stress*. *Science*, 2005. **307**(5711): p. 935-9.
189. Jammi, N.V., L.R. Whitby, and P.A. Beal, *Small molecule inhibitors of the RNA-dependent protein kinase*. *Biochem Biophys Res Commun*, 2003. **308**(1): p. 50-7.
190. Rosen, M.D., et al., *Discovery of the first known small-molecule inhibitors of heme-regulated eukaryotic initiation factor 2alpha (HRI) kinase*. *Bioorg Med Chem Lett*, 2009. **19**(23): p. 6548-51.

191. Hooda, J., M. Alam, and L. Zhang, *Measurement of Heme Synthesis Levels in Mammalian Cells*. J Vis Exp, 2015(101): p. e51579.
192. Park, B.V., et al., *TGFbeta1-Mediated SMAD3 Enhances PD-1 Expression on Antigen-Specific T Cells in Cancer*. Cancer Discov, 2016. **6**(12): p. 1366-1381.
193. Chen, L., et al., *Metastasis is regulated via microRNA-200/ZEB1 axis control of tumour cell PD-L1 expression and intratumoral immunosuppression*. Nat Commun, 2014. **5**: p. 5241.
194. Rutkowski, D.T. and R.J. Kaufman, *All roads lead to ATF4*. Dev Cell, 2003. **4**(4): p. 442-4.
195. Sonenberg, N. and A.G. Hinnebusch, *Regulation of translation initiation in eukaryotes: mechanisms and biological targets*. Cell, 2009. **136**(4): p. 731-45.
196. Hugo, W., et al., *Genomic and Transcriptomic Features of Response to Anti-PD-1 Therapy in Metastatic Melanoma*. Cell, 2016. **165**(1): p. 35-44.
197. Chen, P.L., et al., *Analysis of Immune Signatures in Longitudinal Tumor Samples Yields Insight into Biomarkers of Response and Mechanisms of Resistance to Immune Checkpoint Blockade*. Cancer Discov, 2016. **6**(8): p. 827-37.
198. Krieg, C., et al., *High-dimensional single-cell analysis predicts response to anti-PD-1 immunotherapy*. Nat Med, 2018. **24**(2): p. 144-153.
199. Tumeo, P.C., et al., *PD-1 blockade induces responses by inhibiting adaptive immune resistance*. Nature, 2014. **515**(7528): p. 568-71.
200. Ito, E., et al., *Uroporphyrinogen decarboxylase is a radiosensitizing target for head and neck cancer*. Sci Transl Med, 2011. **3**(67): p. 67ra7.

201. Andant, C., et al., *Hepatocellular carcinoma in patients with acute hepatic porphyria: frequency of occurrence and related factors*. J Hepatol, 2000. **32**(6): p. 933-9.
202. Xu, Y., et al., *Translation control of the immune checkpoint in cancer and its therapeutic targeting*. Nat Med, 2019. **25**(2): p. 301-311.
203. Sengupta, B. and S.A. Siddiqi, *Hepatocellular carcinoma: important biomarkers and their significance in molecular diagnostics and therapy*. Curr Med Chem, 2012. **19**(22): p. 3722-9.
204. Flores, A. and J.A. Marrero, *Emerging trends in hepatocellular carcinoma: focus on diagnosis and therapeutics*. Clin Med Insights Oncol, 2014. **8**: p. 71-6.
205. Ozen, C., et al., *Genetics and epigenetics of liver cancer*. N Biotechnol, 2013. **30**(4): p. 381-4.
206. Strumberg, D., *Preclinical and clinical development of the oral multikinase inhibitor sorafenib in cancer treatment*. Drugs Today (Barc), 2005. **41**(12): p. 773-84.
207. Duffy, A.G. and T.F. Greten, *Liver cancer: Regorafenib as second-line therapy in hepatocellular carcinoma*. Nat Rev Gastroenterol Hepatol, 2017. **14**(3): p. 141-142.
208. El-Khoueiry, A.B., et al., *Nivolumab in patients with advanced hepatocellular carcinoma (CheckMate 040): an open-label, non-comparative, phase 1/2 dose escalation and expansion trial*. Lancet, 2017. **389**(10088): p. 2492-2502.

209. Caviglia, J.M. and R.F. Schwabe, *Mouse models of liver cancer*. *Methods Mol Biol*, 2015. **1267**: p. 165-83.
210. Heindryckx, F., I. Colle, and H. Van Vlierberghe, *Experimental mouse models for hepatocellular carcinoma research*. *Int J Exp Pathol*, 2009. **90**(4): p. 367-86.
211. Tschida, B.R., D.A. Largaespada, and V.W. Keng, *Mouse models of cancer: Sleeping Beauty transposons for insertional mutagenesis screens and reverse genetic studies*. *Semin Cell Dev Biol*, 2014. **27**: p. 86-95.
212. Hansen, L.J., et al., *Differential activation of myc gene family members in hepatic carcinogenesis by closely related hepatitis B viruses*. *Mol Cell Biol*, 1993. **13**(1): p. 659-67.
213. Katz, S.F., et al., *Disruption of Trp53 in livers of mice induces formation of carcinomas with bilineal differentiation*. *Gastroenterology*, 2012. **142**(5): p. 1229-1239.e3.
214. Xue, W., et al., *CRISPR-mediated direct mutation of cancer genes in the mouse liver*. *Nature*, 2014. **514**(7522): p. 380-4.
215. Lee, J.S., et al., *Application of comparative functional genomics to identify best-fit mouse models to study human cancer*. *Nat Genet*, 2004. **36**(12): p. 1306-11.
216. Shachaf, C.M., et al., *MYC inactivation uncovers pluripotent differentiation and tumour dormancy in hepatocellular cancer*. *Nature*, 2004. **431**(7012): p. 1112-7.
217. Conner, E.A., et al., *Dual functions of E2F-1 in a transgenic mouse model of liver carcinogenesis*. *Oncogene*, 2000. **19**(44): p. 5054-62.

218. Lee, J.S., et al., *A novel prognostic subtype of human hepatocellular carcinoma derived from hepatic progenitor cells*. Nat Med, 2006. **12**(4): p. 410-6.
219. Zender, L. and M. Hemann, *Reconstitution of Mice with Modified Liver Stem Cells*. Cold Spring Harb Protoc, 2015. **2015**(7): p. 685-8.
220. Walesky, C., et al., *Hepatocyte nuclear factor 4 alpha deletion promotes diethylnitrosamine-induced hepatocellular carcinoma in rodents*. Hepatology, 2013. **57**(6): p. 2480-90.
221. Richmond, A. and Y. Su, *Mouse xenograft models vs GEM models for human cancer therapeutics*. Dis Model Mech, 2008. **1**(2-3): p. 78-82.
222. Chopra, A.R., et al., *Cellular energy depletion resets whole-body energy by promoting coactivator-mediated dietary fuel absorption*. Cell Metab, 2011. **13**(1): p. 35-43.
223. Chopra, A.R., et al., *Absence of the SRC-2 coactivator results in a glycogenopathy resembling Von Gierke's disease*. Science, 2008. **322**(5906): p. 1395-9.
224. Cvero, A., et al., *Selective estrogen receptor-beta agonists repress transcription of proinflammatory genes*. J Immunol, 2008. **180**(1): p. 630-6.
225. Jeong, J.W., et al., *The genomic analysis of the impact of steroid receptor coactivators ablation on hepatic metabolism*. Mol Endocrinol, 2006. **20**(5): p. 1138-52.

226. Li, X., et al., *Progesterone and glucocorticoid receptors recruit distinct coactivator complexes and promote distinct patterns of local chromatin modification*. Mol Cell Biol, 2003. **23**(11): p. 3763-73.
227. Mukherjee, A., et al., *Steroid receptor coactivator 2 is critical for progesterone-dependent uterine function and mammary morphogenesis in the mouse*. Mol Cell Biol, 2006. **26**(17): p. 6571-83.
228. Stashi, E., et al., *SRC-2 is an essential coactivator for orchestrating metabolism and circadian rhythm*. Cell Rep, 2014. **6**(4): p. 633-45.
229. Xu, J. and Q. Li, *Review of the in vivo functions of the p160 steroid receptor coactivator family*. Mol Endocrinol, 2003. **17**(9): p. 1681-92.
230. Ye, X., et al., *Roles of steroid receptor coactivator (SRC)-1 and transcriptional intermediary factor (TIF) 2 in androgen receptor activity in mice*. Proc Natl Acad Sci U S A, 2005. **102**(27): p. 9487-92.
231. Voegel, J.J., et al., *TIF2, a 160 kDa transcriptional mediator for the ligand-dependent activation function AF-2 of nuclear receptors*. Embo j, 1996. **15**(14): p. 3667-75.
232. Onate, S.A., et al., *Sequence and characterization of a coactivator for the steroid hormone receptor superfamily*. Science, 1995. **270**(5240): p. 1354-7.
233. York, B. and B.W. O'Malley, *Steroid receptor coactivator (SRC) family: masters of systems biology*. J Biol Chem, 2010. **285**(50): p. 38743-50.
234. Lee, P.J., *Glycogen storage disease type I: pathophysiology of liver adenomas*. Eur J Pediatr, 2002. **161 Suppl 1**: p. S46-9.

235. Aragane, H., et al., *Chromosomal aberrations in colorectal cancers and liver metastases analyzed by comparative genomic hybridization*. *Int J Cancer*, 2001. **94**(5): p. 623-9.
236. Chiang, D.Y., et al., *Focal gains of VEGFA and molecular classification of hepatocellular carcinoma*. *Cancer Res*, 2008. **68**(16): p. 6779-88.
237. Parada, L.A., et al., *Frequent rearrangements of chromosomes 1, 7, and 8 in primary liver cancer*. *Genes Chromosomes Cancer*, 1998. **23**(1): p. 26-35.
238. Dasgupta, S., et al., *Coactivator SRC-2-dependent metabolic reprogramming mediates prostate cancer survival and metastasis*. *J Clin Invest*, 2015. **125**(3): p. 1174-88.
239. Bozickovic, O., et al., *A novel SRC-2-dependent regulation of epithelial-mesenchymal transition in breast cancer cells*. *J Steroid Biochem Mol Biol*, 2019. **185**: p. 57-70.
240. Szwarc, M.M., et al., *Steroid Receptor Coactivator-2 Controls the Pentose Phosphate Pathway through RPIA in Human Endometrial Cancer Cells*. *Sci Rep*, 2018. **8**(1): p. 13134.
241. Sandhu, D.S., E. Baichoo, and L.R. Roberts, *Fibroblast growth factor signaling in liver carcinogenesis*. *Hepatology*, 2014. **59**(3): p. 1166-73.
242. Tacconi, C., et al., *Vascular endothelial growth factor C disrupts the endothelial lymphatic barrier to promote colorectal cancer invasion*. *Gastroenterology*, 2015. **148**(7): p. 1438-51 e8.

243. Rutkowski, M.J., et al., *Cancer and the complement cascade*. Mol Cancer Res, 2010. **8**(11): p. 1453-65.
244. Takahashi, M., et al., *Mannose-binding lectin (MBL)-associated serine protease (MASP)-1 contributes to activation of the lectin complement pathway*. J Immunol, 2008. **180**(9): p. 6132-8.
245. Sun, Y., et al., *Modulation of transcription parameters in glucocorticoid receptor-mediated repression*. Mol Cell Endocrinol, 2008. **295**(1-2): p. 59-69.
246. Zhang, Y., et al., *Orphan receptor small heterodimer partner suppresses tumorigenesis by modulating cyclin D1 expression and cellular proliferation*. Hepatology, 2008. **48**(1): p. 289-98.
247. Li, G., et al., *Small heterodimer partner overexpression partially protects against liver tumor development in farnesoid X receptor knockout mice*. Toxicol Appl Pharmacol, 2013. **272**(2): p. 299-305.
248. Sandelin, A. and W.W. Wasserman, *Prediction of nuclear hormone receptor response elements*. Mol Endocrinol, 2005. **19**(3): p. 595-606.
249. Ahn, S.M., et al., *Genomic portrait of resectable hepatocellular carcinomas: implications of RB1 and FGF19 aberrations for patient stratification*. Hepatology, 2014. **60**(6): p. 1972-82.
250. Gao, J., et al., *Integrative analysis of complex cancer genomics and clinical profiles using the cBioPortal*. Sci Signal, 2013. **6**(269): p. p11.
251. Suresh, S., et al., *SRC-2-mediated coactivation of anti-tumorigenic target genes suppresses MYC-induced liver cancer*. PLoS Genet, 2017. **13**(3): p. e1006650.

252. Bavner, A., et al., *Transcriptional corepression by SHP: molecular mechanisms and physiological consequences*. Trends Endocrinol Metab, 2005. **16**(10): p. 478-88.
253. Goodwin, B., et al., *A regulatory cascade of the nuclear receptors FXR, SHP-1, and LRH-1 represses bile acid biosynthesis*. Mol Cell, 2000. **6**(3): p. 517-26.
254. Kerr, T.A., et al., *Loss of nuclear receptor SHP impairs but does not eliminate negative feedback regulation of bile acid synthesis*. Dev Cell, 2002. **2**(6): p. 713-20.
255. Seol, W., H.S. Choi, and D.D. Moore, *An orphan nuclear hormone receptor that lacks a DNA binding domain and heterodimerizes with other receptors*. Science, 1996. **272**(5266): p. 1336-9.
256. He, N., et al., *Epigenetic inhibition of nuclear receptor small heterodimer partner is associated with and regulates hepatocellular carcinoma growth*. Gastroenterology, 2008. **134**(3): p. 793-802.
257. Park, Y.Y., H.S. Choi, and J.S. Lee, *Systems-level analysis of gene expression data revealed NR0B2/SHP as potential tumor suppressor in human liver cancer*. Mol Cells, 2010. **30**(5): p. 485-91.
258. Jeong, Y., et al., *Nuclear receptor expression defines a set of prognostic biomarkers for lung cancer*. PLoS Med, 2010. **7**(12): p. e1000378.
259. Liao, C.H., et al., *Dickkopf 4 positively regulated by the thyroid hormone receptor suppresses cell invasion in human hepatoma cells*. Hepatology, 2012. **55**(3): p. 910-20.

260. Jang, S.M., et al., *Clinicopathological significance of CADM4 expression, and its correlation with expression of E-cadherin and Ki-67 in colorectal adenocarcinomas*. J Clin Pathol, 2012. **65**(10): p. 902-6.
261. Jang, S.M., et al., *Clinicopathological significance of CADM4 expression in invasive ductal carcinoma of the breast*. J Clin Pathol, 2013. **66**(8): p. 681-6.
262. Nagata, M., et al., *Aberrations of a cell adhesion molecule CADM4 in renal clear cell carcinoma*. Int J Cancer, 2012. **130**(6): p. 1329-37.
263. Sugiyama, H., et al., *Interaction of Necl-4/CADM4 with ErbB3 and integrin alpha6 beta4 and inhibition of ErbB2/ErbB3 signaling and hemidesmosome disassembly*. Genes Cells, 2013. **18**(6): p. 519-28.
264. Yamana, S., et al., *The Cell Adhesion Molecule Necl-4/CADM4 Serves as a Novel Regulator for Contact Inhibition of Cell Movement and Proliferation*. PLoS One, 2015. **10**(4): p. e0124259.
265. Stashi, E., B. York, and B.W. O'Malley, *Steroid receptor coactivators: servants and masters for control of systems metabolism*. Trends Endocrinol Metab, 2014. **25**(7): p. 337-47.
266. Wang, L., et al., *Characterization of a Steroid Receptor Coactivator Small Molecule Stimulator that Overstimulates Cancer Cells and Leads to Cell Stress and Death*. Cancer Cell, 2015. **28**(2): p. 240-52.